Analysis and control of complex growth phenomena in physics and biology

von Diplom-Physiker Diplom-Ingenieur (BA)
Michael Block
aus Waren/Müritz

Von der Fakultät II – Mathematik und Naturwissenschaften
der Technischen Universität Berlin
zur Erlangung des akademischen Grades

Doktor der Naturwissenschaften,
Doctor rerum naturalium

genehmigte Dissertation

Promotionsausschuß:

Vorsitzender:	Prof. Dr. E. Sedlmayr
Berichter/Gutachter:	Prof. Dr. E. Schöll, PhD.
Berichter/Gutachter:	Prof. Dr. S. Hess
zusätzlicher Gutachter:	Dr. D. Drasdo

Tag der wissenschaftlichen Aussprache: 5. März 2007

Berlin 2007
D 83

Abstract

Pattern formation and the coarsening of growing surfaces have attracted wide interest in scientific research during the last few decades.

Current fields of interest include not only the development of applications in nanotechnology combined with the fabrication of the corresponding microscopic structures but also the explanation of a wide range of biological growth processes.

In the area of nanotechnology there has, in the last decade, been particular interest in the fabrication of quantum dots, because of the unique electronic and optical properties of these "zero-dimensional" objects. The concept of self-organization holds the key to the effective and cheap fabrication of such structures. Obviously the fabrication of devices on an atomic scale requires rigorous theoretical observations of the underlying processes.

Other fields in which self-organized growth is of great interest are biology and medicine, where the interdisciplinary findings of both physicists and mathematicians are increasingly providing detailed explanations of biomedical processes at a microscopic level. During the last few years in particular, the use of theoretical models to observe the development of cell tissues is becoming more and more important for the development of effective therapies in the treatment of cancer. The aim of the present work is to make a contribution to understanding self-organized growth and to provide the basis for a possible method of control.

We use two well established models.
First we describe epitaxial growth by means of stochastic differential equations in order to manipulate the crystal growth process. To do this we solve various growth equations and combine them with existing methods from control theory to provide a time-delayed feedback. This leads to the theoretical description of in situ influences on the evolution of roughness, where we focus in particular on the experimentally important early phase.

In the second part of the work we use a kinetic Monte Carlo method to describe the formation of cell tissues in in-vitro mono-layers. Using the findings of an off-lattice model and the experimental observations of tumor cells, a simulation tool is generated which enables one to observe the dynamics and morphology of real size cell populations. This tool makes possible the detailed analysis of biologically relevant processes and their impact on growth.

Zusammenfassung

Die wissenschaftliche Untersuchung der Strukturbildung durch Wachstumsprozesse ist seit Jahrzehnten von immenser Bedeutung.

Sowohl die Entwicklung von Anwendungen in der Nanotechnologie verbunden mit der Herstellung entsprechender kleinster Strukturen, als auch die Erklärung von Wachstum in seinen verschiedenen Variationen in der Biologie sind aktuelle Forschungsgebiete.

Im Bereich der Nanotechnologien hat sich innerhalb des letzten Jahrzehnts unter anderem die Fabrikation von Quantenpunkten als eine führende Forschungsrichtung etabliert, nicht zuletzt durch die sehr speziellen elektronischen und optischen Eigenschaften dieser null-dimensionalen Objekte". Die Herstellung von Strukturen auf der atomaren Längenskala erfordert dabei entsprechendes theoretisches Verständnis der grundlegenden Prozesse. Als sehr vielversprechender Ansatz für eine effektive und kostengünstige Herstellung entprechender Halbleiterstrukturen hat sich das Ausnutzen von selbstorganisiertem Wachstum herausgestellt.

Ein weiterer Bereich, in dem selbstorganisiertes Wachstum eine grosse Rolle spielt, ist die Biologie und Medizin, wobei zunehmend Kenntnisse aus der Physik und Mathematik interdisziplinär kombiniert werden, um biologisch-medizinische Prozesse detailliert zu beschreiben. Insbesondere das Verständnis der Entstehung von Zellgewebe gewann in den letzten Jahren immer grössere Bedeutung für die Entwicklung effektiver Therapien in der Krebsforschung.

Ziel der vorliegenden Arbeit ist es, einen Beitrag zum Verständnis von selbstorganisierten Wachstumsprozessen zu leisten und einen Ansatz für eine mögliche Kontrolle dieser zu erarbeiten.

Dazu werden in den Untersuchungen zwei etablierte Modelle genutzt. Zum einen wird das epitaktische Wachstum mit Hilfe stochastischer Differentialgleichungen beschrieben, um anschliessend eine Anwendung zur gezielten Beeinflussung von Kristallwachstum theoretisch herzuleiten. Dazu werden verschiedene bekannte Wachstumsgleichungen numerisch gelöst und anschliessend die aus der Kontrolltheorie bekannte Methode der zeitverzögerten Rückkopplung in die Gleichungen eingeführt. Dies führt zu einer theoretischen Beschreibung einer ’in situ’ Einflussnahme auf die Rauigkeitsentwicklung, wobei besonderes Augenmerk auf die für Experimente wichtige Anfangsphase gelegt wurde.

Im zweiten Teil der Arbeit verwenden wir eine kinetische Monte-Carlo-Methode, um die Bildung von Zellpopulationen in in-vitro Monolayern zu beschreiben. Auf der Basis eines off-lattice Modells und von experimentellen Untersuchungen zu Tumorzellpopulationen wurde eine Simulation erstellt, mit der sich realistische Populationsgrössen hinsichtlich der Dynamik und der resultierenden Morphologie beschreiben lassen. Dabei können im Modell gezielt verschiedene biologisch relevante Prozesse in ihrem Einfluss untersucht werden.

Acknowledgments

First of all, it is a pleasure to thank Prof. Eckehard Schöll for his valuable advice and support and for providing the challenging, interesting, and exciting topic of this thesis.

Cooperation plays a vital role in scientific research.

The part of this work concerning the model for cell population evolution was devoloped within a strong cooperation. For that I would like to thank Dr. Dirk Drasdo from the Interdisciplinary Centre for Bioinformatics (IZBI) Leipzig.

For very intensive and helpful discussions concerning the part of the time-delayed feedback control of stochastic differential equations I would like to thank Prof. Beate Schmittmann from the Virginia Polytechnic Institute and State University Blacksburg (USA).

Very fruitful and stimulating discussions with the members of the theoretical department of the Institute of Crystal Growth (IKZ) are acknowledged. In particular I would like to thank Dr. Torsten Boeck, Dr. Thomas Teubner, and Dr. Wolfram Miller.

Some very helpful discussions with friends are acknowledged. Where Dr. Igor Bjelakovic, Maika Felten, Dr. Gabriel Range, and Dr. Dirk Woywod partly contributed to the physics part, I thank Prof. Jochen Hühn from the German Rheumatism Research Centre (DRFZ) in Berlin for very helpful discussions about the biological part of this work. Where I had to enlarge my knowledge about cell biology, he had to act somehow as a personal biologist.

For the nice working atmosphere in the group of Prof. Dr. E. Schöll I would like to thank all the members, in particular Dr. Frank Elsholz, Pillip Hövel, Johanne Hizanidis, Dr. Gerold Kiesslich, Dr. Roland Kunert, and Dr. Kathy Lüdge.

The Language support by Penny Salter is gratefully acknowledged.

Support in all situations outside this work and thus also support for the work was given by my girlfriend Jana Zastrow. I am deeply grateful for that.

Last, but not least I would like to express warmest thanks to my mom Bürgny Block.

List of publications

Parts of this work were already published as

- M. Block, R. Kunert, E. Schöll, T. Boeck, and Th. Teubner: *"Kinetic Monte Carlo simulation of formation of microstructures in liquid droplet"*. New Journal of Physics **6**, 166 (2004).
- M. Block and E. Schöll: *"Adjusting surface roughness in growth processes by time delayed feedback control"*. In: *Proceedings of the 28th International Conference on the Physics of Semiconductors (ICPS-26)*, Vienna (2006).
- D. Drasdo, S. Hoehme and M. Block: *"On the role of physics in the growth and pattern formation of multi-cellular systems: What can we learn from individual-cell based models?"*. (2006) (accepted for publication in Journal of Statistical Physics).
- M. Block and E. Schöll: *"Time Delayed Feedback Control in growth phenomena"*. Journal of Crystal Growth (2006) doi:10.1016/j.jcrysgro.2006.10.254.
- M. Block, E. Schöll and D. Drasdo: *"Classifying the expansion kinetics and critical surface dynamics of growing cell populations"*. (2006) (submitted to Physical Review Letters).

Preface

If you asked fifty people of various ages what were the most important advances in technology from the last few years, you would get many different answers. Some would say computers, some the internet, photographers would say the digital camera, business people might favour the mobile phone and children play stations.

But what most of the answers would undoubtedly have in common would be a relationship to the miniaturization and optimization of electronic or optical devices. Based on the answers one could say that nanotechnology is one of the most important technological advance in recent years.

Since 2002 there has been a website for very small scale images where the *nanopicture* of the day is chosen [1]. A lot of recent investigations into small scale science are presented and there are also some futuristic speculations about the direction of nanotechnologies.

In Fig. 1 we can see one of the possible future applications of this technology. The 'nanobot' is to be constructed to help doctors destroy unwanted cells. As the authors say, 'this image portrays a tiny, nanometer sized, fully functional autonomous robot helping to destroy a faulty red blood cell.' When we think about the construction of such a nanobot, we need to consider the problems involved. One major goal is to solve the problem of the materials needed for the electronic devices in such a small robot, where length scales are of the order of atoms. Biological behaviour, on the other hand, is explained using length scales of the order of biological cells. The solution is going to involve nanoscale work from a lot of different scientific fields. One could be forgiven for thinking that such a robot is either impossible or will take the whole century to construct, but in fact science is already beginning to solve the first part of the problem. One of the scientific fields involved is the explanation of the properties of materials on an atomic scale and,

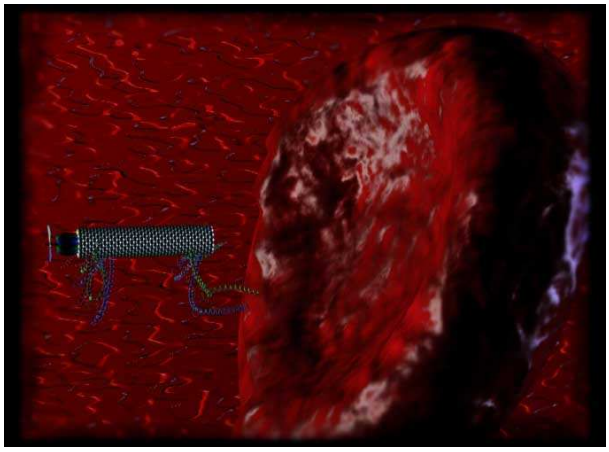

Figure 1: Nanobot destroys a faulty red blood cell [Mav03].

[1] `http://www.nanopicoftheday.org`

of course, the development of the necessary experimental observational methods (see Fig. 2).

In this thesis the reader will find investigations into two specific systems where the concept of *self-organization* generates the kind of growth system we want to explain by statistical methods. First we focus on the formation of structures during the spatio-temporal evolution of the roughening surface. One of the key questions in crystal growth today is the problem of fabricating the surface in a specified way, but cheaply. Epitaxial growth is a well-established method of preparing crystals where self-organization plays a big role. The theoretical investigation of a possible in-situ influence on the growth process could therefore be very helpful. In the second part the reader will find a very different system, that of tumor cell populations in in-vitro mono-layers. Although the length scale is totally different in the two parts, the reader will find a lot of similarities. Both are growth systems with their own self-organization and it was found that similar concepts can be used to model the two systems. So, coming back to the nanobot, our work contributes in a small way to the solution of the problem: both to the preparation of small scale applications and to the explanation of biological tissues, the aim being, of course, to find effective methods of tackling tumor cells. Earlier we stated that work on a nanoscale is a new field of interest for science, but nanotechnology was, of course, used by the ancient Greeks, as Walter *et al* showed in their findings [Wal06]. A 2000-year-old recipe for hair dye shows that they had a method of permanently colouring grey hair black. Basically this method works by biologically inducing the growth of nanocrystals. Presumably the ancient Greeks neither knew why their method worked nor could explain the growth of nanocrystals. Nevertheless, these findings could lead to new methods of growing nanocrystals, where the challenge will be much greater than that of dying hair black.

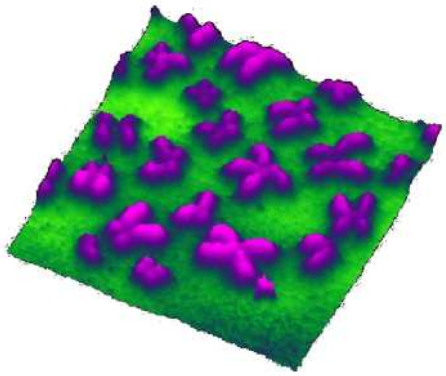

Figure 2: Chromosome image: scanning force microscopy image [McM94].

Contents

Chapter 1

Introduction

Key words like *miniaturization*, *nano*, *lab on chip* are connected to some of the major challenges in science today, those involving the understanding of very small scale processes down to the atomic scale and the development of applications which work on that scale.

Obviously one important part in any kind of theoretical work concerning small scale processes is that of understanding the formation of structures and the interplay of the related particles. A lot of physical, chemical and biological processes can be described as the spatio-temporal evolution of a system which we can explain as a kind of a growth process. The wide range of growth phenomena exhibit very different structures where we can see either very symmetric well-defined structures with for instance circular symmetries like the snow flake crystals (Fig. 1.1), or totally different structures like for example the fire front of a burning sheet of paper, where there is a linear interface, or the growth of trees or the pattern formation on a snail's shell (Fig. 1.2 and Fig. 1.3).

Thus the consideration of growing systems in their spatio-temporal development is an increasingly important field of interest in science, where the accurate description of

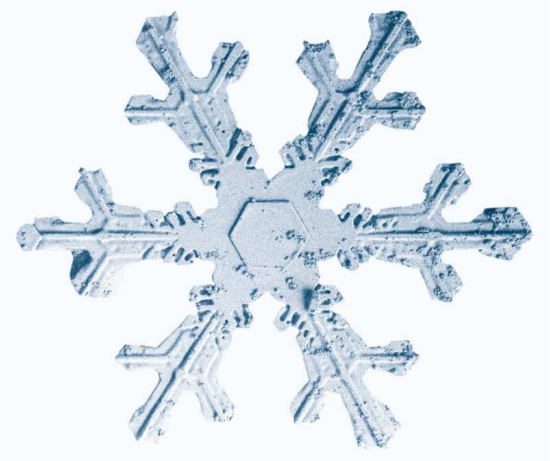

Figure 1.1: Snow crystals: capturing snow flakes for observation with the low temperature scanning electron microscope, Wergin, W. P. and E. F. Erbe Electron Microscopy Laboratory, Agricultural Research Service, U.S. Department of Agriculture, Beltsville, MD 20705 USA 1994.

Figure 1.2: Sample for growth: tree grown on the island Hiddensee.

Figure 1.3: Sample for growth: snail *Conus marmoreus* and behind a simulation result of the model describing the pattern formation due to fronts of pigment reactions. [Mei87](see also [Mei03a] for further examples) .

the basic processes can give an explanation of the similarities and differences between various growth phenomena and thereby a better understanding of the basic mechanisms in general. The microscopic picture can then lead to the description of macroscopic behaviour. We have concentrated here on two different kinds of growth, the roughening of films in epitaxial crystal growth and the formation of cell populations in an in-vitro environment. We shall now give short introductions to both.

1.1 Crystal growth

Current scientific work on crystal growth is focused on obtaining better electronic and opto-electronic devices. Major tasks are the development of better memory chips and effective solar cells together with the optimal miniaturization of these devices using the newly discovered properties of materials. The fabrication of such devices was developed during the last decade on a truly atomic scale with nanocrystals, quantum dots and quantum wells. One application was to lasers. Figure 1.4 shows examples of the wide range of different crystal structures grown by epitaxial methods. It is obviously not only essential to consider the properties of the devices prepared but also the related growth processes needed for their fabrication. A wide branch of experimental meth-

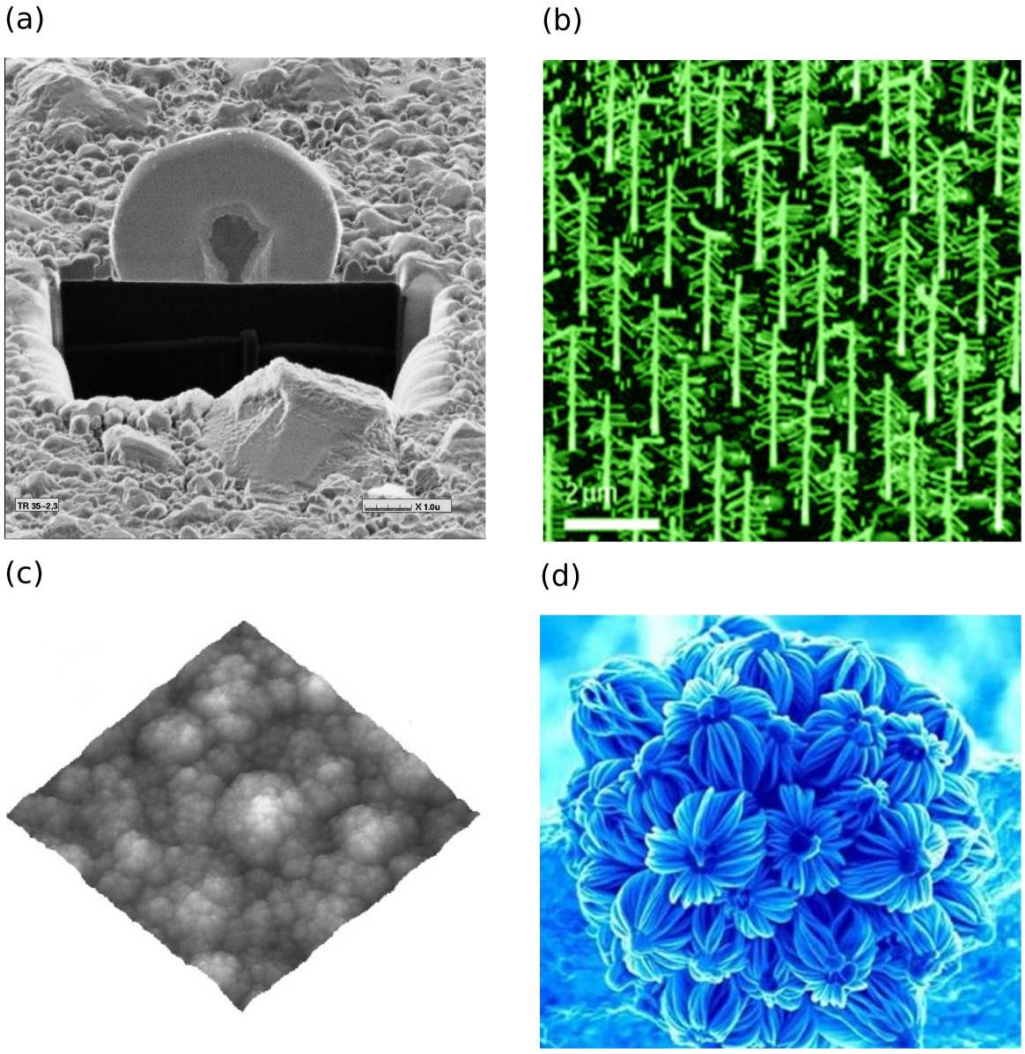

Figure 1.4: Examples for crystal growth: (a) cross-section of an Indium droplet with a Silicon nanocrystallite inside grown by *Liquid Phase Epitaxy* (LPE) [Boe99; Blo04], (b) 'forest' of ordered 'nanotrees' grown by *Metal Organic Vapor Phase Epitaxy* (MOVPE) [Dic04], (c) $14 \times 14 \mu m^2$ AFM images of amorphous SiO_2 films after two days deposition at a temperature of $T = 611K$ grown by *Chemical Vapor Deposition* (CVD) [Oje03] (d) silicon carbide nanobouquet grown by CVD [Ho04].

ods exist for preparing materials with a well defined structure related to the desired and expected properties. There are a lot of experimental methods for growing well defined crystal structures on an atomic scale in different ways for specific applications. Sometimes this involves the growth of highly defined structures like single quantum dots or single crystals, but we are going to concentrate here on roughening surfaces for film growth in experiments. Usually the experimental setups have to be tuned to get a specific structure in thin film growth. A helpful tool would be an 'in-situ' control-

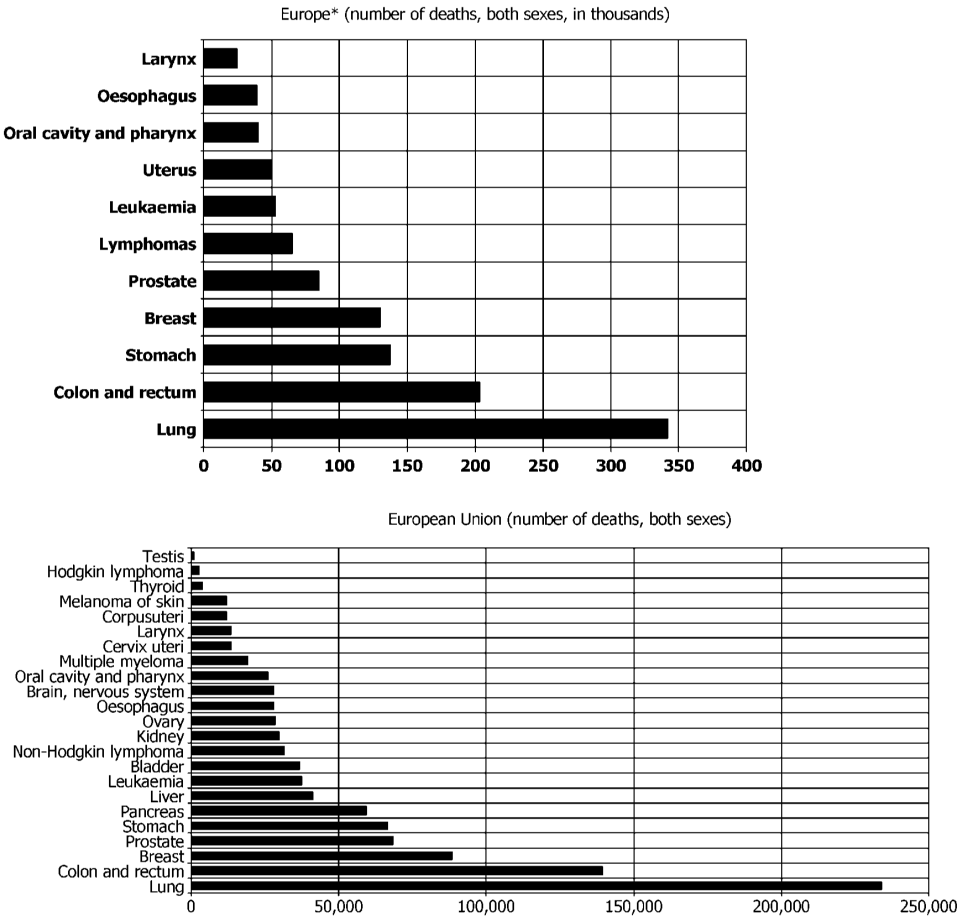

Figure 1.5: Statistics of cancer diseases in Europe, estimated mortality from cancer in Europe and the European Union 2004,* No data for Europe for all the individual sites due to limitations of coding scheme employed. [Boy04].

lable setup to check the structure during growth and then retune the conditions to get a more precise structure without having to start the experiment again. Controlling the roughening process would give one the opportunity of growing a surface with a tuned amplitude of roughness and a tuned correlation function within a well defined time. We would like to present a first contribution to that control process.

1.2 Tumor growth

The most widespread disease in industrial countries today is cancer. As Fig. 1.5 shows, there are a lot of very different types of cancers killing a lot of people every year. Therapies developed during the last decades to tackle this *'scourge of mankind'* often have very strong side effects on the human body and are not always effective. Indeed for some types of cancer there are, as yet, no effective therapies. The development of

effective methods for destroying tumor cells without affecting the surrounding healthy tissue is one of the major challenges to science today.

Scientific work in the field of understanding the mechanisms which lead to these diseases has become more and more interdisciplinary during the last decade. Physical and mathematical methods have been applied to biology and medicine. The development of computers has lead to important advances in diagnostics using, for instance, the new image-processing methods. Physics and mathematics have also helped explain the behaviour of individual cells and their behaviour in a growing structure.

Models developed to explain behaviour on the scale of one cell and of many cells have given us more knowledge about the behaviour of the cells in an organism and helped in the development of effective therapies.

1.3 Structure of this work

In this work we have developed theoretical models for growth and we use two different methods. Whereas stochastic differential equations using a continuous height function are applied to problems in crystal growth, we have developed a kinetic Monte Carlo algorithm as an individual cell based model to explain the growth of in-vitro tumor cell monolayers.

So, this work can be seen both as a further development of the research on epitaxial growth studied in our group during the last years and as a new field of research. Our group has been using kinetic Monte-Carlo methods for about 12 years now as part of an extensive study to explain the growth of semiconductor structures. A second field of interest is the control theory used in part of this work. Both the explanation of biological structures and the study of stochastic growth equations are new.

In this thesis the methods applied to crystal growth are different from those applied to tumor growth. We shall give an introduction to the experimental setup and the processes leading to growth in Ch. 2 and Ch. 3 and explain our modelling methods.

In order to take these different systems into account, we have to think both about how to define the modelling conditions, and about what to take into account when developing an effective and useful model to answer our specific questions.

In this context, Ch. 4 can be seen as a short guide to model growth from the microscopic to the macroscopic range where we show how our findings fit into this general overview.

After these more general aspects of the work we then go further to the first model and growth system type, the control of the stochastic differential equations. We give a detailed explanation for the stochastic differential equations used together with a detailed description of the related processes and their correspondence to epitaxial crystal growth (Ch. 5).

A summary of data analysis as an essential part is given in Sec. 5.4 together with the time-delayed feedback control schemes we discuss in the next chapter (Ch. 6). The combination of these first findings leads to the results for controlled and uncontrolled

equations in 1+1 and 2+1 dimensions (Ch. 7). A detailed variation of the parameters for different growth equations enables us to propose further possible experimental setups.

Whereas up to now we have been working with a continuous description of a growing system, we now change both the growth system and the method in order to consider the spatio-temporal evolution of a biological system. A kinetic Monte Carlo method is used for observing the tumor growth of in-vitro cultures. The following chapter then gives a detailed description of the individual cell based cellular automaton model (CA) on the unstructured lattice used in this work. Ch. 8 explains our model and demonstrates the ability of the simulation tool to study very different detailed mechanisms and processes of biological interest. Thus, this chapter can be seen in part as a manual for the use of the simulation tool in further investigations. We then, using extensive simulations, demonstrate the behaviour of our model and the intrinsic properties of the lattice whereby its advantages in comparison to common lattice types can be seen. We then proceed to show in detail the mechanisms and influences of cell properties on the critical surface dynamics. Comparison to experimental results are made and the result of these findings demonstrates our expectations for realistic biological systems (Ch. 9).

Chapter 2

Crystal growth

In this chapter we want to give a short introduction to the most common methods of growing crystals. We give a detailed description of epitaxial growth, on which we have focused our model, and we look at Czochralski growth as one example of a different method. More detailed overviews of possible experimental methods are given by Scheel and Fukuda [Sch03a] and Byrappa [Byr03] in their books (see also [Wil88; Pam75; Zan88]), where a more general overview of the theory can be found [Mic04; Pim98; Bar95].

2.1 Epitaxial Growth

The theory of continuum stochastic differential equations together with epitaxial growth can be seen as one single major task in the scientific investigation of crystal growth. Epitaxial growth is the targeted deposition of one type of material on a substrate of the same type of material (*homoepitaxial growth*) or on a different material (*heteroepitaxial growth*). Heteroepitaxial systems exhibit different properties because strain effects due to lattice mismatches become important.

The first findings of Volmer and Weber [Vol26] lead to the macroscopic description by Becker and Doering [Bec35] which is still, with a few additions, the major theory describing the formation of nuclei in crystal growth (see also [Sch03a; Wil88]). A lot of recent studies deal with epitaxial methods for fabricating specific structures on an atomic length scale, where for instance one major goal is the use of quantum dots. Where some techniques fabricate the dots 'manually' by putting the individual atoms in the desired position [Eag90], a lot of observations show that self-organized growth is a much more efficient and elegant method of growing such nanostructures. Probably the first self-organized island formation in a semiconductor material system, namely InAs/GaAs, was observed in 1985 by Goldstein *et al* [Gol85]. Self-organized growth was then extensively studied and developed, starting with the first quantum dots [e.g. Mo90; Eag90] and the first quantum dot lasers were developed experimentally in 1994

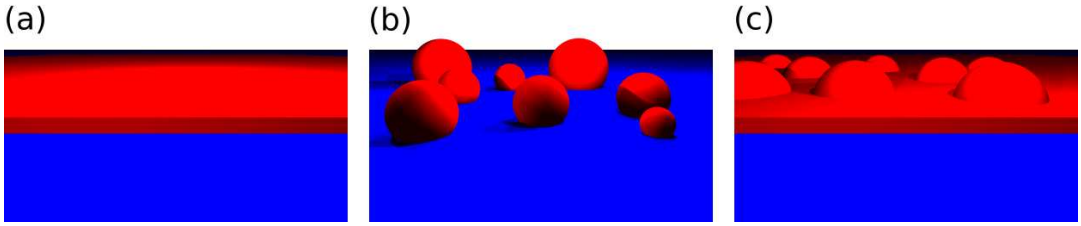

Figure 2.1: Growth modes of epitaxial growth, (a) Frank-van der Merwe growth, (b) Volmer-Weber growth, (c) Stranski-Krastanov growth.

at the Technische Universität Berlin in collaboration with Ioffe Physico-Technical Institute St. Petersburg [Led95].

The theory has become more and more important for applications to information and communication technology. Quantum dot arrays and multilayer systems of quantum dots are of very great interest [Bim96; Spr00; Wan04], and theoretical investigations have helped to explain the opto-electronic properties of these devices.

2.1.1 Growth modes

Epitaxial growth is normally divided into three different modes, where the interfacial free energy and the lattice mismatch determine the growth mode [Bim99; Mar87; Shc04a]. Fig. 2.1 shows these different modes. *Frank-van der Merwe* growth is characterized by layer-by-layer growth or a tendency to fill the individual monolayers [Fra49] (Fig. 2.1 (a)). In contrast *Volmer-Weber* growth is characterized by the formation of island structures [Vol26] (Fig. 2.1 (b)). The *Stranski-Krastanov* mode, where a phase of building a wetting layer is followed by a nucleation of islands, is an intermediate mode [Str39] (Fig. 2.1 (c)). In lattice matched systems only Frank-van der Merwe or Volmer-Weber growth can occur, whereas in lattice mismatched material systems growth in the Stranski-Krastanov mode is more favourable because of strain relaxations [Eag90, and references therein].

2.1.2 Processes in epitaxial growth

The growth process can be explained by different individual atomic processes, namely deposition or desorption processes and diffusion processes. Sometimes the nucleation of islands is referred to as another process, where the nucleation can be seen as just a product of diffusion at the surface together with binding energies, which lead to island growth.

In Fig. 2.2 we can see a scheme of the possible processes on the surface (green arrows show the direction of the events). Where deposition is not explicitly shown we see desorption (Fig. 2.2 (a)) from the surface and desorption from an island (Fig. 2.2 (d)). Fig. 2.2 (b),(c),(e) refer to different diffusion processes, which can be explained by a specific probability p to diffuse.

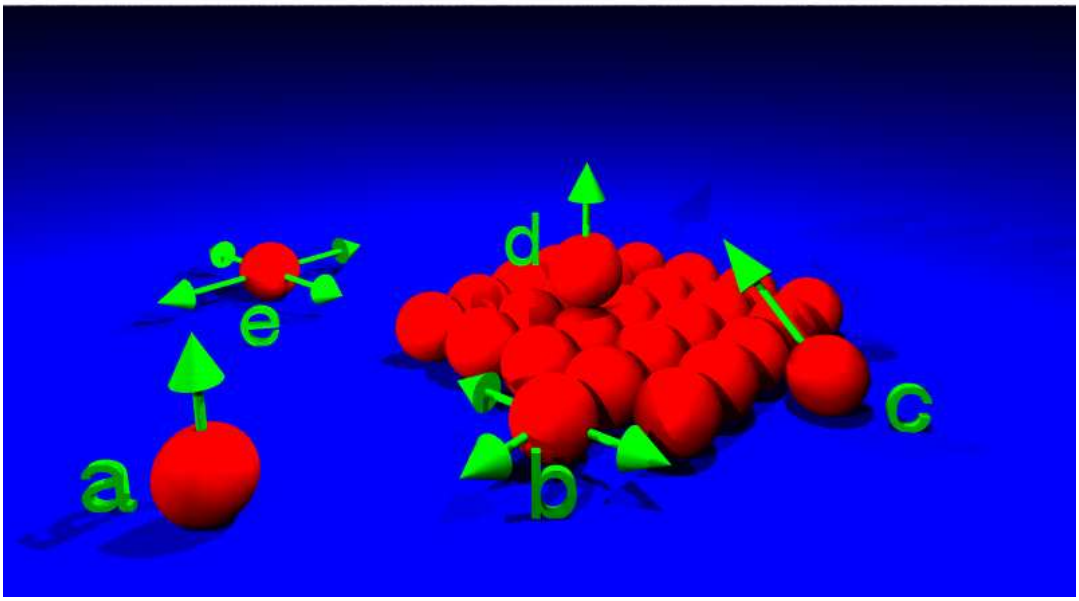

Figure 2.2: Processes at the surface in epitaxial growth: (a) desorption from the surface, (b) diffusion along an island, (c) edge diffusion on an island, (d) desorption from an island, (e) free diffusion.

If we assume that the atoms behave classically, the diffusion probability is expected to follow Arrhenius law [Lai65]:

$$p = \nu_0 \exp(-\frac{E}{k_B T}) \tag{2.1}$$

where ν_0 is the so called attempt frequency, E is the energy barrier for diffusion between the two states defined by the process, k_B is Boltzmann's constant and T denotes the temperature.

Depending on the initial state and on the final state after diffusion we distinguish here between free diffusion (Fig. 2.2 (e)), diffusion along an island (Fig. 2.2 (b)) and edge diffusion (Fig. 2.2 (c)). In Eq. (2.1) these different types of diffusion refer to different energy barriers E. We do not make use of this theory for the stochastic differential equations but explain Arrhenius law in more detail for cell-cell adhesion in the tumor growth model (Sec. 8.3.2).

2.2 Methods in epitaxial growth

A lot of different techniques exist for making semiconductor structures using epitaxial methods.

2.2.1 Molecular Beam Epitaxy

As one of the leading techniques in the fabrication of crystals, *Molecular Beam Epitaxy* (MBE) offers the possibility of growing structures under well defined conditions [Fra03; Shc04b]. This method deals with growth on a surface resulting from the condensation of single atoms or molecules out of the gas phase. The atomic source beams come from the material, which is heated in evaporation cells. Mechanical shutters can interrupt the atomic beam efficiently, so that it is possible to control the deposit of less than one atomic layer. Ultra High Vacuum (UHV, $\approx 10^{-11}$ torr) conditions prevent the incorporation of impurities and ensure that atoms and molecules follow a collision free path towards the substrate. Most MBE systems are equipped with several in-situ monitoring and analysis devices. These could be a mass analyzer, a Reflection High Energy Electron Diffraction (RHEED), an Auger Electron Spectroscopy (AES) and/or others. For detailed descriptions of MBE methods and instruments for the analysis of systems grown by MBE, see the books by Parker [Par85] and Farrow [Far95].

2.2.2 Metall Organic Chemical Vapour Deposition

Chemical vapour deposition (CVD) is used for the deposition of thin films of various materials. In a typical CVD process the substrate is exposed to one or more volatile precursors, which react and/or decompose on the substrate surface to produce the desired deposit. Volatile by-products are frequently produced too and are removed by gas flow through the reaction chamber. CVD is used for a wide range of material systems, for instance $Si0_2$, Ge/Si and TiN. The CVD method can be divided into a wide range of slightly different methods. One kind of chemical vapour deposition is *Metalorganic Chemical Vapour Deposition* (MOCVD). From the point of view of industrial preparation, MOCVD or *Metalorganic Vapour Phase Epitaxy* (MOVPE) has the advantage that the source material can be provided continuously [Moo96]. The disadvantages, on the other hand, are the complicated chemical processes and reactions that take place before and during deposition in the gas phase. While UHV monitoring techniques can not be applied because of the moderate pressure used in MOVPE systems, other in-situ techniques, such as reflectance anisotropy spectroscopy or spectroscopic ellipsometry [Ste96], are commonly used.

2.2.3 Liquid Phase Epitaxy

In contrast to the other methods, *Liquid Phase Epitaxy* (LPE) is a method of growing semiconductor crystal layers from a melt on solid substrates. This happens at tempera-

tures well below the melting point of the deposited semiconductor. The semiconductor is dissolved in the melt of another material. At conditions that are close to the equilibrium between dissolution and deposition the deposition of the semiconductor crystal on the substrate is slow and uniform. The equilibrium conditions depend very much on the temperature and on the concentration of the dissolved semiconductor in the melt. The growth of the layer from the liquid phase can be controlled by a forced cooling of the melt. Impurity introduction can be strongly reduced. Doping can be achieved by the addition of dopants. For one special system, in which Liquid Phase Epitaxy is used to fabricate silicon crystals inside indium droplets, see [Boe99; Blo04].

2.3 Other methods in crystal growth

Having explained the physical properties of epitaxial systems and the related experimental methods, we would now like to refer briefly to another leading crystal growing technique, Czochralski growth.

2.3.1 Czochralski growth

Czochralski growth is named after Jan Czochralski, who discovered the method in 1916. A seed crystal, mounted on a rod, is dipped into molten silicon. The seed crystal's rod is pulled upwards and rotated at the same time. By controlling the temperature gradients, rate of pulling and speed of rotation precisely, it is possible to extract a large, single-crystal, cylindrical ingot from the melt. This process is normally performed in an inert atmosphere, such as argon, and in an inert chamber, such as quartz. While the largest silicon ingots produced today are 400 mm in diameter and 1 to 2 meters in length, 200 mm and 300 mm diameter crystals are the standard industrial size. Thin silicon wafers cut from these ingots (typically about 0.75 mm thick) and polished to a very high degree of flatness are used for creating integrated circuits. Other semiconductors, such as gallium arsenide, can also be grown by this method, although in this case lower defect densities are obtained. So, this method offers a precise fabrication of semiconductor devices by a totally different method. For a detailed description of some other methods we refer to the already mentioned books ([Sch03a; Byr03]).

Chapter 3

The biology of tumor growth

The aim of cell biology is to understand the determining processes in nature in general and to describe the mechanisms and actions at a cellular level in particular. Early work on cell biology tried to observe the behaviour of cells as a kind of rough view of phenomenological behaviour. However, as medicine and biology have developed, scientific investigations have been going deeper and deeper into the detailed structure of the human body and of course into the details of cell biology.
Exploring the details of cell structure and mechanisms requires a description of chemical and physical actions on the cellular level. During the last decades the whole field has become more and more interdisciplinary, and physical biology, mathematical biology and bioinformatics are nowadays well established scientific fields.
Of course the development of better microscopes has opened up a new world of observations and helped us to understand what is happening on the microscopic level right down to the molecular length scale. Increasing knowledge of the cellular structure has also generated more interest in exploring the basic mechanisms of cell growth, the aim being to help biologists and doctors understand cell biology in general and in particular to find effective new therapies.
Until the mid-seventeenth century, scientists were unaware that cells even existed. Probably the first observations of cell biology were made by Robert Hooke, which he described in his 'Micrographia' in 1665. Through his microscope he saw that plant tissues were divided into tiny compartments. He termed them 'cellulae', which is the Latin word for the small rooms of monks. About 200 years later scientists really began to understand the importance of these findings, when Jakob Schleiden and Theodor Schwamm found similarities between animal and plant cells and deduced that all living things are made up of cells.

Nowadays cell biology makes use of modern microscopes to observe the molecular structure of cells and a lot of mechanisms are now well understood. Since the 80's the major goal for cell biology has been to explain the developmental processes, where cell changes and grow. With new apparatuses and the development of computer science, data analysis had a big role to play. A major step was announced in the November 6, 1998 in the Washington Post : "Scientists announced yesterday they had achieved

one of the most coveted goals in biology by isolating from human embryos and foetuses a primitive kind of cell that can grow into every kind of human tissue, including muscle, bone and brain." [1] Gearhart [Gea98] and Thomson et al [Tho98] had isolated embryonic stem cells.

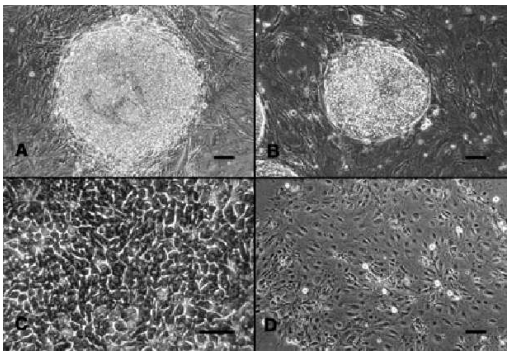

Figure 3.1: Isolation of embryonic stem cells [Tho98].

The major breakthrough of this work was the fact that one could now explain how so many kinds of different cells can develop from only a few cells to form an individuum. A very important field of research today is the explanation of the uncontrolled growth of cells or their uncontrolled division, which is currently a very important disease, *cancer*. Cancer as a Latin word comes from the Greek 'karkinos' which means a crayfish or a crab, maybe because of the image of a destructive crab in the human body. 'karkinos' is also the origin of the word carcinoma, which means the cancer cells. A similarly used word is tumor, meaning a medical excrescence that may be either malignant or benign. The differences between the uses of these words will now be explained. Tumor cells in general are so called because of two basic properties; their uncontrolled reproduction and their invasion and colonization of territories reserved for other cells. As long as the growing tumor or neoplasm is clustered in a single mass the tumor is said to be benign. When the tumor cells become invasive and occupy surrounding tissue or gain access to the blood stream to form secondary tumors, or metastases, the tumor is malignant and in this case the tumors are also called cancer. However these words are often used identically in the literature. In this chapter we are going to give a short description of cell biology and tumor cells, very closely related to our work. We are going to explain the main processes like the basic principles of cell division and the structures inside and outside one individual cell in a cell population but are not going to look into the cell on an atomic scale.

3.1 The biology of the cell

The cell is the structural and functional unit of all living organisms, and is therefore also called the 'building block of life'. [Alb02]. Organisms are divided into unicellular and multi-cellular types. Unicellular organisms consisting of a single cell are, for instance, bacteria, whereas humans, with about 100 trillions of cells, obviously belong to the multi-cellular group. A typical cell size is from 5 to 30 μm in diameter with typical masses around 1 ng. Each cell is to some extent self-contained and self-maintaining: it can take in nutrients, convert these nutrients into energy, carry out specialized functions, and reproduce as necessary. Each cell stores its own set of in-

[1] `http://www.washingtonpost.com/wp-srv/national/cell110698.htm`

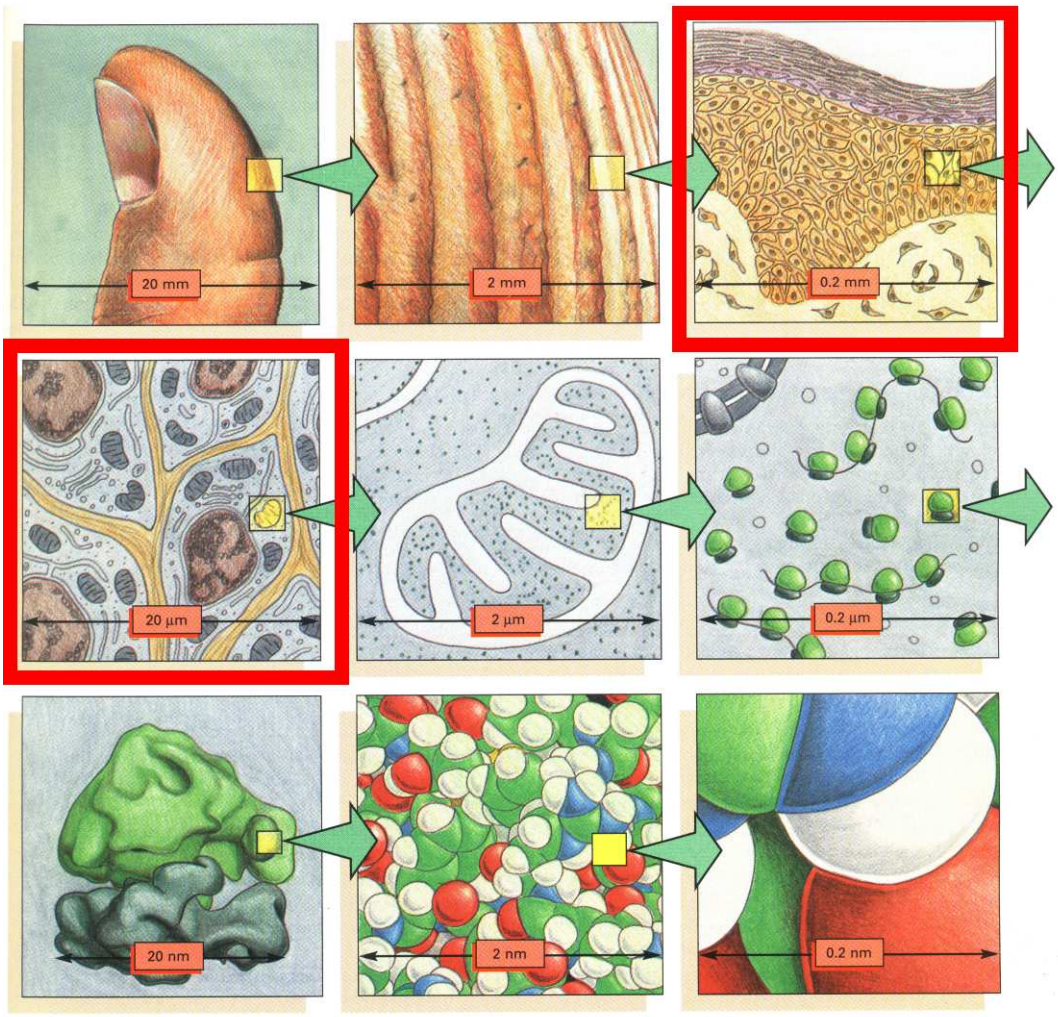

Figure 3.2: View on length scales beetween living cells and atoms where each part show an image magnified by a factor of ten from a thumb to a cluster of atoms part of protein molecules, the scale, which our studies cover, are the image of $0.2mm$ and the image of $20\mu m$ from cell population to an individual cell [Alb02].

structions for carrying out each of these activities. There are two basic kinds of cells, prokaryotic and eukaryotic cells. Whereas eukaryotic cells keep their DNA in a distinct membrane-bounded intracellular compartment called the nucleus, the prokaryotes have no such distinct nuclear compartment. Prokaryotes are normally small and often live as unicellular organisms. According to one estimate, at least 99% of prokaryotic species remain to be classified. A new classification of cells divides them into bacteria, achaea or archeabacteria and eukaryotes, where bacteria and archaea build the prokaryote, but we don't want to go into so much detail here (for more details see [Alb02]). An individual cell is a very complex system and there is no place here to describe all the details from the behaviour of the whole cell to the structure of DNA.

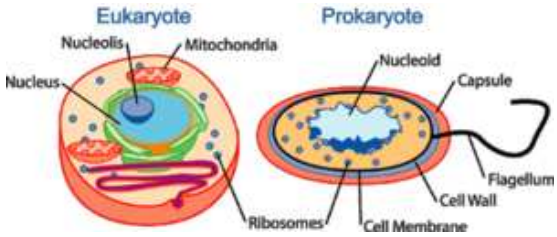

Figure 3.3: Schematic view of cells, left a typical eucaryotic cell, right a procaryotic cell.

Fig. 3.2 shows the different lengthscales one can get by a look on cells. It is obviously not possible to write an introduction to cell biology here.

We shall restrict ourselves here to some basic points related to the model we want to construct later in this work. For very detailed descriptions we refer to the well known and best compendium of molecular cell biology, 'The Cell' by Alberts *et al* [Alb02], where one can find not only an overview but a very detailed description of everything related to an individual cell.

3.1.1 The structure of an individual cell

An individual cell consists of molecules from four major chemical families of organic molecules, which are the important carbon based compounds, the sugars, the fatty acids, the amino acids and the nucleotides. Linked into large macromolecules, these compounds make up approximately 30% of the cell mass, where H_2O fills the remaining 70 $\%$. Fig. 3.3 shows a schematic eukaryotic and a prokaryotic cell. Some prokaryotic cells contain important internal membrane-bound compartments, but eukaryotic cells have a highly specialized endomembrane system characterized by regulated traffic and transport of vesicles. All cells, whether prokaryotic or eukaryotic, have a membrane, which envelopes the cell, separates its interior from its environment, regulates what moves in and out, and maintains the electric potential of the cell. Inside the membrane, a salty cytoplasm takes up most of the cell volume. All cells possess DNA, the hereditary material of genes, and RNA, containing the information needed to build various proteins such as enzymes, the cell's primary machinery.

3.1.2 The cytoskeleton

The cytoskeleton acts to organize and maintain the cell's shape; it anchors organelles in place, organizes the uptake of external materials by a cell, and cytokinesis, the separation of daughter cells after cell division; and moves parts of the cell during the processes of growth and mobility. The eukaryotic cytoskeleton is composed of microfilaments, actin filaments and microtubules. There are a great number of proteins associated with them, each controlling the cell's structure by directing, bundling and aligning filaments. Fig. 3.4 shows an experimental view of an eukaryotic cytoskeleton,

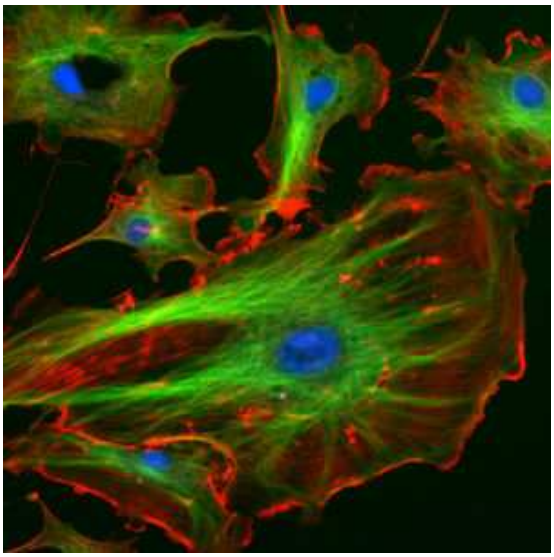

Figure 3.4: Cytoskeleton: Actin filaments are shown in red, microtubules in green, and the nuclei are in blue.

where one can see the actin filaments (red), the microtubules (green) and the nuclei (blue).

3.1.3 The cell cycle

'Where a cell arises, there must be a previous cell, just as animals can only arise from animals and plants from plants'. Rudolf Virchow stated this 'cell doctrine' in 1858. Cell division is such that new cells can only come from existing cells. The ordered sequence of such duplication and division is the *cell cycle*, the essential mechanism for the reproduction of living cells. Cell division is the process by which hair, skin, blood cells, and some internal organs are renewed. A specialized form of cell division is responsible for cellular differentiation during embryogenesis and morphogenesis, as well as for the maintenance of stem cells during adult life.

The cell cycle is specific to the cell type but there are some universal characteristics.

It consists of four distinct phases: G1 phase, S phase, G2 phase (collectively known as interphase) and M phase, which are schematically depicted in Fig. 3.5. The M phase is itself composed of two tightly coupled processes: mitosis, in which the cell's chromosomes are divided between the two daughter cells (see Fig 3.6), and cytokinesis, in which the cell's cytoplasm divides physically. The S phase is characterized by DNA duplication. The gap phases G1 and G2 are influenced by cell signalling and favourable cell conditions, whereby the length can vary in a wide range for the cells. Cells that have temporarily or reversibly stopped dividing are said to have entered a state of quiescence called G0 phase, while cells that have permanently stopped dividing due to age or accumulated DNA damage are said to be senescent. In a typical human cell the interphase I normally take 23 hours in a 24 hour cycle, whereas the M phase takes just one hour. The molecular events that control the cell cycle are ordered and directional; that is, each process occurs in a sequential fashion and it is impossible to 'reverse' the

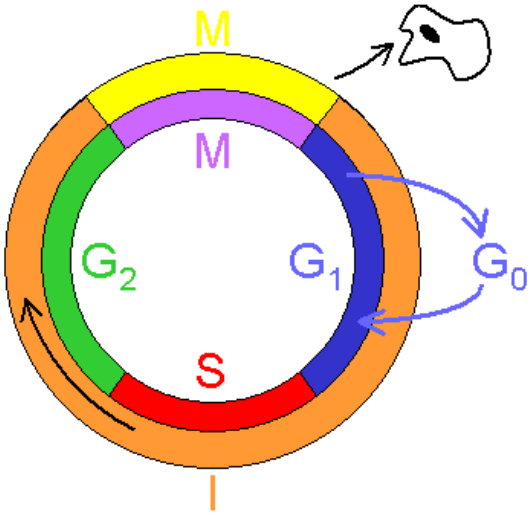

Figure 3.5: Scheme of the cell cycle: M mitosis, G0, G1, G2 the gap phases, S the synthesis phase, G0, G1, G2 and S build the interphase.

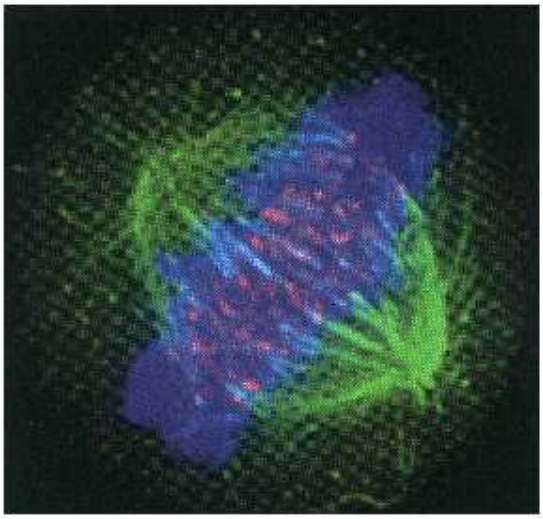

Figure 3.6: Mitosis of a cell.

cycle. Regulatory molecules determine a cell's progress through the cell cycle: cyclins and cyclin-dependent kinases. Leland H. Hartwell, R. Timothy Hunt, and Paul M. Nurse won the 2001 Nobel Prize in Physiology or Medicine for their discovery of these molecules which are central to the regulation of the cell cycle.

There has been a lot of work accorded to the cell cycle, but we don't want to go any further. As we will see in our model, the cell cycle is reduced to a one step event in which the cell divides into two daughter cells. For a more detailed description of the cell cycle see Alberts *et al* [Alb02] and references therein.

3.1.4 Cell types

The type determines the basic properties of a cell, so here we would like to give a short description of how cells can be characterized as animal cells. There are basic types of

tissue in the body of all animals and we are going to explain the most important types.

Epithelial tissue

Tissues composed of layers of cells that cover organ surfaces such as the surface of the skin. The tissues serve for protection, secretion, and absorption.

Connective tissue

As the name suggests, connective tissue holds everything together. Blood is considered to be a connective tissue. These tissues contain an extensive extra-cellular matrix.

Muscle tissue

Muscle cells contain contractile filaments that move past each other and change the size of the cell. Muscle tissue also is separated into three distinct categories: visceral or smooth muscle, which is found in the inner linings of organs; skeletal muscle, which is found attached to bone in order for mobility to take place; and cardiac muscle which is found in the heart.

Nervous tissue

Cells forming the brain, spinal cord and peripheral nervous system.

Areolar connective tissue

A pliable, mesh-like tissue with a fluid matrix whose function is to cushion and protect body organs. There are also different types of tissues in plants.

3.1.5 Cell migration

Cell migration is the central process in the development and maintenance of multicellular organisms. Tissue formation during embryonic development, wound healing and immune responses all require the movement of specific cells in a particular direction to a specific location. Errors during this process have serious consequences, including mental retardation, vascular disease, rheumatoid arthritis, tumor formation and metastasis. An understanding of the mechanisms by which cells migrate may lead to the development of novel therapeutic strategies for controlling, for example, invasive tumor cells. In animal tissues cells often migrate in response to, and towards, specific external signals, a process called chemotaxis. For further information see [Par99] [Lev06].

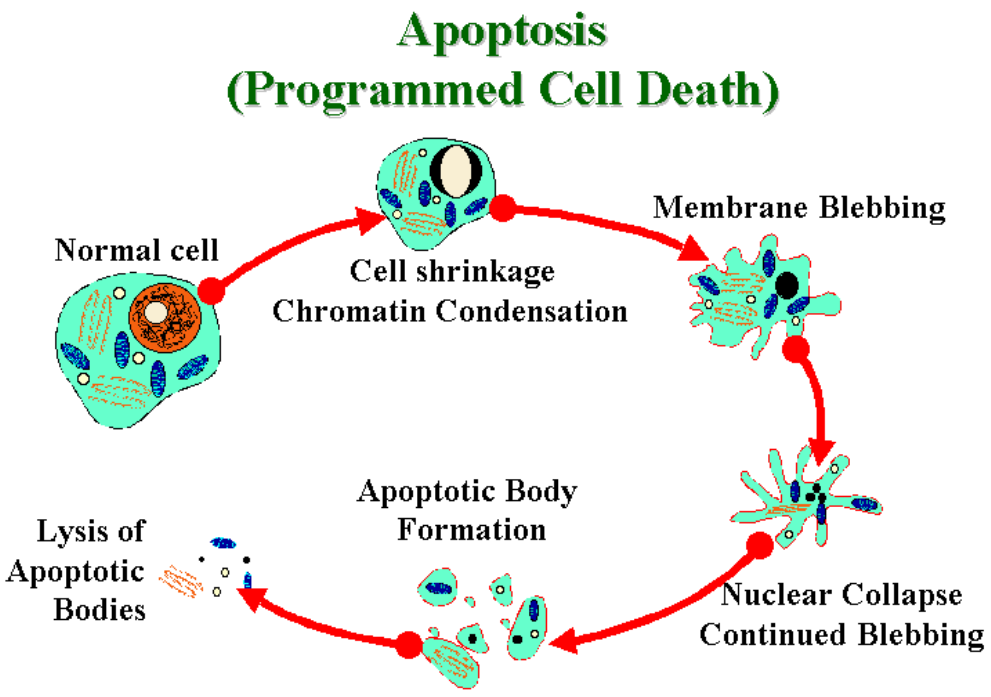

Figure 3.7: Scheme of programmed cell death (Apoptosis).

3.1.6 Apoptosis and necrosis

Apoptosis is also called *programmed cell death*. As such, it is the process of deliberate life relinquishment by a cell in a multi-cellular organism. In contrast to necrosis, which is a form of cell death that results from acute cellular injury, apoptosis is carried out in an ordered process that generally confers advantages during an organism's life cycle [Ker72].

For example, the differentiation of human fingers in the developing embryo requires the cells between the fingers to initiate apoptosis so that the fingers can separate.

Obviously such a mechanism must be well balanced, because too much apoptosis causes cell-loss disorders, whereas too little results in uncontrolled cell proliferation, namely cancerous tumors.

Apoptosis can occur, for instance, when a cell is damaged beyond repair, or infected with a virus. The 'decision' for apoptosis to occur can come from the cell itself, from its surrounding tissue or from a cell that is part of the immune system. If a cell's capability for apoptosis is damaged (for example, by mutation), or if the initiation of apoptosis is blocked (by a virus), a damaged cell can continue dividing without restrictions, developing into cancer. A cell undergoing apoptosis shows a characteristic morphology which can be seen in Fig. 3.7.

The cell becomes circular. The chromatin then undergoes an initial degradation and condensation. It then undergoes further condensation into compact patches against the

nuclear envelope. At this stage, the double membrane that surrounds the nucleus still appears complete. The nuclear envelope becomes discontinuous and the DNA inside it fragments. The nucleus breaks into several discrete chromatin bodies or nucleosomal units due to the degradation of DNA. The cell breaks apart into several vesicles called apoptotic bodies, which are then phagocytosed.

3.2 Biology of cell populations

We now have the basic mechanisms of one individual cell. The next question is how cells work together in a cell population. Cells are often motile and are normally deformable objects filled with some jelly-like medium, so some mechanisms must exist to combine them to give them the strength of the human body. The mechanism is similar to the game of breaking sticks one after the other or trying to break them all together at the same time. Cells form cell-cell junctions, have cell-cell adhesions and are connected by the extracellular matrix.

3.2.1 Extracellular matrix

A substantial part of cell tissues is normally extracellular space, which is largely filled by a network of macromolecules constituting the *extracellular matrix*. Produced by the cells, this matrix composed of proteins and polysaccharides is organized in a meshwork in close association with the surface of the cell. The extracellular matrix in connective tissues is extremely important for physical behaviour. It doesn't determine their behaviour but the properties of the epithelial cells depend on it.

3.2.2 Cell junctions

Cell junctions occur in all cell populations at the points of cell-cell or cell-matrix contacts. They are normally classified into three groups. *Occluding junctions* seal cells together in the epithelium in a way that prevents even small molecules from leaking from one side of the epithelial sheet to the other. *Anchoring junctions* mechanically attach cells and their cytoskeletons to their neighbours or to the extracellular matrix. *Communicating junctions* mediate the passage of chemical or electrical signals from one interacting cell to its partner.

3.2.3 Cell adhesion

The connection between junctions and adhesion is the fact that cells have to adhere in order to build anchoring junctions. A bulky cytoskeletal apparatus must then be assembled around the molecules that directly mediate the adhesion. This results in a well-defined structure and different adhesions can be identified using the electron microscope. For example during the last decade there has been a lot of work on cadherins

mediated Ca^{2+} -dependent cell-cell adhesions. The study of cell adhesion is part of cell biology. Cells are often not found in isolation, but tend rather to stick to other cells or to the non-cellular components of their environment. A fundamental question is: what makes cells sticky? Cell adhesion generally involves protein molecules at the surface of cells, so the study of cell adhesion involves cell adhesion proteins and the molecules that they bind to.

3.3 Carcinogenesis

Cell division (proliferation) is a physiological process that occurs in almost all tissues and under many circumstances. Normally homeostasis, the balance between proliferation and programmed cell death, usually in the form of apoptosis, is maintained by the tight regulation of the processes. Carcinogenesis is caused by the mutation of the genetic material of normal cells, which upsets the normal balance between proliferation and cell death. This results in uncontrolled cell division and tumor formation. The uncontrolled and often rapid proliferation of cells can lead to benign tumors; some types of these may turn into malignant tumors (cancer). More than one mutation is necessary for carcinogenesis. In fact, a series of several mutations to certain classes of genes is usually required before a normal cell is transformed into a cancer cell.

3.4 Tumor cell types

Cancers are generally classified according to the tissue and cell type from which they arise. Tumor in medical language simply means swelling or lump, either neoplastic, inflammatory or other. In common language, however, it is synonymous with 'neoplasm', either benign or malignant. This is inaccurate, since some neoplasms do not usually form tumors, for example leukaemia or carcinoma in situ.

Carcinoma

Tumor cells which arise from epithelial cells are *carcinoma*. Epithelial tissues are well connected tissue divided into epithelial sheets. Cells are tightly bound and the extracellular matrix consists of a thin mat called a *basal lamina*. So in carcinoma cells are attached to each other by cell-cell adhesions.

Sarcoma

A sarcoma is a cancer of the connective or supportive tissue (bone, cartilage, fat, muscle, blood vessels). The term comes from a Greek word meaning 'fleshy growth'.

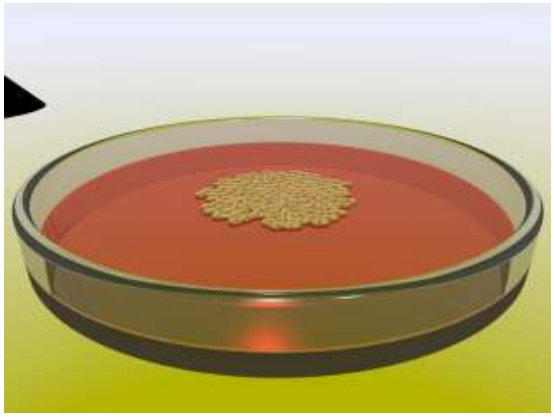

Figure 3.8: Scheme of an in vitro experiment with a petri dish where a solution of nutrients (red) lead to a growth of a cell population monolayer.

Leukemias

Leukemia (or leukaemia; see spelling differences) is a cancer of the blood or of the bone marrow characterized by an abnormal proliferation of blood cells, usually white blood cells (leukocytes). It is one of the broad group of diseases called hematological neoplasms.

3.5 In vitro experiments

All these cell types for tumor cell development have found a lot of interest in cell biology, where the determination of possible explanations is feasible thanks to the high resolution of modern microscopes which are able to distinguish the complexity of the cells in a complex tissue. In vitro experiments have been established as a very successful tool for studying the mechanisms of cells in a well defined environment where the setup is such that unknown influences can, on the whole, be neglected. A precise change of the properties of the cultured growth of cells therefore makes it possible to study the basic mechanisms of cells in detail.

Fig. 3.8 gives an impression of a possible setup for in vitro experiments - of course real apparatuses are much more complicated.

Chapter 4

Modeling growth phenomena

In the previous chapters we gave an overview of the systems we want to model. Obviously it is impossible to include all the details of the real growth process in a useful and effective model.

A model is, by definition, a simplification of reality, made in order to answer a specific question about real behaviour. So of course the first very important part of the work is to determine the limits and decide what assumptions have to be made, using the questions we want to answer as guidelines. Basic tasks are the timescales, length scales and the related methods.

In this chapter we follow this guideline in order to obtain the rules our representation have to fulfil. The method of building up the model may look obvious, but a closer look at the systems we want to explain - and in our opinion all other growth systems - shows that it is important and one of the first problems to solve. So this chapter may be a help in the construction of growth models in general and we shall apply it later on to crystal growth and cell population growth.

4.1 Get the right view

As shown in Fig. 4.1, different length scales explore very different views of the system, where each is related to individual properties of the system. So posed in a slightly different manner our question is, whether to look at the forest, at the individual tree or at an individual leaf.

Here we want to describe many-particle systems in order to get results for the dynamical behaviour of growth processes of as many particles as possible. On the other hand we want to include details of the basic actions of the individual particles. Thus, a well balanced description is required to ensure large scale simulations.

(a) (b) (c)

Figure 4.1: Zoom from macroscopic to microscopic view: Three different views on the same problem, (a) forest, (b) tree (c) leaf.

4.1.1 The microscopic view

A first approach could be the explanation of the most detailed view. In the case of particles such as atoms we go directly to the quantum mechanical potentials on the surface. If we explain the cell as a complete system together with all the processes inside one individual cell we rapidly come to the DNA structure and again to molecular structures. All these processes are of great interest and importance, firstly for the behaviour of individual particles and thereby also for collective behaviour.

However our questions are on a macroscopic scale. The microscopic view does not help us with our problem if we do not want to derive a model that explains all the processes of nature. But nevertheless findings from the microscopic view are essential for our model in order for us to make suitable assumptions.

4.1.2 The macroscopic view

Another way of tackling the problem is to explain the system by a macroscopic view. In case of atoms that view could be of the whole surface or in case of the cell the grown cell population. But if we want to decide between processes which lead to this behaviour and to model the growth itself this view seems too blunt.

4.1.3 The mesoscopic view

We need an approach that lies somewhere between the two previous approaches. This is the mesoscopic view, where we don't explain the structure of the particles but take particles with known properties and see what happens when we model the processes. So our scale for atomic behaviour is the lattice constant ($\sim 0.5 - 1.0\ nm$) and a time scale of the order of milliseconds. For cells our scale starts with a cell size ($\sim 10 - 40 \mu m$) and a time scale of hours to days (doubling time for cells $10 - 30$ hours).

4.2 Scaling theory

Having decided on our range for length scales, we are still left with the question of how much information and how many assumptions to include. If one considers a surface where in epitaxial growth some islands arise, an important question is whether we can deduce the behaviour of the whole surface from looking at a small section of it. The answer to that question is the concept of *'scaling'*, where by measuring quantities on a small section one can deduce values for bigger systems. A lot of growth systems show such relations. In our case one can find scaling laws for the morphological structures of the developing growth system.

4.2.1 Concept of self-similarity and self-affinity

As already explained, the basic concept in scaling approaches is the idea that one can divide a big system into 'similar parts'. Similarity means that when one looks at two maps with different magnifications and different measurements of a defined quantity, they look similar. Mathematically that is either an isotropic transformation, in which case the system is said to be *self-similar*, or anisotropic transformation, which defines a *self-affine* system. We can then extrapolate from small parts of the system to behaviour on a larger scale by using the *scaling laws* which we now want to introduce.

4.2.2 Roughening and scaling in growth systems

For surface growth the main quantities that describe the developmental processes are the velocities and spatial dimensions of the system and its morphological structure. Assuming either self-affinity or self-similarity we then measure the root mean square (rms) surface roughness given by

$$w_{RMS}(L,t) = \sqrt{\frac{1}{L}\sum_{i=1}^{L}[h(i,t) - \overline{h}(t)]^2} \tag{4.1}$$

where L is the system-size, $h(i,t)$ denotes the height function of the surface at the i-th point at time t, and $\overline{h}(t)$ is its average.

It follows from this equation that the rms roughness describes the standard deviation of the height function $h(i,t)$. In Fig. 4.2 we can see an example of a rough surface. Here the situations in 1+1 (1 spatial coord. + height) and in 2+1 (2 spatial coord. + height) dimensions are depicted: In the middle a rough surface in 2+1 in terms of a three dimensional height profile is shown, where the mean height is emphasized by the green line. Under the profile a two dimensional projection is shown, where the height increases from black to white colors, the plane on the left shows the same situation in 1+1 dimensions, where the height now depends on just one coordinate.

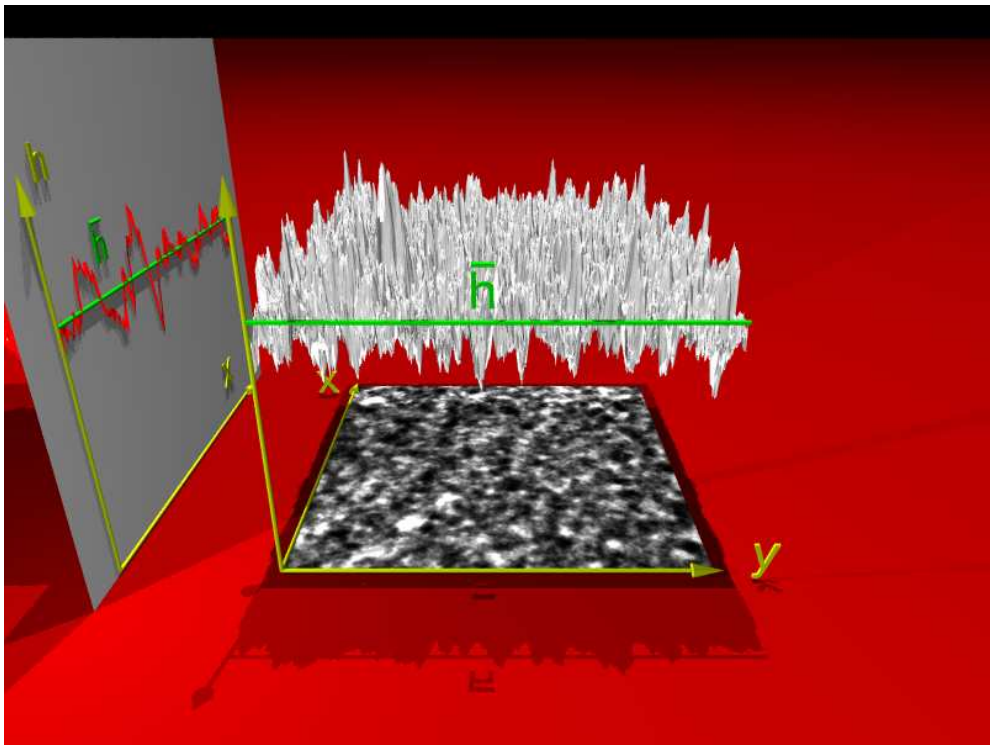

Figure 4.2: Illustration of a rough surface: in the middle a 2+1 dimensional surface with the height profile and the projected density plot of the height profile, on the left the height function in 1+1 dimensions (red line), the mean height $\overline{h}$ is shown by a green line.

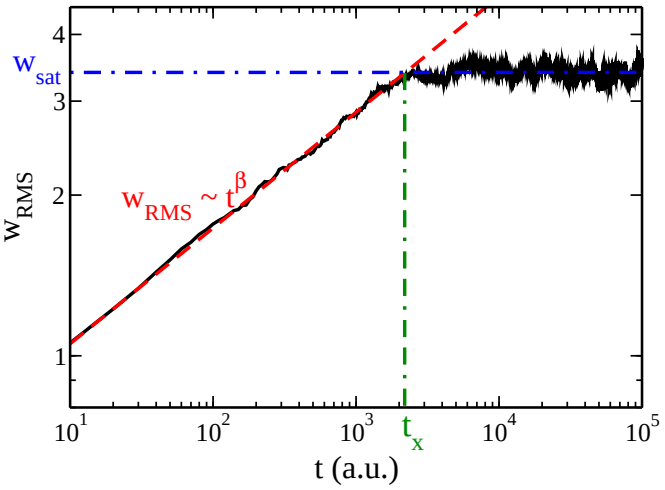

Figure 4.3: Typical temporal evolution of the root mean square roughness w_{RMS} (black line, example taken form long-time simulations for the Molecular Beam Epitaxy equation in Sec. 7.2), blue dash-dotted line: the saturation roughness, red dashed line: the early phase with $w_{RMS} \propto t^{\beta}$, green dash-dotted line denotes the crossover time t_x (double-logarithmic plot).

If growth now starts from a flat surface with system size L, the system roughens. In Fig. 4.3 we see a typical evolution divided into two phases, namely the roughening and the saturation phase, divided by crossover time t_x.

The early phase can be characterized by an exponent β, the so called *growth exponent*, whereas the late phase can be explained by a *roughness exponent* α.

After a certain time, depending on the spatial dimension and system size, the roughness saturates: The saturation roughness w_{sat} has been reached (blue). The exponents are then defined by the following power laws:

$$w_{RMS}(L,t) \propto t^{\beta} \quad \text{for} \quad t \ll t_x \tag{4.2}$$

$$w_{sat}(L) \propto L^{\alpha} \quad \text{for} \quad t \gg t_x \tag{4.3}$$

where t_x is the crossover time between the two regimes of evolution (green). Fig. 4.3 shows this behaviour for the Molecular Beam Epitaxy equation in 2+1 dimensions. We discuss this later in more detail (Sec. 7.2). Time t is in arbitrary units. We infer the growth exponent $\beta = 1/5$ from the simulated data, and then derive the roughness exponent $\alpha = 2/3$ from the amplitudes of the saturation values. t_x and L are linked by a further power law.

$$t_x \propto L^z \tag{4.4}$$

This third exponent z, the *dynamic exponent*, is not independent of α and β, as can easily be checked using the Family-Vicsek scaling relation [Fam85],

$$w_{RMS}(L,t) \propto L^{\alpha} f\left(\frac{t}{L^z}\right) \tag{4.5}$$

where f is the so-called *scaling function* and the exponents then obey the relation:

$$z = \frac{\alpha}{\beta} \tag{4.6}$$

The scaling exponents α, β (in our case they are independent of one another) determine the *universality classes*, which are then related to different kinds of growth. In general these methods can be applied to a wide range of systems developing in time, wherever one can define a height function and find self-similar growth in the system.

4.3 Lattice approaches

Once we know the relationship between the basic processes and the universality classes we can describe the evolution of growth. For computer simulations of growth we obviously need a well defined underlying structure to work on. We now want to introduce different approaches to defining it. In general there are two basic kinds, off-lattice models and lattice models.

Off-lattice models

Off-lattice models are normally used to describe either the exact position of unstructured surfaces like glassy or amorphous materials in crystal growth or the changeable or determined position of a cell in cell populations.

The question then arises as to whether the exact position is of crucial importance in the model or whether one can use one's a priori knowledge of an off-lattice model to replace it by an effective model on a defined lattice. The choice here is between two different explanatory systems. In the case of a crystal the best underlying structure is given by the structure of the crystal itself, namely the discrete positions of the effective atoms. The approximations for the processes are then in the choice of the method, where one can either try to solve the many body quantum mechanical problems or consider effective atoms and effective energies at the lattice points in order to simplify the problem and move from the microscopic to the mesoscopic scale. The situation changes if we then have an amorphous substrate where it is rather difficult to define the lattice. For cell population growth the situation is totally different, because here the possible positions are continuous, so a model which aims to reflect reality perfectly has to be an off-lattice model. Here the lattice model is only the first approximation, which not only fixes the position in some way but also restricts the overall area of the cells, so that one can think about local changes. So these questions are again, as explained in Sec. 4.1, the choice of including the microscopic view or staying on a mesoscopic scale.

That question is obviously very important for computer experiments because working on an off-lattice model structure uses much more computer time. So, in the case of both crystal growth and tumor growth off-lattice or detailed quantum mechanical approaches are normally taken for small systems, whereas a coarse-grained approach with lattices and without detailed solutions of the quantum mechanical wave functions is successful for larger systems.

Lattice models

In most cases it is useful to take a well defined structure for large growth systems. There are a lot of different very special lattice constructions and here we shall explain the three most common.

First there is the square lattice or the cubic lattice which is also called the *von Neumann* lattice, where every point is connected in two dimensions to the four neighbors with equal x or y values. For a three dimensional structure every point then has six neighbors (Fig. 4.4 (a)). The simplicity of this structure makes it easy to use in computer experiments.

Depending on the structure, it can be useful for crystal growth to take a *hexagonal* lattice where every point has six neighbors in two dimensions and 12 in three dimensions (Fig. 4.4 (b)).

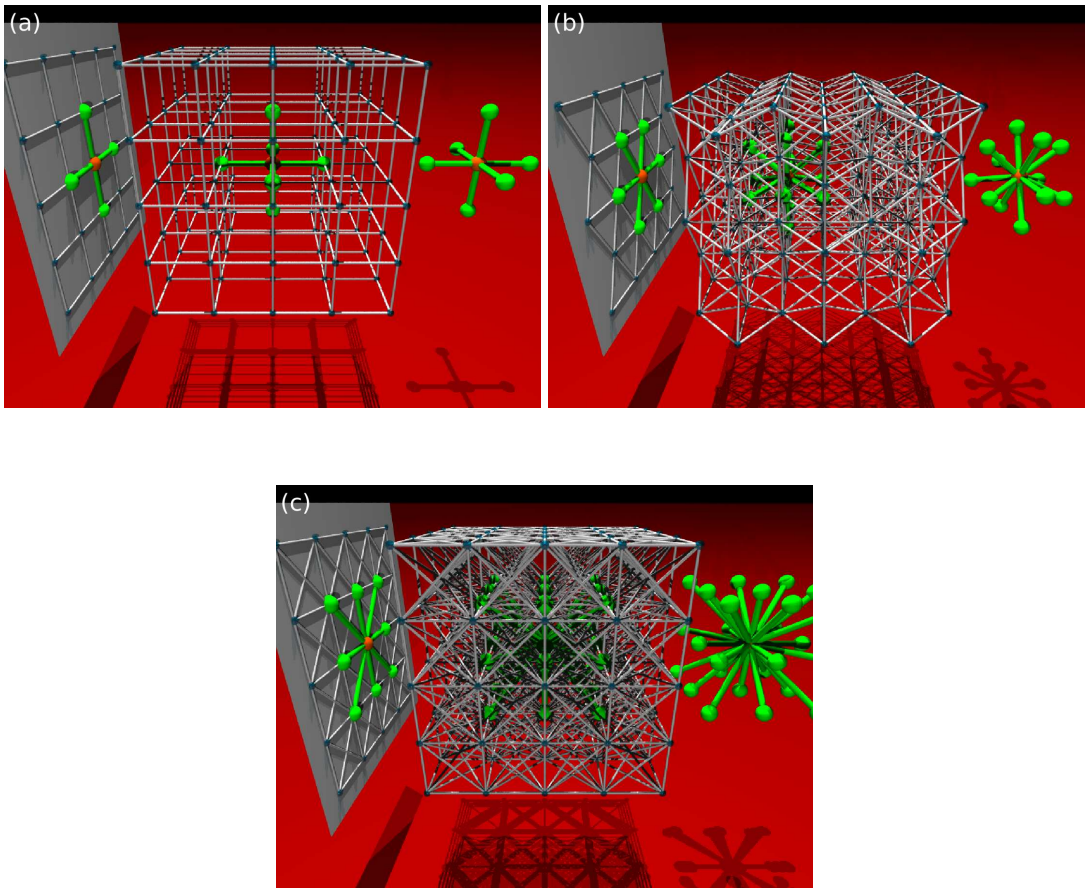

Figure 4.4: Different lattice types: (a) von Neumann neighborhood, (b) hexagonal lattice, (c) octogonal lattice Moore neighborhood with 8 neighbors, left the projections to twodimensional systems with the neighbors, on the right are the neighbors in three dimensions.

In a way similar to the cubic lattice one can also define the diagonals as neighbors which leads to a so called Moore neighborhood with eight neighbors and 26 neighbors in three dimensions (Fig. 4.4 (c)).

All of these structures are extensively used and implemented as models. The problem of lattice approaches is the reflection of the lattice structure in computer experiments. These artefacts can cause mistakes if they don't reflect realistic physical behaviour in the experiments. A new and different construction related to the special conditions of growing cell populations will be introduced in Sec. 8.2. It has been developed to avoid such artefacts.

4.4 General methods

Once we have made use of the scaling concepts and chosen a well defined structure to work on, we have to choose the method. We now explain some of the common methods and model types with their advantages, disadvantages and special constructions.

4.4.1 Monte Carlo approach

Monte Carlo simulations provide a very good tool for explaining growth. Monte Carlo methods are numerical methods, where random numbers are used to describe statistical quantities. Based on the early findings of Metropolis and Ulam [Met49], who named the method after the famous city, a variety of different Monte Carlo techniques are nowadays widely used to solve problems in statistical physics.

The name was chosen because of the relationship of the method to the huge random number generators used in gambling. And in fact, Monte Carlo methods can still be seen as a form of gambling, but just a little bit more advanced.

Nevertheless, the basic idea of such methods goes back to the 18th century to Buffons' famous needle problem to calculate the value of number π, which was solved in 1873 (A. Hall). These early experiments made use of known probabilities to solve integrals, and methods today still have the same rules. Monte Carlo simulations rely on the assumption that the state of a system can be described by all its transition probabilities to reach a different state. When one knows the transition rate of the incoming and outgoing processes, one can then try to describe the global or macroscopic behaviour of the system. In general there are two types of Monte Carlo methods, firstly time independent methods which explain the equilibrium or local equilibrium behaviour of the system and then time dependent methods which also try to give the development a time scale.

Markov processes

Markov processes are stochastic processes which fulfil the *Markov property*. So by definition all the possible states which can be reached from a given state depend solely on the current state of the system and not on any past state.

A sequence of random variables X_0,X_1,...X_{k-1},X_n then is called a *Markov chain*, if X_k just depend on X_{k-1}.

Markov chains are said to be *ergodic*, if there is a nonzero probability of reaching any possible state of the system from any other state.

So, if we have a system in the state $\boldsymbol{i}$ with a transition probability $p_{\boldsymbol{i}\to\boldsymbol{j}}$ of reaching state $\boldsymbol{j}$ after a certain time t, the probabilities for all the transitions obey the relationship

$$p_{\boldsymbol{i}\to\boldsymbol{j}} > 0 \tag{4.7}$$

Assuming a given ergodic Markov chain we can describe evolution in the state space by a master equation:

$$\partial_t P_{\boldsymbol{i}}(t) = \sum_{\boldsymbol{j}} [P_{\boldsymbol{j}}(t) r_{\boldsymbol{j}\to\boldsymbol{i}} - P_{\boldsymbol{i}}(t) r_{\boldsymbol{i}\to\boldsymbol{j}}] \tag{4.8}$$

where $P_{\boldsymbol{j}}(t) r_{\boldsymbol{j}\to\boldsymbol{i}}$ represents the processes that reach the state $\boldsymbol{i}$ and $P_{\boldsymbol{i}}(t) r_{\boldsymbol{i}\to\boldsymbol{j}}$ are the processes which leave the initial state. $P_{\boldsymbol{i}}(t)$ are the probabilities of finding the system at time t in state $\boldsymbol{i}$, and $r_{\boldsymbol{i}\to\boldsymbol{j}}$ is the rate of change to state j (transition probability per unit time).

In general all simulations which are made by kinetic Monte Carlo techniques represent the solution of such a master equation.

When we want to explain systems which tend to an equilibrium state, the property of *detailed balance* is required [Lan05].

$$P_{\boldsymbol{i}} p_{\boldsymbol{i}\to\boldsymbol{j}} = P_{\boldsymbol{j}} p_{\boldsymbol{j}\to\boldsymbol{i}} \tag{4.9}$$

Taking the required properties into account, one can now define the transition probabilities which generate such Markov chains.

Classical Monte Carlo methods

The two most famous methods are

Metropolis algorithm

$$p_{\boldsymbol{i}\to\boldsymbol{j}} = \begin{cases} 1 & \text{if} \quad E(\boldsymbol{j}) - E(\boldsymbol{i}) < 0 \\ \exp(-\beta(E(\boldsymbol{j}) - E(\boldsymbol{i}))) & \text{otherwise} \end{cases}$$

Kawasaki algorithm

$$p_{\boldsymbol{i}\to\boldsymbol{j}} = \frac{1}{1 + \exp(\beta(E(\boldsymbol{j}) - E(\boldsymbol{i})))} ,$$

where $\beta = 1/(k_B T)$ where k_B is Boltzmann's constant and T the temperature.

In the simplest form of a Monte Carlo algorithm for simulating lattice dynamics, a particle is chosen randomly and a jump direction is also chosen randomly. If the arrival site is empty, the probability $p_{\boldsymbol{i}\to\boldsymbol{j}}$ is computed and compared with a random number $0 < r_{\text{rand}} \leq 1$. If the final site is occupied or $r_{\text{rand}} > p_{\boldsymbol{i}\to\boldsymbol{j}}$ the move is rejected. The cycle now starts from the beginning again.

The essential drawback is clear. There are always a certain number of cycles which do not produce new states since they are rejected, yet consume computing time. In low temperature systems, where transition probabilities are low too, this effect becomes dominant.

Continuous time Monte Carlo methods

To overcome this problem, each event needs to be chosen according to its *a priori* probability, and *every* step needs to be accepted. Methods based on this idea are the so-called *time dependent Monte Carlo* methods (the method used in this work), sometimes referred to as *event based Monte Carlo, continuous time Monte Carlo, BKL algorithm* after Bortz, Kalos and Lebowitz [Bor75] or *Gillespie algorithm* after Gillespie [Gil76].

Consider a system with a total number of states N in the state $\boldsymbol{i}$. Labelling all states $\boldsymbol{j}$ which may be reached from $\boldsymbol{i}$ with $k \in \{1, \ldots, K\}$, the total transition rate is given by

$$R(\boldsymbol{i}) = \sum_{\boldsymbol{j}} r_{\boldsymbol{i}\to\boldsymbol{j}} = \sum_{k=1}^{K} r(\boldsymbol{i}; k)\,.$$

Here, the rate $r_{\boldsymbol{i}\to\boldsymbol{j}}$ to the final state $\boldsymbol{j}$ being labeled by the number k is described by $r(\boldsymbol{i}; k)$. The partial sums can be written as

$$R(\boldsymbol{i}; k) = \sum_{l=1}^{k} r(\boldsymbol{i}; l)\,.$$

Now one specific event k can be selected by a uniformly distributed random number $0 < \tilde{r}_{\text{rand}} \leq R(\boldsymbol{i})$, for which the condition

$$R(\boldsymbol{i}; (k-1)) < \tilde{r}_{\text{rand}} \leq R(\boldsymbol{i}; k) \tag{4.10}$$

must be met.

Under the constraint that time is incremented proportionally to the lifetime $\tau(\boldsymbol{i}) = \tau_0/R(\boldsymbol{i})$, a detailed balance is always ensured. One can therefore model the transition probabilities with respect to the physical needs of the specific problem rather than being restricted by the constraints mentioned above.

The time step Δt in the event based Monte Carlo simulation is calculated as follows [Fic91]:

$$\Delta t = -\frac{1}{\sum_i p_i} ln(1-\xi) \tag{4.11}$$

where ξ is a random number equidistributed in $[0, 1)$ and $\sum_i p_i$ is the sum of all possible events i which may occur at time t.

We now have a situation where, instead of wasting computation time on unnecessary rejections which do not contribute to a change of configuration, the main part of the computing time is spent calculating total and partial transition rates. So by implementing the time dependent Monte Carlo algorithm with care, the drawbacks on the non-time dependent algorithm can be minimized and this method is much faster. Finally, as the last comment in this section, the difference between kinetic Monte Carlo (KMC) and classical Monte Carlo should be emphasized. While the latter is used for the calculation of a quantity in the thermodynamic equilibrium state of a system the

former describes the *path* of the system towards the equilibrium state. So, by using a KMC algorithm, we ensure not only realistic equilibrium behaviour, but also realistic kinetic behaviour.

4.4.2 Discrete models

Discrete models of crystal growth are closely related to kinetic Monte Carlo methods. Here one defines the properties of the main processes and thereby gets different types of models with well defined properties that can be identified by their critical exponents. Because the stochastic differential equations and our tumor growth model work with comparable quantities, we want to point out here the basic model types. In general they differ in their definition of the deposition processes and in determining the diffusion, or relaxation of particles on the surface, respectively. Where the discrete models and the stochastic differential equations aimed to explain roughening by a height function, the height here is discretized, normally corresponding to the actions of effective particles, for instance atoms in a lattice.

Ballistic deposition models

In ballistic deposition models the particles which fall perpendicular onto the surface stick to the first nearest neighbor (NN) they find, or to the next nearest neighbor (NNN) (see [Mea93; Mea90; Bai88; Fam85]).

Solid on Solid models

The solid on solid approximation (SOS) is an idealization whereby neither bulk vacancy nor surface overhang is allowed to form during growth. One also normally neglects desorption or evaporation processes from the front.

Random Deposition model

The easiest SOS model is the random deposition model, where we neglect diffusion on the surface. The random deposition of particles at a position $\boldsymbol{x}$ on a given surface at a deposition rate F increases the height function $h(\boldsymbol{x}, t)$ locally. Obviously, by definition, in the random deposition model no correlations can occur without relaxation processes.

Family model

Since most real growth systems show relaxations, a further development of the random deposition model is the *random deposition with surface relaxation* [Fam86] sometimes also referred to as the Family model. The deposited particles do not then stick irreversibly at the position, but can relax to a nearest neigbor with a lower height.

Wolf-Villain model

The Wolf-Villain model determines the relaxation after deposition by a move to the neighboring site, when the particle is thereby able to increase the number of bonds [Wol90].

Das Sarma-Tamborena model

This model is just a variation of the Wolf-Villain model, where in addition the particles only relax if they do not have any lateral neighbors, otherwise they stay in their position [Sar91].

A variety of other dynamic relaxation models exist but all these models have the problem that the relaxation process is determined by the local environment at the position of the deposited particle.

The advantage of these models is their easy implementation in a computer simulation with low computational demand.

4.4.3 Stochastic SOS models

The so called *stochastic Solid on Solid* models offer a more realistic modelling of diffusion processes. The deposition of particles occurs in the same manner as in the other models and the models are also only described by events to neighboring sites. But in contrast to the other models, here any surface atom could be selected at any time for a diffusion process, not only at deposition time. For instance a diffusion by Arrhenius law can give the transition probabilities of such events.

In Sec. 2.1 we described the diffusion processes in epitaxial growth using Arrhenius law, and we don't want to go into the subject any further here but refer readers to the publications for kinetic Monte Carlo simulations on SOS models extensively studied in our group during the last 12 years in the framework of Sfb 296 ([Sch98; Bos99a; Bos99b; Bos00; Mei01c; Mei01a; Mei01b; Liu01; Mei02; Mei03c; Mei03b; Man03; Els03; Wet04; Els04; Blo04; Els05b; Els05a; Kun06b; Kun06a; Kun06c].

4.4.4 Continuum Equations

A different method of describing growth or evolutionary processes is to use continuum equations. Using scaling theory (see Sec. 4.2) there are different equations related to different universality classes. To construct such continuum equations one has to expand the so called generalized equation, which includes all the processes.

$$\frac{\partial h(\mathbf{x},t)}{\partial t} = G(h,\mathbf{x},t) + \eta(\mathbf{x},t) \tag{4.12}$$

where G is the generalized function depending on interface height, position and time [Bar95]. If we now assume that the incoming flux of particles is not constant, then

we use the term $\eta(\mathbf{x}, t)$ to describe the random deposition. This means that random fluctuations then have zero mean and normally the second moment is assumed to have no correlations in space or time (Gaussian white noise).

$$\langle \eta(\mathbf{x}, t) \rangle = 0 \tag{4.13}$$

$$\langle \eta(\mathbf{x}, t)\eta(\mathbf{x}', t') \rangle = 2D\delta^d(\mathbf{x} - \mathbf{x}')\delta(t - t') \tag{4.14}$$

Whereas one can also introduce correlated fluctuations, in this work we use white noise as defined in Eq. (4.13). Now the individual definition of the function G characterizes a specific growth process by a specific continuum equation. The general function can be simplified by using the symmetry principles of roughening systems.

Time translation invariance
The growth equation does not depend on where we define the origin of time so the invariance has to fulfil the relationship $t \rightarrow t + \delta_t$

Translation invariance along the growth direction
Growth has to be independent of the choice of h = 0 so the invariance has to fulfil the relation $h \rightarrow h + \delta_h$

Translation invariance in perpendicular growth direction
The growth has to be invariant under translation perpendicular to growth $\mathbf{x} \rightarrow \mathbf{x} + \delta_x$

Rotation and inversion symmetry about growth normal vector
Growth has to be invariant if we invert or rotate the height profile about the growth normal $\mathbf{n}$.

Up/down symmetry for h
One can include a symmetry which states that interface fluctuations are similar with respect to the mean height, but this property is only fulfilled by linear equations.

Further reading about the symmetry principles can be found in text books [Bar95].

When we include the knowledge about growth gained from the symmetry principles, we first obtain an expansion of terms described as follows

$$\frac{\partial h(\mathbf{x}, t)}{\partial t} = (\nabla^2 h) + (\nabla^4 h) + ... + (\nabla^{2n} h) + (\nabla^2 h)(\nabla h)^2 + ... + (\nabla^{2k} h)(\nabla h)^{2j} + \eta(\mathbf{x}, t) \tag{4.15}$$

were n, k, j can take any positive value. For simplicity the coefficients in front have not been written down explicitly. Neglecting the different coefficients in this expansion now leads to different growth equations which are classified by different critical exponents β, α and z.

If the growth is self-similar and fulfils the properties of scaling theory, then the different growth equations extracted from the generalized equation lead to the different universality classes described in Sec. 4.2 which can be classified using the related scaling exponents.

Chapter 5

Stochastic Differential Equations

In the last chapter we gave a general explanation of methods of modelling growth phenomena and stated that stochastic differential equations have been established as one of the leading methods of modelling growth. We now want to describe this kind of modelling in more detail, and will use it later on to control the roughening process.

The theory of stochastic differential equations for growth, also referred to as stochastic growth equations, is based on Langevin equations.

Whereas Langevin equations were widely used earlier, Edwards and Wilkinson first used stochastic differential equations for the roughening process in the early eighties [Edw82].

With the observations of Kardar, Parisi and Zhang [Kar86] the theory of stochastic differential growth equations became a well established tool to explain growing systems.

A lot of different equations have been proposed during the last 20 years to describe different universal classes of growth, but there are still a lot of unsolved problems. Some of the questions arise because of the nonlinear form of some of the equations and the impossibility of solving them analytically. The equations can be used as idealized versions of realistic growth properties, but the relation of realistic growth to its corresponding universality class is not always obvious. In Sec. 4.4.4 we developed the equations as the result of an expansion with the addition of certain symmetry principles and we now want to describe the specific equations that are most frequently used. We shall explain the terms related to the different processes together with their specific physical meaning.

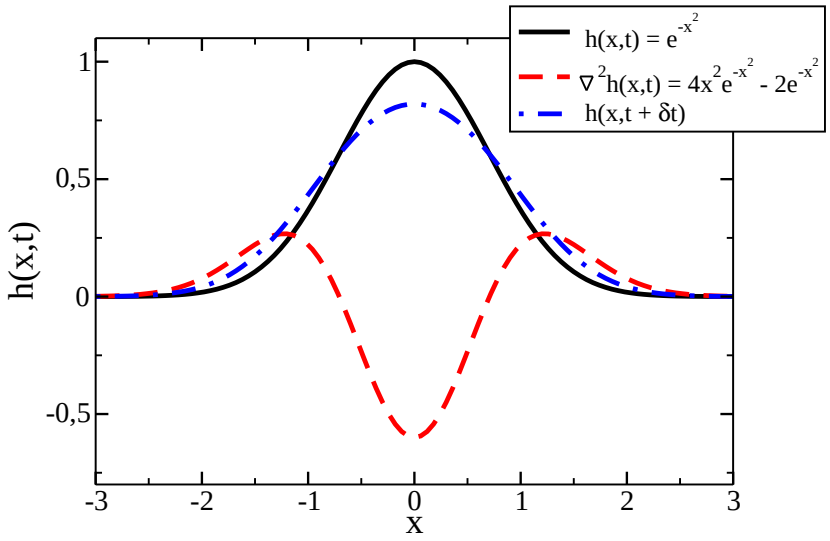

Figure 5.1: Behaviour of the Edwards-Wilkinson term (red dashed line) on an artificial height profile $h(x,t) = \exp(-x^2)$ (black line) leads to small variation in the resulting profile (blue dash-dotted line).

5.1 The Edwards-Wilkinson and the Kardar-Parisi-Zhang Equation

For an explanation of the relevant terms in this work we shall now discuss the hypothetic generalized function $G(h, \mathbf{x}, t)$ in Eq. (5.1).

$$\frac{\partial h(\mathbf{x},t)}{\partial t} = G(h,\mathbf{x},t) + \eta(\mathbf{x},t) \tag{5.1}$$

The basic question arising from this growth equation is the question as to which realistic processes dominate the roughening.

5.1.1 The Edwards-Wilkinson equation

The easiest generalized function to think about is the Edwards-Wilkinson (EW) equation [Edw82],

$$\partial_t h(\mathbf{x},t) = \nu\nabla^2 h(\mathbf{x},t) + \eta(\mathbf{x},t) \tag{5.2}$$

where we take only the linear second order term from the expansion (Sec. 4.4.4). Originally developed to describe an Ising spin system, it also exhibits some properties relevant to growth phenomena.

In Fig. 5.1 we see how this term acts on a given surface profile. We take a simple Gaussian height profile $h(x,t) = \exp(-x^2)$ and calculate the second derivative $\nabla^2 h(x,t)$ for a pre-factor $\nu = 0.1$ in one spatial dimension.

If we now add a small variation to the height function corresponding to a small change of the function in time, we see that the Edwards-Wilkinson term acts as a smoothing term on the height profile and as a conservative relaxation. Surface tension behaves similarly, which is why this term is normally called the *surface tension term*.

The Edwards-Wilkinson equation is valid in the small gradient approximation, i.e. in the limit $|\nabla h| \ll 1$.

It corresponds to the well known discrete random deposition model with surface relaxation [Fam86] (see also Sec. 4.4.2).

The main difference from a random deposition model without relaxation is the presence of correlations.

There are different ways of solving the Edwards-Wilkinson equation and calculating the scaling exponents. Both an approach using scaling and an exact solution [Nat92] are possible. The EW equation is one of the rare solvable equations and we shall now show the solution. For the solution by scaling we only require a self-affine interface with a height function $h(\boldsymbol{x}, t)$. As explained in Sec. 4.2, rescaling in the horizontal and vertical directions produces interfaces which are statistically indistinguishable from the original one.

$$\begin{aligned} \mathbf{x} \to \mathbf{x}' &\equiv b\mathbf{x} \\ h \to h' &\equiv b^{\alpha} h \end{aligned} \tag{5.3}$$

When we measure the height function at different times, the two interfaces are also rescalable in time.

$$t \to t' \equiv b^{z} t \tag{5.4}$$

Due to the fact that the rescaled quantities obey these relations, by substitution in d dimensions we get

$$\frac{\partial h'(\mathbf{x}', t')}{\partial t'} = \nu \nabla^2 h'(\mathbf{x}', t') + \eta(\mathbf{x}', t') \tag{5.5}$$

$$b^{\alpha - z} \frac{\partial h(\mathbf{x}, t)}{\partial t} = \nu b^{\alpha - 2} \nabla^2 h(\mathbf{x}, t) + b^{-\frac{d}{2} - \frac{z}{2}} \eta(\mathbf{x}, t) \tag{5.6}$$

$$\frac{\partial h(\mathbf{x}, t)}{\partial t} = \nu b^{z-2} \nabla^2 h(\mathbf{x}, t) + b^{-\frac{d}{2} + \frac{z}{2} - \alpha} \eta(\mathbf{x}, t) \tag{5.7}$$

and by multiplying the term $b^{\alpha - z}$ on both sides we come to the rescaled height function which is invariant under the transformation and therefore fulfils the following relations (independent of b, comparison of coefficients)

$$z - 2 = 0 \tag{5.8}$$

$$-\frac{d}{2} + \frac{z}{2} - \alpha = 0 \tag{5.9}$$

which leads to the exponents of the EW universality class,

$$\alpha = \frac{2-d}{2}, \qquad \beta = \frac{2-d}{4}, \qquad z = 2 \tag{5.10}$$

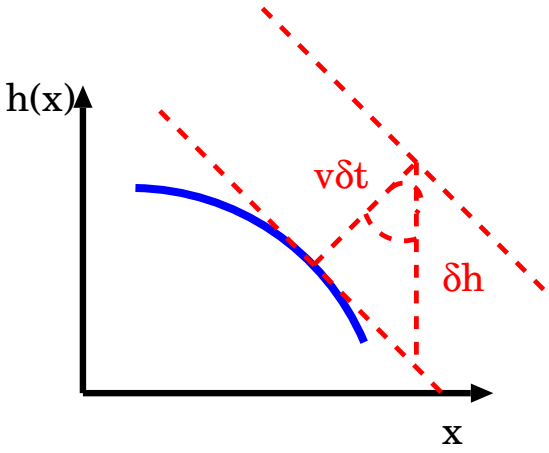

Figure 5.2: Scheme of the lateral growth, height function $h(x)$ (blue), lateral growth on the surface (red dashed lines).

where d is the spatial dimension.

So in 1+1 dimensions the exponents are $\alpha = 0.5$, $\beta = 0.25$, whereas in 2+1 dimensions the exponents for the above equations are $\alpha = 0.0$, $\beta = 0.0$ and $z = 2$. This means that scaling is logarithmic in 2+1 dimensions for the Edwards-Wilkinson equation.

Whereas we solved the equations before by scaling arguments in a phenomenological way, this equation can be solved exactly, as shown by the findings of Nattermann *et al* [Nat92]. The Edwards-Wilkinson equation fulfils up/down symmetry (Sec. 4.4.4). If the growth is non-linear, the scaling has to change and this property is no longer fulfilled. We now come to an equation where processes related to nonlinear terms play an essential role.

5.1.2 The Kardar-Parisi-Zhang Equation

Once again we first think of the easiest nonlinear term possible, which is the $(\nabla h)^2$ term. The simplest such equation is the Kardar-Parisi-Zhang (KPZ) equation [Kar86] which describes the growth of a surface in the absence of any conservation laws.

$$\partial_t h(\mathbf{x},t) = \nu\nabla^2 h(\mathbf{x},t) + \frac{\lambda}{2}(\nabla h(\mathbf{x},t))^2 + \eta(\mathbf{x},t) \tag{5.11}$$

We have already explained the surface tension term ν. The nonlinear term determines the strength and direction of both lateral growth and growth normal to the interface. The origin of the nonlinear term can be seen in Fig. 5.2. Lateral growth normal to the interface can be described locally by a term related to the Pythagorean theorem

$$\delta h^2 = (v\delta t)^2 + (v\delta t\nabla h)^2 \tag{5.12}$$

where δh is the small difference in the height function in the general growth direction and $(v\delta t)$ the lateral growth normal to the interface. We are using the small gradient approximation, so one can easily see that an expansion of δh leads to

$$\frac{\partial h(\mathbf{x},t)}{\partial t} = v + \frac{v}{2}(\nabla h)^2 + ... \tag{5.13}$$

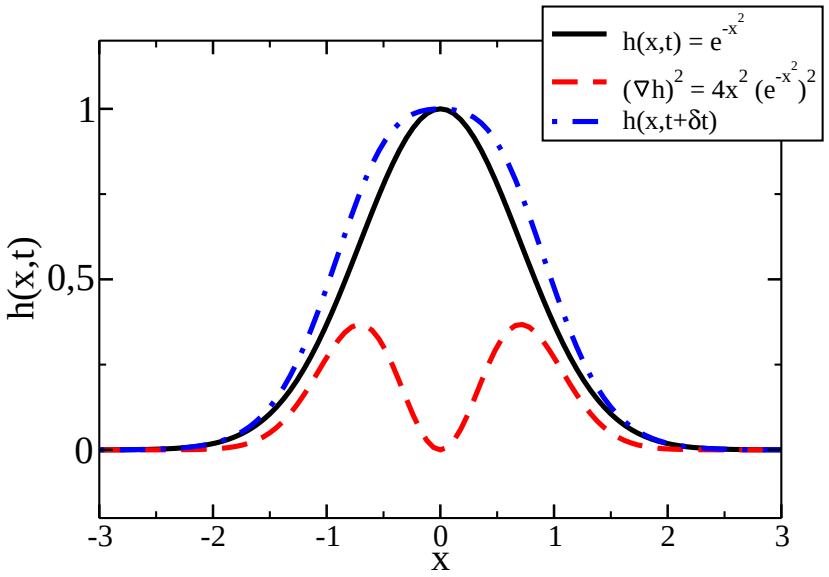

Figure 5.3: Behaviour of the nonlinear KPZ term (red dashed line) on an artificial height profile $h(x,t) = \exp(-x^2)$ (black line) leads to small variation in the resulting profile (blue dash-dotted line).

and thereby exhibits the nonlinear term. The velocity is nothing but an included term in the mean average height development of the flux F to the surface. In Fig. 5.3 we show the behaviour of the KPZ term on the roughening surface in the same way as we showed it for the EW equation. Two main features are to be seen. Growth is related to the normal of the interface and its strength to the local gradient. What one can also observe is a lost mean height, so growth is not conserved relative to the mean height development. So, whereas we can write a continuity equation for the total number of particles for the Edwards-Wilkinson equation where $\boldsymbol{j}$ is the particle flux.

$$\frac{\partial h}{\partial t} = -\nabla \mathbf{j}(\mathbf{x}, t) \tag{5.14}$$

this relation is not fulfilled by the Kardar-Parisi-Zhang equation. The consequence is that, although we can generally describe a growth process with a constant flux to surface which can be neglected for the continuity equation and conserved for growth related to the mean height, this growth process can not be described by a non-conserved equation like the KPZ equation. The KPZ equation cannot be solved analytically because of its nonlinear character [Mic04; Bar95]. Nevertheless there are some proposed scaling exponents for the equation.

5.1.3 Relations beetween EW and KPZ equation

The relationship between the Edwards-Wilkinson equation and the Kardar-Paris-Zhang equation lies in the strength of the nonlinearity. Moser *et al* demonstrated

that fact by using an effective coupling constant g defined by the parameters of the KPZ equation [Mos91].

$$g = \frac{\lambda^2 D}{\nu^3} \tag{5.15}$$

The coupling constant is related to the fixed point of a renormalization group theory approach not discussed in this work. They describe the changed roughening for non-zero nonlinearities due to a change in this coupling constant g. So, to ensure that the behaviour we describe here is similar, we choose numerical parameters for our 'strong coupling' behaviour that ensure a coupling constant in the same range as that in this paper. The critical exponents for the KPZ equation are well known in 1+1 dimensions and are given by

$$\alpha = 0.5, \qquad \beta = \frac{1}{3}, \qquad z = \frac{3}{2} \tag{5.16}$$

In higher dimensions, where the renormalization group analysis fails, there exist two different competing results from numerical simulations

$$\alpha = \frac{1}{d+1}, \qquad \beta = \frac{1}{2d+1}, \qquad z = \frac{2d+1}{d+1} \tag{5.17}$$

and

$$\alpha = \frac{2}{d+3}, \qquad \beta = \frac{1}{d+2}, \qquad z = 2\frac{d+2}{d+3} \tag{5.18}$$

which are both compatible with Eq. (5.16) for $d = 1$. The numerical observations of Wolf and Kertész [Wol87] (Eq. (5.17)) and Kim and Kosterlitz [Kim89] (Eq. (5.18)) lead to the same exponents in 1+1 dimensions as given by Eq. (5.16) but they differ for higher dimensions.

A lot of further calculations where made to determine these exponents. The values of calculated growth exponents vary widely in a range from the models below, with $\beta = 0.20$ from Wolf and Kertész to values close to and in between the two predictions, where the exact value is still an open question (for numerical results see also [Mos91; Ama90; Cha89; Guo90].

More recent findings by Lässig [Läs98] and Chin and den Nijs [Chi99] show the values of the Kim-Kosterlitz model (Eq. (5.18)). A summary of the latter findings together with some new numerical findings can be found in [Gha06]. We will see later whether our findings without control fall within this range.

5.2 The Molecular Beam Epitaxy Equation

Molecular beam epitaxy (MBE) is a major technique in crystal growth of thin films. Growth takes place in vacuum conditions under which particles from a molecular beam are deposited on the surface (see also Sec. 2.2.1).

Because of the growth temperature, desorption processes do not play an important role in comparison with the diffusion processes on the surface. So models which aim to describe a MBE process normally neglect desorption processes. Once one neglects them one has to take surface diffusion as the determining process. If one now describes the surface current $\boldsymbol{j}$ by the local chemical potential $\mu(\boldsymbol{x}, t)$, it is driven by the gradient

$$\mathbf{j}(\mathbf{x}, t) \propto -\nabla\mu(\mathbf{x}, t) \tag{5.19}$$

If one explains the movement of particles as a process depending on the number of bonds, then this number increases with the local curvature. The chemical potential then depends on $-1/R$ and thereby on $\nabla^2 h(\mathbf{x}, t)$, which gives us a relation

$$\mu(\mathbf{x}, t) \propto -\nabla^2 h(\mathbf{x}, t) \tag{5.20}$$

Combining that with the continuity equation (Eq. (5.14)) our height function is

$$\frac{\partial h}{\partial t} = -K\nabla^4 h \tag{5.21}$$

where K is the strength of this diffusion term.

So we now have a growth equation describing relaxation by diffusion just as we have in epitaxial growth for Molecular Beam Epitaxy. The equation is also sometimes referred to as the Mullins or Herring-Mullins equation, because the first findings came from the observations of Herring [Her50] and Mullins [Mul57]. To avoid confusion with the notation of the control strength, later on we use ν_1 instead of K as the strength of the diffusion. Equation 5.21 is deterministic. It was introduced for MBE growth by Wolf and Villain [Wol90]. With some additional changes it becomes the normal type of 'MBE growth equation' we shall discuss later. Calculating the critical exponents we arrive at [Sar91; Bar95]

$$\alpha = \frac{4-d}{2}, \qquad \beta = \frac{4-d}{8}, \qquad z = 4 \tag{5.22}$$

So in 1+1 dimensions the exponents are $\alpha = 1.5$, $\beta = 0.375$ where in 2+1 dimensions the exponents related to the above equations would be $\alpha = 1$, $\beta = 0.25$ and $z = 4$. The MBE growth equation that is normally used was described by Lai and das Sarma [Lai91]. Also known as the conserved KPZ equation [Mic04], this equation takes an additional term into account.

$$\frac{\partial h(\mathbf{x}, t)}{\partial t} = -\nu_1\nabla^4 h + \lambda_1\nabla^2(\nabla h)^2 + \eta(\mathbf{x}, t) \tag{5.23}$$

The origin of the additional term is described as arising from the situation where 'particles landing at high steps (large derivatives) relax to lower steps (smaller derivatives)' [Lai91]. The authors believe that it corresponds to 'high temperature' regimes, where the atoms at kink sites can break bonds and hop to steps with a smaller height and a higher probability, so they propose the above equation as the ideal MBE growth

equation for intermediate to high temperatures. Obviously the explanation includes a variation of the nonlinear term with temperature which is an essential factor in our further findings. The change in this term also is quite similar to the situation explained for the coupling in the KPZ equation, so here we have either strong or weak coupling according to the different temperatures. Whereas these equations explain MBE growth in an idealized way, the question arises as to what happens when the physical process involves both surface relaxation related to deposition or desorption processes and a diffusing term like in the following equation.

$$\frac{\partial h}{\partial t} = \nu\nabla^2 h - \nu_1\nabla^4 h + \eta(\mathbf{x}, t) \tag{5.24}$$

The long term behaviour is obviously the behaviour of the EW equation, because for large length scales the Laplacian either governs the equation or is its leading term. The terms generate a characteristic length scale which determines whether the diffusion term is still the leading term or whether the length is so large that the EW term is the relevant one for the exponents.

That fact can be explained if we rescale the terms using the known exponents. We then get $\nu b^{\alpha-2}\nabla^2 h$ and $\nu_1 b^{\alpha-4}\nabla^4 h$. Thus for $b \to 0$ the diffusion term dominates and for $b \to \infty$ we get Edwards-Wilkinson scaling. In terms of length scales the term

$$L_1 = \left(\frac{\nu_1}{\nu}\right)^2 \tag{5.25}$$

describes the behaviour ($L \gg L_1 \to$ MBE-like, $L \ll L_1 \to$ EW-like). So which length scale we choose depends on the growth conditions, but for realistic MBE conditions one can normally neglect the EW term in comparison with diffusion, and the length scale L_1 is so large that one can see the MBE exponents. There are a lot of different models and equations related to Molecular Beam Epitaxy, a good overview of the discrete models and their relations to the equations is given in [Sar96].

5.3 Crystal growth and stochastic differential equations

We have already discussed the behaviour of the most referenced and used equations for growth. We are now going to have a short look at the different types. There are a few articles which try to describe experiments using such growth equations but it is still a developing field. It is quite difficult to find crystal growth experiments where the growth conditions are as ideal as assumed in the generic equations. The measured exponents vary over a wide range for the same system and it is not easy just to measure the roughness and then write down one of the equations.

5.3.1 Observations by Raible *et al*

The observations of Raible *et al* [Rai00a; Rai00b; Rai01] provide an example of a more complicated growth equation applied to amorphous metallic thin films. Here a specific equation is solved by numerical integration. The equation

$$\frac{\partial h(\mathbf{x},t)}{\partial t} = a_1\nabla^2 h + a_2\nabla^4 h + a_3\nabla^2(\nabla h)^2 + a_4(\nabla h)^2 + \eta(\mathbf{x},t) \tag{5.26}$$

is proposed to describe growth. One can see immediately that it is a combination of the terms of the KPZ equation (Eq. (5.11)) and the conserved KPZ or MBE equation (Eq. (5.23)). Guided by the measured experimental roughness evolution of $Zr_{65}Al_{7.5}Cu_{27.5}$ the equation was solved by a numerical scheme and fitted to the experimental findings. The parameters were identified as

$$F = 0.79\ nm/s \qquad D = 0.0174 nm^4/s \tag{5.27}$$

$$a_1 = -0.0826 nm^2/s \qquad a_2 = -0.319 nm^4/s \tag{5.28}$$

$$a_3 = -0.1\ nm^3/s \qquad a_4 = 0.055 nm/s \tag{5.29}$$

The parameter a_1, normally identified with surface tension in the equations, is negative. The authors explain that irritating fact by growth instabilities "due to the deflection of the initially perpendicular incident particles caused by the inter-atomic forces between the surface atoms and the incident particles". The instability referred to is explained by Villain as due to an instability on terraces in growth with a diffusion bias at a crystallite layer [Vil91]. A test with our numerical simulation scheme shows agreement with the findings but also shows that the numerical solution with exactly the same parameters is extremely sensitive to very small changes in the fitted parameters. Although one can easily show that small differences in the pre-factors lead to a non-convergent growth equation, small differences between experiments cannot be explained by this model. Fig. 5.4 (a) shows that, with exactly the same parameters as used in the numerical scheme, the evolution of roughness can be reproduced exactly by our numerical scheme.

The authors do not explicitly report the roughness exponents. They showed the height-difference correlation, where one can see from the plots, that α should be close to a value $\alpha \in [0.85, 0.9]$. We explicitely determined this quantity using the height-height correlation (Fig. 5.4 (b)) and the height-difference correlation function (Fig. 5.4 (c)) and got exponents $\alpha = 0.88$ and $\alpha = 0.87$, so our numerical solution and the data analysis are consistent with the findings of Raible (see next Section for the method). Whereas the determination of the correlations once again reproduces the behaviour found by Raible et al, one can easily check that the exponents are not related to any one of the explained equations. Obviously a mixture of different terms can lead to much more complicated behaviour in roughening. To summarize, it is quite difficult to simulate very complex behaviour with the growth equation and to unambiguously

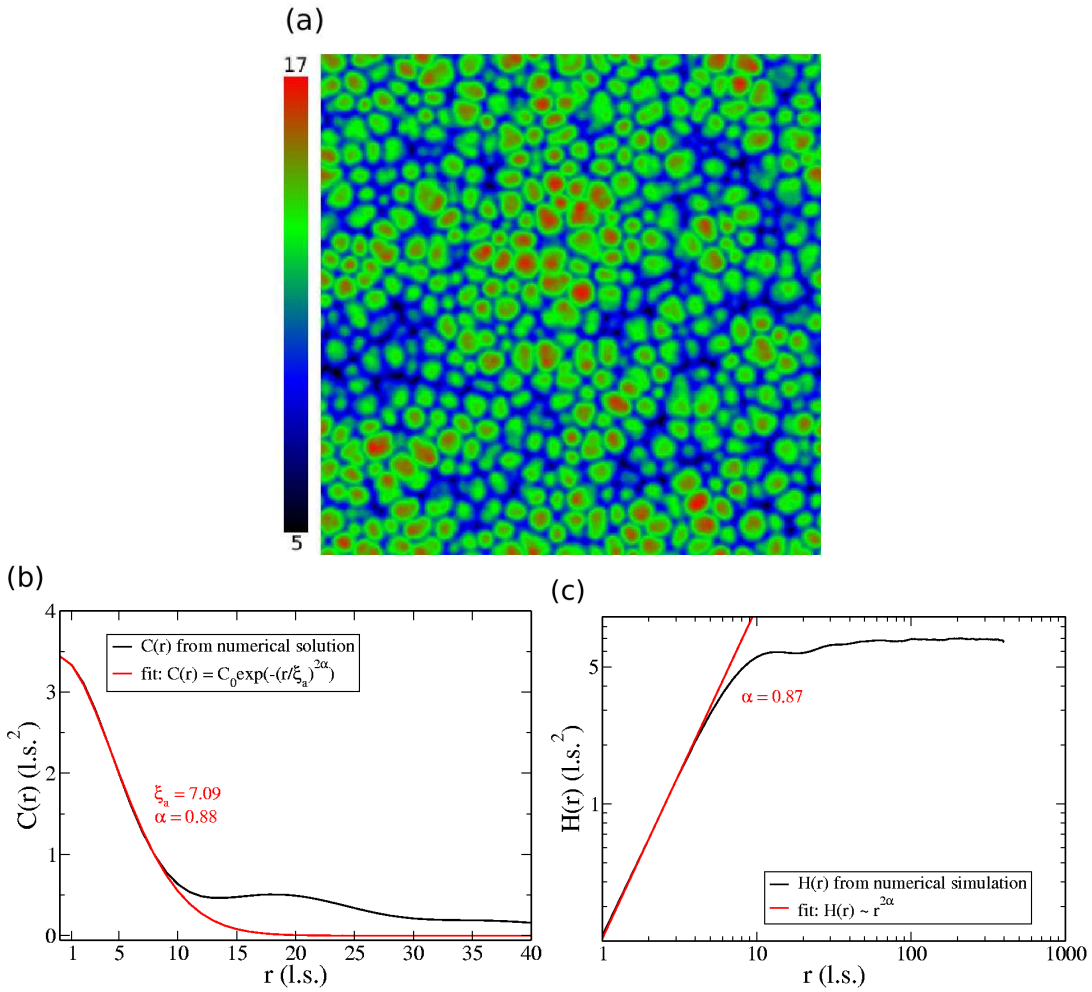

Figure 5.4: Verification of the Raible model for thin film growth: (a) height profile for a 400×400 l.s. simulation at time $t = 1000$, (b) the height-height correlation with a fit function, (c) the height-difference correlation function with a fit function.

identify the basic processes which lead to the experimental behaviour. For amorphous substrates discrete modelling with, for instance, KMC simulations can help to solve these problems [Els05b; Els05a]. In general one has to be very careful when explaining the different processes.

Nevertheless, observations using the easier equations can lead to a better knowledge of complicated roughening systems.

5.4 Data analysis

For computer experiments in general, and in our work too, it is fundamentally important to calculate the quantities in a proper way and to construct the computer codes

and the numerical scheme in a way most closely related to reality, in order to avoid discretization artefacts as much as possible. It is also extremely important to include the parameters in a simulation in a way that makes sense. The competing difficulty is then nevertheless to ensure a numerical solution in an appropriate real time and not to tune the computational expense to infinity. The first step in a data analysis is to think about the discretization scheme to be applied to the equations, and only after that can one think about how to calculate the observed quantities.

5.4.1 Numerical scheme of solving the growth equations

The numerical solutions of the stochastic growth equations are normally based on lattice or on discretized points, for which the height function has to be solved. If we focus on crystal growth, the natural approach is to identify the different points with atoms in a lattice where the spatial position on the interface is discrete and the height function is then quasi-continuous. The height function $h(\mathbf{x}, t)$ depends on discrete points, so when we speak about the continuum height function for the growth equation our simulations must approximate most closely not a continuum but a discrete version of it. The spatial discretization Δx and the discretization of the time steps dt are the discrete quantities that determine the distance to a real growth process. In the ideal case dt goes to zero, and the minimal discretization reflects a lattice constant a. In the case of an amorphous substrate the normal approach is also an effective lattice constant [Els05b; Els05a].

$$\text{Discrete growth equation} \rightarrow \text{Continuum growth equation} \tag{5.30}$$

$$dt \rightarrow 0 \tag{5.31}$$

$$\Delta x \rightarrow a \tag{5.32}$$

In our case we want to investigate the behaviour of those equations where scaling is dependent on the system size L. If we had, for instance, a system of real size $64 \times 64\ nm$ with a lattice constant a of approximately $0.5\ nm$, we would have 128×128 discrete points on an atomic scale. If we now simulated a system with 256×256 discrete points, it would refer to a system of four times the area and would be related to $128 \times 128\ nm$, or with a lattice discretiation of $\Delta x = 1\ nm$ it would refer to $256 \times 256\ nm$. The scaling laws are not affected. But, for good results for different system sizes, one needs to take the same underlying spatial discretization Δx as we do in this work. This shows that the choice of spatial discretization is not important for the simulation itself but becomes important with its interpretation for real sizes.

So a rough view of a $128 \times 128\ nm$ with describing every second atom by a lattice point of the system is an even rougher view of a $64 \times 64\ nm$ where all atoms are represented by one point, but from the point of view of the simulation they are the same and in the case of scaling laws they ought to be the same. These statements are obviously a direct outcome of fulfilling the scaling laws.

The discretization of time dt is much more difficult. If the discretization is too rough, the fluctuations that naturally appear in numerical schemes lead the growth

and the results don't explain the equations. There is no general law to determine the discretization that will ensure realistic behaviour. In general it has to be small in comparison with the timescale we want to analyze.

The lower cut-off is computationally demanding, so we have to find a rule to check our simulations. If fluctuations dominate growth, in the worst case the height function goes to infinity at a certain point. We then know that we have chosen the wrong timescale for the simulation. That can easily be demonstrated using the algorithm. A more difficult case occurs when the discrete version is not close enough to the realistic equation. We can check this by using a smaller time discretization, and then, if the behaviour does not change, we know that a suitable discretization has been chosen.

5.4.2 Discretization scheme

We have now explained how we prepare the discretization of the lattice and of time in our numerical scheme. We now come to our discretization of the equation by terms. The first observations by Moser and Kertész used a normal forward-backward differences scheme on a cubic grid and integrated it using an Euler algorithm [Mos91].

$$\begin{aligned} h_n(t+\Delta t) &= h(t) + \frac{\Delta t}{\Delta x^2}\sum_{i-1}^{d}(\nu[h_{n+e_i}(t) - 2h_n(t) + h_{n-e_i}(t)] \\ &\quad + \frac{1}{8}\lambda[h_{n+e_i}(t) - h_{n-e_i}(t)]^2) + \delta\sqrt{12\Delta t}R_n(t) \end{aligned} \tag{5.33}$$

While some of the newer investigations still make use of this simple discretization scheme, Lam *et al* demonstrated that in 1+1 dimensions it produces some mistakes in transitions from zero nonlinear terms to nonzero. They showed that the results of individual roughness evolution produce the right exponents, but when one want to get, for instance, the transition from the behaviour of the Edwards-Wilkinson equation to the KPZ equation, some numerical mistakes occur [Lam98a; Lam98b].

Lam *et al* showed in their findings that in the transition from Edwards-Wilkinson ($\lambda = 0$) to KPZ behaviour ($\lambda > 0$) a shift of the amplitude A for the saturation function appears ([Kru92]).

$$w_{sat} = \left(\frac{A}{12}\right)^{1/2} L^{\alpha} \tag{5.34}$$

They conclude that this conventional discretization is not a genuine approximation to the continuum KPZ equation. They propose a new discretization in 1+1 dimensions and show in detail that their scheme is a solution of the continuum equation that does not produce these instabilities.

A more generalized study of the problem provides a scheme which solves these problems for more than just the 1+1 dimensional case [Buc05b].

In order to ensure that the proposed numerical scheme really avoids unwanted behaviour we want to use here the scheme from Lam *et al* instead of the older scheme of Moser and Kertesz [Lam98b; Mos91].

So as to avoid such mistakes we use the discretization scheme of Lam *et al*, while ensuring that the exponents are not affected.

$$\begin{aligned} h_{i,j}^{n+1} &= h_{i,j}^n + \frac{\Delta t_n}{(\Delta x)^2}[w_{i+1,j}^n + w_{i-1,j}^n + w_{i,j-1}^n - 4w_{i,j}^n] \\ &+\frac{a_4}{3(\Delta x)^2}[(h_{i+1,j}^n - h_{i,j}^n)^2 + (h_{i+1,j}^n - h_{i,j}^n)(h_{i,j}^n - h_{i-1,j}^n) \\ &+(h_{i,j}^n - h_{i-1,j}^n)^2 + (h_{i,j+1}^n - h_{i,j}^n)^2 \\ &+(h_{i,j+1}^n - h_{i,j}^n)(h_{i,j}^n - h_{i,j-1}^n) + (h_{i,j}^n - h_{i,j-1}^n)^2] \\ &+\sqrt{\frac{24D\Delta t_n}{(\Delta x)^2}} r_{i,j}^n \end{aligned} \tag{5.35}$$

$$\begin{aligned} w_{i,j}^n &= a_1 h_{i,j}^n + \frac{a_2}{(\Delta x)^2}[h_{i+1,j}^n + h_{i-1,j}^n + h_{i,j+1}^n + h_{i,j-1}^n - 4h_{i,j}^n] \\ &+\frac{a_3}{3(\Delta x)^2}[(h_{i+1,j}^n - h_{i,j}^n)^2 + (h_{i+1,j}^n - h_{i,j}^n)(h_{i,j}^n - h_{i-1,j}^n) \\ &+(h_{i,j}^n - h_{i-1,j}^n)^2 + (h_{i,j+1}^n - h_{i,j}^n)^2 \\ &+(h_{i,j+1}^n - h_{i,j}^n)(h_{i,j}^n - h_{i,j-1}^n) + (h_{i,j}^n - h_{i,j-1}^n)^2] \end{aligned} \tag{5.36}$$

Here the $h_{i,j}^n$ is the discretized height function depending on x_i, y_j and time t_n. $r_{i,j}^n$ is a random number taken from a uniform distribution $[-0.5, 0.5)$.

From this general discretization we arrive at the specific equations by setting $a_2 = 0$ and $a_3 = 0$ for the KPZ equation ($a_1 = \nu$, $a_4 = \lambda$) or by setting $a_1 = 0$ and $a_4 = 0$ for the MBE equation ($K = \nu_1 = a_2$, $a_3 = \lambda_1$).

5.4.3 Determination of the critical exponents

In our work the basic quantities calculated from simulations are the critical exponents which determine the universality classes. We are going to use a lot of different methods so we shall explain them here. The basic measured quantities in our work are the rms roughness evolution in time $w_{RMS}(t)$ and the related exponents α β and z. We now present the different methods of calculating of the exponents, and we shall use almost all of them to obtain the resulting structures.

Calculation of the growth exponent β

There are different methods of determining the growth exponent β, direct and methods using the exponents α and z. A direct measurement of β can be made by tracking

the temporal evolution of roughness and then taking the slope of the double logarithmic plot which reflects the law explained in Eq. (4.2). In this case the roughness is not saturated. We have already explained the roughening phase in Sec. 4.2.2 so will not explain this direct method again. The second method of measuring the growth exponents is by determining the other exponents, using Eq. (4.6).

Calculation of the roughness exponent α

First we have to measure the roughness exponents. Direct measurement of the roughness exponent α is possible if we can reach the saturation point of the surface for different system sizes L. Then the scaling law for saturation roughness (Eq. (4.3)) can be mapped to the curves to get the related exponent. That may be the easiest method, but it is not the best way of obtaining the roughness exponent, as we shall see later for the tumor growth model (Sec. 9.7).

This method obviously fails for most crystal growth systems where saturation is not always reached during growth. A different method assumes that, even if we do not reach the saturation value, it is still possible to determine the roughness exponent from locally saturated regions of the surface. The so called *local width method* then takes the dependence of the locally saturated roughness (width)

$$w_L(l,t) = \sqrt{< [h(\mathbf{x},t) - h_l(\mathbf{x},t)]^2 >_{\mathbf{x}}} \tag{5.37}$$

where h_l is the mean height of the local window of size l. The scaling of local roughness for small l is the same as for the whole system, so for small l we obtain the roughness exponent using the relation

$$w_L(l,t) \propto l^{\alpha} \tag{5.38}$$

This method works very well for saturated systems but for unsaturated surfaces one has to verify that $l \ll \xi_{||}$.

Another method is to determine the height-difference correlation function

$$H(r) = \sqrt{[< (h(\mathbf{x}) - h(\mathbf{x}'))^2 >_{\mathbf{x}}]} \qquad (|\mathbf{x} - \mathbf{x}'| = r) \tag{5.39}$$

If we again assume a self-similar roughening system with an arbitrary factor b then

$$h(\mathbf{x}) \rightarrow b^{-\alpha} h(b\mathbf{x}) \tag{5.40}$$

(see also Sec. 5.1), and invariance implies the relation

$$H(r) = b^{-2\alpha} H(br) \tag{5.41}$$

By setting $b = 1/|r|$ it follows that

$$H(r) \propto |r|^{2\alpha} \tag{5.42}$$

With this relationship it is possible to determine the roughness exponent from the height-difference correlations.

A more general correlation is the height-height-correlation function

$$C'(\mathbf{r}) = < (h(\mathbf{x}+\mathbf{r}) - \overline{h})(h(\mathbf{x}) - \overline{h}) >_{\mathbf{x}} \quad (5.43)$$

$$C(r) = < C'(\mathbf{r}) >_{|\mathbf{r}|=r} \quad (5.44)$$

From the radius averaged correlation $C(r)$ we can then calculate the roughness exponent using the relation:

$$C(r) = C_0 exp(-(\frac{r}{\xi_a})^{2\alpha}) \quad (5.45)$$

where ξ_a is the so called self-affine correlation length. The functions $H(r)$ and $C(r)$ are related to the correlation length by

$$H(r) \to 2w_{RMS}^2 \qquad \text{for} \quad r \gg \xi_a \quad (5.46)$$

$$C(r) \to 0 \qquad \text{for} \quad r \gg \xi_a \quad (5.47)$$

The structure function $S(\mathbf{k}, t)$ makes use of the power spectrum of the interface. Defined by

$$S(\mathbf{k}, t) =< h(\mathbf{k}, t)h(-\mathbf{k}, t) > \quad (5.48)$$

with

$$h(\mathbf{k}, t) = \frac{1}{L^{d/2}} \sum_x [h(\mathbf{x}, t) - \overline{h}]e^{i\mathbf{k}\cdot\mathbf{x}} \quad (5.49)$$

the Fourier transform of the height function $h(\mathbf{x}, t)$, the scaling concepts lead to the relation

$$S(\mathbf{k}, t) = k^{-d-2\alpha} g(t/k^{-z}) \quad (5.50)$$

with the Fourier space scaling function $g(u)$ which fulfils the relations

$$g(u) \propto u^{(2\alpha+d)/z} \qquad \textit{for} \qquad u \ll 1 \quad (5.51)$$

$$g(u) = const. \qquad \textit{for} \qquad u \gg 1 \quad (5.52)$$

and is quite similar to the scaling function in normal space (Eq. (4.5)). It allows one to determine two of the three exponents directly.

If we now measure the slope of the log-log plot of the structure function we can measure $-(2\alpha+d)$ directly. By then rescaling the function with the measured exponent we get the scaling function u.

Rescaling again with the expected value of z for the structure function for different times t we end up with a data collapse where the curves match one another, provided we choose the right value of z.

This method also indirectly measures the growth exponent β. It is used for the stochastic differential equations of the tumor growth model, as we shall see later.

Although there are a lot of other methods of calculating the exponents, in this work we shall restrict ourselves to those we have already explained (see [Bar95]).

Chapter 6

Control of stochastic differential equations

In the last chapter we described the equations whose universal exponents determine the classes of the different growth phenomena. We discussed the properties and influence of the terms corresponding to the physical mechanisms of realistic roughening; we now want to answer the question of how to influence and control growth.

In crystal growth normally the first step, when growing defined structures, is to calibrate the system. Although for a lot of systems it is rather difficult to measure local conditions on the substrate, this procedure can be combined with an extensive number of repeated tests, until one reaches the conditions under which growth shows the required behaviour.

A more elegant and, of course, cheaper way is to tune the conditions during growth. So an in-situ setup that adjusts the surface roughness is a very helpful tool.

When we use stochastic differential equations in the theoretical approach, the basic question is how to implement a useful control in the equation in order to tune the roughening process.

In this chapter we want to explain how we control the roughening surface using the stochastic differential equations we described previously. We introduce the basic concepts and then proceed to our method [Blo06b; Blo06a].

6.1 Control theory

Controllers are an essential part of daily life. Although one might first think of applications to engineering like the 'anti-skid system' in a car or the automatically tuned temperature of rooms, one of the most complex systems involving controllers is the human body itself.

An example of this is the 'erect posture'. We first use our tactile and visual senses to summarize the information from the environment. The brain then acts as the complex

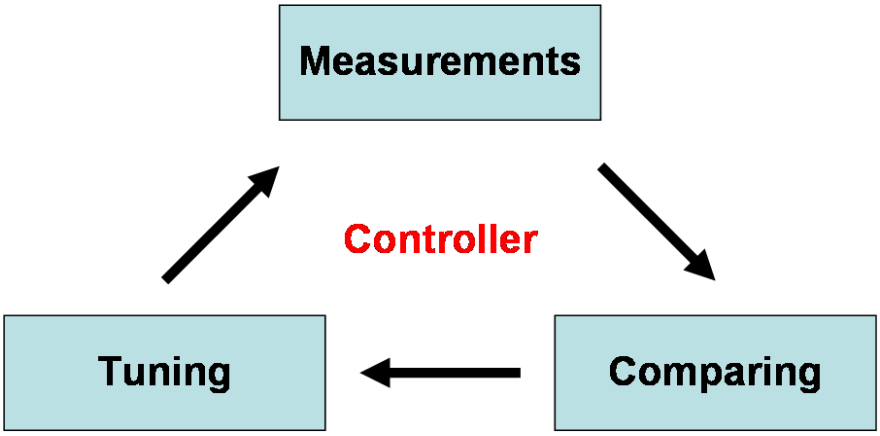

Figure 6.1: General scheme of a control system with the basic actions, measuring, comparing, tuning.

controller which send the signals to the muscles to act in the right way. If this controller fails for any reason, the corresponding actions fail to occur.

Although the design of this controller is very complicated, it shares certain universal properties with other systems.

The design of a controller like that in Fig. 6.1 can be described by the process of adjusting a specific quantity, which we measure in the system. The required value of this quantity then gives, by comparison, the direction for tuning. So the cycle of measuring, comparing and tuning is the basic concept and the controller determines the changes needed to reach the desired value.

The properties of the system then decide the specific design.

There are two general types of controllers, the feedback method and the non-feedback method (often called feed-forward). In this work we only use the feedback method.

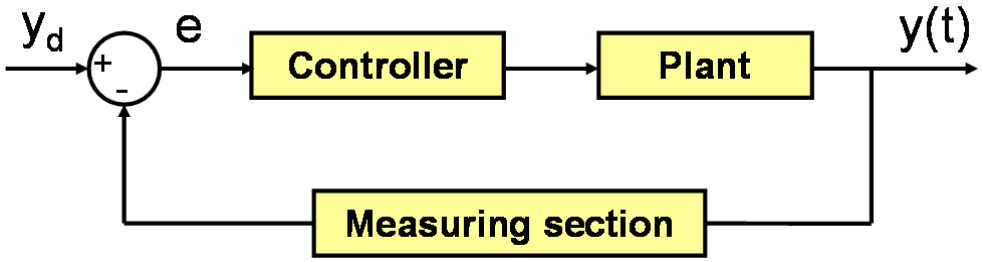

Figure 6.2: Mathematical scheme for a control of a system with y_d the desired value of y, e the difference from the measured value to y_d and $y(t)$ the output of the system acting together with the measuring section, the controller and the plant.

In Fig. 6.2 we see how feedback control works. The control is designed to tune quantity y to the desired value y_d. During the development of the system, the time dependent quantity $y(t)$ is measured in the *measuring section*.

It is compared to the required value and the difference e is given to the *controller*. The controller then uses the information and responds by tuning the so-called *plant*, which is the system to be controlled.

By constantly following the defined feedback loop, a properly designed controller will reach y_d. In the ideal case e goes to zero. The control has to be reset if some disturbance z occurs in the system.

The properties of the system we want to tune help us to decide between the various methods of control theory. We call the adjustment of the value of a quantity in a system which doesn't show any chaotic behaviour *"classical control"*. However, during the last decade, methods of controlling systems with a huge number of unstable periodic orbits have been developed in the field of nonlinear dynamics. When such systems show chaotic behaviour we have to decide between "classical" and *"chaos control"*.

Although the basic concepts like the choice of feedback or feed-forward methods are similar, the systems exhibit different behaviour under control.

6.1.1 Classical control methoods

The most important class of mathematical approaches in classical control methods is the so called *"Proportional Integral Differential"* (PID) controller. As the name indicates, the controller is made up of three different terms, some of which can be neglected, depending on the specific problem.

These three parts determine the behaviour of the control. The P-part works as an amplifier of the difference e, the I-part sums up the measured values of e and thereby memorizes the development of the quantity and the D-part measures the gradient of the difference.

In general these parts of a controller are well defined by the answer from the step response. The equation u for a PID control follows directly from the transfer function f.

$$f(s) = K_P + \frac{K_I}{s} + K_D\, s \tag{6.1}$$

$$u(t) = K_P\, e + K_I \int e\, dt + K_D \frac{de}{dt} \tag{6.2}$$

The weights of the controller parts are the pre-factors K, and s denotes the time interval in which we measure the differences e. $u(t)$ is then given by the controller to the plant of the system.

More complicated kinds of P-parts or time delay parts can be included. These make the controller much more complicated. For a detailed overview of the concepts of PID we refer the reader to the book by Åstrom and Hägglund [Åst95].

Fuzzy control is a different approach to controlling a system. The basic concepts were developed from fuzzy logic theory by Lotfi Asker Zadeh in 1965. Fuzzy logic includes not only the set 'true' or 'false' but also logical states in between. Fuzzy control then answers the question of how close the measurement is to the correct value.

The detection of edges on a poor grey colored picture is an example. If we define white to be the edge and black to be not at the edge, then most of the points are in between. For further reading we suggest the book by Passino and Yurkovich [Pas98].

6.1.2 Chaos control

Where normally, for classical methods, the aim is to tune a specific quantity to a certain target value, for fluctuating systems the aim is sometimes to stabilize or destabilize certain chaotic attractors. Control then usually means adjusting the essential oscillation properties of the system by imposing a small perturbation.

Control of complex irregular motion is one of the central problems in nonlinear dynamics [Sch01; Sch04; Sch89; Sch99; Sch07].

The phase space of such systems contains a large number of unstable periodic orbits embedded in a chaotic attractor. Therefore a small change in initial conditions can lead to a completely different evolution.

There are several different methods, which once again can be divided into feedback and feed-forward methods.

An important class is called *non-invasive* control. Here only weak external forces are coupled into the system. They do not change the dynamics of the system completely, but stabilize an already existing orbit embedded in the chaotic attractor.

The most important non-invasive methods are the Ott-Grebogi-Yorke (OGY) method [Ott90], and the Pyragas control scheme [Pyr92], which is also known as *time-delayed auto-synchronization* (TDAS). The TDAS scheme uses the time-delayed feedback of a system variable, which is coupled back into the system. It can easily be applied to a great number of systems and has proved to be successful in real experiments. See [Ben02; Boc00; Jus03a; Sch06a], or for various classes of theoretical models [Bab02; Bec02; Fra99; Höv04; Höv03; Jus03b; Bal05; Höv05; Yan06; Sch06b], and for models of semiconductor nanostructures [Sch93; Ama03; Ama02; Sch03b; Unk03]. A wide range of applications of this method have been tested and there have been a great many theoretical investigations. A further development of control was then proposed as *extended time-delayed auto-synchronization* (ETDAS) [Soc94]. Time-delayed feedback control has also been applied to noise-induced oscillations [Jan04; Bal04; Sch05; Pom05; Ste06; Hiz06; Hau06; Bal06].

We have briefly discussed chaos control, but for more detailed explanations of the methods and a state of the art review of theoretical methods and their experimental applications see the book by [Sch07].

6.2 Control in this work

In this work we use the observed methods explained above to control the stochastic differential equations and thereby the behaviour of the roughening interface by means of a time-delayed feedback control method.

6.2.1 Control variable

The main quantity for the stochastic differential equations is the rms-roughness. The development of roughness is correlated to three exponents, which determine the universality class of growth and thereby determine the growth process. Any possible control has to influence this evolution and so our control variables are restricted to the growth exponent β, the roughness exponent α and the dynamic exponent z.

In order to be included in a setup, the variables have to be directly measurable. We have seen in Sec. 4.2, that, in self-affine systems, the exponents are not independent. While it is rather difficult to determine the dynamic exponent z directly by measuring the crossover time t_x or by using the structure function, we can in general control both other exponents.

For α we have to calculate the correlation functions (see Sec. 5.4) or the structure function during control. If we want our tool to be related to realistic growth, the direct method is very complicated, because it requires the comparison of different system-sizes. And as already pointed out (see Sec. 5.4), a lot of systems do not reach saturation during growth. So both for the theoretical model and for an experiment the natural choice of control is the growth exponent β.

Our control variable in the roughness evolution represents the early phase, so for a lot of epitaxial systems it can be measured directly from development.

6.2.2 Time delay

The determination of β requires the roughness evolution to be tracked during development. According to the definition of the growth exponent β, our algorithm has to calculate β in-situ by taking the slope of the roughness $w(t)$ on a logarithmic scale and therefore requires the previous roughness values to be memorized.

For a measurement in a numerical scheme it is obviously important not to measure the growth exponent at every single time step dt in order to avoid large effects of discretization. As control theory is widely used for a lot experimental setups, we give the system a time delay τ before it reacts to control tuning. So our scheme calculates the roughness for a time interval $[t-\tau, t]$ from the actual and the memorized value of time $t-\tau$ and therefore is a *time-delayed feedback control* method.

6.2.3 Scheme of control

We have now explained the basic quantities and our control scheme follows as a direct result.

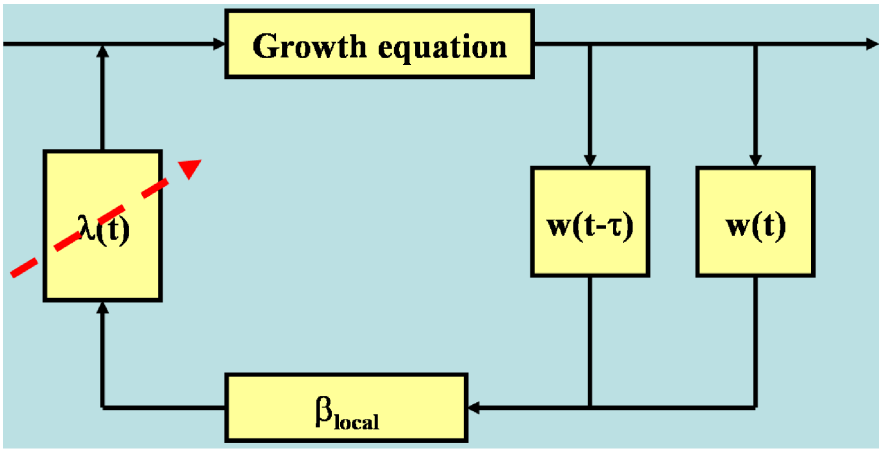

Figure 6.3: Control of the growth exponent β.

As shown in Fig. 6.3, measurements from the stochastic differential equations we have solved give the time dependent roughness, which determines the behaviour. The algorithm calculates the actual growth exponent at time t from the roughness evolution, compares it with the desired value of β and then changes the behaviour using a well defined strategy.

In detail, the scheme is as follows. First we choose the desired value of the growth exponent, β_0, and select an appropriate time delay τ. Generating sufficiently many samples of $h(x,t)$, we record $w(t-\tau)$ and $w(t)$ (the argument L will be omitted from now on). The *local exponent* β_{local} at time t is defined as

$$\beta_{local}(t) \equiv \frac{\log w(t) - \log w(t-\tau)}{\log t - \log(t-\tau)} \tag{6.3}$$

Depending on the sign and value of $\beta_{local}(t) - \beta_0$, we adjust the nonlinear coupling, λ, of the KPZ equation, as follows. First we introduce a control function $F(t)$.

For *digital control*, we define

$$F(t) \equiv \begin{cases} a, & if\ \beta_{local} \leq \beta_0 \\ -a, & if\ \beta_{local} > \beta_0 \end{cases} \tag{6.4}$$

where the parameter a defines the control 'bit', i.e. the amount by which λ changes at each control step.

Alternatively, we also investigate a *differential* method for which

$$F(t) \equiv K(\beta_0 - \beta_{local}) \tag{6.5}$$

and K sets the amplitude of the control strength. Given one of the two choices of $F(t)$, the control scheme kicks in at time t_0 and acts on the nonlinear terms of the different equations, as we will explain in more detail for each specific equation.

Our scheme is successful if $\beta_{local}(t)$ approaches β_0 and then settles at the desired value within a reasonable period of time after the control has been activated.

Control of the KPZ equation

We have already explained in Sec. 5.1 the relationship between the KPZ equation (Eq. (5.11)) and the EW equation (Eq. (5.2)) when we have zero nonlinearity. The best method of controlling the exponents is to control the leading term, which is the nonlinearity λ. The value of the nonlinear term is then no longer constant in time but changed by the control force $F(t)$ in the following way

$$\lambda(t) = \begin{cases} \lambda_0, & if\ t < t_0 \\ \lambda(t-\tau) + F(t), & if\ t = t_n \\ \lambda(t_n), & if\ t_n < t < t_{n+1} \end{cases} \tag{6.6}$$

The control scheme starts at time t_0. From then on, the nonlinearity λ is updated at times $t_n \equiv t_0 + n\tau$, $n = 1, 2, ...$, starting from an initial value λ_0. As we know, zero nonlinearity leads to EW like behaviour of the growth exponent β, where the value $\beta_{EW} = 0.25$ (for 1+1 dimensions) is smaller than that for the KPZ equation $\beta_{KPZ} = 1/3$.

The algorithm has to include that fact. Therefore the control force is added to the nonlinearity if the local exponent is smaller than that desired (Eq. (6.6)). This assumption is valid if we look at positive nonlinearities $\lambda > 0$. For negative nonlinearities the situation is just the opposite. We have to subtract if the difference $\beta_{local} - \beta_0$ is negative, showing that the KPZ equation is symmetric in that sense.

Negative lateral growth corresponds to a negative nonlinear term. Such a process seems to be unusual in crystal growth. But there are quite similar systems with corrosive behaviour at the interface which exhibit negative lateral growth.

In Table 6.1 we see a typical setup for our simulations with the initial parameters $\nu = 0.1$ and $D = 0.5$ kept constant for all simulations. The parameters of the control β_0, τ, λ_0 and the control strength a and K determine the control force $F(t)$.

Control of the MBE equation

The situation for controlling the MBE equation (Eq.(5.23)) is in some ways different from the control of the KPZ equation. The MBE equation with just the fourth order term has a proposed exponent of $\beta = 0.375$ in 1+1 dimensions and the exponent

EW term (surface tension)	$\nu = 0.1\ nm^2/s$
Strength of the Gaussian white noise	$D = 0.5\ nm^4/s$
Initial nonlinear term	$\lambda_0 = 0.00 \ldots 0.40\ nm/s$
Strength of the digital control	$a = 0.001 \ldots 0.100\ nm/s$
time discretization	$dt = 0.001 \ldots 0.1$ s
System size	$L = 256 \ldots 16384$ lattice sites (l.s.)
desired value of the growth exponent	$\beta_0 = 0.25 \ldots 0.33$
time delay for the feedback	$\tau = 0.1 \ldots 10$ s

Table 6.1: Typical set of parameters for the control of the KPZ equation.

Surface diffusion term	$\nu_1 = 0.1\ nm^4/s$
Strength of the Gaussian white noise	$D = 0.5\ nm^4/s$
Initial nonlinear term	$\lambda_{1,0} = 0.00 \ldots 0.10\ nm^3/s$
Strength of the digital control	$a = 0.001 \ldots 0.100\ nm/s$
Strength of the differential control	$K = 0.001 \ldots 0.100$
time discretization	$dt = 0.001 \ldots 0.1$ s
System size	$L = 256 \ldots 8192$ lattice sites (l.s.)
desired value of the growth exponent	$\beta_0 = 0.33 \ldots 0.375$
time delay for the feedback	$\tau = 0.1 \ldots 10$ s

Table 6.2: Typical set of parameters for the control of the MBE equation.

decreases with a nonzero additional term of the nonlinearity λ_1. For two dimensions the same situation occurs when the exponent for a zero nonlinearity λ_1 is higher.

That is essential for the control scheme. If we want to tune an effective exponent β_0 by our time-delayed feedback control scheme, we have to increase the nonlinearity λ_1 to get smaller values of the exponents by increasing the function $\lambda_1(t)$. So our control force $F(t)$ has to work in opposition to the force from the KPZ equation. For simplicity we change the sign in the control scheme, but one could alternatively redefine the control forces with a change of sign in Eq. (6.4) (6.5). If we control the exponents using λ_1, our control scheme has to be

$$\lambda_1(t) = \begin{cases} \lambda_{1,0}, & if\ t < t_0 \\ \lambda_1(t-\tau) - F(t), & if\ t = t_n \\ \lambda_1(t_n), & if\ t_n < t < t_{n+1} \end{cases} \tag{6.7}$$

where the procedure for the time delay is the same as for the KPZ equation. In Table 6.2 we see a setup of the parameters for this type of equation.

We have now defined a control procedure for the growth equations which will be applied to control the growth exponent. So the question arises as to whether it is possible to tune β to all the desired values if the choice is restricted to universality classes. As one would expect, the answer is no.

But if we conceive of the exponents as defined quantities for the long term and long range behaviour of the roughening surface, we can control the early states with a well defined system size L by effective exponents, so the behaviour can be different.

A second question concerns the behaviour of the roughness exponent α during the control. α does not differ for the Edwards-Wilkinson and the KPZ equation. So a useful and successful control maintains these values during the control, otherwise we would leave the universality classes and the above equation would not explain a adjustment of local growth exponents within these classes.

For the MBE equation the situation changes, the roughness exponents are not the same for the two extreme cases, but one would expect α to lie somewhere in a range between the universality classes for the controlled equation. Table 6.3 sums up the exponents of the different regimes for the equations we want to control by the methods explained above. The different exponents for the KPZ equation in 2+1 dimensions denote the different values proposed by Wolf and Kertész [Wol87] and Kim and Kosterlitz [Kim89].

Kardar-Parisi-Zhang equation	β	α	
1 + 1 dimensions $\lambda = 0$	0.25	0.50	
1 + 1 dimensions $\lambda > 0$	0.33	0.50	
2 + 1 dimensions $\lambda = 0$	0.00	0.00	
2 + 1 dimensions $\lambda > 0$	0.20	0.33	Wolf-Kertesz
2 + 1 dimensions $\lambda > 0$	0.25	0.40	Kim-Kosterlitz
MBE equation			
1 + 1 dimensions $\lambda_1 = 0$	0.375	1.50	
1 + 1 dimensions $\lambda_1 > 0$	0.33	1.00	
2 + 1 dimensions $\lambda_1 = 0$	0.25	1.00	
2 + 1 dimensions $\lambda_1 > 0$	0.20	0.66	

Table 6.3: The critical exponents for the growth equations.

6.2.4 Relation to control methods

A short look at our control scheme shows its relationship to the general methods explained above. First, of course, we have a time-delayed feedback method as for the classical control and for chaos control.

Obviously we do not control a chaotic system. On the other hand we have a system driven by stochastic noise as noise induced roughening. The main difference from a lot

of chaotic systems is the absence of a chaotic attractor and in this sense it is closer to the classical methods of tuning a developing system. So it is rather difficult to include classical or chaos control.

The method contains not only the properties of PID controllers but also those of the TDAS scheme. Our differential control scheme acts in a similar way to a proportional controller, in that it amplifies the difference of the desired exponent. The digital scheme answers with a step on a step function.

So our scheme combines some properties and findings of both the classical and chaos control approaches.

Chapter 7

Simulating Stochastic Differential Equations

In the previous chapters we showed how to control surface roughness by adjusting the growth exponent β in the early phase of the roughening. We now apply the time-delayed feedback control method defined in Ch. 6.2 to the equations for crystal growth.

7.1 The Kardar-Parisi-Zhang Equation

In case of the KPZ equation we want to tune the growth exponent β by means of the nonlinear term λ. We have to ensure that the related exponents are valid for 1+1 dimensions and have to check if we get similar results in comparison to previous findings for 2+1 dimensions or to the proposed exponents, respectively (see table 6.3). So we first check our numerical scheme for this equation without any control and then continue with the feedback scheme.

7.1.1 The uncontrolled equation in 1+1 dimensions

For a satisfactory check of the exponents without control the best method is to look at the long time behaviour of scaling. In Fig. 7.1 we provide a data collapse for the equation in 1+1 dimensions, where we used two different system sizes $L = 1024$ and $L = 4096$ for the numerical scheme.

Simulations were made for long times. 'Long time' here means that the roughness is in the saturation phase as shown in Fig. 7.1. The data collapse was made using the Family-Vicsek relation (Eq. (4.5)).

First the roughness $w(t)$ was rescaled by $w \rightarrow w/L^{\alpha}$, then the timescale was rescaled by $t \rightarrow t/L^{z}$. If we have chosen the right values for α and z, the curves collapse into single curves, as can be seen for the three initial setups.

In all three cases $\alpha = 0.50$ measured by the height-difference correlation $H(r)$ (see Sec. 5.4.3 for the method) and is the right value for both the EW universality class

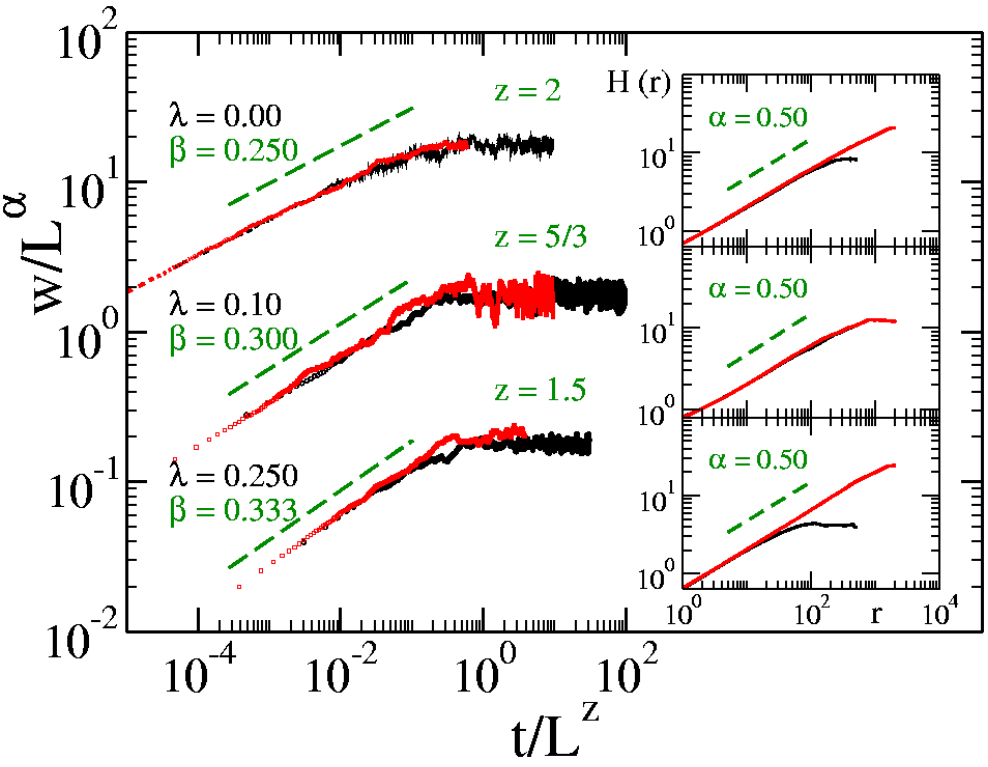

Figure 7.1: Data collapse for the KPZ equation in 1+1 dimensions w/L^{α} vs t/L^{z} plotted on a logarithmic scale for three different initial setups for the nonlinearity λ for systemsizes $L = 1024$ (red lines) and $L = 4096$ (black lines) (i) $\lambda = 0$ shifted by a factor of 4 (ii) $\lambda = 0.1$ shifted by a factor of 2 (iii) $\lambda = 0.25$, insets show the height difference correlation function $H(r)$ measured for $r \in [0, L]$, the broken green lines are guides to the eyes for the extracted exponents α and β, respectively.

and the KPZ universality class. The dynamic exponent z differs and therefore so does the growth exponent β.

Three different initial nonlinearities λ were used. For zero nonlinearity we see that the Edwards-Wilkinson equation ($\beta = 0.25$, $\alpha = 0.5$ and $z = 2$) behaves as expected. The other extreme case has a sufficiently strong nonlinearity ($\lambda = 0.25$) to provide a case of KPZ behaviour ($\beta = 1/3$). Here the other exponents $\alpha = 0.5$ and $z = 3/2$ stay at the KPZ values.

The third case ($\lambda = 0.1$) is surprising. We find a local exponent $\beta_{local} \sim 0.30$ which is neither the EW value nor the KPZ value but is nevertheless constant over a range of more than two decades.

There are several possible explanations for this behaviour.

- It is possible that saturation sets in before the exponent reaches the KPZ value. Alternatively the opposing processes, the roughening phase and early saturation, cancel one another out to give an effective exponent.
- It is also possible, though extremely unlikely, that we have found a totally new universality class.
- It is also possible that there are some difficulties with the numerical scheme. If this is true then the numerical scheme needs to be changed.

To get a more detailed view, we made simulations of the early phase for a wide range of different nonlinearities λ. As simulations of long time behaviour are extremely computationally demanding, we used shorter simulations and took ensemble averages.

In Fig. 7.2 we have changed the nonlinear term in the range $\lambda \in [0.0, 0.8]$. The dashed lines help one to see the limiting exponents, which are the EW ($\beta = 1/4$) and the KPZ value ($\beta = 1/3$).

For small nonlinearities we get clear effective exponents, which seem to increase monotonically with the value of λ. If λ is not too large we see the behaviour we expect

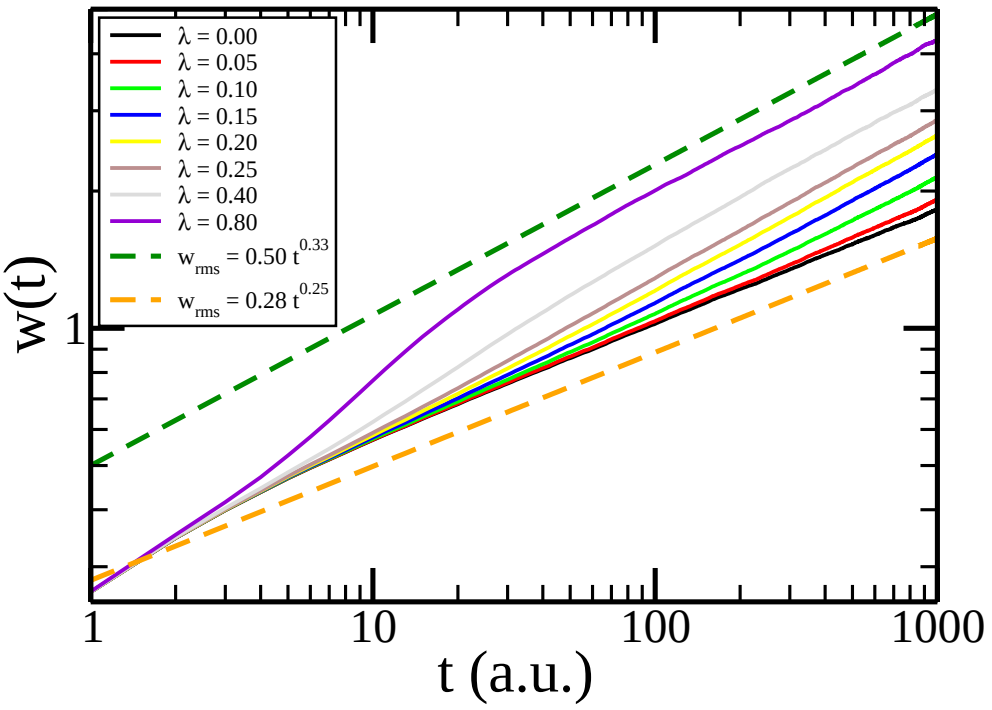

Figure 7.2: Early roughness evolution of the KPZ equation $w(t)$ vs time t with $\lambda \in [0.0, 0.8]$ for $L = 4096$ and time $t = 1000$ with a time discretization $dt = 0.02$, dashed lines denote the limits of the growth exponents for $\beta_{EW} = 0.25$ (orange) and $\beta_{KPZ} = 1/3$ (green) as guides to the eye.

and have observed before in Fig. 7.1. For a large enough nonlinearity $\lambda = 0.80$ we see a local exponent which increases and then saturates at the KPZ value $\beta = 1/3$. This indicates that we have not found a new universality class for the equation but rather a local regime of early development in which the growth exponent β is tunable to a certain value.

Quite similar behaviour has been found by other authors [Mos91; Gha06]. So we are not proposing a new universality class, and the limits of the numerical solutions are still within the expected range. The universality class explains long time and, more importantly, large scale behaviour, so our results explain behaviour during early development. But this behaviour could be relevant to realistic setups when we have a defined limited scale and obviously also a limited time scale.
We have determined the limits and range of the KPZ equation in 1+1 dimensions where control can adjust the growth exponent β.
We now take a more detailed look at the calculation of the roughness exponents for long time behaviour. As one can see in Fig. 7.3, the methods we have already described (see Sec. 5.4.3) do actually work. We test the calculation using the height-difference correlation $H(l)$ (Fig. 7.3 (a)), the height-height correlation $C(l)$ (Fig. 7.3 (b)) and the structure function $S(k,t)$ (Fig. 7.3 (c)). As expected, the exponent $\alpha = 0.5$ is the same in all three cases, with a zero nonlinearity $\lambda = 0$, a strong nonlinearity $\lambda = 0.25$ and an intermediate value of $\lambda = 0.10$. In Fig. 7.3 (b) the simulation plots (solid lines) are fitted (dashed lines) to the function $C(l) = C_0 exp(-(l/\xi)^{2\alpha})$ (see Sec. 5.4.3). For the structure function $S(k,t)$ we see that all the curves match a single curve with a slope corresponding to $\alpha = 0.5$. Here k is scaled so that $k = 1$ corresponds to $l = L$ in phase space and we shall use this scaling in further calculations.

7.1.2 Definition of parameters for the control

The first thing to determine for control is the range of time in which we want to apply the control. As we can see, for our simulations in arbitrary units the range of clear effective exponents is $t \in [10, 1000]$, where saturation normally sets in after $t = 1000$. So, in order to avoid effects produced by the saturation process, control should not be applied for too long a period. We have therefore restricted our control to this range for all our simulations.

The next step is to define the time delay τ and the strength of the control forces by means of the parameters a and K from Eq. (6.4), (6.5). Because our simulations are highly computationally demanding, we aim as far as possible to restrict the range and use the parameters as a control before starting any simulation. This avoids both long parameter changes and wasting too much time reaching the right parameters.

Obviously, τ, a and K are not independent of one another during control. When we have a very small time delay, we do not take too large a control parameter in order to avoid numerical instabilities in the scheme. If we take a larger time delay, we have to ensure that the control force can tune the exponent to the desired value in time, or else we have to choose parameters a and K that are not too small. There are limits

to the parameters defined by the equation and the control range determined above. If we assume a limit for our control function $\lambda(t) \in [0, 0.25]$, which is a reasonable assumption looking at the changeable exponents in Fig. 7.2, then we have to determine our control using that range. To get a more generalized view we now define a control factor for digital control.

$$C_a = \frac{a}{\tau} \tag{7.1}$$

From this factor we can easily calculate the maximum of our range for $\lambda(t)$ by

$$\Delta\lambda(t) = C_a(t_{c,end} - t_{c,0}) \tag{7.2}$$

where $t_{c,0}$ is the time of the beginning of control and $t_{c,0}$ is the end. So for a time delay $\tau = 1$ and a control step $a = 0.005$ the range is $\Delta\lambda \sim 0.5$ which is twice the range of $\lambda(t)$ and therefore a good choice. Similar possible choices would then be $\tau = 10$ and

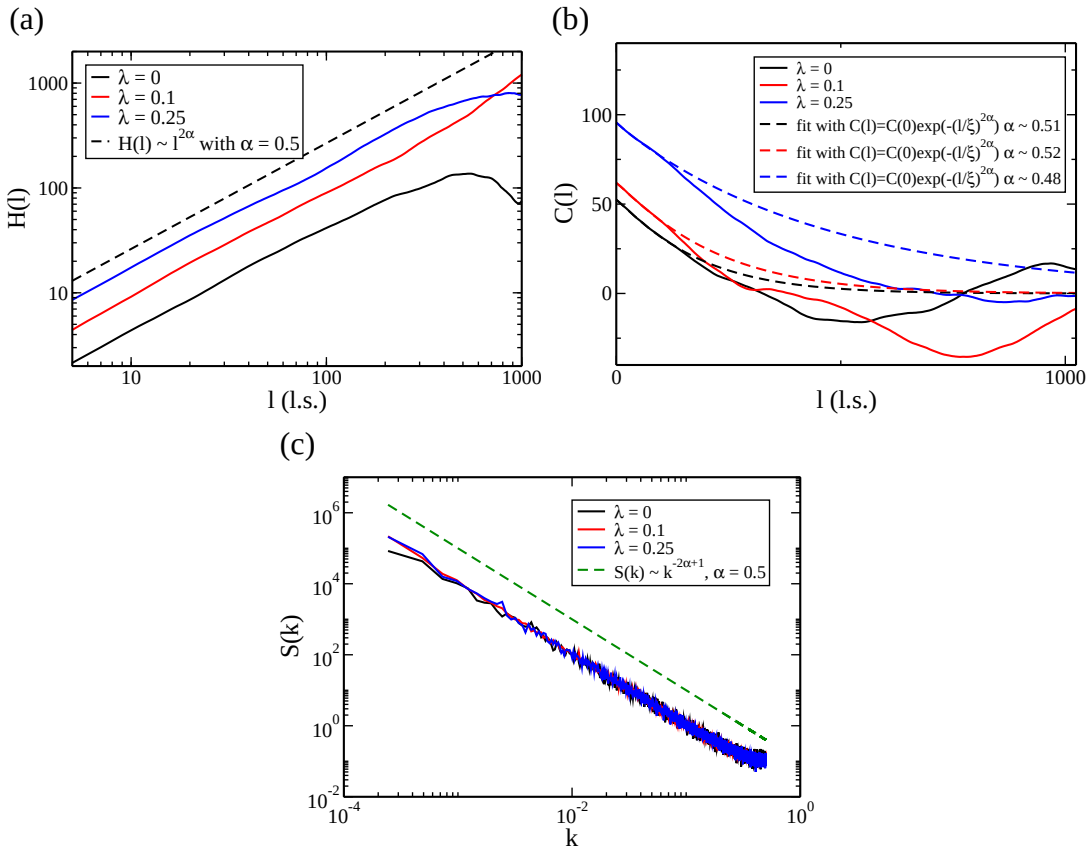

Figure 7.3: Calculation of the roughness exponent α for the KPZ equation in 1+1 dimensions in the long time behaviour: (a) the height-difference correlation function $H(l)$, (b) the height-height correlation function $C(l)$, (c) the dynamic structure function $S(k,t)$ for three different nonlinearities $\lambda = 0.0$ (black), $\lambda = 0.1$ (red) and $\lambda = 0.25$ (blue) with $L = 4096$, $t = 10^6 a.u.$ and $dt = 0.01$, the dashed lines show the fit functions for calculation of the roughness exponents.

$a = 0.05$ or $\tau = 0.1$ and $a = 0.0005$ which give the same maximum $\Delta\lambda$. So the factor C_a gives general predictions as to how to set the initial parameters. The best choice then depends on the specific development of roughness. A *'coarse control'* or a control which only changes a few times in the control range of the function $\lambda(t)$ defines the upper limit of time delay. A very small time delay is more sensitive to the fluctuations from the numerical scheme which appear in the numerical integration. Of course one also has to ensure that the time delay is large enough in comparison with the time step dt.

For differential control the control factor has a similar definition

$$C_K = \frac{K}{\tau} \tag{7.3}$$

which is obviously impossible to calculate without some 'test' simulations of the initial conditions for K and τ. This is because it depends directly on the difference $\beta_0 - \beta_{local}$. Digital control only reacts to the sign of this difference. In this sense differential control is more difficult to apply but, on the other hand, is probably a much faster control method.

We now need to define either the range in which we want our control to influence the roughening phase or the times t_0 for the onset of control and for the end of control. We therefore clarify the restrictions in our numerical scheme. In Fig. 7.4 we see the development up to a time $t = 10000$ for a setup with $L = 4096$ and a nonlinearity value of $\lambda = 0.25$. In the left panel we show the linear plot and the insets show that the power law is relatively stable up to $t = 1000$, with fluctuations appearing in the range from $t = 1000$ to $t = 2000$ and becoming very obvious at $t = 10000$, whereas this does not show up so clearly in the logarithmic plot.

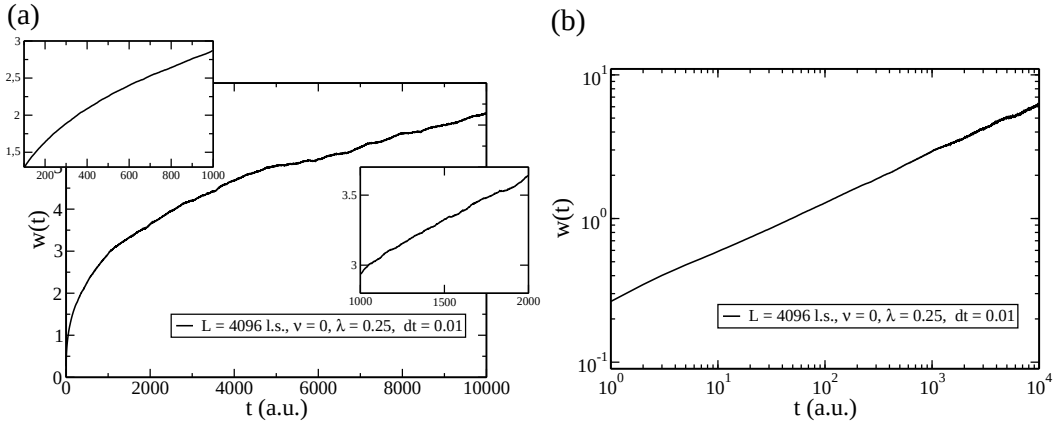

Figure 7.4: Roughening of the early time KPZ equation with $L = 4096$, $w(t)$ vs t: (a) linear plot, (b) logarithmic plot with a time discretization of $dt = 0.01$ and a nonlinearity of $\lambda = 0.25$

The origin of these fluctuations can be explained both by the start of a change in roughening before the saturation phase and by the strong influences of numerical

System size	$L = 4096$
Time of onset of control	$t_0 = 10$
End of control	$t_e = 1000$
Initial nonlinear term	$\lambda_0 \in [0, 0.25]$
Time delay	$\tau \in (0, 1000]$
Strength of the digital control	$a \in (0, 0.05]$
Strength of the differential control	$K \in (0, 0.10]$
desired value of the growth exponent	$\beta_0 \in [1/4, 1/3]$
time discretization	$dt \in (0, 0.05]$
Averages	25 realizations

Table 7.1: Parameter ranges for the control of the KPZ equation in 1+1 dimensions.

fluctuations. When the evolution obeys a power law, small fluctuations in the numbers lead to bigger changes in the local exponent for the later times. This is because the absolute values of the differences between the values of the roughness decrease due to the logarithmic scale.

Of course, we also get these fluctuations for smaller values, but ours seems to be a suitable choice for controlling roughening up to $t = 1000$. Up to $t = 10$ the roughening depends on the initial flat surface, so we set our time $t_0 = 10$.

So we now have determined our basic parameters for the control of the KPZ-equation and also the range within which control of the local exponent is possible. Table 7.1 lists a summary of these parameters.

7.1.3 Control of the KPZ equation in 1+1 dimensions

We now test our control scheme for the KPZ equation in 1+1 dimensions with these restriction on the parameters. We check how control works and to what extent the scheme depends on the basic parameters for certain setups.

Influence of τ on control

First we want to test the reaction on different time delays τ. We set an initial nonlinearity $\lambda_0 = 0$ and take a control strength with constant values $a = 0.01$ and $K = 0.01$. The desired growth exponent is set to be $\beta_0 = 0.29$.
We now test this setup for three time delays $\tau \in \{0.01, 0.1, 1\}$. In order to make the influence of the time discretization dt as negligible as possible, we set it to $dt = 0.0005$. This increases the simulation time but we get clear results that only depend on τ. In Fig. 7.5 we see the results of the control for a variation of the time delay τ. In Fig. 7.5 (a) we see that digital control works for the time delay $\tau = 1$ (blue) and for a value of $\tau = 5$ (orange), where the control adjusts the exponent a little bit later in the second case. For the smaller values control fails (black, red). In the

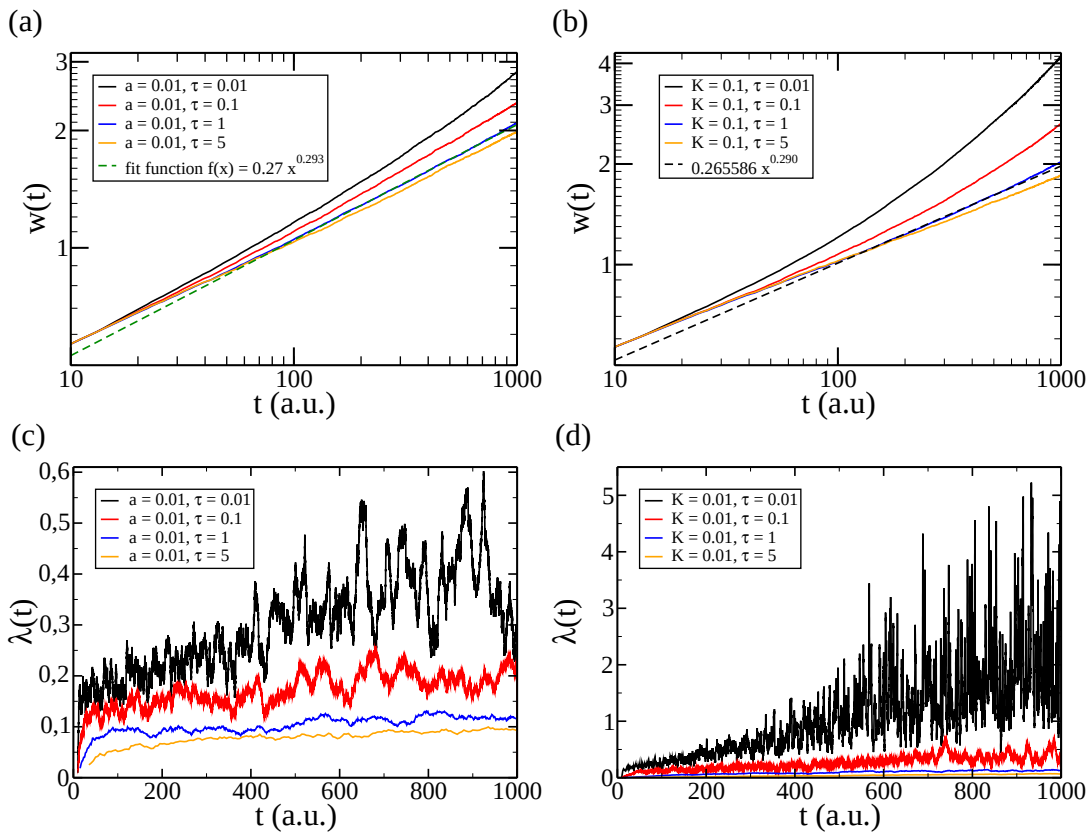

Figure 7.5: Influence of time delay on control for digital and differential control, (a) w vs t for the digital control with $a = 0.01$, (b) for the differential control with $K = 0.01$, (c) $\lambda(t)$ for the digital control, (d) $\lambda(t)$ for the differential control, time delay vary in $\tau \in \{0.01, 0.1, 1, 5\}$, $dt = 0.0005$, $\lambda_0 = 0.00$, $\beta_0 = 0.29$ and 25 averages for all simulations.

corresponding control functions (Fig. 7.5 (c)) we see the reason for this behaviour. Whereas for the successful control the function first increases and then stays nearly constant, it fluctuates widely for smaller τ. This is obviously a reaction to the much faster control with the smaller time delays. So differences from the ideal case of the power law of roughening here lead to over-controlled behaviour and thereby to a larger effective exponent β.

For differential control the situation is much more extreme. In general we see similar behaviour: the control works for $\tau = 1$ and in the case of $\tau = 5$ does not reach the value of β_0, but stays close to $\beta = 0.25$. Control fails for the smaller time delays.

Because of the direct dependence of the control strength on the absolute value of the difference from the desired value of β_0, the fluctuations are much stronger here.

In conclusion, we have found a possible control but anticipate better tuning of the control strength for other cases of digital control using different time delays. So although differential control reacts faster, the digital scheme of changing the time delay

under constant conditions offers a wider range of possibilities.

Influence of control strength on control efficiency

We now take a closer look at how controllers react to a change in the strength of the control parameters a and K. We again take setups with time delays of $dt = 0.0005$, $\beta_0 = 0.29$, $\lambda_0 = 0$ and set the time delay to a constant value $\tau = 1$ for both types of control. In Fig. 7.6 (a) we see that the control works for a digital parameter of $a = 0.005$ (red), but fails for $a \in \{0.001, 0.02, 0.05\}$. The dashed line here is a fit to the working control parameter which shows only a slight difference from the desired value of the effective exponent. Obviously, too small an a leads to a control function which does not adjust the exponent in the given range of time. This is because of the absolute added value of the parameter. For parameters that are too large, the changes are too large for a given difference, so the control functions $\lambda(t)$ fluctuate more and the required exponent cannot be reached: the control is too fast for the system to react normally. That can be seen from looking at the functions $\lambda(t)$ in Fig. 7.6 (c). For differential control the behaviour is very similar: the lowest value $K = 0.001$ gives a smaller effective exponent and the control strengths $K = 0.02$ and $K = 0.05$ produce larger effective exponents than desired and also cause large fluctuations in the functions $\lambda(t)$ (Fig. 7.6 (d)). The adjustment $\beta_0 = 0.29$ only works for $K = 0.006$ (red).

So a change in the strength of control using parameters a and K leads to quite similar behaviour in both types of control.

If we look at the introduced control factors C_a (Eq. (7.1)) and C_K (Eq. (7.3)), control works here for values of $C_a = 0.005$ and $C_K = 0.006$.

Simulations with constant C_a and C_K

We now want to take a look at these artificial parameters.

We again take our setups with time discretizations of $dt = 0.0005$, $\beta_0 = 0.29$, $\lambda_0 = 0.00$ and now set the factors at $C_a = 0.01$ and $C_K = 0.01$, close to the values of our previous working control. Then we change both the control parameters and the time delay in simulations and ensure these factors stay constant. In Fig. 7.7 show the results for constant factors. For digital control, the roughness evolution is adjusted perfectly for two setups, $a = 0.005$ with $\tau = 0.5$ (orange) and $a = 0.002$ with $\tau = 0.2$ (blue). For the other setups control fails. The absolute changeable range during control using the factor C_a is constant (here $\Delta\lambda_{max} = 0.99$, (see Eq. (7.1)), the reason being slow reaction to changes in the local effective exponent.

For the differential control method this is not the case and therefore all setups show very similar behaviour. Due to the direct amplifying nature of C_K this leads to a working control in all cases. The inset in Fig. 7.7 (b) shows that roughness increases slightly for higher τ and K.

If we take a look at the control functions for digital control we see that values increase for increases in τ and a. In the early stage the function increases fast with

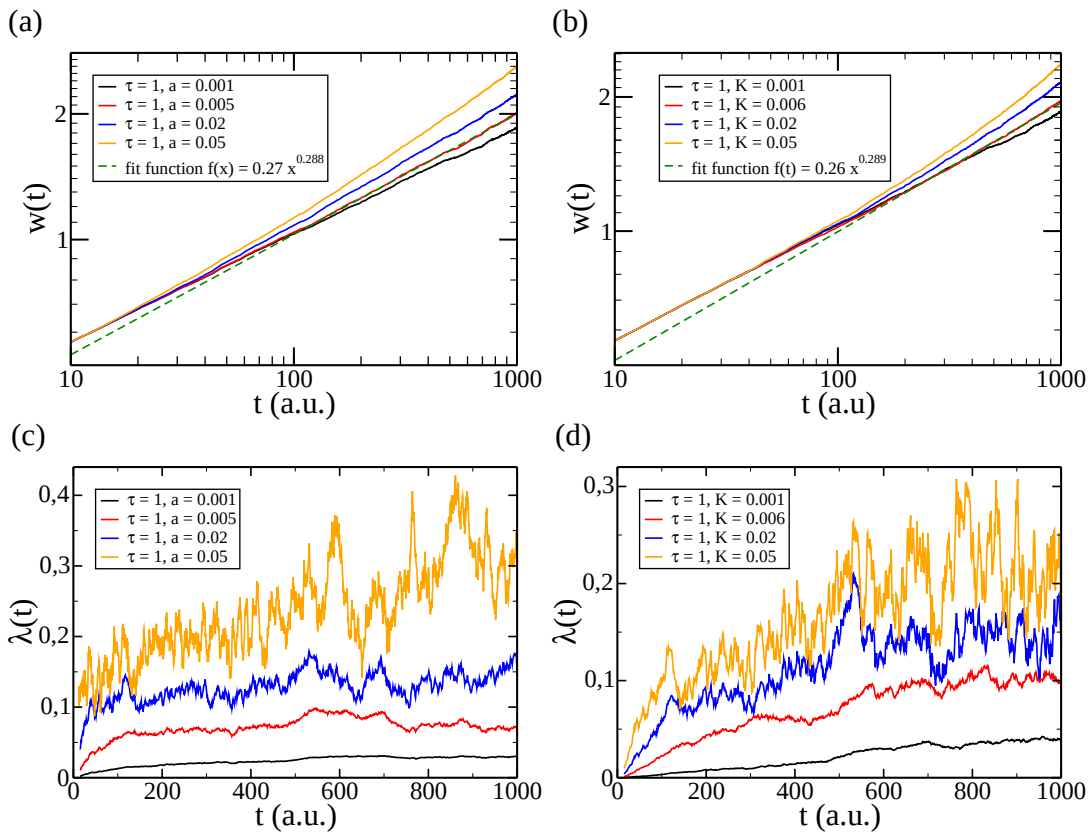

Figure 7.6: Influence of control strength on control for digital and differential control, (a) w vs t for the digital control with $a \in \{0.001, 0.005, 0.02, 0.05\}$, (b) for the differential control with $K \in \{0.001, 0.006, 0.02, 0.05\}$, (c) $\lambda(t)$ for the digital control, (d) $\lambda(t)$ for the differential control, time delay in $\tau = 1$, $dt = 0.0005$, $\lambda_0 = 0.00$, $\beta_0 = 0.29$ and 25 averages for all simulations.

high values, whereas later, because of fluctuations, it cannot decrease fast enough to give the right exponent.

To conclude: the fast reacting differential control has the advantage of being independent of τ and K for constant values of C_K, thereby reducing the degrees of freedom.

Simulations with nonconstant C_a and C_K

Fig. 7.8 gives a summary of a wide range of possible variations for τ, a and K for the setup we used before. We have classified the results using a color code: green squares for a very good adjustment in the range $\Delta\beta < 0.005$ around β_0, blue squares for a functional but imperfect control at $\Delta\beta < 0.01$ and red squares denote a non-functional control for $\Delta\beta > 0.01$. For digital control we see in Fig. 7.8 (a) that the possible control works around values of $\tau = 1$ and $a = 0.01$ for small changes. In

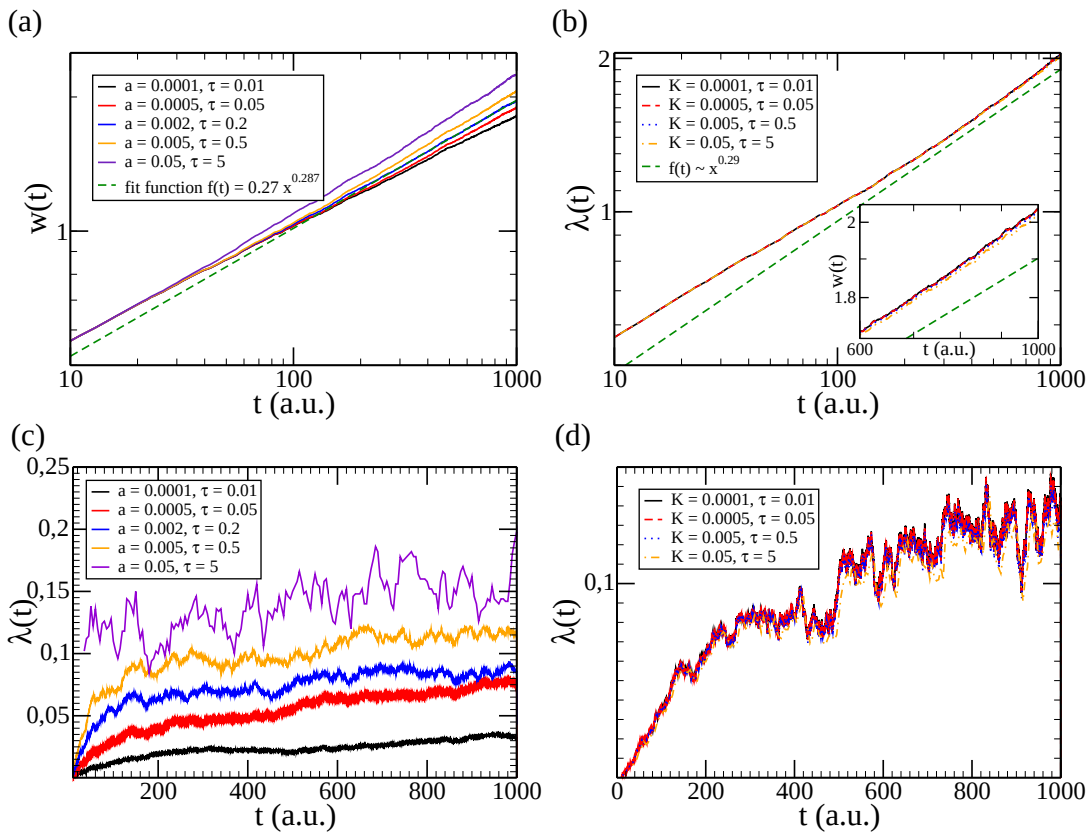

Figure 7.7: Influence of constant factors $C_a = a/\tau$ and $C_K = K/\tau$ on control, (a) roughness $w(t)$ vs time t for different parameters a and τ and $C_a = 0.01$ by digital control, (b) roughness $w(t)$ vs time t for different parameters K and τ and $C_K = 0.01$ by differential control, insets show the curve in smaller range to see the differences, (c) and (d) the corresponding control functions $\lambda(t)$

comparison with the differential control in Fig. 7.8 (b), the range is larger but generally more limited by an upper and lower bound to both τ and a. The differential control for constant K only shows control for a smaller range of τ but does not seem to be limited by choice of K. So for all K a corresponding τ can be found.

Nevertheless there are limits due to the fact that when small τ are of the same order of magnitude as the time discretization , τ and K do not lead to useful control if the function $\lambda(t)$ reacts strongly to differences.

So, as explained above, in the case of differential control we can reduce the parameters over a wide range to the factor C_K which determines the efficiency of control. In the case of the initial setup of $\beta_0 = 0.29$ and $\lambda_0 = 0$ this control works for $C_K \in [0.005, 0.01]$.

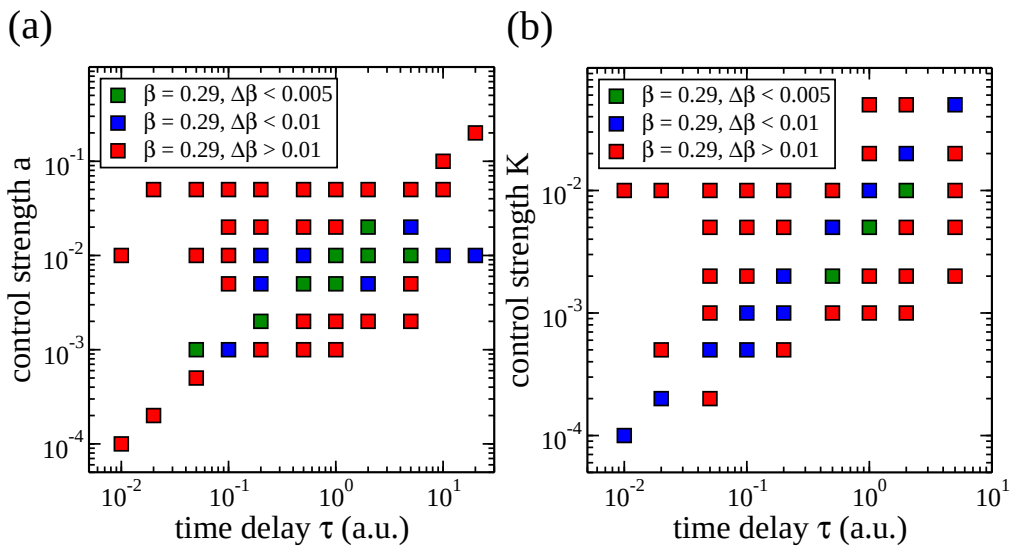

Figure 7.8: Influence of the constants C_a and C_K delay on control, digital and differential, (a) digital control for different setups of τ and a, (b) differential control for different setups of τ and a, categorization in both cases by green squares (good working control), blue quares (working control) and red squares (no working control), parameters in all cases $\lambda_0 = 0.0$, $\beta_0 = 0.29$, $dt = 0.0005$ for 25 averages.

Other control setups

We have made a detailed investigation of one specific initial setup for the time delayed feedback and know how the method works and what influences determine and restrict the ranges. It is now possible to tune the control parameters more efficiently for other setups.

As we saw for the uncontrolled case, we can generate the full range of exponents between the EW and the KPZ universality classes by changing λ within a range of $\lambda \in [0, 0.25]$.

There are three different setups in which our control works for *extreme* cases. These cases are:

- an initially zero $\lambda_0 = 0$ corresponding to the KPZ universality class ($\beta = 1/4$) to be controlled to a desired $\beta_0 = 1/3$ corresponding to the KPZ universality class
- an initially strong $\lambda_0 = 0.25$ corresponding to the EW universality class ($\beta = 1/3$) to be controlled to a desired $\beta_0 = 1/4$ corresponding to the KPZ universality class
- different initial λ_0 which stabilize the effective exponents in a range of $\beta_0 \in (1/4, 1/3)$

By testing these setups we showed that all other possible relevant setups with initial partial nonlinearities in the range between them also work.

We have already partly shown the third case of analysis of the parameters; we now check the whole range for an initial nonlinearity of $\lambda = 0$ and desired values of $\beta_0 \in \{0.25; 0.27; 0.29; 0.31; 0.33\}$. From the simulations for β_0 we know that $\tau \sim 1$ seems to be the best choice for optimal control in both digital and differential control.

We therefore normally restrict simulations to $\tau = 1$, although we have also partly tested setups with other time delays.

For the control strengths we use setups of $a \in \{0.005, 0.01\}$ and $K \in \{0.005; 0.01\}$ and partly test other setups for the differential control to reproduce the behaviour explained above, where control seems to depend only on C_K. Because simulations with the prior time discretization $dt = 0.0005$ are too computationally demanding (a few hours for single simulation), we reduce the time discretization by a factor of 10 to $dt = 0.005$. We thereby reduce the whole simulation time from days to hours, which suggests that the precision of control is slightly affected.

To analyze the results we took the roughness evolution and measured the change in the control function $\lambda(t)$ in situ starting at time t_0 with λ_0. The insets in the upper left of the diagram show the development of this function during control. We have already seen slight changes in the late phase of the control time range due to the more important numerical fluctuations in this range and we shall now take a closer look at the late phase of all the simulations, as shown in the lower right of the diagram (also double logarithmic plot). The figures show the fitted effective exponent in the time range after the control has tuned it to a nearly constant value. In Fig. 7.9 we show the results for digital control with $\lambda_0 = 0$, $a = 0.005$ and $\tau = 1$. In general there is the possibility of control in all cases. Whereas there is nearly perfect control for the required exponent $\beta_0 > 0.25$ (Fig. 7.9 (b - e)), the case of $\beta_0 = 0.25$ is more problematic. Normally one would expect that, when the initial nonlinearity $\lambda = 0$ corresponds to this required value, it would be easily adjustable, as the scheme just has to stay at a zero value. In fact we see the effects of numerical solutions, where small changes in the roughness evolution activate a change of λ. So, in all cases of nonzero λ, which we always get in the case of partly measured values $\beta_{effective} < 0.25$, the tendency is to produce $\beta > 0.25$. Summing gives an exponent of $\beta > 0.25$. Changing the condition that $\lambda \geq 0$ does not change the problem, because negative λ also leads to bigger growth exponents due to the symmetric nature of the equation (see [Mos91; Bar95]).

As already explained, we are going neglect that case, because in experimental setups it would be difficult to change the sign of the nonlinear term corresponding to a real physical quantity. Nevertheless we also tested the control without any restrictions on the sign of λ, but did not find noticeable differences, so here we only show results that neglect such schemes. In the control functions we see that a small increase in nonlinearity leads to the control behaviour, which then stabilizes for higher values of β_0. For the higher values of β_0 the control is perfectly stable, and in the case of $\beta_0 = 0.27$ too, as can be seen in the inset, small fluctuations lead to a bigger local exponent, which is then compensated for by the control.

In the differential scheme we see exactly the same behaviour, except in the problematic case of $\beta_0 = 0.25$ (Fig. 7.10). Here we get better control behaviour with a faster control, which gives a stable exponent of $\beta = 0.254$. Nevertheless fluctuations, which are then controlled by the scheme, can also be seen in this case (inset).

If there is a problem adjusting the exponents to the EW universality class from a zero nonlinearity due to the numerical behaviour described above, then other setups usually fail to stabilize $\beta = 0.25$. A control that works for $\beta_0 > 0.25$ can be seen in Fig. 7.11. The question is whether the good working control in the case of β_0 is only an effect of the numerics or if it is relevant for experimental setups. We do not want numerical fluctuations in experimental setups, so the control of a setup which normally tends to have EW-behaviour should tune the nonlinearity to zero.

A good indication that there is a numerical reason for the behaviour is that the initial conditions are chosen so that the value of λ stays at zero.

For the reasons already explained for the symmetric border at $\lambda = 0$, this behaviour is not seen in other setups, not even in the opposite case of a strong nonlinearity ($\lambda_0 = 0.25$), which can be controlled to a KPZ exponent ($\beta_0 = 0.33$).

We now check other setups for the control with different initial nonlinearities. We restrict ourselves here to setups with $\lambda_0 = 0.10$ and $\lambda_0 = 0.25$, which mark the important changes in the initial nonlinearity. For further information about additional simulations see the Appendix.

Now we look at an initial nonlinearity of $\lambda = 0.10$ for both the digital and the differential control. In Figs. 7.12 and 7.13 we can see the setups for $\lambda_0 = 0.10$. As already described, control fails for $\beta_0 = 0.25$, but the other cases show stable behaviour and differential control seems to be nearly perfect in all cases.

The range in which control changes the nonlinearity is much smaller than for the case $\lambda = 0.00$. That is obviously the case for these setups, because the initial conditions are closer to those required. So, as can be seen in the scheme without control (Fig. 7.4), this initial setup without control produces an exponent between the EW and the KPZ class. So here it is much easier to tune the function $\lambda(t)$ to the correct value. That is why, in the case of $\beta_0 = 0.29$, the range for both control types fluctuates between $\lambda(t) \in [0.1, 0.12]$, and increases in the case of higher exponents to a maximum of $\lambda(t) \sim 0.16$ for $\beta_0 = 0.33$.

These values give also an indication of how the system tends to behave in the KPZ class. It complies with the proposed value $\lambda = 0.25$ as a "strong coupling" value.

For the setup of this strong nonlinearity we now look again at the results. In Fig. 7.14 we see that the control works very well for higher β_0 and higher control strengths also lead to control behaviour (see appendix). It is not surprising that when the control works for small initial nonlinearities, it also works for larger ones. We can see that the function decreases slightly and then stabilizes, with more fluctuations in the late phase, but with a clearly stabilized growth exponent.

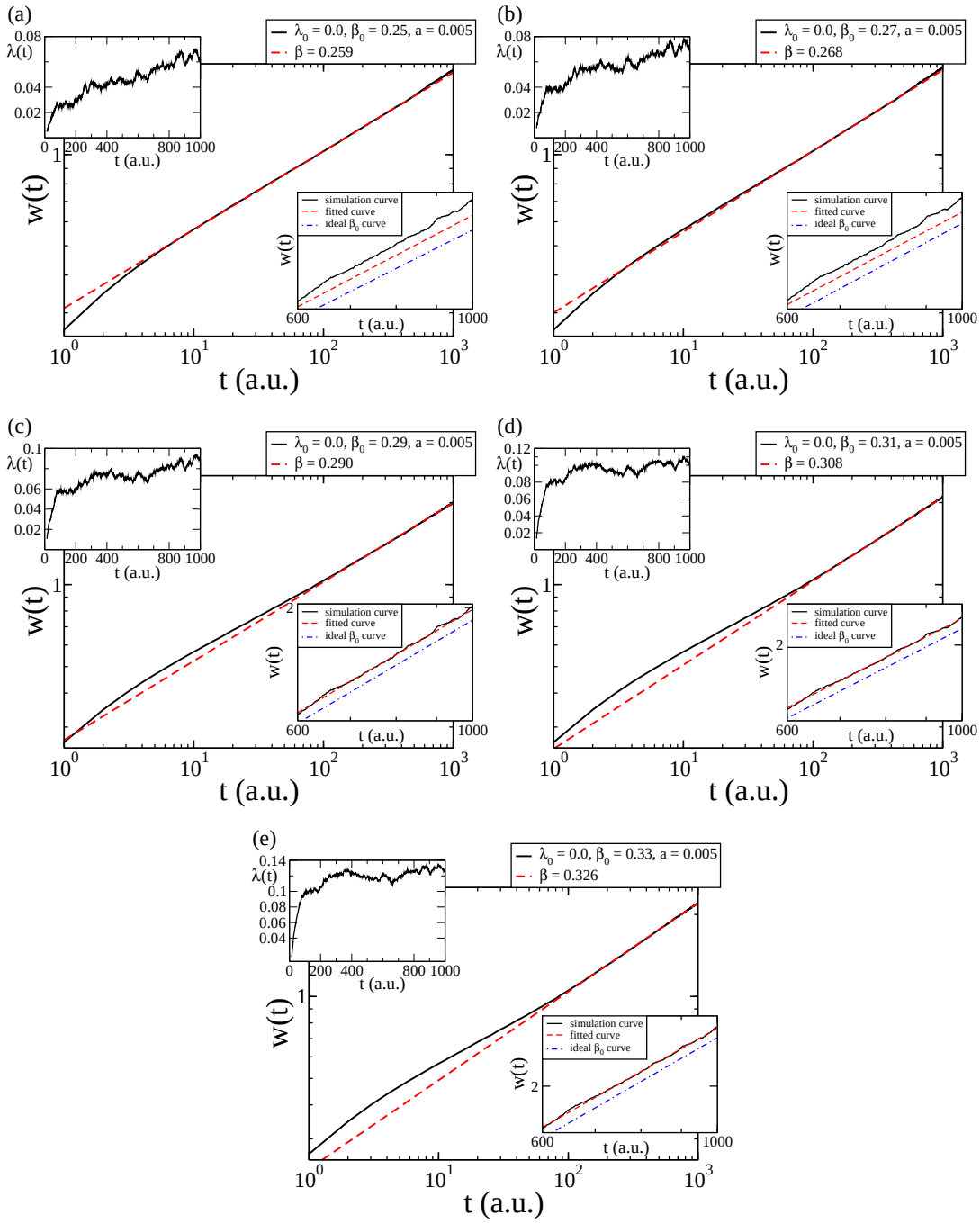

Figure 7.9: Digital control for the KPZ equation in 1+1 dimensions with a control setup: $\lambda_0 = 0.00$ and $a = 0.005$ for five different desired control values of: (a) $\beta_0 = 0.25$, (b) $\beta_0 = 0.27$, (c) $\beta_0 = 0.29$, (d) $\beta_0 = 0.31$, (e) $\beta_0 = 0.33$, time discretization $dt = 0.005$, upper left insets show the functions $\lambda(t)$, lower right insets show the roughness in the late phase in double logarithmic plot.

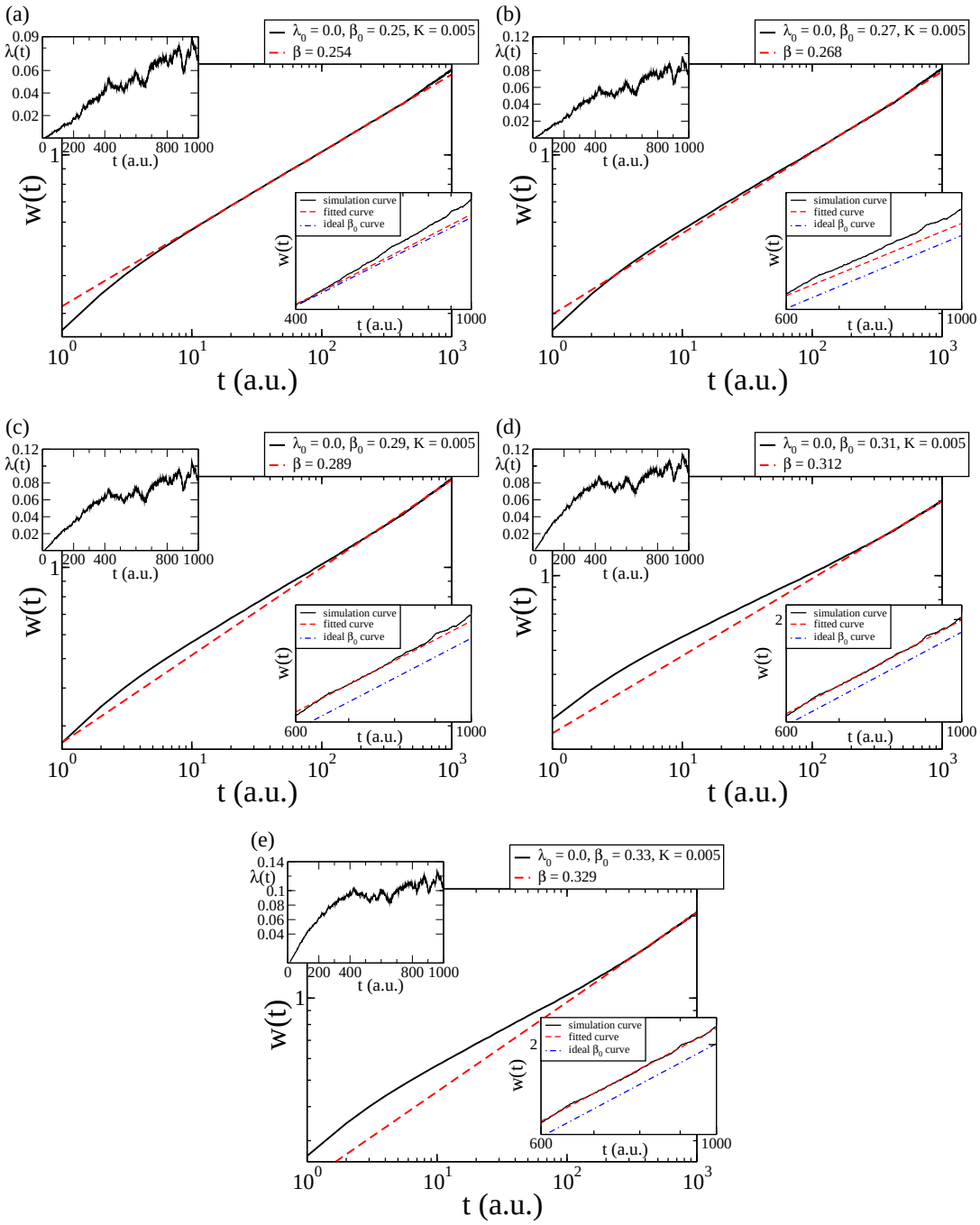

Figure 7.10: Differential control for the KPZ equation in 1+1 dimensions with $\lambda_0 = 0.00$ and $K = 0.005$ for five different desired control values of: (a) $\beta_0 = 0.25$, (b) $\beta_0 = 0.27$, (c) $\beta_0 = 0.29$, (d) $\beta_0 = 0.31$, (e) $\beta_0 = 0.33$, time discretization $dt = 0.005$, upper left insets show the functions $\lambda(t)$, lower right insets show the roughness in the late phase in double logarithmic plot.

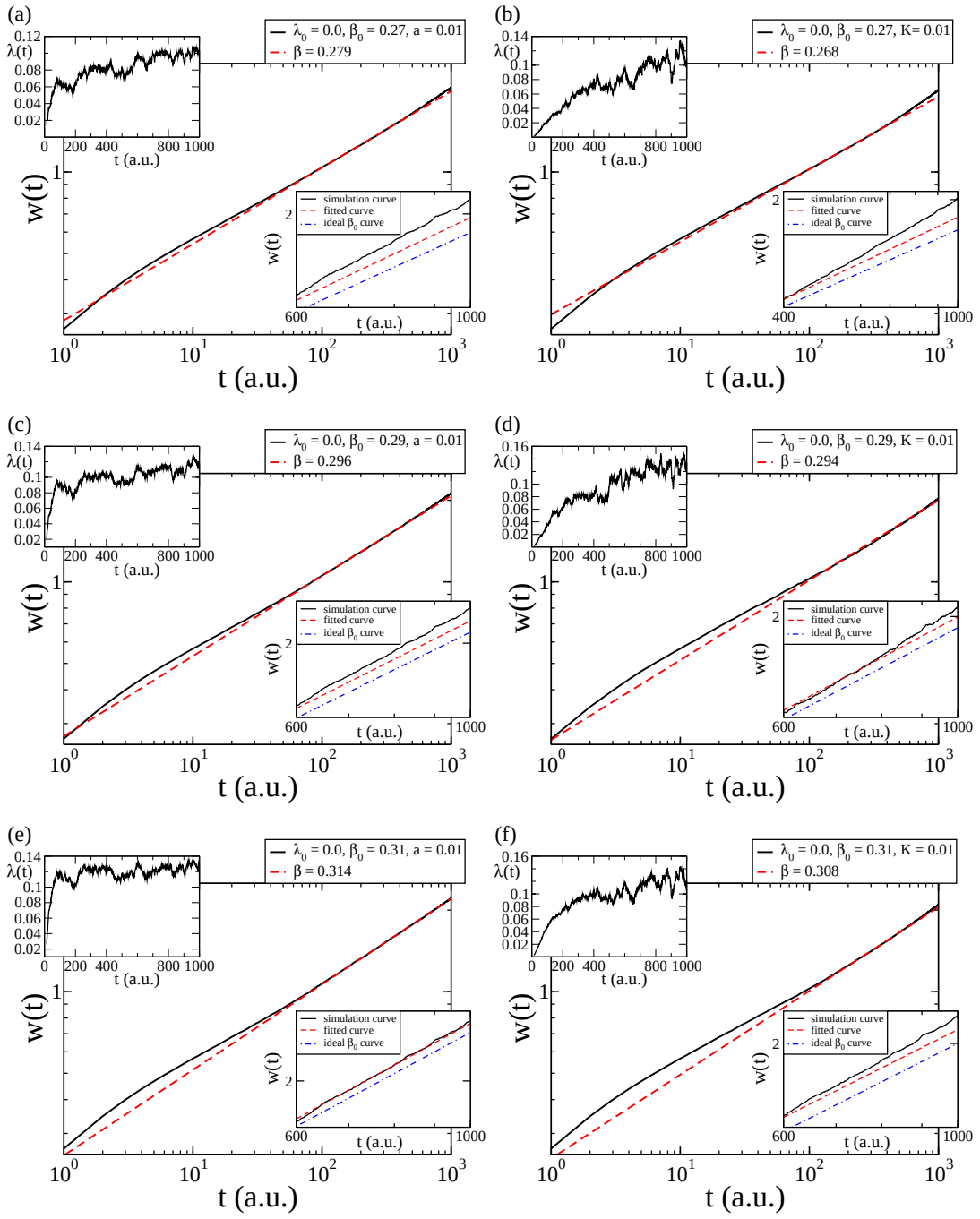

Figure 7.11: Digital and differential control for the KPZ equation in 1+1 dimensions with $\lambda_0 = 0.00$, $a = 0.01$ respectively $K = 0.01$ for three different desired control values of: (a,b) $\beta_0 = 0.27$, (c,d) $\beta_0 = 0.29$, (e,f) $\beta_0 = 0.31$, time discretization $dt = 0.005$, upper left insets show the functions $\lambda(t)$, lower right insets show the roughness in the late phase in double logarithmic plot.

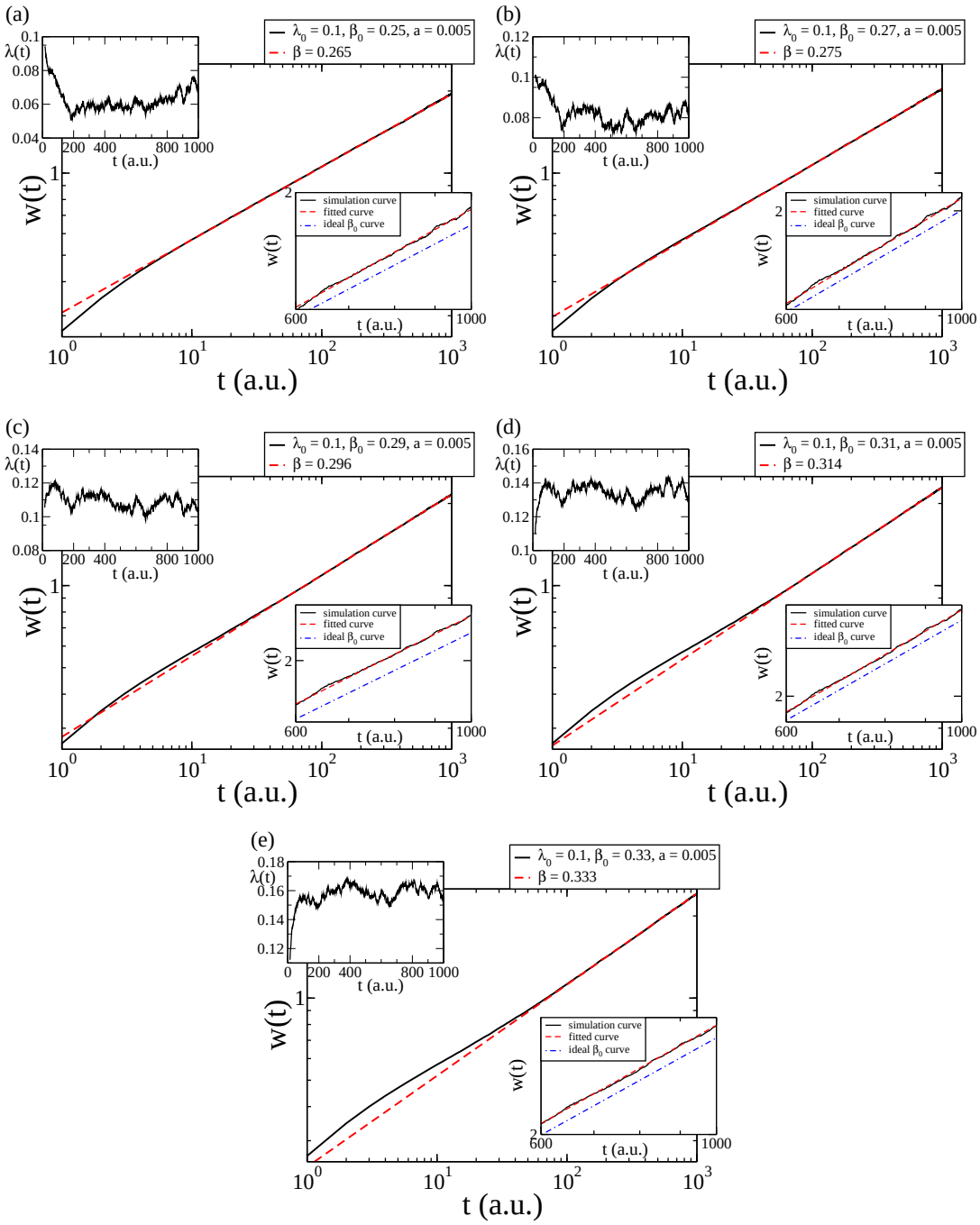

Figure 7.12: Digital control for the KPZ equation in 1+1 dimensions with a control setup: $\lambda_0 = 0.10$ and $a = 0.005$ for five different desired control values of: (a) $\beta_0 = 0.25$, (b) $\beta_0 = 0.27$, (c) $\beta_0 = 0.29$, (d) $\beta_0 = 0.31$, (e) $\beta_0 = 0.33$, time discretization $dt = 0.005$, upper left insets show the functions $\lambda(t)$, lower right insets show the roughness in the late phase in double logarithmic plot.

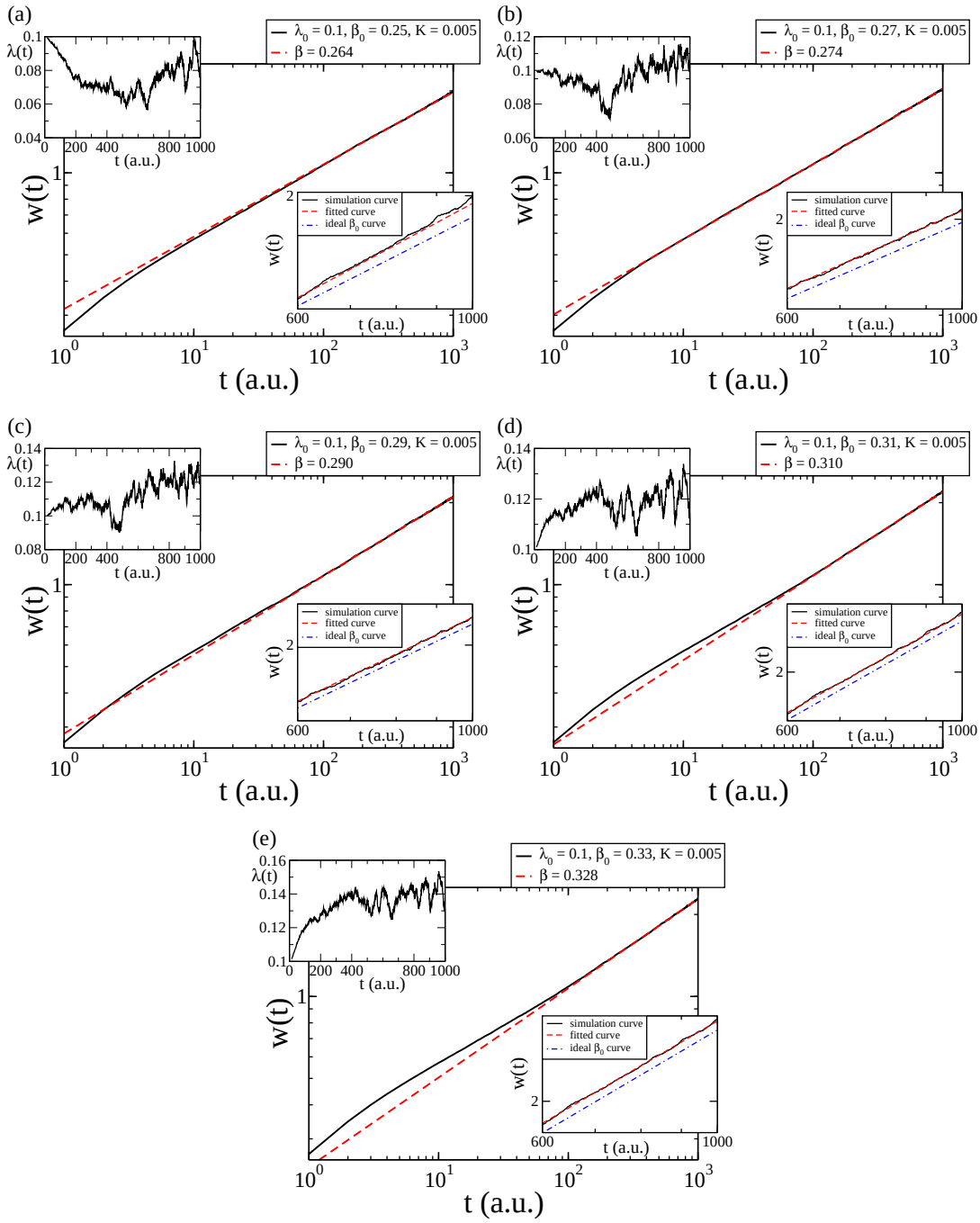

Figure 7.13: Differential control for the KPZ equation in 1+1 dimensions with $\lambda_0 = 0.10$ and $K = 0.005$ for five different desired control values of: (a) $\beta_0 = 0.25$, (b) $\beta_0 = 0.27$, (c) $\beta_0 = 0.29$, (d) $\beta_0 = 0.31$, (e) $\beta_0 = 0.33$, time discretization $dt = 0.005$, upper left insets show the functions $\lambda(t)$, lower right insets show the roughness in the late phase in double logarithmic plot.

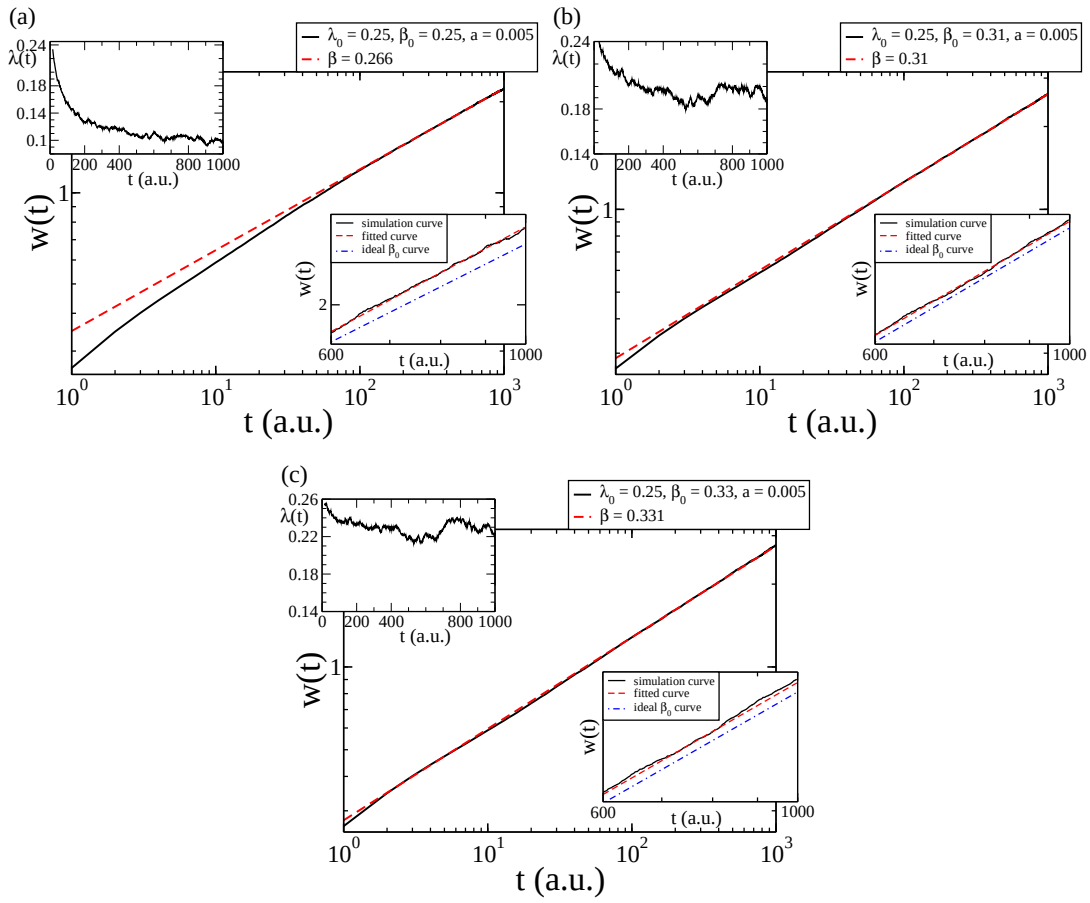

Figure 7.14: Digital control for the KPZ equation in 1+1 dimensions with a control setup: $\lambda_0 = 0.25$ and $a = 0.005$ for three different desired control values of: (a) $\beta_0 = 0.25$, (b) $\beta_0 = 0.31$, (c) $\beta_0 = 0.33$, time discretization $dt = 0.005$, upper left insets show the functions $\lambda(t)$, lower right insets show the roughness in the late phase in double logarithmic plot.

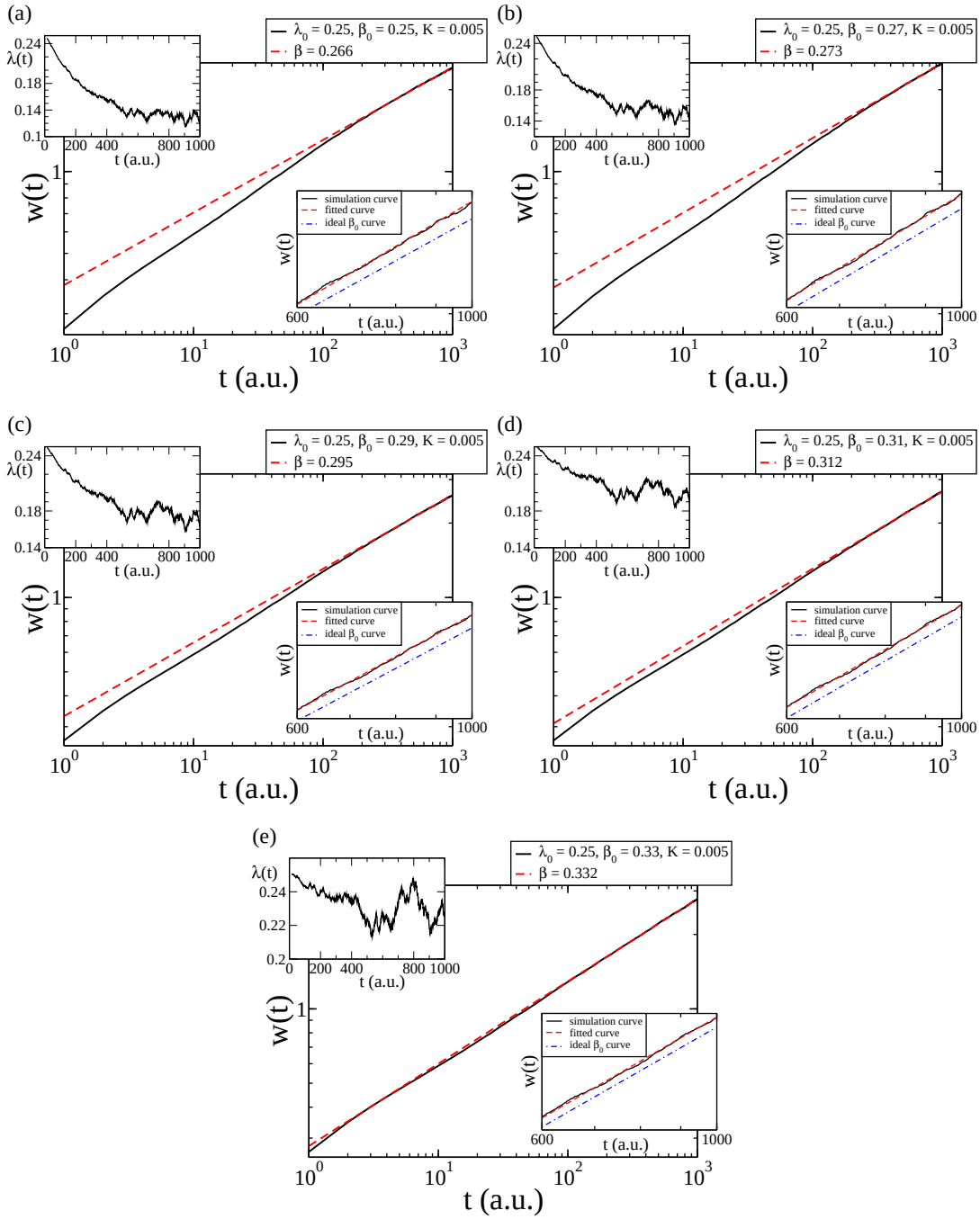

Figure 7.15: Differential control for the KPZ equation in 1+1 dimensions with $\lambda_0 = 0.25$ and $K = 0.005$ for five different desired control values of: (a) $\beta_0 = 0.25$, (b) $\beta_0 = 0.27$, (c) $\beta_0 = 0.29$, (d) $\beta_0 = 0.31$, (e) $\beta_0 = 0.33$, time discretization $dt = 0.005$, upper left insets show the functions $\lambda(t)$, lower right insets show the roughness in the late phase in double logarithmic plot.

7.1.4 The uncontrolled equation in 2+1 dimensions

We now want to look at the behaviour of the KPZ equation in 2+1 dimensions. As depicted in Fig. 7.16, the situation here is much more complicated. In the 1+1 dimensional case we got clear effective exponents in the early phase but they do not appear here. We used setups for the nonlinear terms in the equation in the range $\lambda \in [0, 0.1]$

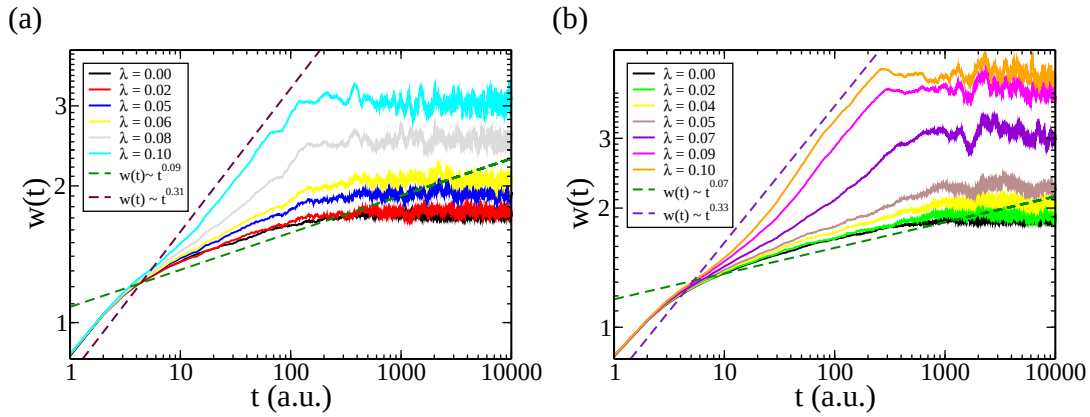

Figure 7.16: Longtime roughness evolution of the KPZ equation in 2+1 dimensions: w vs time t for different values of λ ($\lambda \in [0.0, 0.10]$) for (a) $L = 32 \times 32$ and (b) $L = 64 \times 64$ and time $t = 1000$, dashed lines denote the limits of the growth exponents for (a) $\beta \sim 0.09$ (b) $\beta \sim 0.07$ (green) and (a) $\beta \sim 0.31$ and (b) $\beta \sim 0.33$.

with system sizes $L = 32 \times 32\, l.s.$ (Fig. 7.16 (a)) and $L = 64 \times 64\, l.s.$ (Fig. 7.16 (b)).

Although we can not determine the exponents exactly by a direct method, we can nevertheless get an impression of the range in which β is valid for our scheme.

We can thereby check if our numerical scheme works. The bounds of possible exponents in the early phase are denoted by the dashed lines. We do not see a wide range of exponents over more than one decade, but on the other hand the dashed lines indicate that the exponents could be in the range $\beta \in [\sim 0.09; \sim 0.3]$ for both system sizes. This agrees with recent studies of the values of the KPZ-equation in 2+1 dimensions [Mos91]. Additionally, as in our findings for 1+1 dimensions, the local exponents and also the roughness w(t) increase with the value of λ.

This behaviour is not surprising since, as we have already pointed out in Sec. 5.1.2, the determination of the critical exponents of the KPZ equation in 2+1 dimensions is still an open problem. It would be much more surprising if we could determine them by a simple direct method.

Most recent studies have tried to tackle this problem using stochastic models and Monte Carlo or Kinetic Monte Carlo methods. The renormalization method fails in this case [Bar95; Mic04]. Models (see also Sec. 4.4.2) proposed for KPZ behaviour are expected to be in the class of ballistic deposition models (see Sec. 4.4.2). A variety of these models have appeared during the last decade, some using deposition to explain crystal growth ([Sar96; Osk06; Chi99]), others describing the two type particle

system ([Kol06]) and treating a lot of very different problems concerning growth and fluctuation phenomena.

All these slightly different approaches make the assumption that ballistic deposition models can explain phenomena related to the KPZ equation described above. The extracted exponents vary between $\beta \in [0.1, 0.25]$ and are close to the expected exponent $\beta = 0.25$. But the exact values remain unknown (newer findings for specific problems can be found in [Hor06; Rei06; Gha06; Fog06]). A very short analysis of simple ballistic deposition where we implemented the simple version introduced by Meakin *et al* [Mea86] and later further explained by Baiod *et al* [Bai88] can be seen in the App. B.1. Our results agree with their findings and the exponents are in the range expected for the KPZ universality class.

If our numerical solution of the equation does not give the growth exponent directly, nevertheless the control can give some indication of its value.

Because of the behaviour shown in Fig. 7.16 we can not ensure that our numerical scheme will work, so we have to strengthen the approach by looking at the roughness exponents.

For this calculation we make use of both the height-height correlation and the height-difference correlation function. In Fig. 7.17 we see the behaviour of the correlation functions for one setup with three different initializations of the random generator. We took a nonzero nonlinearity $\lambda = 0.05$ for a now larger system of $L = 128 \times 128\, l.s.$ and we use this for the control too. Although the extracted exponents α for the height-

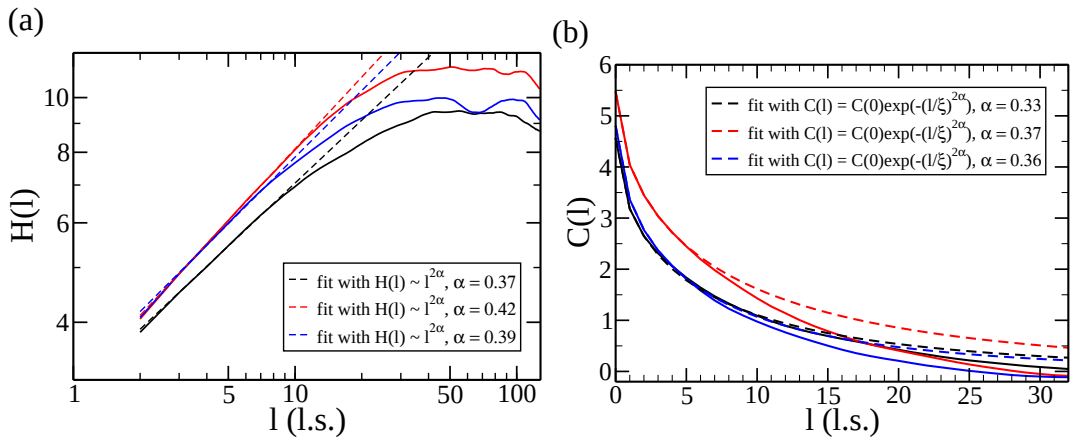

Figure 7.17: Determination of the roughness exponent for different samples for $L = 128 \times 128$, $\lambda = 0.05$ and time $t = 1000$, (a) height-difference correlation, dashed lines are fits for the small length behaviour to calculate α (b) height-height correlation, three initializations of the random generator were used, dashed lines are fits with $C(l) = C_0 exp(-(l/\xi)^{2\alpha})$.

height correlation give smaller values ($\alpha \sim 0.35$) than for the height-difference method ($\alpha \sim 0.40$) both values are in the range proposed for the KPZ model by numeri-

System size	$L = 128 \times 128$
Time of onset of control	$t_0 = 10$
End of control	$t_e = 1000$
Initial nonlinear term	$\lambda_0 \in [0, 0.1]$
Time delay	$\tau = 1$
Strength of the digital control	$a \in (0.005 : 0.01]$
Strength of the differential control	$K \in (0, 0.10]$
desired value of the growth exponent	$\beta_0 \in [0, 1/4]$
time discretization	$dt = 0.005$
Averages	10 realizations

Table 7.2: Parameter ranges for the control of the KPZ equation in 2+1 dimensions.

cal solutions of the equation [Mos91] or using different ballistic deposition models [Bai88; Bar95; Mic04; Gha06; Sar96].

We do not see clear growth exponents. That may be due to the fact that saturation sets in when the nonlinear term in the equation becomes responsible for roughening. Alternatively we see a short very early phase, also called *random growth* ([Rei06]), which then reaches the saturation phase very fast. The phase in between, called the *correlated* growth phase by Reis (it is responsible for the growth exponent), then can become very small (see [Rei06]).

In this case, control can be applied to the equation to stabilize it in a given range.

7.1.5 With control in 2+1 dimensions

We now determine the range for control. We again use a range $t \in [10, 1000]$. Once again the control sets in at time $t_0 = 10$ in order to exclude effects occurring during the very early phase (Fig. 7.16).

The question is, if it is useful to apply our scheme here. Further investigations will have to clarify what control can tell us about the behaviour of the continuum function, but we nevertheless tried control and got surprising results.

At first setups for $L = 128 \times 128\ l.s.$ with a strong initial nonlinearity $\lambda = 0.10$ were investigated, which should give larger β corresponding to the KPZ class (consistent with Moser *et al* [Mos91]).

As we can see in Fig. 7.18, the equation for the digital scheme shows control behaviour in 2+1 dimensions, too. We tried to adjust the exponents between those expected from the EW class ($\beta = 0$) and the KPZ class ($\beta \sim 0.25$). Control for $\beta > 0.30$ failed in all cases, but we got local control for $\beta_0 \leq 0.25$. The scheme adjusts the lower value of β_0 for only a very small time range, but seems to work very well for the desired exponents $\beta_0 \in \{0.20; 0.25\}$.

Looking at the insets, it can be seen that fluctuations arise in the cases of $\beta_0 = 0.2$ and $\beta_0 = 0.25$, where the roughness increases briefly and is then restabilized by the scheme to the desired exponent.

For values of β closer to the EW class the local increase in roughness is not restabilized. So if the aim is to adjust and then stabilize the values using the time delayed feedback, then control obviously fails in this case.

The function $\lambda(t)$ shows similar behaviour as in the 1+1 dimensional case: it first decreases and then stabilizes at a certain value. When the setups fail we observe first an initial decrease and then a monotonic increase in the fluctuations of λ. We had similar problems controlling the EW value in the case of the 1+1 dimensional equation, but here this deviation is much more relevant and, in contrast to the case in 1+1 dimensions, can not be controlled. Different factors could give rise to this behaviour:

- the problem of a zero nonlinearity λ which acts as a border, where all other λ lead to higher exponents (symmetry of the equation)
- too large fluctuations in the late time range
- too small system sizes, which encourage fluctuations
- the EW class exponent is generally not adjustable

The first point is partly responsible but, as we saw for 1+1 dimensions, its influence can be decreased by decreasing the time discretization dt. We proved that point, but got no noticeable differences.

If those fluctuations which can not be compensated for fast enough play an essential role, then differential control should be more stabilizing as a fast reacting control (see the results for KPZ equation in 1+1 dimensions). And in fact, if we look at the results for the same initial setups with the differential scheme, the control is also better for smaller exponents (see Fig. 7.19).

But there are still effects on the evolution of roughness. The tendency to late roughening against the control is still present.

The fourth point we can simply not prove here. If we see an improvement when we change from digital time delay to differential time-delayed feedback, it might indicate that control is also possible for small values of β_0.

However the EW class with $\beta = 0$ is a special case. Here we can not see a really stable exponent in the roughness evolution (see Fig. 7.16). So $\beta = 0$ just means that the roughness scales logarithmically with t.

Although we have not entirely solved this problem, we strongly suggest that tests be made with ballistic deposition models and control to reproduce the behaviour and give further information.

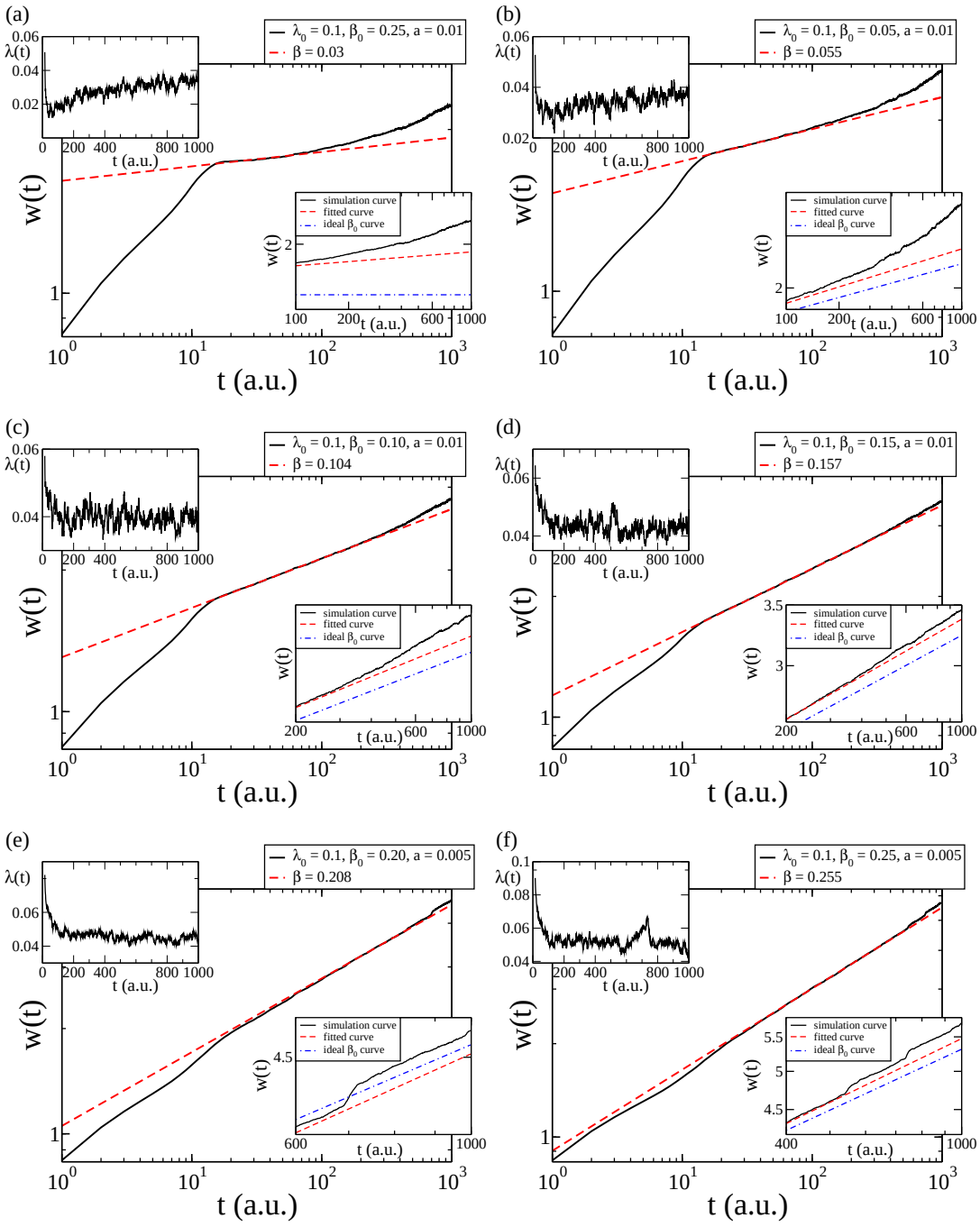

Figure 7.18: Digital control for the KPZ equation in 2+1 dimensions with $\lambda_0 = 0.10$, $\beta_0 \in \{0.00; 0.05; 0.10; 0.15; 0.20; 0.25\}$, time delay $\tau = 1$ and control strengths of $a = 0.01$ ((a), (b), (c), (d)) and $a = 0.005$ ((e), (f)), upper left insets show the functions $\lambda(t)$, lower right insets show the roughness in the late phase in a logarithmic plot.

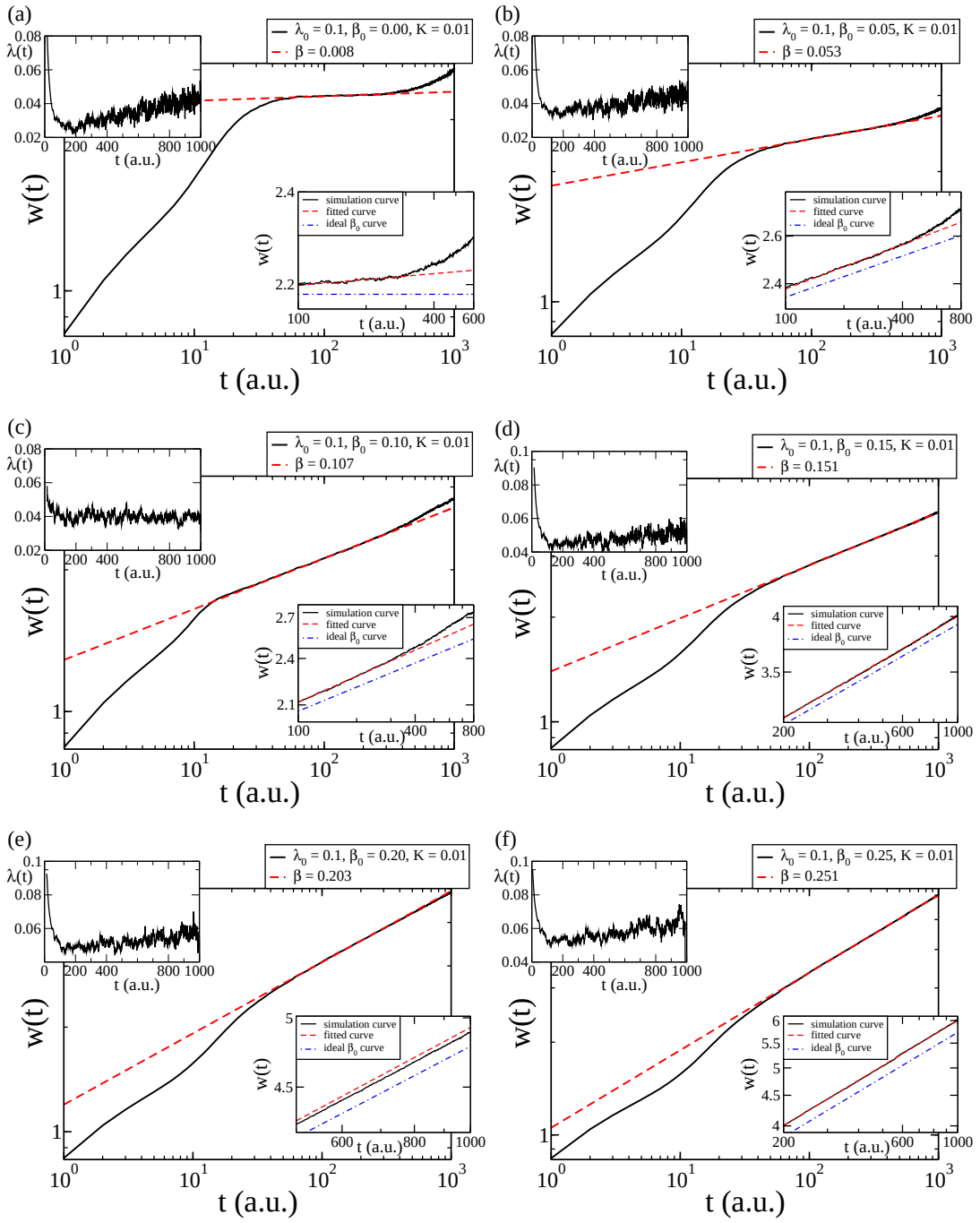

Figure 7.19: Differential control for the KPZ equation in 2+1 dimensions with $\lambda_0 = 0.10$, $\beta_0 \in \{0.00; 0.05; 0.10; 0.15; 0.20; 0.25\}$, time delay $\tau = 1$ and a control strength of $K = 0.01$, upper left insets show the functions $\lambda(t)$, lower right insets show the roughness in the late phase in a logarithmic plot.

We get the best results for the desired exponents around the values expected for KPZ-behaviour ($\beta_0 \in \{0.2; 0.25; 0.3$). Here we see really stable exponents in the region where the control acts on the equation. This is surprising, because we do not get such clear behaviour without control. There could be various reasons for this. Where the nonlinearity is the leading term in the equation and depends strongly on local gradients of the height function, then, by definition, the control acts not only to control the equation but also to control the unwanted numerical fluctuations.

The nonlinearity decreases briefly in all cases, and then stabilizes at different values for the desired exponents. In the late phase, where numerical fluctuations are much more in evidence, small β_0 can not be controllled. So roughness increases again for small β_0, whereas it does not increase for the nearby KPZ exponents.

This may indicate that in this case we can control roughness and also get some information about a realistic KPZ exponent in 2+1 dimensions.

We now also show digital control and differential control setups for $\lambda_0 = 0.00$ in Fig. 7.20,

Whereas the control adjusts the exponents in the expected way for the higher exponents, it fails for small β_0 (not shown). In the setups the control functions $\lambda(t)$ show behaviour similar to that observed for 1+1 dimensions. For small initial nonlinearities and higher exponents the functions increase to a certain value.

So also in this case, the growth exponent seems to be only adjustable around the value $\beta_0 = 1/4$, where it is very well tunable.

Nevertheless, there should be some comparable results from, for instance, ballistic deposition models related to KPZ-behaviour to ensure that the above explanations are indeed responsible for the behaviour.

For initial nonlinearities in between the presented values we see very similar behaviour, some of the additional simulations can be seen in the Appendix A.2.

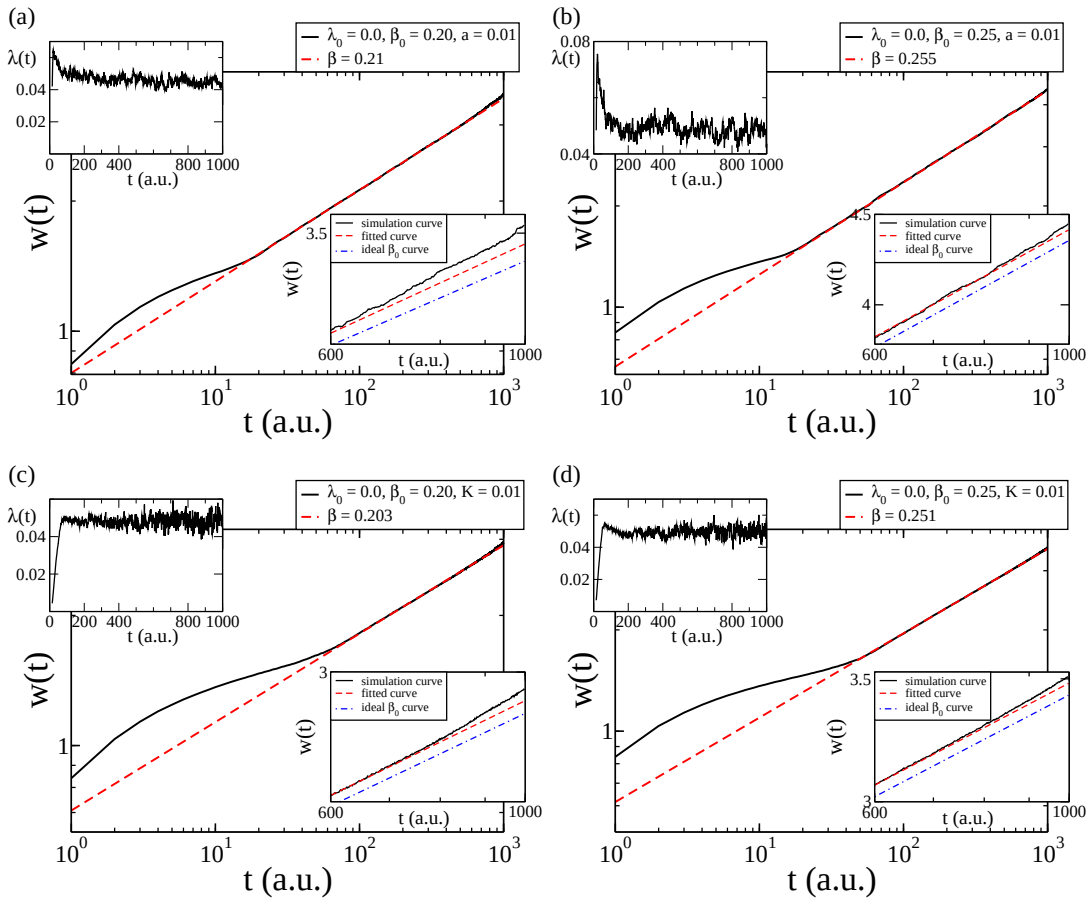

Figure 7.20: Digital and differential control for the KPZ equation in 2+1 dimensions with $\lambda_0 = 0.0$, $\beta_0 \in \{0.20; 0.25\}$, time delay $\tau = 1$ and a control strength of $a = 0.01$,$K = 0.01$, respectively. Upper figures: digital contro, lower figures: the corresponding differential cases. Upper left insets show the functions $\lambda(t)$, lower right insets show the roughness in the late phase in a logarithmic plot.

7.2 The MBE Equation

We have already shown that our control scheme works for the KPZ equation in 1+1 dimensions and have the impression that it could also partly work in 2+1 dimensions. We now want to apply our scheme to the growth equation proposed to explain Molecular Beam Epitaxy. In general control should also be applicable to the growth exponent in this equation. For the MBE equation with $\lambda_1 = 0$ (Eq.(5.21)) and the equation with $\lambda_1 > 0$ (Eq.(5.23)) the roughness exponents α are not the same, as has already been explained in Sec. 5.2.

The proposed exponents are:

$$\begin{aligned} \beta &= 3/8 \qquad \alpha = 3/2 \qquad z = 4 \qquad \text{for} \qquad \lambda_1 = 0 \\ \beta &= 1/3 \qquad \alpha = 1 \qquad z = 3 \qquad \text{for} \qquad \lambda_1 > 0 \end{aligned} \tag{7.4}$$

We follow the same steps as for the KPZ equation. First we apply our scheme to 1+1 dimensions.

7.2.1 Without control in 1+1 dimensions

In the case of 1+1 dimensions the fourth order term makes it rather difficult to see any saturation in the roughness. Therefore we first use very small systems $L = 32\ l.s.$ and $L = 64\ l.s.$ which obviously are not useful for control. Nevertheless they should show saturation and thereby help test the numerical scheme and the determination of the exponents without control by rescaling.

In Fig. 7.21 we see the data collapse from the rescaled functions and can determine the exponents. As before, we have used three different setups, $\lambda_1 \in \{0, 0.05; 0.10\}$ for a time $t = 100000$. We see that the data collapse into single curves for all setups and we get slightly different values for the growth exponent consistent with the proposed exponents.

We now look more closely at the early behaviour of a larger system $L = 8192$, which appears reasonable for the control scheme. As we can see in Fig. 7.22, we get differences that look very small on the logarithmic scale. Obviously the differences appear more clearly in the late phase between $t \sim 500$ and $t = 10000$.

The zero nonlinear term gives an exponent of $\beta = 0.374$ close to $\beta = 3/8$ and the nonlinear term $\lambda_1 = 0.08$ gives a value $\beta = 0.336$ close to the value $\beta = 1/3$.

Of course, if our solution reproduces the scaling of the MBE class, the saturation for this system size can not be reached in a computationally useful time. If we assume an exponent of $\alpha = 1$ for nonzero nonlinearity and get a time t_x from the above simulation, the saturation then sets in at $t \sim 500000$ and can be clearly seen for $t > 10000000$ with one decade saturation. For zero nonlinearities the case would be much more extreme. As we see in Fig. 7.21, saturation sets in later for $t_x \sim 5000$ and with an expected exponent of $\alpha = 1.5$ we would see saturation at approximately $t \sim 20 \cdot 10^6$.

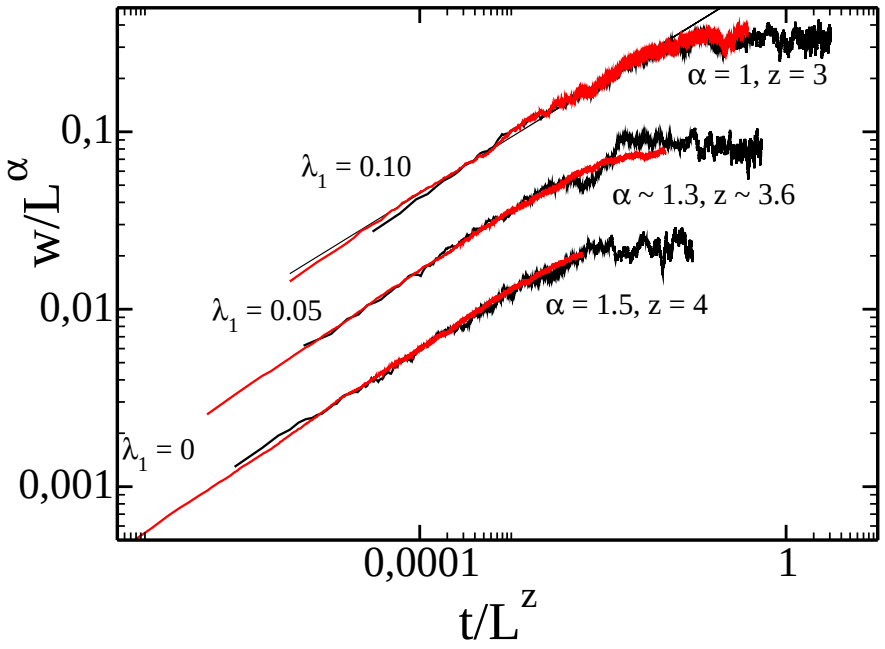

Figure 7.21: Roughening of the MBE equation in 1+1 dimensions for setups with $L = 32$ and $L = 64$, $t = 100000$ and three different initial nonlinearities $\lambda \in \{0; 0.05; 0.10\}$ with a time step $dt = 0.05$, setup for $\lambda = 0.1$ shifted by a factor 4 in y-axis, setup for $\lambda = 0.05$ shifted by a factor 2 in y-axis, 20 averages for both systems.

So it is obviously impossible to reach saturation with a simulation. The time scale is different for the MBE equation in 1+1 dimensions so we have to change the time range in which we apply the scheme of control. We can use the same onset of control time $t_0 = 10$ and, if early roughening from the flat surface does not influence the behaviour of the equation, we expand the control to $t_e = 10000$. This is much more computationally demanding but promises clear results. In the case of the KPZ equation we saw that distinguishing the five different desired growth exponents β_0 is quite easy, but here we restrict ourselves to three different values: the limiting exponents $\beta_0 = 3/8$ and $\beta_0 = 1/3$ and one exponent in between, $\beta_0 = 0.35$. The control results would otherwise be speculative.

As already explained, the critical exponents depend on long time scaling behaviour. To ensure scaling for the early development of the interface as well we have to check the roughness exponents.

Therefore we calculate the structure function. In Fig. 7.23 we see the results of rescaling, once again using the Family-Vicsek relation. We used very different setups with different system sizes $L \in \{256; 1024; 4096; 8192\}$, a nonlinearity $\lambda_1 = 0$ and different times. In this case not all interfaces reach saturation. In the left hand panel we see the unrescaled functions, which in the case of scaling have to match the others in the descending part of the curve. After rescaling by $k \to kt^{1/z}$ and $S(k,t) \to S(k,t)k^{-(2\alpha+1)}$ they have to collapse into one single curve as we can see in the right

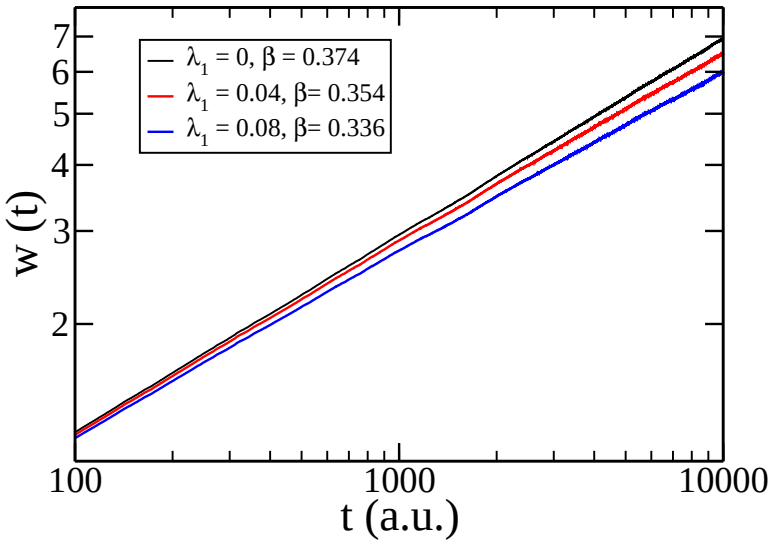

Figure 7.22: Early roughening of the MBE equation in 1+1 dimensions for a setup with $L = 8192$, $t = 10000$ and five different initial nonlinearities $\lambda \in \{0; 0.04; 0.08\}$ with a time step $dt = 0.01$.

hand panel. This rescaling only works if we use the correct exponents, so we used $\alpha = 3/2$ and $z = 4$, giving a growth exponent $\beta = 3/8$ ($\beta = \alpha/z$). Having described

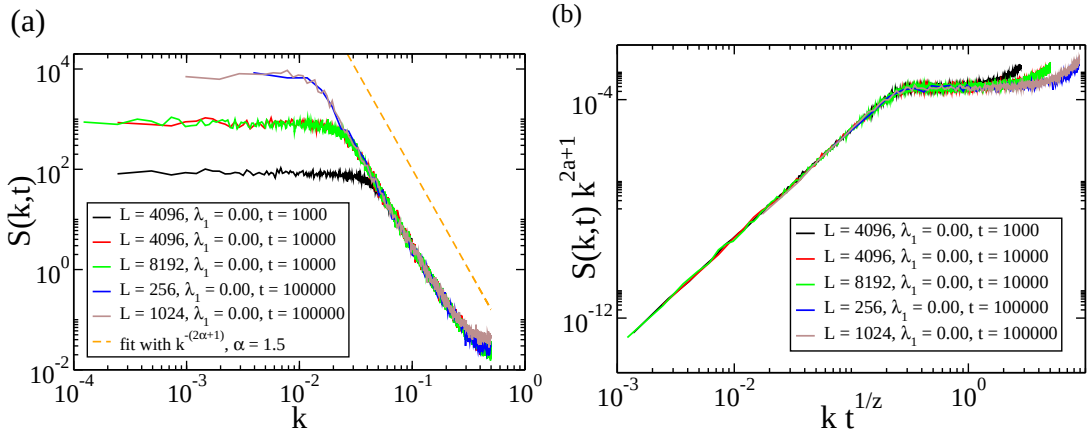

Figure 7.23: Data collapse by structure function $S(k, t)$ for the MBE equation in 1+1 dimensions for five different setups (legends): (a) the structure function, (b) the rescaled function by the Family-Vicsek relation.

the scheme without control, we now take a look at behaviour for "small" times. In case of the MBE equation for 1+1 dimensions we get relatively clear-cut behaviour for the growth exponent over a wide range. In comparison to the KPZ equation, the difference between zero and nonzero nonlinearity λ_1 appears at a much later phase of the roughness evolution for similar values of the simulation parameters, namely

System size	$L = 8192\, l.s.$
Time of onset of control	$t_0 = 10$
End of control	$t_e = 10000$
Initial nonlinear term	$\lambda_{1,0} \in [0, 0.1]$
Time delay	$\tau = 1$
Strength of the digital control	$a \in (0.0005, 0.002]$
Strength of the differential control	$K \in (0.0005, 0.002]$
desired value of the growth exponent	$\beta_0 \in [1/3, 3/8]$
time discretization	$dt = 0.01$
Averages	10 realizations

Table 7.3: Parameter ranges for the control of the MBE equation in 1+1 dimensions

$L = 4096 l.s.$, $D = 0.50$ and $\nu_1 = 0.10$.

7.2.2 With control in 1+1 dimensions

By tests for control with that parameters, our control seemed to work, but did not show really clear exponents without large fluctuations (not shown).

So we have to enlarge the systemsize and the control time.

In the simulations here shown we used $L = 8192\ l.s.$ (see appendix for further simulations) and a larger time $t_e = 10000$. Time discretization is set to $dt = 0.01$ in all setups. Table 7.3 lists the used parameters for the shown results.

In Fig. 7.24 and Fig. 7.25 we show the results for an initial nonlinearity of $\lambda_{1,0} = 0.0$.

In contrast to the KPZ equation, this initialization corresponds to a higher value of the growth exponent as explained in detail in Sec. 6.2. A working control also has to react in a contrasting way. This behaviour can be seen for the setups in both digital and differential control. In order to adjust the desired exponents, the control functions now increase to tune the lower β_0, as predicted by the theory.

As expected we get a control behaviour for the MBE equation in 1+1 dimensions. Due to the required long time simulations to clarify the difference between the two universality classes we here restrict to the setups shown, where the uncontrolled results and the results with digital and differential control for λ_1 show, that also for other setups one can expect working adjustment of the desired exponents (see Appendix for further simulations).

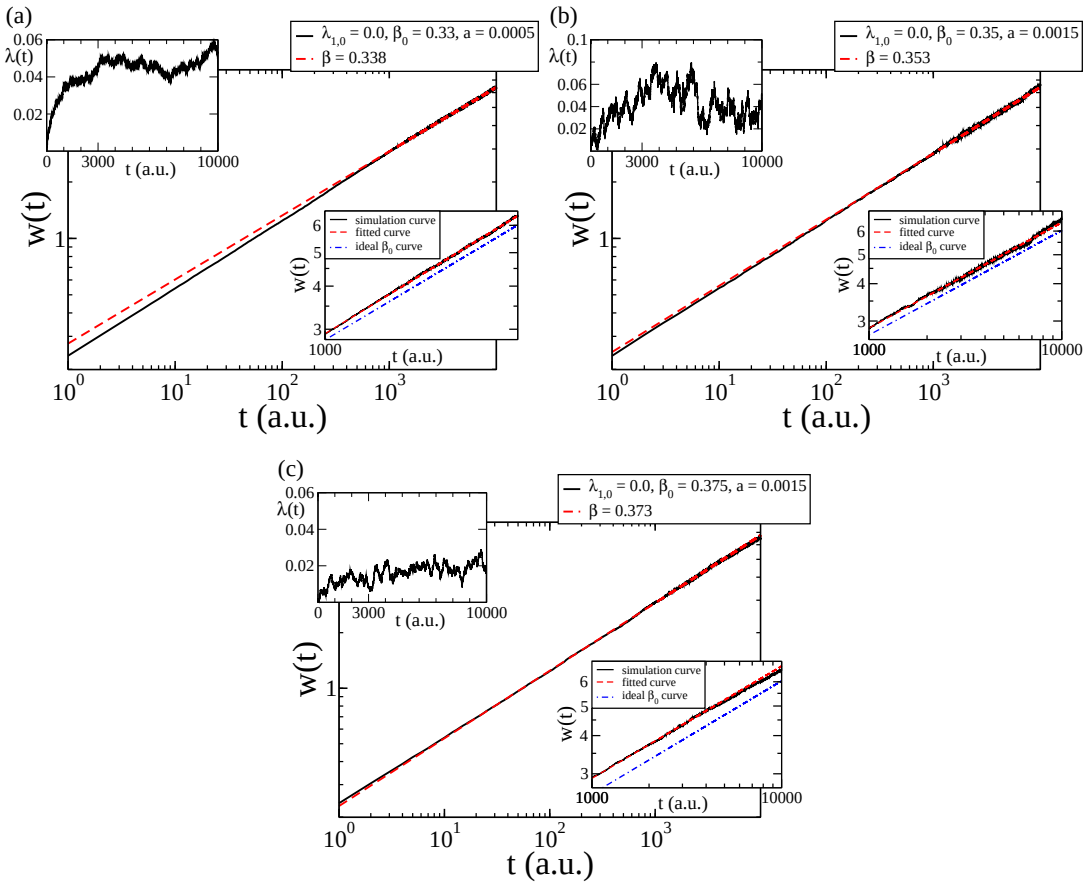

Figure 7.24: Digital control for the MBE equation in 1+1 dimensions with a control setup: $\lambda_{1,0} = 0.00$ and $a = 0.005$ for three different desired control values of: (a) $\beta_0 = 0.33$, (b) $\beta_0 = 0.35$, (c) $\beta_0 = 0.375$, time discretization $dt = 0.01$, upper left insets show the functions $\lambda(t)$, lower right insets show the roughness in the late phase in a logarithmic plot.

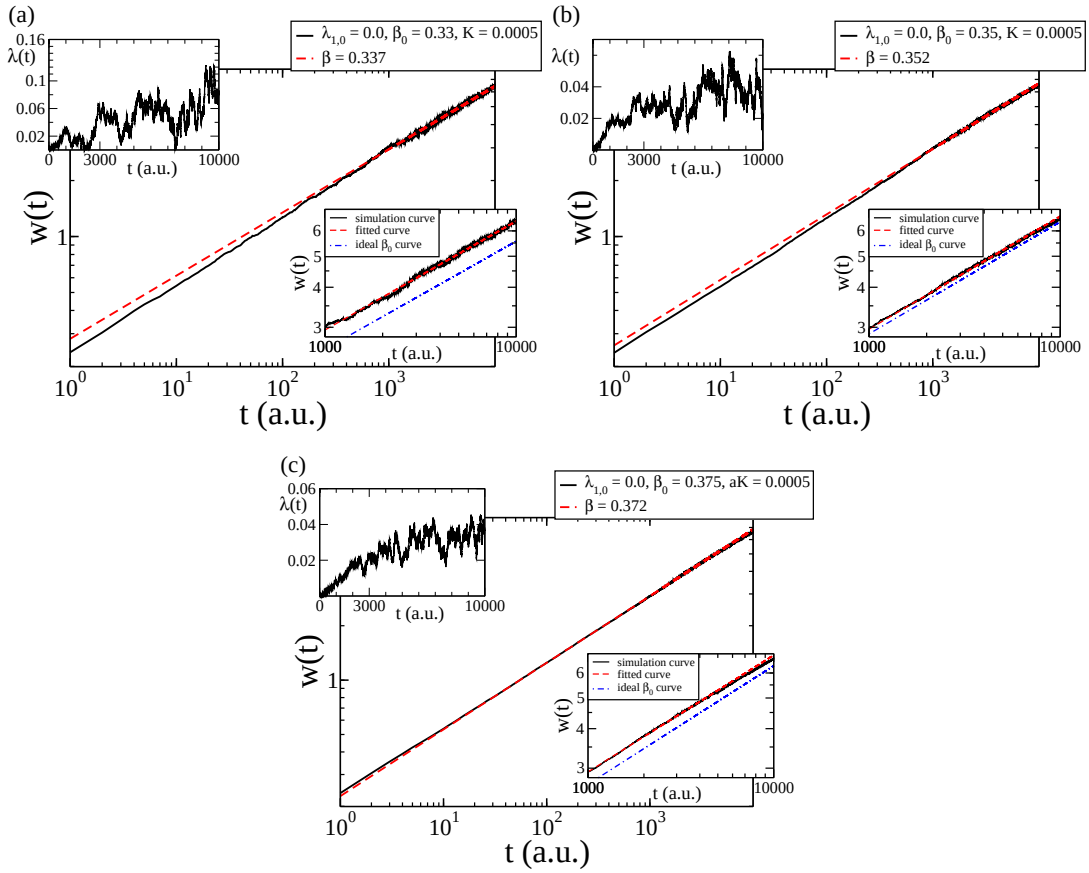

Figure 7.25: Differential control for the MBE equation in 1+1 dimensions with $\lambda_{1,0} = 0.00$ and $K = 0.005$ for three different desired control values of: (a) $\beta_0 = 0.33$, (b) $\beta_0 = 0.35$, (c) $\beta_0 = 0.375$, time discretization $dt = 0.01$, upper left insets show the functions $\lambda(t)$, lower right insets show the roughness in the late phase in a logarithmic plot.

7.2.3 Without control in 2+1 dimensions

We now come to the 2+1 dimensional case. For the KPZ equation in 2+1 dimensions we obtained a control that was very difficult to apply. The control behaviour was very difficult to interpret as we could not find a clear exponent for the roughening phase. Obviously here the situation seems to be much easier, as can be seen from Fig. 7.26. We used setups for $L = 32 \times 32\ l.s.$ and $L = 64 \times 64\ l.s.$ for the data collapse. The

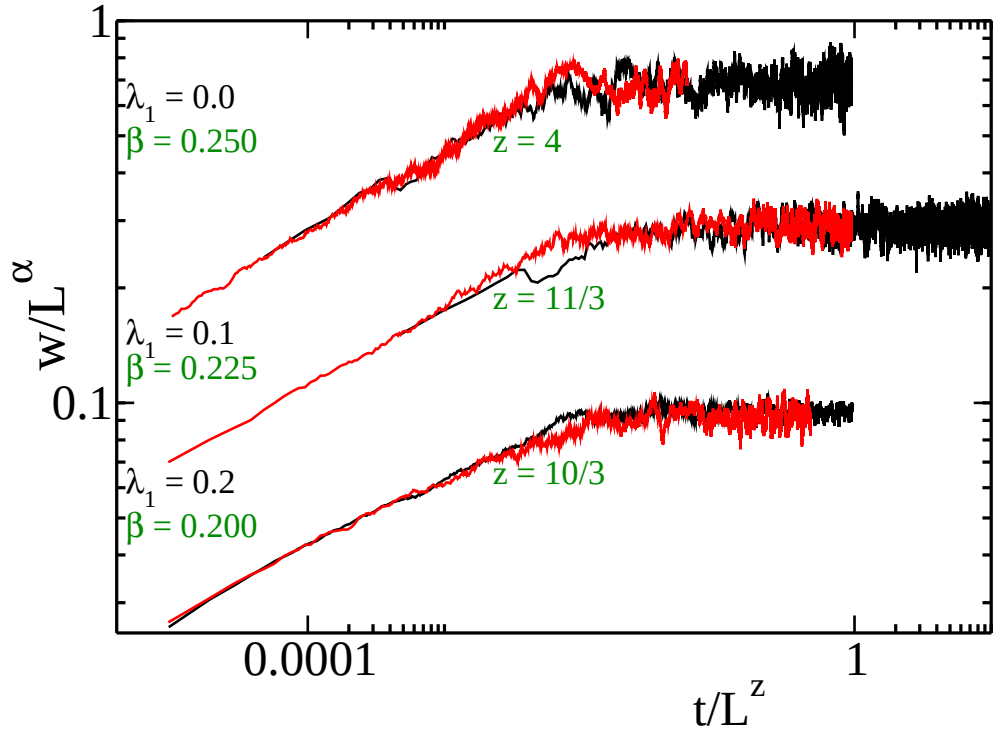

Figure 7.26: Data collapse for the MBE equation in 2+1 dimensions with two system-sizes $L \times L = 32 \times 32$ (black) $L \times L = 64 \times 64$ (red) and with three different initial λ_{1_0}, $\nu_1 = 0.1$ and $D = 0.5$ kept constant for all simulations.

parameters for the uncontrolled case were $\lambda_1 \in \{0; 0.1; 0.2\}$ with times $t = 10000000$ for the smaller system and $t = 1000000$ for the second system size. All setups give a data collapse for rescaling with $t \to t/L^z$ and $w \to w/L^\alpha$. For zero nonlinearity $\lambda_1 = 0$ we see that the exponents for rescaling $\alpha = 1$ and $z = 4$ agree with the expected exponents for the equation. The strongly nonlinear term of $\lambda_1 = 0.2$ also produces the expected exponents $\alpha = 2/3$ and $z = 10/3$. As for the other equations, the third case shows clear behaviour, where exponents of $\alpha \sim 0.82$ and $z \sim 3.7$ lead to a data collapse.

So the requirements for possible control are fulfilled. We have a clear behaviour at the limiting borders determined by the zero nonlinearity and a strong enough nonlinear term. Additionally we see an effective exponent in between the limiting borders.

We now look at the short time behaviour of larger systems $L = 128 \times 128\, l.s.$.In Fig. 7.27 we see that we can measure the different values of β very well in this case. The borders are given by the critical exponents of the universality classes. We now

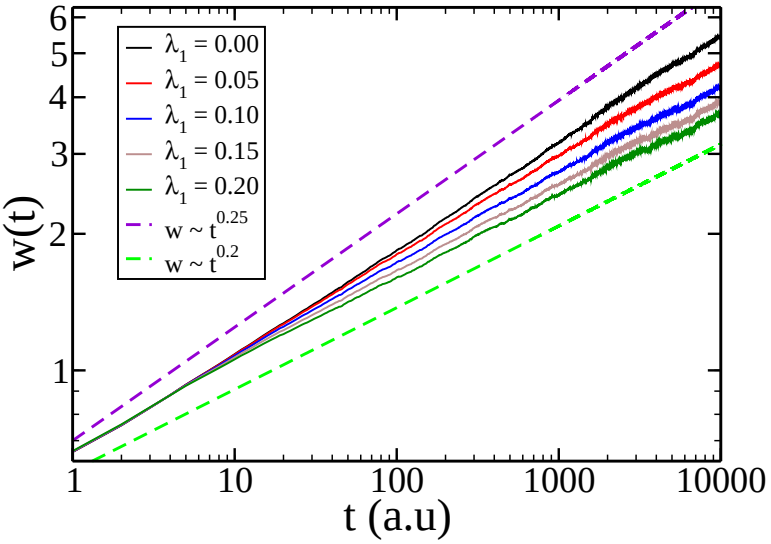

Figure 7.27: Early roughness evolution of the MBE equation in 2+1 dimensions $w(t)$ vs time t with $\lambda_1 \in [0.0, 0.2]$ for $L = 128 \times 128$ and time $t = 1000$ with a time discretization $dt = 0.01$, dashed lines denote the limits of the growth exponents for $\beta_1 = 0.25$ (violet) and $\beta_2 = 0.20$ (green) as guides to the eye.

want to look briefly at roughening by means of the surface structure. In Fig. 7.28 we compared the surface structure after $t = 10$ (upper panels) and after $t = 10000$ (lower panels) for $\lambda_1 = 0$ (left) and $\lambda_1 = 0.20$. Whereas after $t = 10$ we see very similar results with a rough surface, the structure formation differs at $t = 10000$, as can be seen in the lower panels. For $\lambda_1 = 0.20$ we can see small clear structures overlaying a local rough surface. These structures do not arise in the left hand surface for $\lambda_1 = 0$. Although this analysis is just visual, a more precise analysis is possible using the height-height correlations in Fig. 7.29. The results of the extracted exponents for $\lambda_1 = 0$, $\alpha \sim 0.93$ and for $\lambda_1 = 0.2$ $\alpha \sim 0.67$ are close to those expected. In addition we can see greater roughness for the nonzero nonlinearity and a more pronounced first maximum in the correlation, which indicates the mean distance between the structures that occur (note that $C(0) = w^2$). Although it is quite difficult to depict this behaviour in 1+1 dimensions, we have the impression that it could be changed experimentally by controlling the roughening.

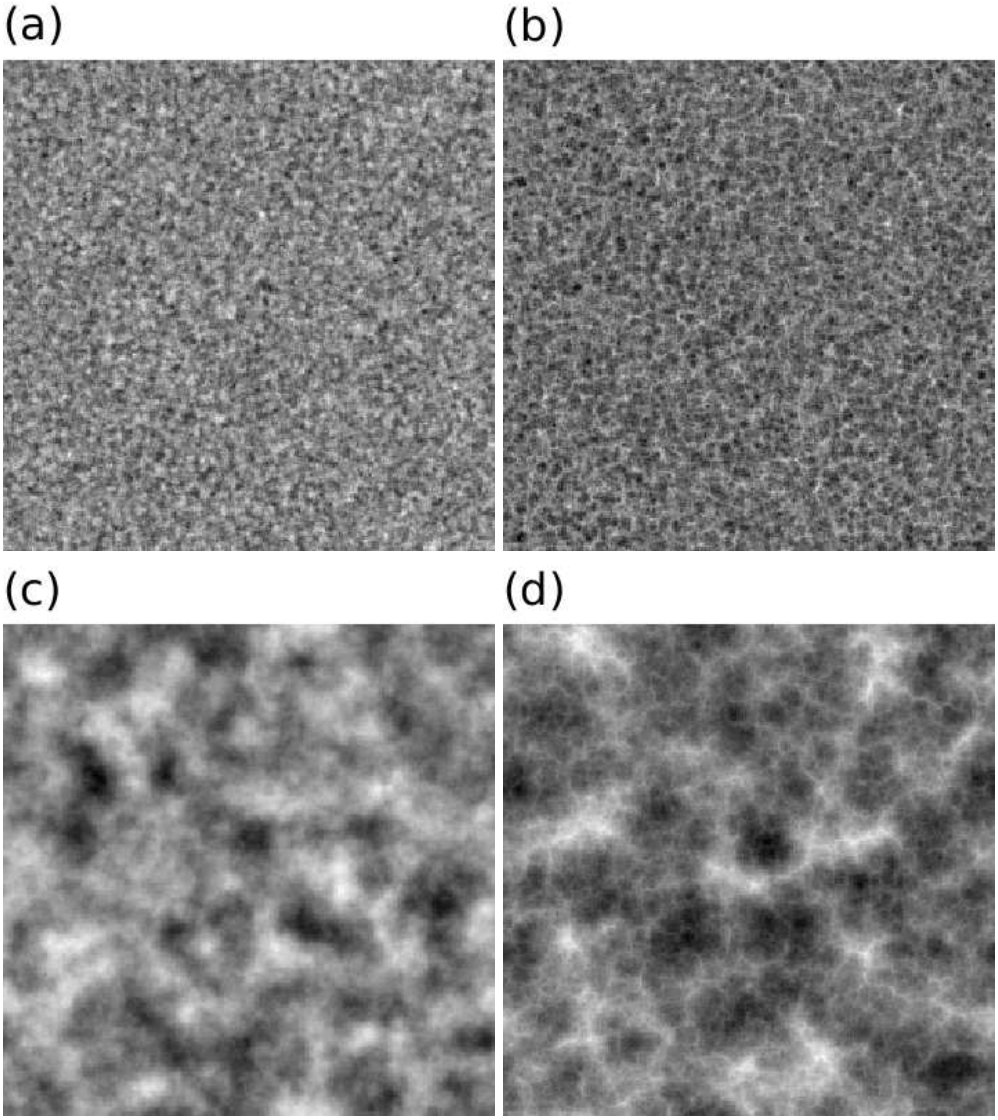

Figure 7.28: Roughening in the MBE equation in 2+1 dimensions, system size $L = 256 \times 256\ l.s.$, $t = 10000$ for two nonlinear terms $\lambda_1 = 0$ and $\lambda_1 = 0.2$, (a),(c) show for zero λ_1 the surface after $t = 10$, $t = 10000$ respectively, (b), (d) show the surface for $\lambda_1 = 0.2$ after $t = 10$, $t = 10000$ respectively, the images are scaled from lowest to highest value of the height function, the roughness for $t = 10000$ are both given in Fig. 7.29 by $C(0)$.

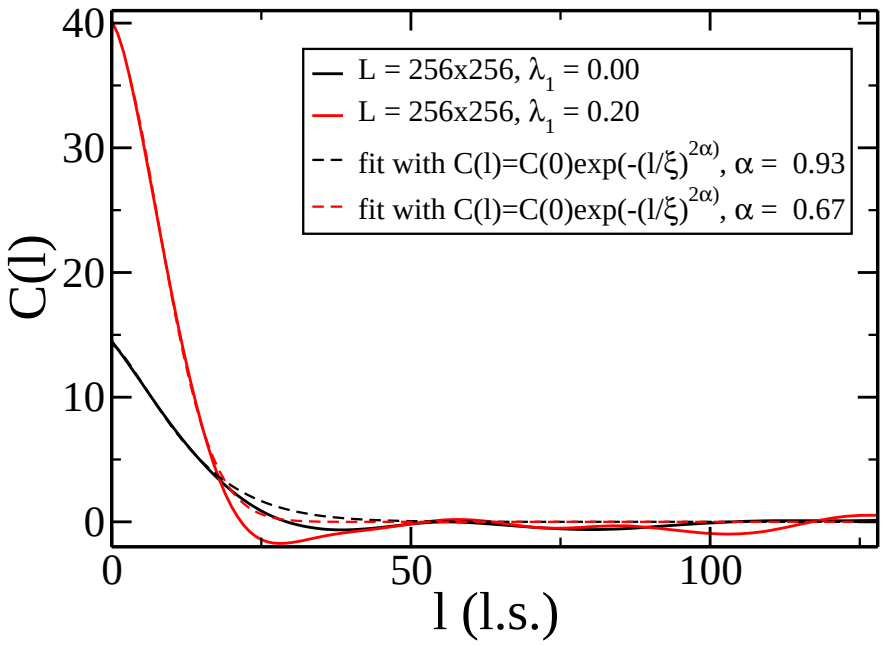

Figure 7.29: Correlations of roughening surfaces for the MBE equation in 2+1 dimensions, here we used the same setups as for Fig 7.28.

System size	$L = 256 \times 256\ l.s.$
Time of insetting control	$t_0 = 10$
End of control	$t_e = 1000$
Initial nonlinear term	$\lambda_{1,0} \in [0 : 0.2]$
Time delay	$\tau = 1$
Strength of the digital control	$a \in (0.005 : 0.01]$
Strength of the differential control	$K \in (0.005 : 0.02]$
desired value of the growth exponent	$\beta_0 \in [1/5 : 1/4]$
time discretization	$dt = 0.04$
Averages	10 realizations

Table 7.4: Parameter ranges for the control of the MBE equation in 2+1 dimensions.

7.2.4 With control in 2+1 dimensions

We now go on to the control of the MBE equation in 2+1 dimensions. Here we use a system $L = 256 \times 256\ l.s.$, time discretization $dt = 0.04$ and set the time range to $t_0 = 10$ and $t_e = 1000$. Where the system size is chosen as large as possible, the other parameters are again guided by the detailed investigations for the KPZ equation and partly tested for some setups before generally applied.

In Fig. 7.30 and Fig. 7.31 we showed solutions of the equation for initial $\lambda_{1,0} = 0.0$ with control strengths of $a = 0.005$ and $K = 0.005$.

We get really clear control behaviour with both types of control for all setups . So from a zero initial nonlinearity, the MBE equation is adjustable to any desired growth exponent between the universality classes $\beta_0 \in [0.2, 0.25]$. The behaviour of the control functions, well known from the other equations, is also present in the solution. As can be seen in the other setups with $\lambda_{1,0} = 0.1$ and $\lambda_{1,0} = 0.2$, the function at first either increases or decreases, depending on the desired exponent, until it reaches the exponent, and then stabilizes at the corresponding value. For $\lambda_0 = 0$ and $\beta_0 = 0.2$ we get a strong increasing function $\lambda(t)$ which then stabilize at a value $\lambda \sim 0.08$. for the other cases the stabilization values are lower as expected, where the desried value of β increases.

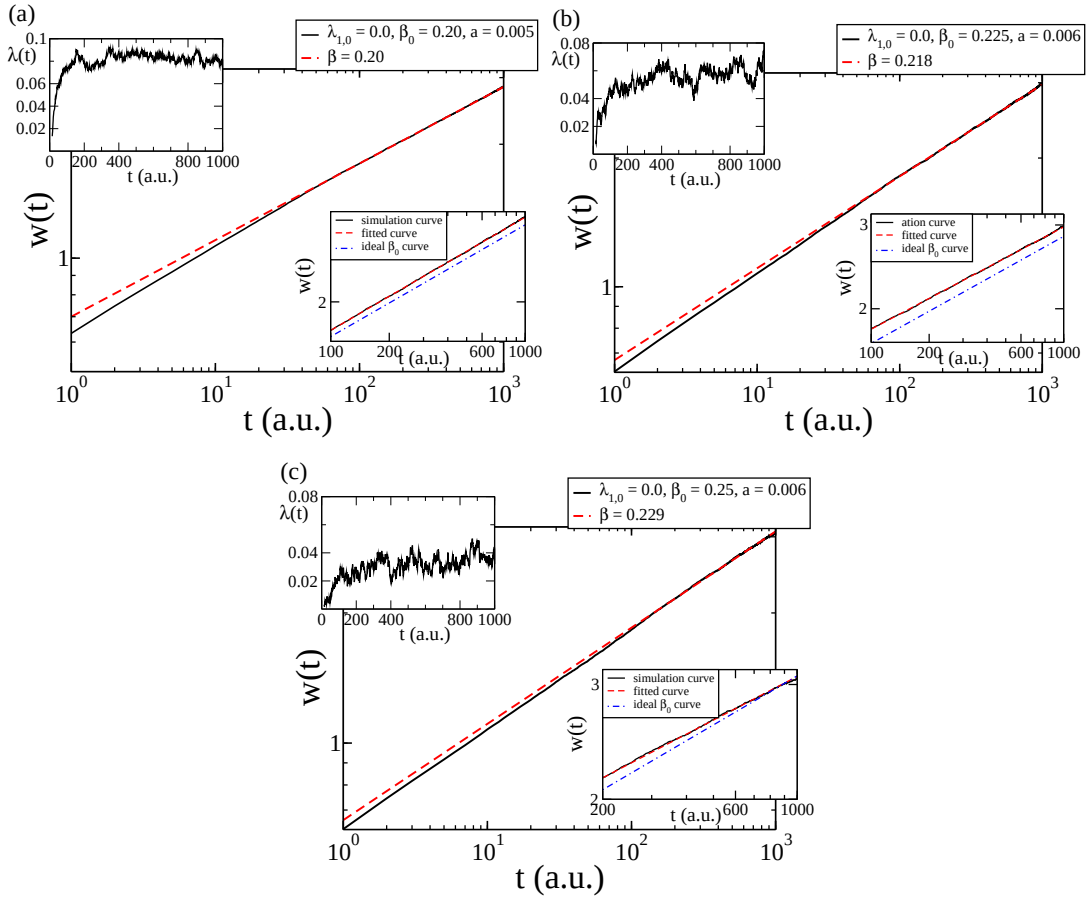

Figure 7.30: Digital control for the MBE equation in 2+1 dimensions $\lambda_{1,0} = 0.0$, $L = 256 \times 256\ l.s.$, $dt = 0.04$, (a) $\beta_0 = 0.2$, (b) $\beta_0 = 0.225$, (c) $\beta_0 = 0.25$, upper left insets show the functions $\lambda(t)$, lower right insets show the roughness in the late phase in a logarithmic plot.

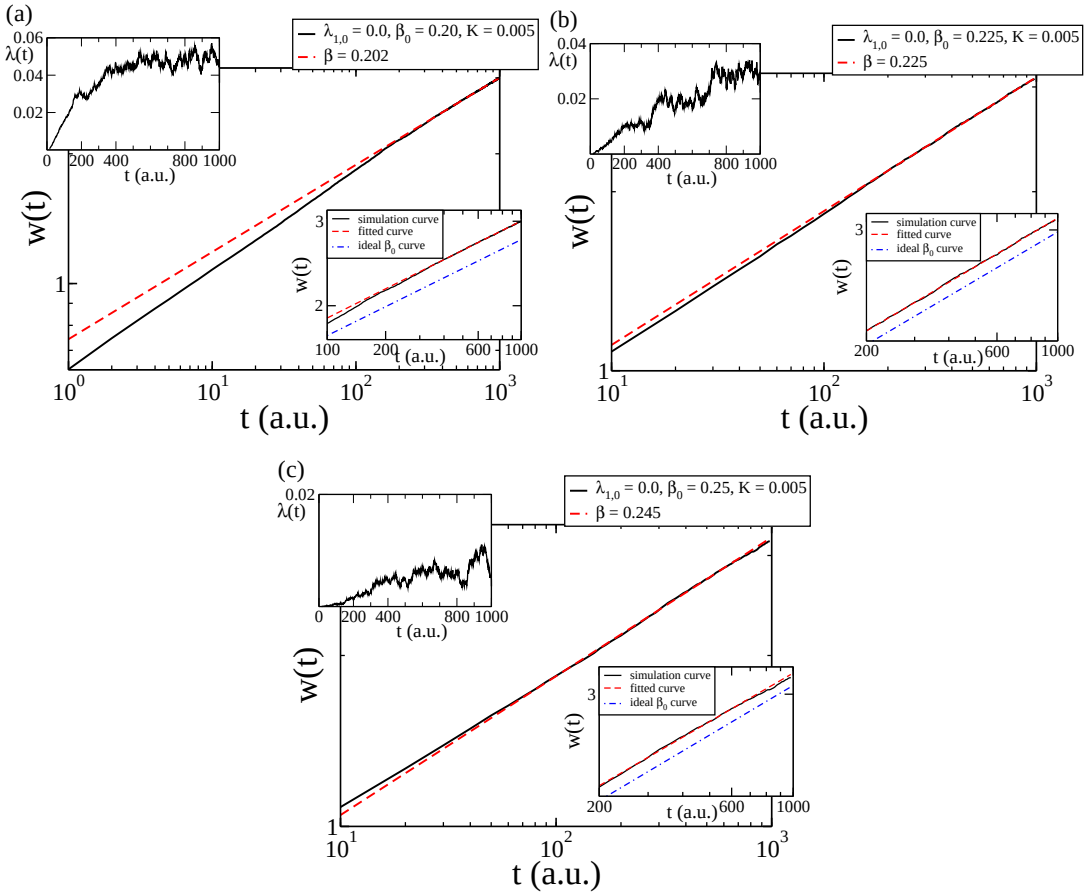

Figure 7.31: Differential control for the MBE equation in 2+1 dimensions $\lambda_{1,0} = 0.0$, $L = 256 \times 256\ l.s.$, $dt = 0.04$, (a) $\beta_0 = 0.2$, (b) $\beta_0 = 0.225$, (c) $\beta_0 = 0.25$, upper left insets show the functions $\lambda(t)$, lower right insets show the roughness in the late phase in a logarithmic plot.

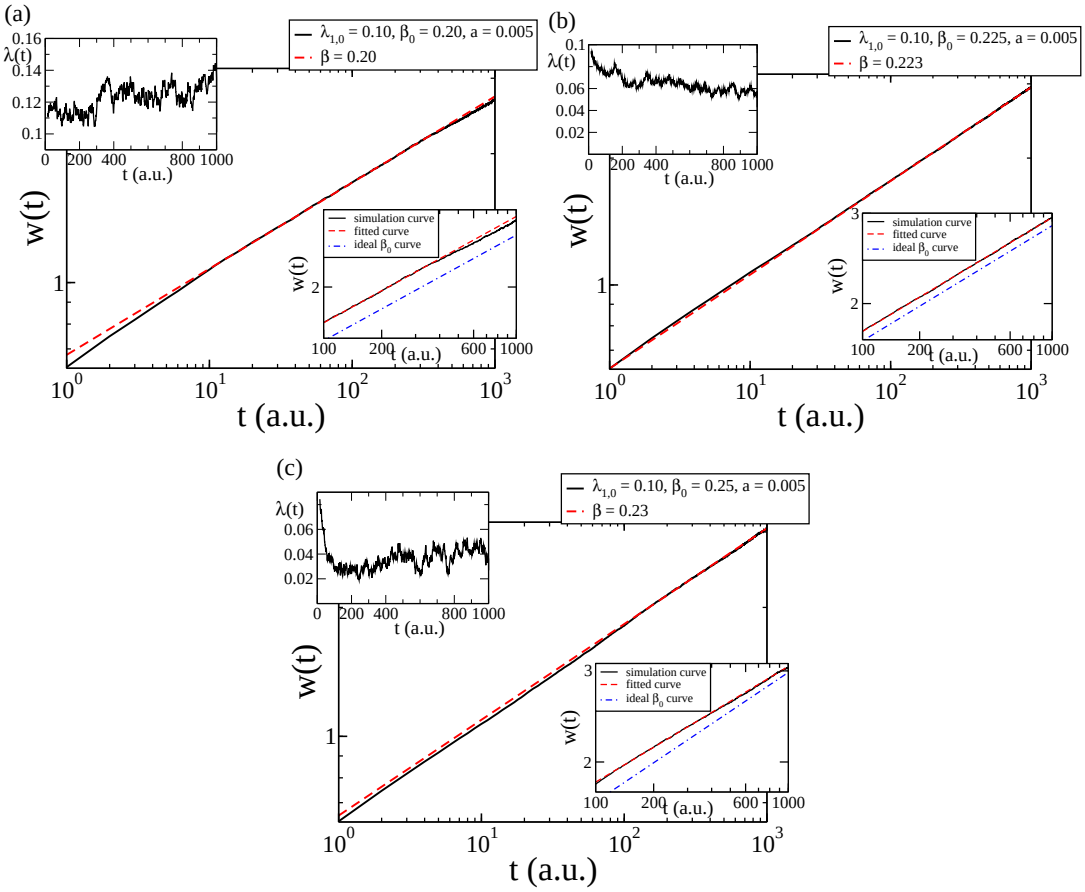

Figure 7.32: Digital control for the MBE equation in 2+1 dimensions $\lambda_{1,0} = 0.1$, $L = 256 \times 256\ l.s.$, $dt = 0.04$, (a) $\beta_0 = 0.2$, (b) $\beta_0 = 0.225$, (c) $\beta_0 = 0.25$, upper left insets show the functions $\lambda(t)$, lower right insets show the roughness in the late phase in a logarithmic plot.

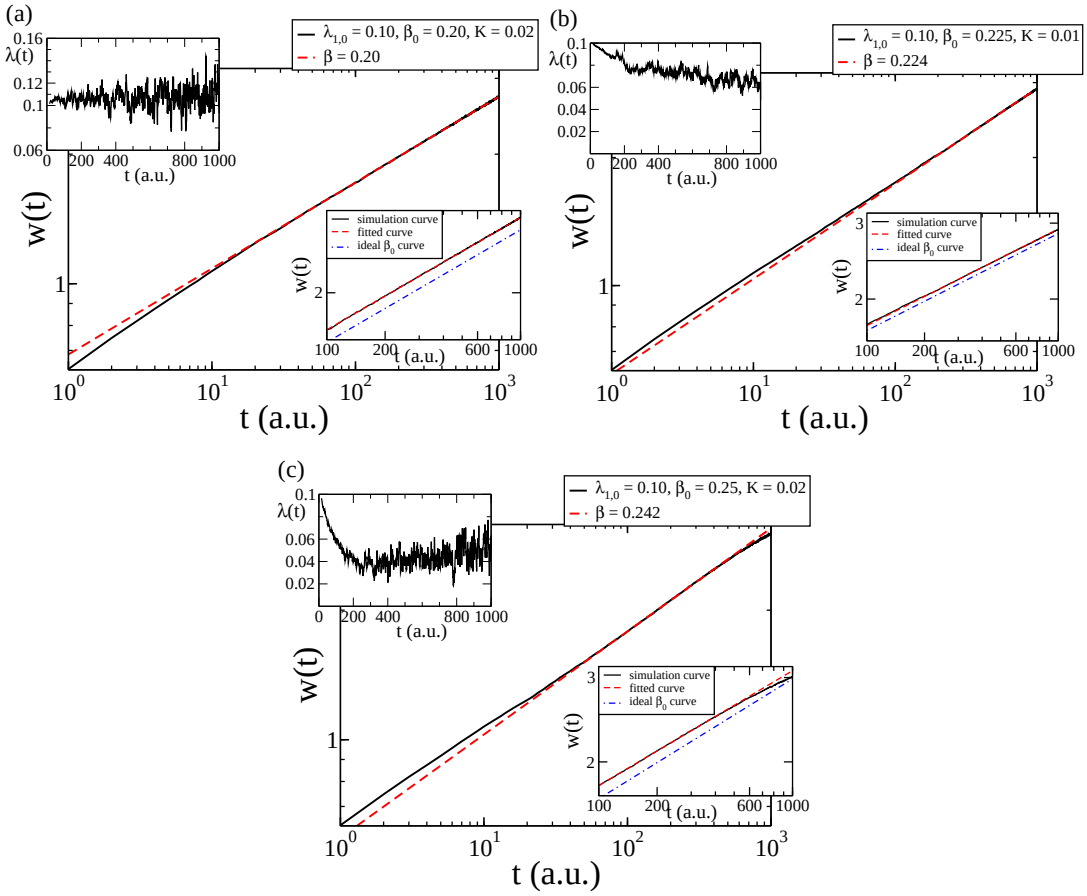

Figure 7.33: Differential control for the MBE equation in 2+1 dimensions $\lambda_{1,0} = 0.1$, $L = 256 \times 256\ l.s.$, $dt = 0.04$, (a) $\beta_0 = 0.2$, (b) $\beta_0 = 0.225$, (c) $\beta_0 = 0.25$, upper left insets show the functions $\lambda(t)$, lower right insets show the roughness in the late phase in a logarithmic plot.

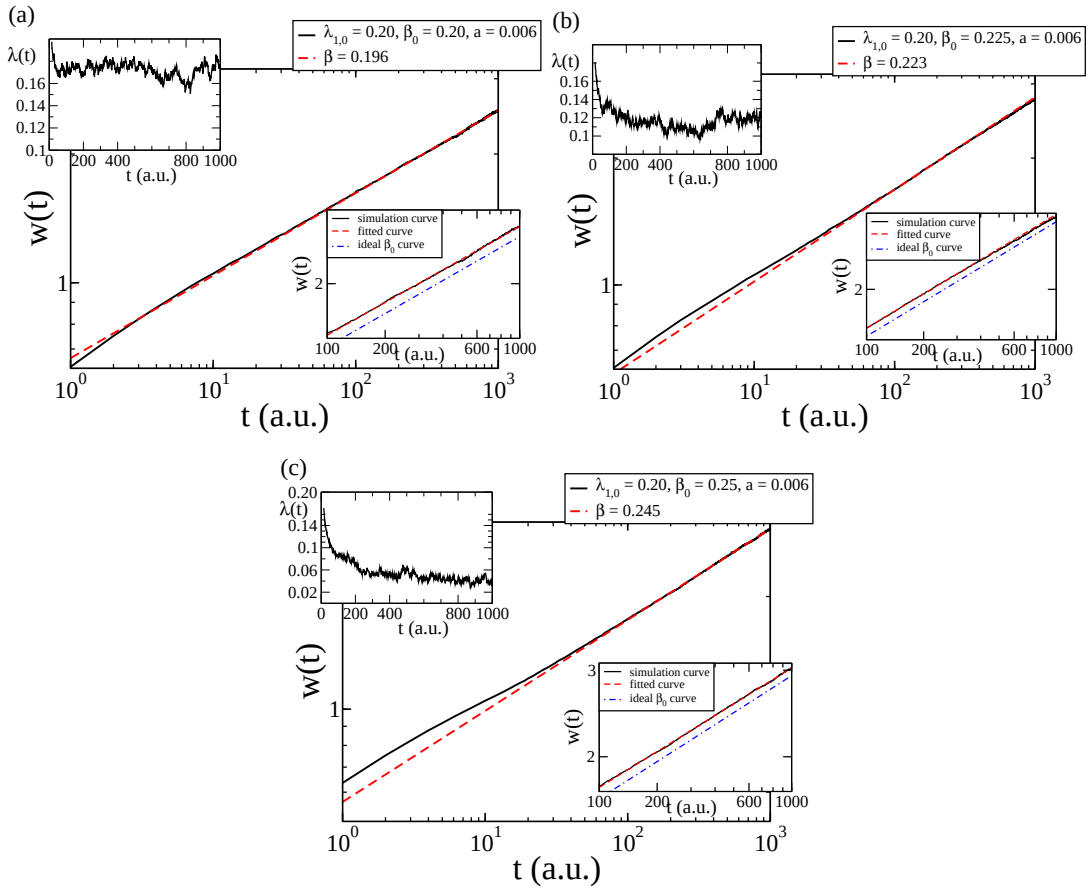

Figure 7.34: Digital control for the MBE equation in 2+1 dimensions $\lambda_{1,0} = 0.2$, $L = 256 \times 256\ l.s.$, $dt = 0.04$, (a) $\beta_0 = 0.2$, (b) $\beta_0 = 0.225$, (c) $\beta_0 = 0.25$, upper left insets show the functions $\lambda(t)$, lower right insets show the roughness in the late phase in a logarithmic plot.

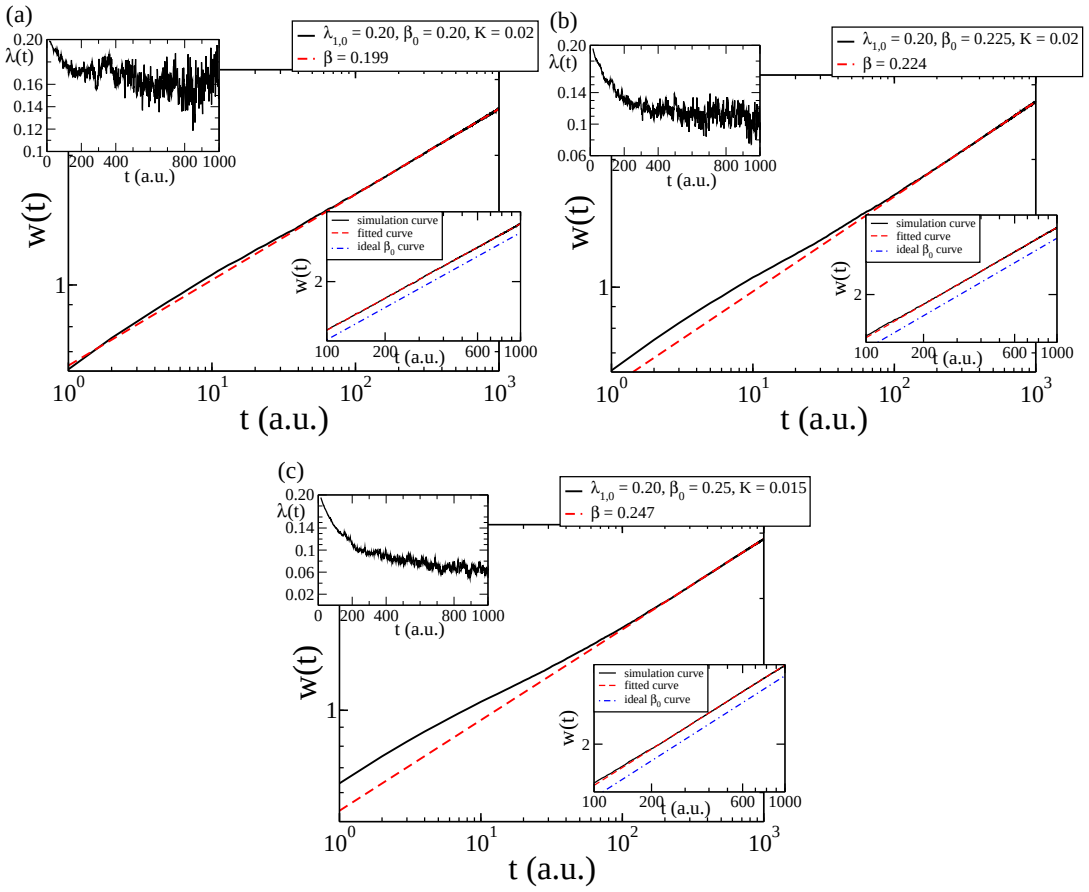

Figure 7.35: Differential control for the MBE equation in 2+1 dimensions $\lambda_{1,0} = 0.2$, $L = 256 \times 256\, l.s.$, $dt = 0.04$, (a) $\beta_0 = 0.2$, (b) $\beta_0 = 0.225$, (c) $\beta_0 = 0.25$, upper left insets show the functions $\lambda(t)$, lower right insets show the roughness in the late phase in a logarithmic plot.

7.3 Summary for the control of the growth equations

To conclude, the stochastic differential equations, described here for modelling growth phenomena, are adjustable, within a certain range, to values of the effective growth exponent β_0 for different universality classes.

We explained in great detail the mechanisms and considerations for the KPZ equation in 1+1 dimensions, showing the restrictions on the possible ranges and the borders of the possible control setups. In the case of the EW exponent $\beta = 1/4$ it is difficult to tune the control strength due to numerical fluctuations, but for all other setups we get clear control behaviour.

We applied the knowledge acquired from this equation to other equations. In case of the KPZ equation in 2+1 dimensions there are indications that the control might also work. For the proposed KPZ value $\beta = 1/4$ we can stabilize by control the effective exponent very well, where a control for small values is rather difficult. In these cases without more detailed investigations we can not be sure that the behaviour as explained is responsible for a realistic control. This is because of the numerical fluctuations, which can not be determined without controlling the exponents. This is not surprising as the exact values are still unknown. Our control here could establish a different method to determine the right exponents, as by definition a working control is possible in the range between the universality classes and a nonworking control defines the border and therefore the realistic exponents.

But it would be helpful to get such behaviour with a different type of model, such as a Kinetic Monte Carlo method with a stochastic model, currently under consideration [Wün07].

For the MBE equation the control works in both 1+1 dimensions and 2+1 dimensions.

We have demonstrated control for 1+1 dimensions for different setups with extensive numerical simulations restricted to a smaller parameter space than for other equations due to the computational expense.

For 2+1 dimensions the exponents are also adjustable between the two values which determine the universality classes. For these equations, control of the growth exponents β leads to an automatic change of the roughness exponent α relating to the same universality class as the desired growth exponent.

The MBE equation is proposed to explain the corresponding experimental setup where also KPZ-behaviour was found in crystal growth. The difference between the equations is the absence of relevant lateral growth for the MBE equation. KPZ-behaviour is found for low temperature systems, where under high temperatures, diffusion dominates the growth and the MBE equations are corresponding.

So, where simulations by means of a Kinetic Monte Carlo method can help to reproduce the findings of the time-delayed feedback control the aim then has to be a test with experimental setups.

7.3.1 Experiments

By our theoretical investigations we showed in detail that in case of the stochastic differential equations a time-delayed feedback control scheme can lead to an adjustment of the growth exponent and thereby to a deliberate tuning of the surface roughness. Now we want to discuss some hyptheses, how those schemes could be applied to experiments.

While in the literature there is still a lack of comparison of scaling theory with roughening of crystal growth systems, the work by Ojeda *et al* [Oje00; Oje03] can be seen as a guide and a proof that such schemes are relevant, where the hypothetic specific application depend on the experiment.

If we want to predict, how one can tune the roughness, we first have to look at the parameters of the equation, in case of KPZ namely ν and λ or ν_1 and λ_1, respectively, for the MBE equation.

The question for real-world systems then is, what is a corresponding tunable quantity. In case of crystal growth that could be first the temperature and then pressure as influences from the experimental conditions and second, all material parameters as intrinsic conditions.

What can we influence by temperature? Of course, the surface tension is coupled to the temperature, diffusion of particles strongly depends on the temperature and the deposition for almost all crystal growth experiments is related to temperature.

Obviously we just repeated all terms we used in the equations, thus the next question has to be: Can we tune these parameters independent from each other by temperature?

Ojeda *et al* showed in great detail in their findings that in case of a chemical vapor deposition of silicon films, where they find exponents corresponding to KPZ class, it is first possible to change the nonlinear term experimentally by change of the temperature and second, this procedure does not affect in their setup the smoothing term ν of the equation. For different temperatures they showed thereby, that different exponents appear in response to that change.

That is exactly what we use in our setups, an independently changable λ.

Our control is related to constant ν and ν_1, so λ and λ_1 seem to be needed independent from the other parameters. But as we already have shown in Sec. 5.1.3 the KPZ equation can be also characterized by a factor g depending on the equation parameters. So in case ν and λ are not independent changable by temperature, a study concerning this factor g have to be the method, to characterize a control scheme of the equation.

7.3.2 Other control schemes

We have applied a control scheme which is similar to classical Proportional-controllers and the Time-delayed autosynchronization method in chaos control.

If we think of Proportional-Integral-Differential control (PID), we could possibly improve the working adjustment by including integral parts or differential parts as explained.

An integral control would average memorized values of the local growth exponents within a pre-defined time interval and then the control force would depend on these values.

$$\overline{\beta} = 1/L \sum_{i=1}^{L} \beta_i \tag{7.5}$$

$$F(t) = K(\overline{\beta} - \beta_0) \tag{7.6}$$

where t_i denote the times where β_i has to be measured. The range from t_1 to t_L would define an additional time delay. We tested such a scheme, but did not find noteworthy differences to the presented setups. Some selected results are shown in the appendix.

A additional part of the controller could also react on the changes of the differences to the desired value and thereby establish a D-part.

We did not test such a scheme here.

We explained the difficulties to get good results for large time control due to numerical fluctuations. The absolute differences of the roughness between to points, where the control acts on the development, decreases due to the power law behaviour. So, a possibly better control setup up could be a changed strength of the control for late phase, especially for the differential control. We have seen, that for the MBE equation in 1+1 dimensions the enlarged time range lead to smaller control strengths for a working control, that may be an indication for a changed control strength for later times. So this might neglect strong fluctuations in the functions $\lambda(t)$.

A further development of our findings could also be the test of a control of the roughness exponents α. While for our equations such a scheme would be only meaningful for the MBE equation, also in other equations it could be interesting to apply methods for the other exponents.

7.3.3 Other equations

While we explained and reproduced by our numerical scheme the observations by Raible *et al*, a time-delayed feedback could also be applied to such a complex equation.

As already explained, KPZ behaviour is proposed for low to medium temperature behaviour, whereas the MBE universality should be obtained in high temperature systems. So, a generalized equation, containing both situations and the transition between the classes would be an equation, where all terms here explained in two different equations are included. A change of the prefactors ν, ν_1, λ and λ_1 then would correspond to a change of the temperature.

We made firsts steps towards the control of the so-called noisy Kuramoto-Sivashinsky equation (KS), where we just solved the equation without control.

$$\partial_t h(\mathbf{x},t) = \nu\nabla^2 h(\mathbf{x},t) + \frac{\lambda}{2}(\nabla h(\mathbf{x},t))^2 - \nu_1\nabla^4 h + \eta(\mathbf{x},t) \tag{7.7}$$

As can be seen in Eq.7.7 the KS equation combines the terms of both, the MBE and the KPZ equation. While the long time behaviour thus must be KPZ-like, for early times the exponents should depend on the strengths of the terms, so this equation could explain the transition from low-temperature (KPZ) to high-temperature (MBE) behaviour, where a control possibly could act to tune the universality class.

The problem of more complex equations is the fact that we normally can not see a clear scaling in the early roughening due to the different terms responsible for the behaviour. So, control of the growth exponents here is much more difficult and requires extensive precending investigations of the uncontrolled equations (see appendix for results of the uncontrolled KS equation).

Chapter 8

The Model for the evolution of cell populations

A lot of models describing the development of cell populations have been used during the last few years [Mor02; Dra05a; Dra05b; And05]. In this chapter we introduce the individual cell based model we used to observe the growth of tumor cells in an in-vitro environment.

Following the basic steps for modelling growth phenomena explained in Ch. 4, we first want to look at the system and define the underlying structure (lattice) on which our simulation has to work.

We want to describe the dynamics and surface morphology of large cell populations and to include the most relevant biological properties about the cells themselves and their interactions at a multi-cellular level. We consider the system at an individual cell length scale that does not explicitly explain the sub-cellular structure and is therefore a kind of mesoscopic view.

We have used the experiments of Bru *et al* [Brú03] as guidelines for our model. We have also used detailed information about the off-lattice model introduced by Drasdo and Hoehme [Dra05b]. Here extensive simulations were used to explain cell structure and then give information about the multi-cellular structure.

8.1 Experiment and Off-lattice model

We now want briefly to introduce the main results from the observations of Bru *et al* and the off-lattice model of Drasdo and Hoehme before we proceed to our model.

8.1.1 Experiments by Bru *et al*

In these experiments [Brú03] colonies of 15 in vitro cell lines and 16 types of in vivo cultures were extensively studied to explain the growth dynamics and to study the morphological structure of the tumor border. The cell lines were grown in Petri dishes

of diameter $5\ cm$ under specific conditions and analyzed by taking photographs at 24 hour intervals. Previous results needed scaling analysis methods to explain the border structure for one cell line [Brú98], but here [Brú03] they analyzed the critical exponents for all the cell lines studied.

For the growth dynamics they found an initial exponential growth law followed by a regime, in which the cell population radius grows linearly in time. They concluded that a proliferating zone restricted to a rim at the tumor border is responsible for such a behaviour.

For the scaling analysis they took photographs of the tumor border and analyzed the structure. Due to their interpretation, the critical exponents correspond to the MBE universality class (see Sec. 5.2) and explained this behaviour by a migration at the tumor border which depends either on the coordination number of the cell, or on the number of neighboring cells.

They found these critical exponents for all cell lines and suggested a general MBE like critical surface dynamic for tumor cell lines.

The mathematical treatment of the universality class was critically discussed by Buceta and Galeano [Buc05a], who concluded that the analysis was incorrect. They suggested that the critical exponents could belong to other universality classes, for instance to the KPZ universality class. We aim to clarify this discrepancy and also to explain the dynamics found in the studies.

8.1.2 The off lattice model

For our model we use the results of an off lattice model. Drasdo and Höhme [Dra05b] developed a model based on individual cells. Cells are described as sticky, elastic particles of limited compressibility and deformability. Cell division is modelled by the spherical shape of the cell after division, though it deforms during mitosis into a dumb-bell.

Cell adhesion is defined by adhesive bonds which are affected by the distance between cell centers. When cell pressure and nutrient supply are taken into account, the results for the dynamics are in good agreement with the findings of Bru.

So our lattice model, which also aims to explain the dynamics of Bru, uses some of the results from observations of that model.

8.2 The Dirichlet lattice construction

We consider a model on a lattice. We want to combine the advantage of lattice structures without the artifacts often produced by such models. We are now going to introduce, as an alternative construction to the common lattice types, the construction of the cell structure on an irregular lattice by a Delauney triangulation.

8.2.1 Voronoi diagrams and Delauney triangulation

We construct a lattice based on concepts of Dirichlet, Voronoi and Delauney [1]. Descartes first used Voronoi like diagrams in 1644. In the nineteenth century Dirichlet (1850)used Voronoi diagrams in theoretical studies (Dirchlet) and Snow used them in a study of the Soho cholera epidemic of 1854 (John Snow) [Oka00]. He showed that the people who died lived closer to the infected pump than to any other water pump. This also illustrates one of the fields where Voronoi or Dirichlet tessellations are most often applied, because of the properties of a Voronoi cell.

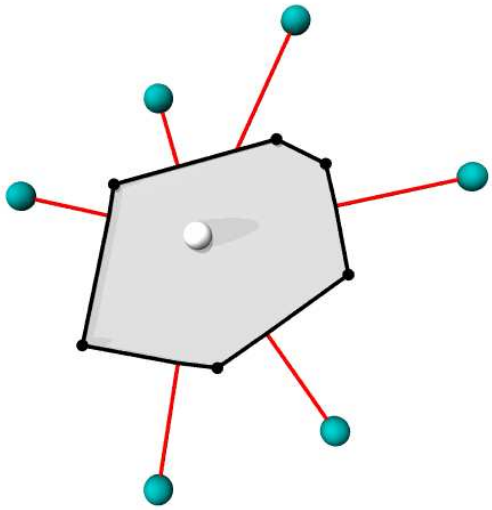

Figure 8.1: An individual Voronoi cell: seven points distributed on a twodimensional surface define the set M, the white point denote x_i and the grey area defines the Voronoi cell (black polygon), where all interior points have x_i as the closest point of set M.

The diagram in Fig. 8.1 demonstrates the properties of a Voronoi cell. If we have a set M of points in a space, then the set of all points closer to a point x_i than to any other point of set M defines the '*Voronoi cell*' or '*Dirichlet domain*' (black polygon). If we optimize the distributed points in an area and then define the nearest point for cells, the solution is a Voronoi diagram. Taking post offices as points this optimization problem is very famous as the "Post Office" problem. The tessellation of polytypes then defines the Voronoi diagram, named after Georgy Voronoi [Vor08]. The dual graph of the Voronoi diagram is the Delauney triangulation. Delauney triangulations are a well-covered topic; for an overview of the possible applications for these concepts see e.g. [Oka00; Ber97].

[1] Delauney is the french pronouncation of the Sovjet mathematician Boris Nikolajevitch Delone

8.2.2 The construction in our model

In our model we apply these concepts to construct a lattice that is unstructured but has a well defined distribution of the cell area. The algorithm is depicted in Fig. 8.2. Our

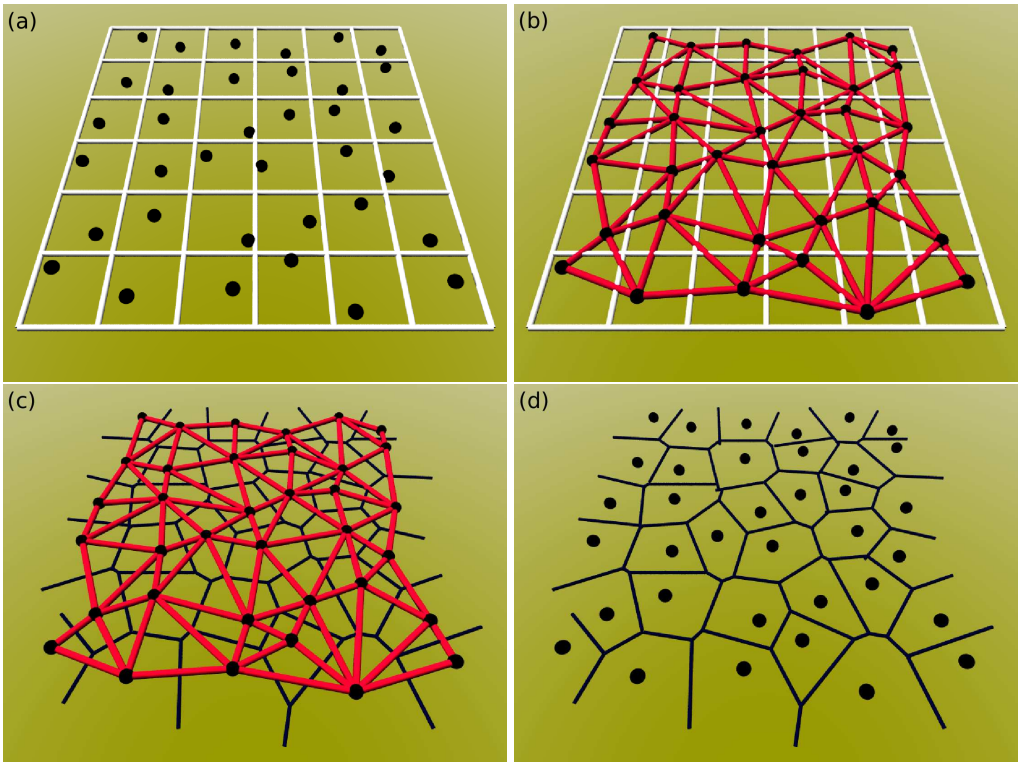

Figure 8.2: Construction of the Dirichlet lattice in four steps: (a) distribution of Voronoi points (black) in the square lattice, (b) Delauney triangulation (red), (c) Delauney triangulation and the corresponding dual graph, the Voronoi tesselation (black), (d) the Dirichlet lattice corresponding to cells.

construction is divided into the following steps:

We take a simple square lattice of size $L = l \times l$ points with a lattice constant a. All cells here then have a cell area $A = a^2$, where the overall area is $((l-1)a)^2$ (denoting that a lattice with l points has $l-1$ divisions).

The second step is to distribute points randomly in every square. Later we briefly discuss different ways of doing this, but for these simulations we insert exactly one point into each square. So we now have $(l-1) \times (l-1)$ newly constructed points as the points of our lattice (Fig. 8.2 (a)).

We now define the neighborhood of all points by a Delauney triangulation. As the name says, we construct triangles using the selection rule, which says that if, by connecting the points, we produce a square, we divide the square into two triangles by the shorter connecting line (Fig. 8.2 (b)). In the case where two connections have the same length, the choice is random [Oka00].

So our lattice fulfils the basic properties of an unstructured lattice with a well defined neighborhood.

The cell structure corresponding to our construction is given by the Voronoi graph, which is the dual graph of the Delauney triangulation (Fig. 8.2 (c)). If we take the perpendicular bisector of the connecting lines from the Delauney triangulation the intersections determine our cell structure (Fig. 8.2 (d)).

The lattice given by this algorithm has the following properties.

- lattice of $(l-1) \times (l-1)$ points with a well defined neighborhood of on average six neighbors as a result of the Delaunay triangulation.
- a pre-described average cell area of $\overline{A} = a^2$ with a well defined sharply peaked distribution around the average (determined by the choice of one point in each square)
- a well-defined correspondence of the lattice points to the cell structure on the dual graph

In order to be able to compare simulations using our lattice with other types of lattice simulations, we included the possibility of loading the lattice types as explained in Sec. 4.3, namely the square lattice, the hexagonal lattice and the octagonal lattice. To ensure a direct comparison, we consider types with the same cell area as those in our Voronoi tessellation, where in the regular case their size is exactly the cell area ($A = \overline{A}$) which in our case is the mean cell area.

With this lattice construction we now proceed to explain the model for our growth simulation.

8.3 Modeling the basic processes

The basic processes in a cell population growth model are obviously the division and migration of cells. Additionally we here also include other relevant processes like apoptosis, mutations and fluctuations which could be responsible for a change in the developmental behaviour.

8.3.1 Cell division

The lattice structure in our model does not determine anything about the structure of the cell, so cell division is reduced to modelling the cell cycle time and its distribution.

As already explained, the cell cycle consists of distinct phases, namely the mitosis phase (M-phase), the DNA duplication phase (S-phase) and Gap phases, in which cell signalling and individual cell conditions determine the time.

Because the cell cycle is controlled by cell cycle check points [Alb02] and experiments indicate a Γ-like distribution, we here model the cell cycle time τ using the discrete analogue to the Γ distribution, the Erlang distribution in Eq. (8.1).

$$f(\tau') = \lambda_m \frac{(\lambda_m \tau')^{m-1}}{(m-1)!} exp\{-\lambda_m \tau'\} \tag{8.1}$$

Here $\lambda_m = m$ such that $\langle \tau' \rangle \equiv \tau = 1$.

As can be easy seen from the equation, $m = 0$ corresponds to a Poisson distribution. So the parameter m ensures a realistic distribution of the cell cycle time.

In our model cell division is the same as the occupation of a new lattice point. We describe the biological process of one mother cell dividing into two daughter cells by choosing one cell to divide and then setting the new cell at a neighboring site on the lattice, adjacent to the mother cell. Volume exclusion (one cell on one point) then determines the possible choices of newly occupied cell as shown in Fig. 8.3. Although

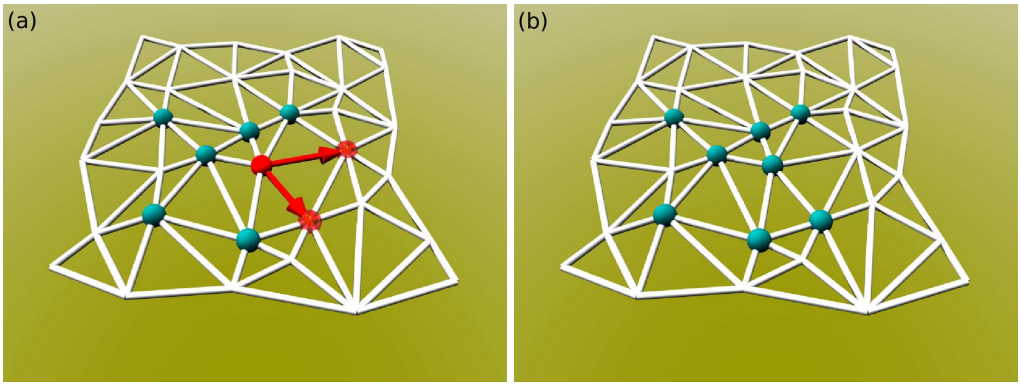

Figure 8.3: Division in the model: a) a dividing cell with two possible choices to divide to a lattice point, b) randomly chosen point of possible choices is occupied.

we normally choose the point for division randomly, we also include different rules for division in the model. As already explained, the cell is able to sense its environment. If one considers a choice of position which promises the best environment for the cell, for instance maximum nutrients or maximum free volume, then the rules have to be changed. We discuss these different choices later, but the first approach has to be random choice.

Proliferating rim

By experimental observations of many tumor cell lines Bru *et al* found a dynamics that shows an exponential growth in the early phase of the development of the cell diameter that then changes to a linear growth rate, so correspondingly a proliferating rim has to be included in the model. The experimental growth velocities do not agree with a proliferating rim $\Delta L = 1$. Thus, $\Delta L > 1$ is needed. Cells are able to divide

inside this rim. We model this by a environment of size ΔL for each lattice point. A cell then is able to divide if a free lattice point is available within a circle radius ΔL.

If there is no free point in the direct neighbourhood, we give the cell the ability to push aside other cells in its neighborhood. This algorithm allows a cell to divide if, and only if, there is at least one free neighboring site within a circle of radius ΔL around the dividing cell. We see this environment for one individual cell in Fig. 8.4. A sample simulation for 641 cells shows both the cell and the lattice structure with an enlarged section showing the movement of cells (red cells) inside the rim along a line (green). One interpretation is that a dividing cell is able to exert a sufficiently large force to

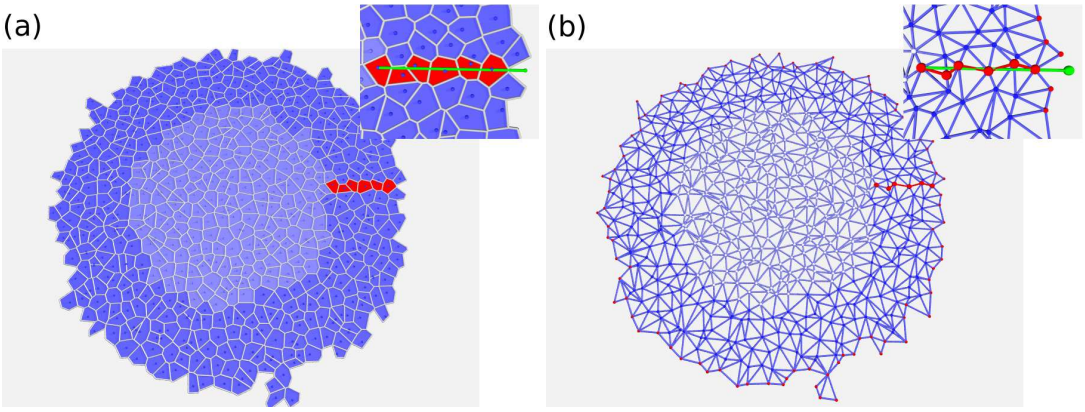

Figure 8.4: Cell and Point structure in the simulation, (a) the cell structure by the Voronoi tesselation, (b) the corresponding Delauney triangulation with the lattice points and the connections to the neighboring points, light blue cells are quiescent and the dark blue proliferating, insets show a sample for pushing cells inside the proliferating rim along the greeen line.

push at most $\Delta L/l$ cells aside in a certain direction in order to obtain free space for its division. Another interpretation of this rule is that only a limited number of cells can be stimulated to migrate away and leave free space for a dividing cell. It is noteworthy that as $\Delta L \to \infty$ lattice asymmetries in the growth patterns disappear from a regular (square) lattice; usually $\Delta L/l \sim 2-3$ already gives reasonable results [Dra05a].

To determine the growth sites we draw a circle of radius $\Delta L/l$ around the dividing cell and shift the neighboring cells towards the closest free site within this circle (shifts by more that $\Delta L/l$ lattice positions are prohibited). If division is permitted, we place one of the daughter cells on the site of the mother cell, and the other daughter cell on the neighboring site that has become free as a consequence of the previous cell shift. A biological interpretation of the assumption of limited shifts is that a cycling cell stops in one of the cell cycle check points if the division would require a shift of surrounding cells over a distance of more than $\Delta L/l$ cell diameters. As a consequence, the size of the proliferating rim within the expanding monolayer cannot exceed ΔL if the cells are dense (as they are here), which is why we call ΔL the proliferation depth. In the lattice model ΔL is a free parameter, while in the off-lattice model ΔL is a consequence of

the biomechanical and migrational properties of the cells and may be influenced by, for example, the cell stiffness and motility [Dra05b].

8.3.2 Cell migration

We want to describe the dynamics and surface morphology of large cell clusters. The migration of cells is responsible for changes in the general behaviour. For tumor cell populations in general, processes related to migration play a crucial role. If a mutation causes a cell to lose its ability to adhere to other cells, it becomes invasive. Migration can then cause these cells to invade other parts of the human body and form new tumors. This metastatic process is one of the most important processes in tumor growth.

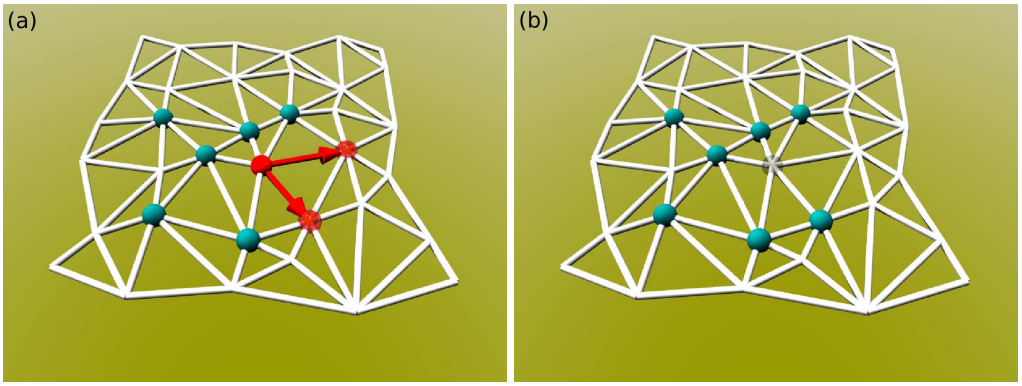

Figure 8.5: Migration in the model: a) a migrating cell with two possible choices to migrate to a lattice point, b) by type of migration chosen point of the two possible points is occupied, where the old position is now free again.

Although it is not our aim to model the metastatic processes of invasive cells explicitly, we consider cell migration (Fig. 8.5). Bru *et al* explained the behaviour of cell population growth relying on the Molecular Beam Epitaxy universality class. We use our model to explain how different migration rules change the growth behaviour. We consider the following types of cell migration.

Free migration

A cell moves with rate ϕ to an unoccupied neighboring site, irrespectively of the number of neighboring cells before and after its move. This rule corresponds to the case of no cell-cell adhesion.

Border migration

Cells move with rate ϕ if by this move the cell is not isolated. This may be seen as the easiest way to model cell-cell adhesion.

Cell-Cell adhesion

The most complex behaviour to model is cell-cell adhesion by the kinds of bonds between the cells. Cells move with a rate $\phi \exp\{-\Delta E/F_T\}$ with $\Delta E = E(t+\Delta t) - E(t)$, where Δt is the time step, $E(t)$ is the total interaction energy of the multi-cellular configuration, $F_T \sim 10^{-16} J$ is a "metabolic" energy [Bey00], $\Delta E/F_T \sim \mathcal{O}(1) - \mathcal{O}(10)$ [Dra05b]. This induces migration towards locations with a larger number of neighboring cells. After considering the basic properties of particle diffusion in other systems with energies corresponding to neighboring sites, we define our energy by

$$E = E_s + n \cdot E_B \tag{8.2}$$

where E_s is an energy normally related to the bonds to the substrate, here it may correspond to the bond to the extra-cellular matrix, n is the number of occupied neighboring cells and E_B denote the bond energy stored in each cell-cell contact. Whereas in simulations for crystal growth such definitions are widely used in the application of Arrhenius law (see Sec. 2.1), here the pre-factor ϕ corresponds to the frequency with which a cell is able to perform a hopping trial.

While the findings of Bru et al suggest a migration related to Molecular Beam Epitaxy, which is a diffusion-dominated type of growth (see Sec.5.2), the above assumptions should explain the migration of cells, as also shown in the off-lattice model [Dra05b].

8.3.3 Apoptosis of cells

Simple apoptosis

We partly include apoptosis (programmed cell death) in our model in order to obtain the specific dynamics for a change from no apoptotic cells to a situation where cells are undergoing development apoptosis. The simple way is to include the rate γ at which the cells undergo apoptosis.

Complex apoptosis

We have defined a constant rate which defines the ability of the cell to undergo apoptosis, however other rates might be needed to describe realistic behaviour. Carcinogenesis is the process whereby cells mutate into tumor cells and it is often partly associated with a change in the rate at which cells undergo apoptosis. A combination of knocked-outs of tumor suppressor genes and the suppression of apoptosis are processes which can lead to the uncontrolled growth of the cell population. We therefore add to the rate of apoptosis a probability for the suppression of apoptosis.

In detail: if we have a general rate of apoptosis in a cell population giving a 5% rate of cells undergoing apoptosis, this rate is decreased by a mutation rate γ_{ko}.

8.3.4 Necrosis

Whereas cells dying of apoptosis die without damaging their neighbors, those dying of necrosis normally die as a result of acute injury, causing a potentially damaging inflammatory response. In in-vitro monolayers of cultured cells, destruction is an unwanted process and does not have to be taken into account. But in general necrosis plays a role in cell populations, so we include a necrosis rate in our model.

8.3.5 Mutations and fluctuations

Tumor growth in general is a result either of changes in cell cycle behaviour or of a change in the suppression and promotion of cell conditions, and is therefore a kind of mutated condition.

Mutation in the cell cycle

Of course, during the development of a cell population consisting of cells mutated and thereby supporting the uncontrolled growth, additional mutations can occur. We want to denote a mutation of the cell cycle by a change the rate to divide within a certain range around the original cell division rate.

So we randomly mutate the rate τ by $\Delta\tau$ with

$$\tau_{new} = \tau_{old} + \Delta\tau \tag{8.3}$$

where $\Delta\tau$ is a random number $\Delta\tau \in [-\Delta\tau_{max}/2, \Delta\tau_{max}/2]$.

So our mutation does not show a preference for faster or slower divisions of the individual cells, but a change in the cell population caused by such a mutation can of course effect the dynamics.

Mutation of apoptosis rate

Whereas a mutation of the cell cycle probably has more effects on the dynamics, the properties of cells undergoing apoptosis can also be changed and could have effects on the behaviour of the cell population. We include a change of the apoptosis rate γ similar to the mutation of the cell cycle time τ.

$$\gamma_{new} = \gamma_{old} + \Delta\gamma \tag{8.4}$$

Here the cell cycle mutation $\Delta\gamma$ is a randomly selected number in the range $[-\Delta\gamma_{max}/2; \Delta\gamma_{max}/2]$.

Fluctuations of the environment

We have already included parameters for change which take into consideration intrinsic cell conditions such as mutation and apoptosis, but the cell cycle is also influenced

by external properties like, for instance, the accessibility of nutrients. So fluctuations of the external conditions may affect the cell cycle. In our model such fluctuations are shown either by the underlying structure or by the lattice. So we have built into our model the possibility of defining the lattice with random fluctuations related to the lattice sites. In our structure this leads to a local change of the cell cycle time τ. We would like to emphasize that this is a fluctuation of the environment in which the cells grow as opposed to the mutation of a single cell, where change is an intrinsic property of the cell.

8.4 The Kinetic Monte Carlo method

We have already defined our underlying structure, namely the Delauney triangulation, and we have described the possible processes and parameters in the model. We are now going to describe our method of observing cell population growth.

In contrast to the simulations for the crystal growth equations, we here use the Kinetic Monte Carlo method. This method has been described in Sec. 4.4.1 and we now describe the specific conditions for our simulation. We have already defined the processes we included by mean cell cycle times and mean migration and we now include probabilities.

The rules given in this chapter can be formalized by the master equation

$$\partial_t p(Z,t) = \sum_{Z' \to Z} W_{Z' \to Z} p(Z',t) - \sum_{Z \to Z'} W_{Z \to Z'} p(Z,t). \tag{8.5}$$

Here $p(Z,t)$ denotes the multivariate probability of finding the cells in configuration Z and $W_{Z \to Z'}$ denotes the transition rate from configuration Z to configuration Z'. A configuration $Z = \{..., x_{i-1}, x_i, x_{i+1}, ...\}$ consists of local variables $x_i = \{0, 1\}$ with $x_i = 0$ if lattice site i is empty, and $x_i = 1$ if it is occupied by a cell.

The kinetic Monte Carlo method or event-based Monte Carlo then makes use of all possible events in the system at time t [Bor75; Gil76; Fic91]. According to the specific probability of the event, we then step by step choose an event to happen and increase the time by the well known time step

$$\Delta t = -\frac{1}{R} ln(1 - \xi) \tag{8.6}$$

Here, ξ is a random number uniformly distributed in $[0, 1)$, and $R = \sum_i p_i$ is the sum of all transition probabilities p_i of possible events which may occur at time t.

We have now included all the parameters and can analyze tumor growth using our simulation tool. For a detailed description of the options for the simulation tool see Appendix C.

8.5 Data analysis

We want to explain the development of the cell population and the critical surface dynamics, so our main quantities are the cell diameter of the population and the border cells.

Gyration radius

It is obviously important to have a measurement of the size of the cell population which is independent of the morphology. Although we can also analyze growth kinetics using the cell population size $N(t)$, in this case we take the gyration radius defined by

$$R_{gyr} = \sqrt{\frac{1}{N}\sum_{i=1}^{N}(\underline{r}_i - \underline{R}_0)^2} \tag{8.7}$$

Here $\underline{R}_0 = \frac{1}{N}\sum_{i=1}^{N}\underline{r}_i$ is the position of the center of mass. For a compact circular cell aggregate (in $d = 2$ dimensions), R_{gyr} is related to the mean radius $\overline{R}(t) = \frac{1}{2\pi}\int_0^{2\pi} R(\varphi, t)d\varphi$ (polar angle φ) of the aggregate by $\overline{R} = R_{gyr}\sqrt{2}$.

Structure function

To determine the cell population border we use the structure function we have already described above. For completeness we would like to point out the special conditions needed for this approach, and for the scaling theory and data analysis for the critical exponents we refer the reader to sections 4.2 5.4.

Here we want to explain a roughening process that is different in the sense that we have a circular environment. So the border is not as easy to determine as in the case of the development of a single line by roughening. Additionally we have an unstructured lattice.

There are two basic differences from the scaling in 1+1 dimensions we described before: the circular environment and the size of the developing system. Curvature may have an effect on the structure function and we make the assumption that the tumor border is large enough to avoid artifacts.

The developing system should reflect the basic properties of scaling. Although this effect makes it difficult to observe a stable growth exponent, the assumption that the tumor border shows scaling requires the observation of α and z by the structure function.

$$S(k,t) = \langle R(k,t)R(-k,t)\rangle \tag{8.8}$$

where $R(k,t)$ is the Fourier transform of the local radius $R(s,t)$ and $\langle ...\rangle$ denotes the average of the growth process over different realizations (e.g. [Ram00]).

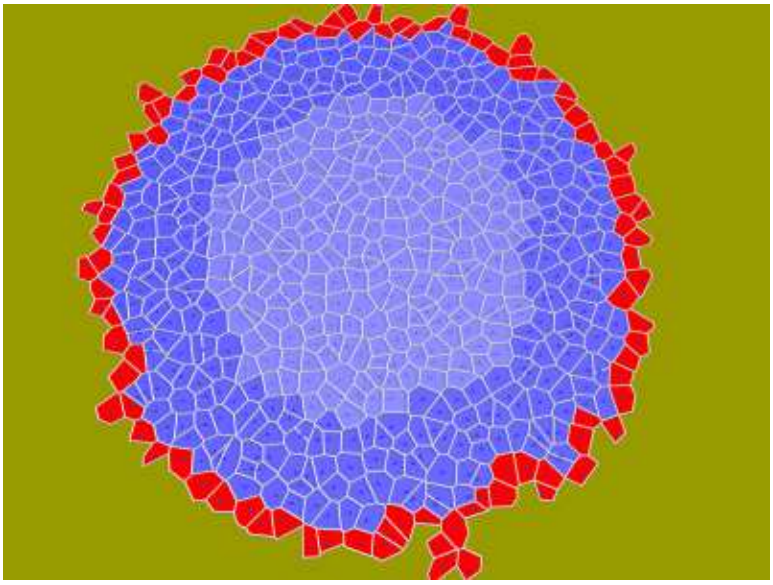

Figure 8.6: Structure extracted from simulations, red cells here denote the tumor border, where the light blue cells are quiescent and the dark blue proliferating.

In order to determine the tumor border using an algorithm, we can either use all the cells at the border and follow the individual points along the border by arc length, or use a discretization by angles $\Delta\phi$ from the center of mass. When we include both types, we normally make use of the first method guided by the algorithm described in the findings of Bru *et al* [Brú03].

In Fig. 8.7 we show the scheme of the simulation tool. A detailed description of the options can be found in App.C.

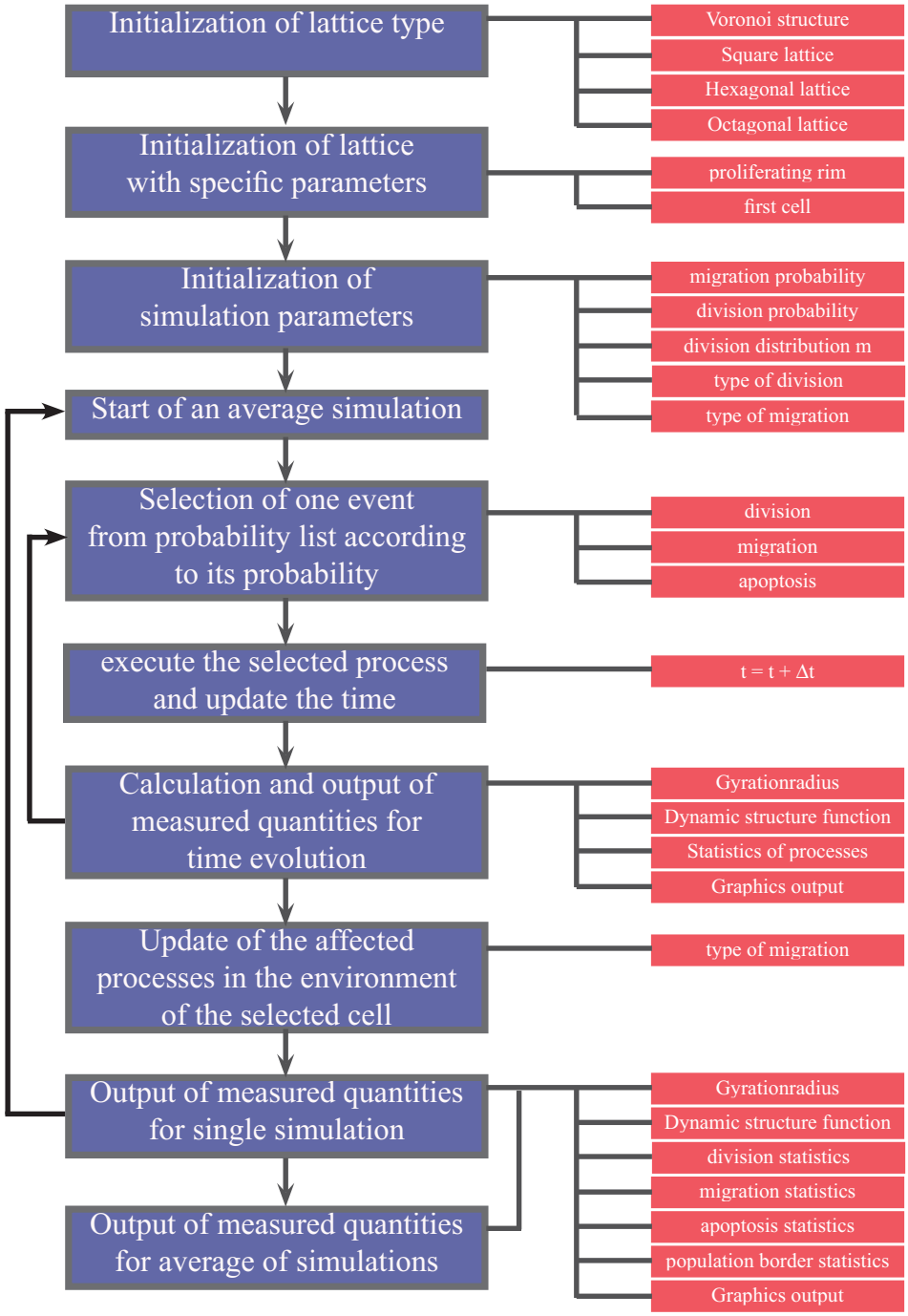

Figure 8.7: Scheme of the Kinetic Monte Carlo simulation.

Chapter 9

Simulations of the evolution of cell populations

We now apply different parameters to our Kinetic Monte Carlo simulation tool to investigate how expansion kinetics and critical surface dynamics depend on the various properties and mechanisms. In the first part we want to test the properties of our model and show how its behaviour differs from that of other types of model.

For all simulations we use reference time scales and length scales, more specifically the mean cell cycle time $\overline{\tau}$ and the mean cell area $\overline{A}$ or, for linear quantities in space, $\sqrt{\overline{A}}$. So all quantities are multiples of these scaling factors; for instance, the gyration radius R_{gyr} is described by the mean average cell diameter $\overline{A}^{1/2} = l$. For direct comparison with experiments the quantities are then rescaled, and we use these scales to investigate generic growth behaviour in our model.

9.1 Lattice artifacts

First we consider our lattice. We need to show that our construction avoids lattice artifacts. Such lattice-induced asymmetries could significantly disturb the analysis of the surface growth dynamics in circular geometries. If the lattice type is chosen properly for crystal growth, it reflects the actual lattice and therefore the actual properties of the crystal, but here realistic behaviour is not directly coupled to a regular morphology because of the absence of a regular underlying lattice structure.

Our simulation tool can decide between four different types of the underlying structure (see Sec. 8.2.2) and we now use this to compare our lattice to the other lattice types, namely the square lattice (von Neumann neighborhood), the hexagonal neighborhood and the Moore neighborhood with eight neighbors.

In order to check for any possible lattice artifacts we let the parameter τ corresponding to the sharpness of the cell cycle time increase $m \to \infty$. This corresponds to a δ-function for the distribution where all cells divide after exactly τ , and reduces the effects of the random nature of realistic cell cycle times.

At large m the tumor border then becomes smoother and the tumor shape reflects the symmetry of the underlying lattice. This effect is known as *noise reduction* [Bat91].

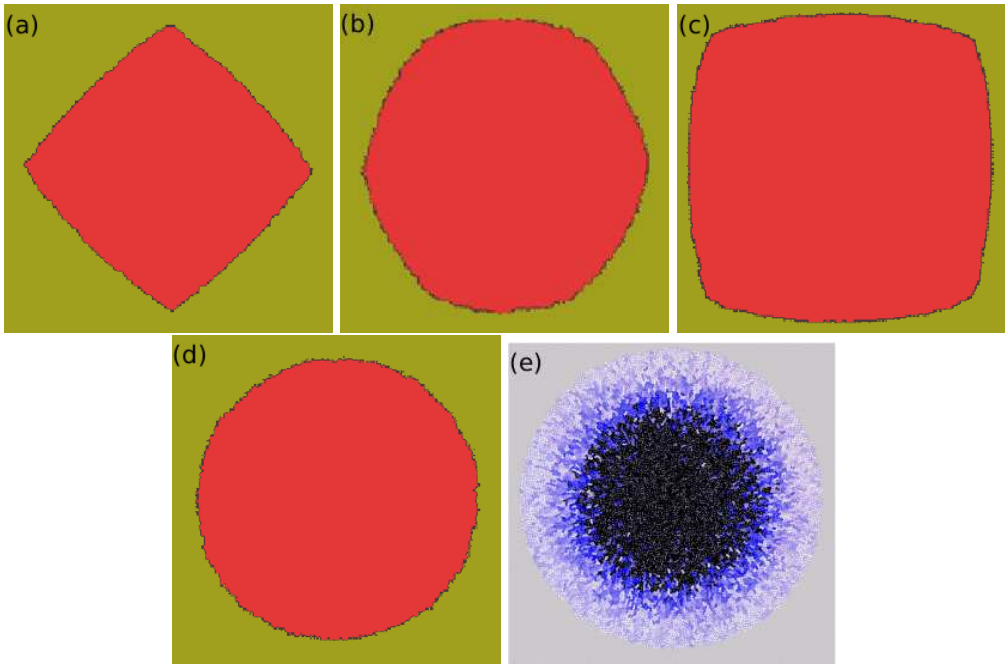

Figure 9.1: Lattice artifacts: (a) von Neumann neighborhood, (b) hexagonal neighborhood with six neighbors, (c) Moore neighborhood with eight neighbors, (d) the Dirichlet lattice construction with an average of six neighbors, (e) for comparison a simulation with the off-lattice model [Dra05a], all lattice simulations with no migration $\Delta L = 0$ and $m = 10000$ for time $t = 120$.

In Fig. 9.1 we show the resulting morphology of the noise reduced simulations. For the setups we used $m = 10000$ for all lattices and let all the cell populations expand for $t = 120$. There was no migration and we took a proliferating rim $\Delta L = 0$ to avoid the effects of parameters other than m.

As anticipated, the three regular lattice types show the underlying structure (Fig. 9.1 (a - c), whereas our lattice type (Fig. 9.1 (d)) and, of course, the off-lattice model (Fig. 9.1 (e)) do not show any regular structure other than the circular shape of the cluster.

It can be seen that, in this case, the lattice construction of our model produces a simulation free from lattice artifacts. So the construction our model is an advance on the regular structure based models.

There is one additional property of the regular lattices. For the same simulation times the number of cells increase with the number of neighbors in the regular lattice, whereas our lattice shows similar values of cell divisions in comparison with the hexagonal structure. This agrees with the fact that our points have, on average, six neighbors due to the triangulation procedure.

The underlying lattice structure does not only appear as a result of noise reduction in the cell cycle. Similar behaviour can be seen in simulations for crystal growth if we have a large rate of diffusion at the surface and a comparatively low deposition rate [Blo04].

In this case the islands that are grown normally tend to form squares of a specific size on a cubic lattice. The diffusion in such simulations is defined by an Arrhenius law with the energy difference depending on the number of neighbors (coordination number) as explained in Sec. 2.1.2 and as also defined in our tool (Sec. 8.3.2).

Because Bru *et al* [Brú03] suggested exactly this type of migration, we test our lattice type again to compare it with the others. If our lattice type has no artifacts associated with this type of noise reduction, then it should not show any regular structure.

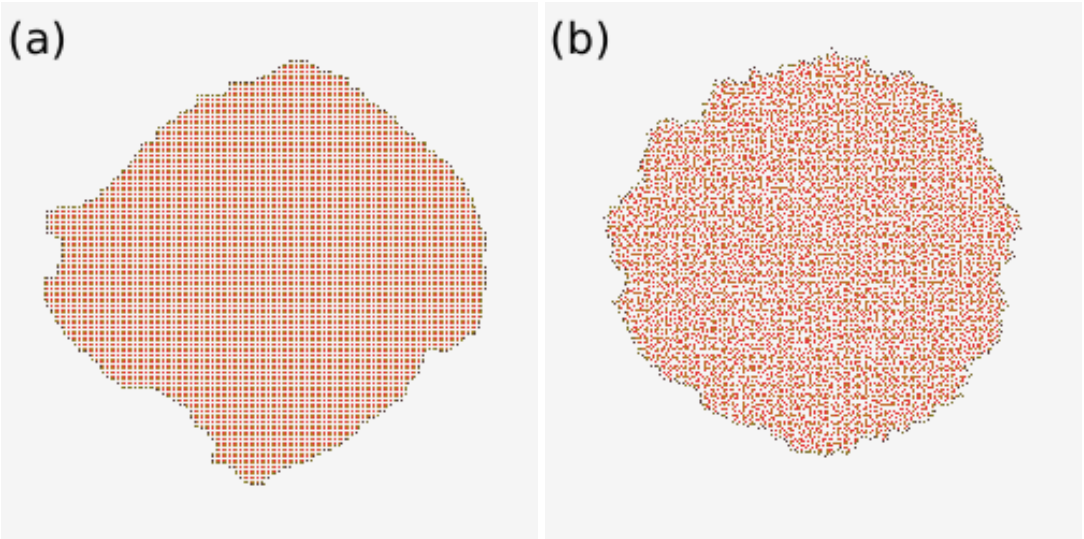

Figure 9.2: Lattice artifacts: (a) von Neumann neighborhood (square lattice), (b) the Dirichlet lattice construction with an average of six neighbors, all lattice simulations with migration $\phi = 100$, $\Delta L = 0$ and $E_s = 1$ $E_B = 6$ and divided cells $N = 10000$ before proliferation stops.

In Fig. 9.2 we compare the square lattice (Fig. 9.2 (a)) with our structure (Fig. 9.2 (b)). We let 10000 cells divide, then stop the proliferation and let the cells migrate ($\phi = 100$) only by means of a coordination number depending on diffusion, as defined in Sec. 2.1.2. This procedure corresponds to the fast equilibration of a conserved model. Conservation here means that the number of particles is constant due to the elimination of the division process after 10000 divisions. If the migration is chosen in such a way that the cells tend to adhere to a maximum number of other cells, then migration could cause this tendency of equilibrium behaviour to reflect the underlying structures.

The parameters for the adhesion energies in our case are $E_s = 1$ and $E_B = 6$ for both lattice types.

Once again we can see the underlying structure of the regular lattice, which does not appear in our construction. Obviously the underlying symmetry is not as clear as for noise reduction by cell division, but whereas in this case the cells can reach local equilibrium, the probability of reaching global equilibrium is not so large. One therefore has to run the simulation for very long times to see the perfect square lattice structure, whereas we can already see the underlying structure locally.

So for both types of noise reduction we have shown that our lattice type, as opposed to the regular type, seems to be free of any lattice artifacts.

Of course we have shown extreme cases, but whereas the artifacts may not be obvious in other simulations, they affect the results to a greater or lesser degree and so normally require explanations for a recalculation of the measured quantities, if possible.

9.2 Cell area distribution

The second major difference between our construction and regular lattice types is that it produces a realistic cell area distribution. We demonstrate the distribution our construction produces using the steps that have already been explained. Therefore we make the Voronoi tessellation inside the simulation and calculate the cell area by Herons formula (see appendix for details).

Obviously for regular lattice types, like the three included in the tool, the distribution is sharp where biologically it should vary slightly around the average area.

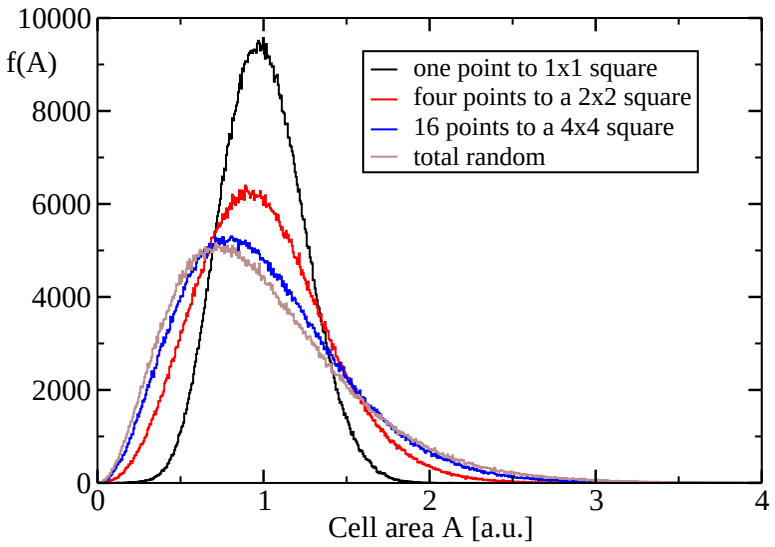

Figure 9.3: Cell area distribution for different lattices: Lattice points: 1000×1000 for the basic lattice construction, four different distributions to the squares, random distribution of 1000×1000 points to the square lattice (brown), 16 points to a 4×4 squares (blue), 4 points to a 2×2 squares (red) and 1 point to each square (black)

To emphasize the nature of our algorithm for construction, we have chosen different methods of distributing the Voronoi points to the square lattice.

In Fig. 9.3 we see the dispersion of the cell area for our construction with one point in each square, giving a totally random distribution on the predefined lattice.

So as expected, our distribution gives a pre-described average with a sharp distribution. An upper border of the sharp distribution is of course given by $A = 4a^2$ because of the maximum distance between two points.

If we now distribute more points randomly to a larger area by definition of our construction this maximum increases and the distribution disperses.

If we expect the cell area to be sharply peaked around an average, our best choice seems to be the first (black line), whereas for very flexible and fast growing cell lines other choices might be better.

9.3 Proof of cell cycle time distributions

We now proceed to prove the cell cycle time τ using the Erlang distribution. We tested the distribution of the cell cycle for different setups with different m.

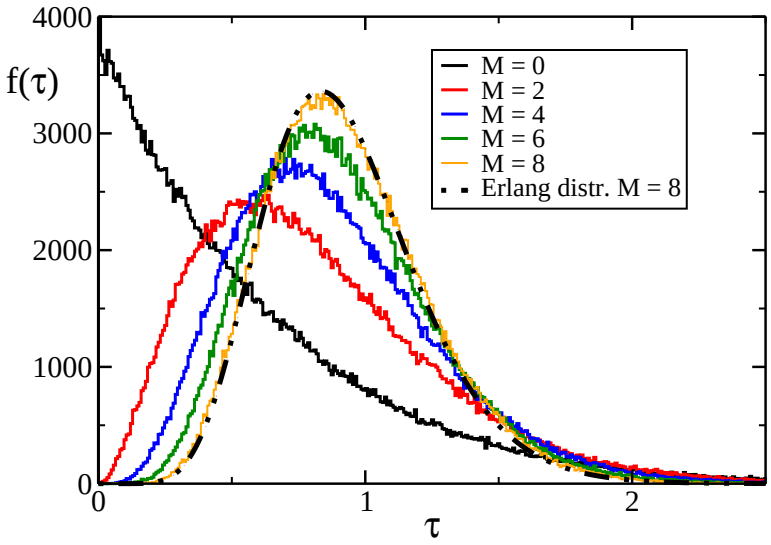

Figure 9.4: Cell cycle time distribution for different parameters m: 300000 cells were grown for the different setups, no migration and $\Delta L = 0$, the dash-dotted line denote for $M = 8$ the corresponding Erlang distribution.

We can see that for $m = 0$ the cell cycle has a Poisson distribution and for larger m the cell cycle becomes sharper around the average of $\tau = 1$ for all distributions. We show the "ideal" Erlang distribution (dash-dotted black line) for comparison for the setup with $m = 8$.

9.4 Expansion kinetics of cell populations

We now want to investigate the expansion kinetics of cell populations with specific properties. We therefore vary the basic parameters ,i.e., migration and the proliferating rim, for the division of cells over a wide range. Additionally we look at the dependence of the cell cycle time distribution on the mean velocity of developing cell populations.

9.4.1 General expansion

We first want to focus on the general growth behaviour we see in all simulations without mutations.

We took the simplest case, namely a simulation with $\Delta L = 0$ $m = 0$ and $\phi = 0$. In Fig. 9.5 (a) we see the development of the gyration radius R_{gyr} vs time t and in Fig. 9.5 (b) the morphology of the developed cluster. The general growth behaviour can be seen. After an early exponential phase the gyration radius enters a linear phase where the velocity stay at a nearly constant value (inset). v_{gyr} denote the velocity of the gyration radius R_{gyr}.

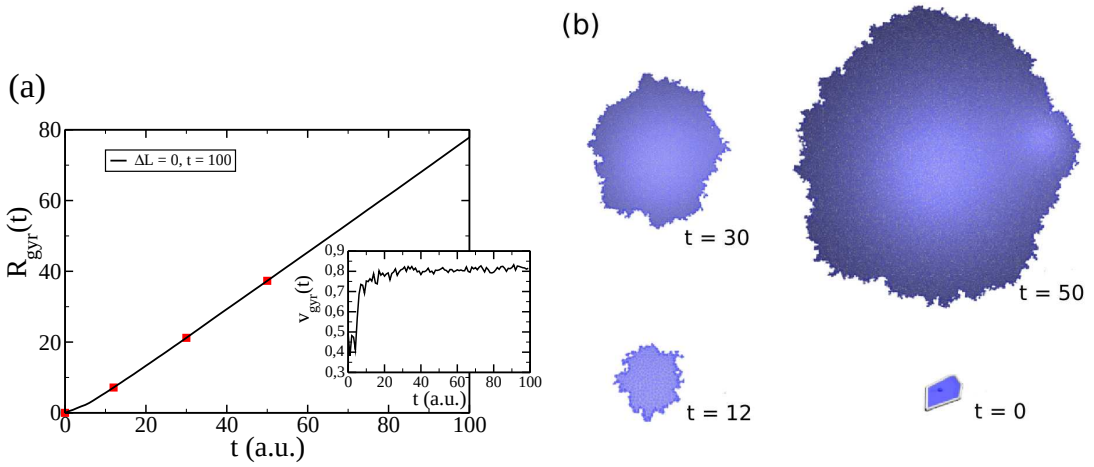

Figure 9.5: General dynamics of cell populations, parameters: proliferating rim $\Delta L = 0$, rate for proliferation $1/\tau = 1$, rate of diffusion $\phi = 0$, (a) Gyration radius R_{gyr} vs time scale t/τ, inset show the velocity for the Gyration radius $v_{gyr} = \dot{R}_{gyr}$, points denote the steps, where the clusters are depicted in (b); (b) shows the development of the morphology of the cell cluster, dark blue: the proliferating cells at the border, light blue: quiescent cells in the interior.

The behaviour corresponds to the expansion observed by Bru *et al* and also to the findings for the off-lattice model [Dra05b]. As we shall see for other setups, this general behaviour is found for all simulations without mutations.

9.4.2 Influence of the proliferating rim

We now proceed to observe the influence of the proliferating rim, one of the basic parameters in our model. In experiments the proliferating rim is responsible for linear expansion in the late phase of development.

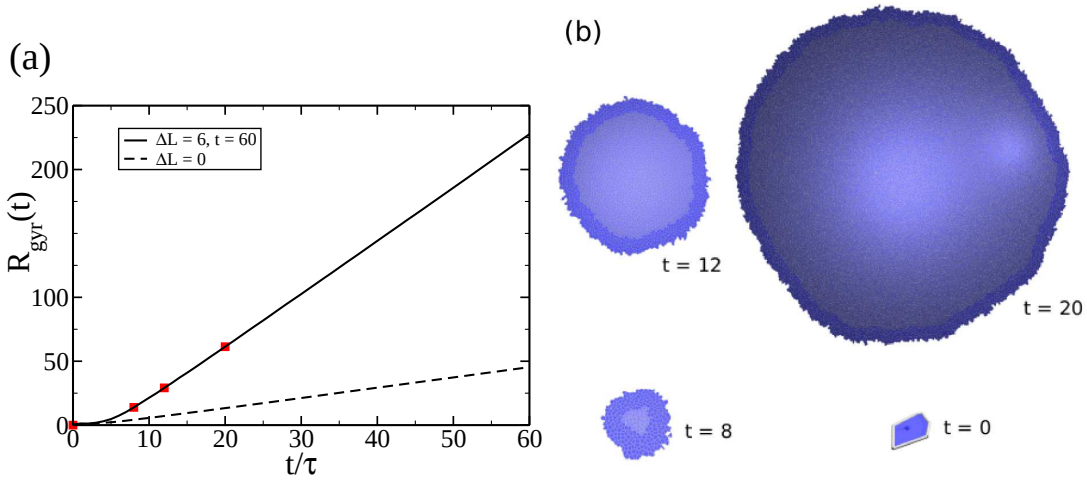

Figure 9.6: General dynamics of cell populations, parameters: proliferating rim $\Delta L = 6$, rate for proliferation $1/\tau = 1$, rate of diffusion $\phi = 0$, (a) Gyration radius R_{gyr} vs time scale t/τ, dashed black line show the setup from Fig. 9.5, points denote the steps, where the clusters are depicted in (b); (b) shows the development of the morphology of the cell cluster, dark blue: the proliferating cells at the border, light blue: quiescent cells in the interior.

We tested a change of expansion using a setup with $\Delta L = 6$ and otherwise the same conditions as before. In Fig. 9.6 we see the general influence of the proliferating rim on both the velocity and the morphology. The linear phase can also be seen in this case: under constant conditions the velocity increases with ΔL and the tumor border smoothes out, as can be seen in Fig. 9.6 (b). A larger number of proliferating cells obviously leads to an increase in the expansion velocity as the dividing cells push their neighbors in a direction corresponding to the local radius of ΔL and this then leads to the smoothening effect. We discuss the role of the proliferating rim in detail later.

9.4.3 Influence of free migration

The first main process in our simulation is the division of cells, but we now look at the second main process, migration. We include here the free migration of cells or the absence of any cell-cell adhesion, respectiveley.

When we look at the behaviour under conditions of free migration, we see that the gyration radius again increases in comparison with the first setup, but that the behaviour of the developing cluster is slightly different. Initially the morphological

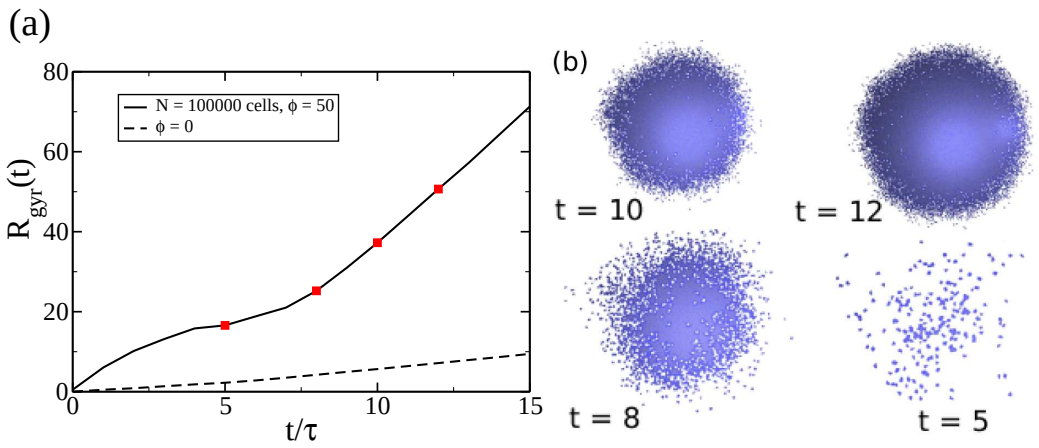

Figure 9.7: General dynamics of cell populations, parameters: proliferating rim $\Delta L = 0$, rate for proliferation $1/\tau = 1$, rate of diffusion $\phi = 50$, (a) Gyration radius R_{gyr} vs time scale t/τ, dashed black line show the setup from Fig. 9.5, points denote the steps, where the clusters are depicted in (b); (b) shows the development of the morphology of the cell cluster, dark blue: the proliferating cells at the border, light blue: quiescent cells in the interior.

structure is not a compact cluster (Fig. 9.7 (b)), but later, as more cells divide, the tumor population becomes denser. So although the linear phase is similar to the increases of the proliferating rim, the way it is reached is very different. The early development can be described by a square root function of the gyration radius corresponding to a free migration of particles.

9.4.4 Systematic parameter variation

We have shown the influence of the basic parameters by looking at the morphology and the general expansion using the gyration radius R_{gyr}, and we now proceed to a more systematic study using the parameters ΔL, ϕ, m.
Fig. 9.8 shows a systematic study of growth kinetics for free migration.

Initially, the cell population size grows exponentially fast with

$$N(t) = N(0)exp(t/\tau_{\text{eff}}) \tag{9.1}$$

where the relationship

$$\tau_{\text{eff}}^{-1} = (2^{1/m} - 1)m\tau^{-1} \tag{9.2}$$

is fulfilled [Dra05a].

The duration of the initial phase increases with ΔL and ϕ. The growth law for the diameter depends on ϕ. If $\phi = 0$, the initial expansion of the diameter is exponentially fast. If $\phi > 0$, cells initially detach from the main cluster and the diameter grows diffusively, with

$$L \equiv 2\sqrt{2}R_{gyr} \propto \sqrt{A(\phi + 1/\tau_{\text{eff}})t} \tag{9.3}$$

where $A \approx 1.2$ is a lattice-dependent fit constant (Fig. 9.8(a)).

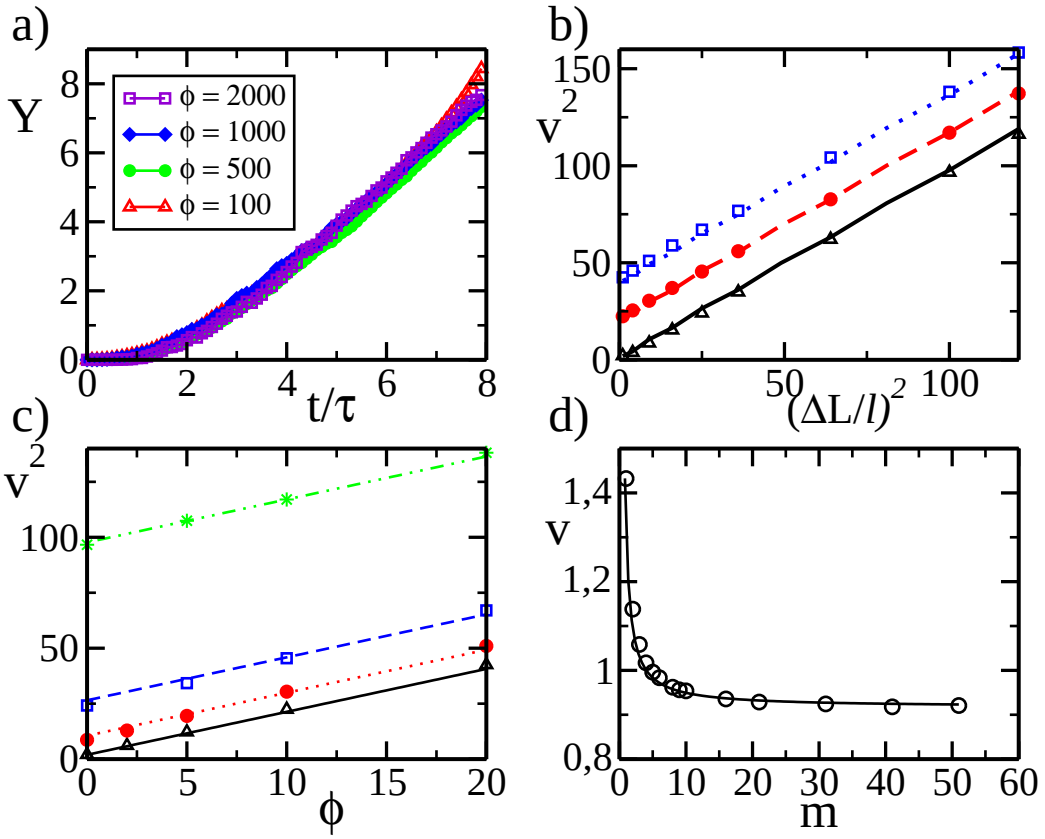

Figure 9.8: Dynamics of tumor cell populations: (a) $Y = R_{gyr}^2/(\phi + 1/\tau_{\text{eff}})$ vs. t/τ for $m = 0$, $\Delta L = 1$ and different values for ϕ. (b-d): Growth in the linear expansion regime ($N \sim 10^5$). (b) Square of expansion velocity, v^2, vs. square of the proliferation zone, ΔL^2 (triangles: $\phi = 0$, circles: $\phi = 10$, squares: $\phi = 20$; $m = 0$). (c) v^2 vs. ϕ (triangles: $\Delta L = 1$, circles: $\Delta L = 3$, squares: $\Delta L = 6$, stars: $\Delta L = 10$; $m = 0$). (d) v vs. m ($\Delta L = 1$, $\phi = 0$). The lines are fits using eqn. (9.4).

For $t/\tau \leq 2$, $R_{gyr} \propto t$ (Fig. 9.8(a)). This regime disappears for $N(0) \gg 1$ (see [Dra05a]). As soon as cells in the interior of the aggregate are incapable of further division the exponential growth crosses over to a linear expansion phase.
Fig. 9.8 shows v^2 vs. (b) $(\Delta L)^2$, (c) ϕ, and (d) m for large N ($N \sim 10^5$ cells).

The model can explain the experimentally observed velocity-range in Ref. [Brú03]. As $t \to \infty$, $L = v(m, \phi, \Delta L)t$ with

$$v^2 \approx B^2([\Delta L'(\Delta L)]^2/\tau_{\text{eff}}^2 + \phi/\tau_{\text{eff}}), \tag{9.4}$$

$B \approx 1.4$ (lines in Fig. 9.8b-c). $\Delta L'(\Delta L)$ ($\approx 1 + 0.685(\Delta L - 1)$) results from the average over all permutations to pick boundary cells within a layer of thickness ΔL.

For $\Delta L/\tau_{\text{eff}} \ll \sqrt{\phi/\tau_{\text{eff}}}$ eqn. (9.4) has the same form as for the *Fisher-Kolmogorov-Petrovskii-Piskounov* (FKPP) equation. (e.g. [Mor01][Mur02]). This equation is frequently used to model tumor growth phenomena by continuum models [Swa00]. Here the FKPP equation is used to predict the distribution of tumor cells for high-grade glioma in regions which are below the detection threshold of medical image techniques. Where we can get the same velocities for expansions depending on different proliferating rims and migration and as we will see, for different apoptotic behaviour, we believe, that these predictions require additionally measurement to decide the different biologically parameters which can lead (as we show) to the same expansion velocity.

9.4.5 Proliferating rim

Where the role of division and migration is clear, we want to explain the role of ΔL here in more detail.

The size ΔL of the proliferating rim controls the growth velocity in both, the off-lattice and the cellular automaton model. In the simulations we found that $v \approx \Delta L'/\tau_{eff}$ with $\tau_{eff} = \tau/\omega$ being the cell cycle time

Here $\Delta L'/l \approx [1 + (\Delta L/l - 1)0.685]$ and $\omega = (2^{1/m} - 1)m$ (and thereby the expansion velocity) depends on the dispersion of cycle time distribution. The parameter $m \in [0, 1, 2, ...)$ controls the shape of the cycle time distribution $f(\tau')$.

Hence the larger the dispersion of the cycle time distribution (by choosing m to be smaller) the smaller is ω, and the larger are τ_{eff} and consequently the expansion velocity v of the monolayer. At no dispersion the expansion velocity is the smallest. The factor 0.685 results from the order in which the cell divisions take place. Although our simulations are in two dimensions, the occurrence of this factor can best be understood if one considers a one-dimensional segment of a two-dimensional growing cell population, ideally a one-cell-thick column ranging from the center of mass of the monolayer until its surface.

If only the outermost cell is able to divide ($\Delta L/l = 1$), the increment within τ is ΔL. However, if the proliferation depth is $\Delta L \gg l$ then the order of divisions determines whether a cell is able to divide or not. To see this assume an almost precise cell cycle length (i.e., a cycle time distribution sharply peaked at $\tau = \langle\tau\rangle$ which is obtained for $m \gg 1$). Then, if it is the innermost cell that divides first then all cells closer to the border are still able to divide while, if it is not the innermost cell that divides first, then the innermost cell cannot divide anymore since this would require to shift more than $\Delta L/l$ cells. So even if $f(\tau') \to\sim \delta(\tau' - \tau)$ the order at which the cells divide matters since for $\Delta L > l$ the cell divisions are not completely parallel. The factor ~ 0.685 can be calculated from investigating the expected growth increment from all permutations of choosing the cells in the proliferative rim for division. Note that the factor ~ 0.685 marks the difference between an asynchronous and a parallel update. To understand

this first note, that since we start each simulation with a single cell, a precise length of the cycle time would mean that all cells divide at the same point of time. The factor ~ 0.685 results from the asynchrony as argued above. For a parallel update this factor would not be expected; the expansion velocity should instead be $v \approx \Delta L/\tau$. (Note that in a circular geometry the expansion velocity may slightly deviate from this value due to the boundary curvature which decreases with increasing monolayer size as $1/R$ with R being the monolayer radius.)
Note also, however, that the factor ~ 0.685 may disappear also in asynchronous updates if the choice of how cells are divided is slightly changed. If one would assume that a cell that once has passed the restriction point divides with probability one that is, if one assumes the decision on whether a cell divides or not is made immediately after its birth and not when it is chosen for division, then the dependency of the velocity upon the order at which the cell divisions in the proliferating rim are performed would no longer be expected.

9.5 Comparison with experiments

Now we want to compare our model directly with the experimental data.

Findings from the off-lattice model [Dra05b] were able to explain the growth velocity found by Bru *et al* [Brú03] for the developing population, and in our simulation we use parameters that are consistent with these findings, namely a proliferating rim of $\Delta L = 9$ and a parameter for cell cycle time distribution $m = 60$.

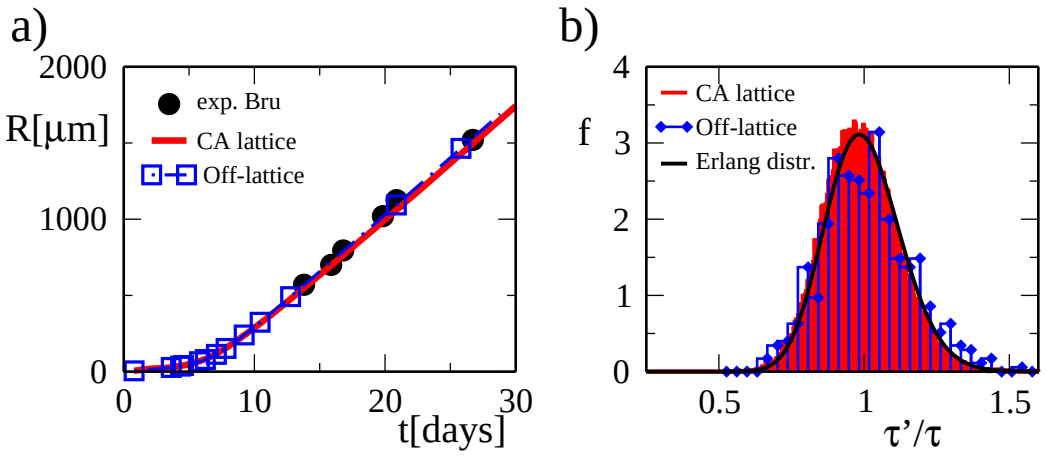

Figure 9.9: Dynamics of experiments:(a) Mean radius $\overline{R}$ of the cell aggregate vs. time t. Full circles: experimental findings for C6 rat astrocyte glioma cells ([Brú03]). (b) Cell cycle time distribution $f(\tau')$ for the off-lattice model and the CA growth model in comparison with the Erlang distribution ($m = 60$, $\Delta L = 9$, $\phi = 0$).

After the simulations we rescaled the resulting expansion parameters using the real size of the cell diameter as also used by [Dra05b] (cell size $l = 10\mu m$ cell cycle time

$\tau = 19h$). As can be seen in Fig. 9.9 our simulation is consistent with both, the experimental data and the off-lattice model.

9.6 Cell density

We have already explained how different parameters and therefore different biophysical properties can lead to the same velocities in the linear phase. We now consider the properties that determine them. A variety of mechanisms can give the same velocity, one being the cell density at the tumor border. If, for example, we have the same velocity but a different migration strength at the border, and cells are also able partly to migrate away from the cluster, this can be determined by measuring the cell density. Cell density here means the mean volume filled within a given radius.

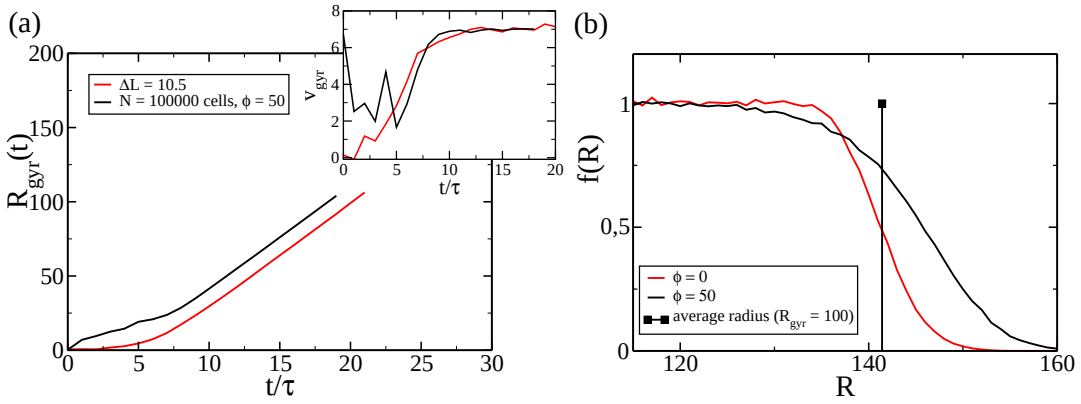

Figure 9.10: Comparison of cell density at the tumor border for simulations with $m = 0$ and two different setups: proliferating rim $\Delta L = 10.5$ and migration rate $\phi = 0$ and $\Delta L = 0$ and $\phi = 50$, $R_{gyr} = 100$ for both simulations, profiles are rescaled to normal radius (factor $\sqrt{2}$) and shifted to recent region.

We have used simulations with the same velocity and the setup of a proliferating rim $\Delta L = 10.5$ and zero migration (black) compared to $\Delta L = 0$ and $\phi = 50$ (red). In both simulations $m = 0$. To make the simulations comparable, we stop the simulations at a gyration radius $R_{gyr} = 100$.

At first we see the same expansion velocities (inset of Fig. 9.10 (a)), but the initial phase is different. The velocity measurement alone obviously does not give us enough information to decide between the two setups, but when clusters without migration are denser, large migration rates lead to more active cells at the border and additionally to unoccupied points, so the density decreases more slowly at the border as shown in Fig. 9.10 (b).

This setup shows that further measurement of either the initial phase or the cell density is required for the model in order to decide between expansions with the same velocity. So the relationship to the FKPP equation can not determine all the relevant parameters.

9.7 Surface dynamics

We now go further to look at the behaviour of the tumor border in terms of the structure function. As already explained, different suggestions have been made for the critical surface dynamics of the tumor cell lines. Whereas Bru et al suggest an MBE like behaviour, the critical comments by Buceta and Galeano suggest a KPZ like behaviour. First we want to look at the behaviour of the case with no migration and $\Delta L = 0$ for different times t. In Fig. 9.11 we see the structure functions for different times

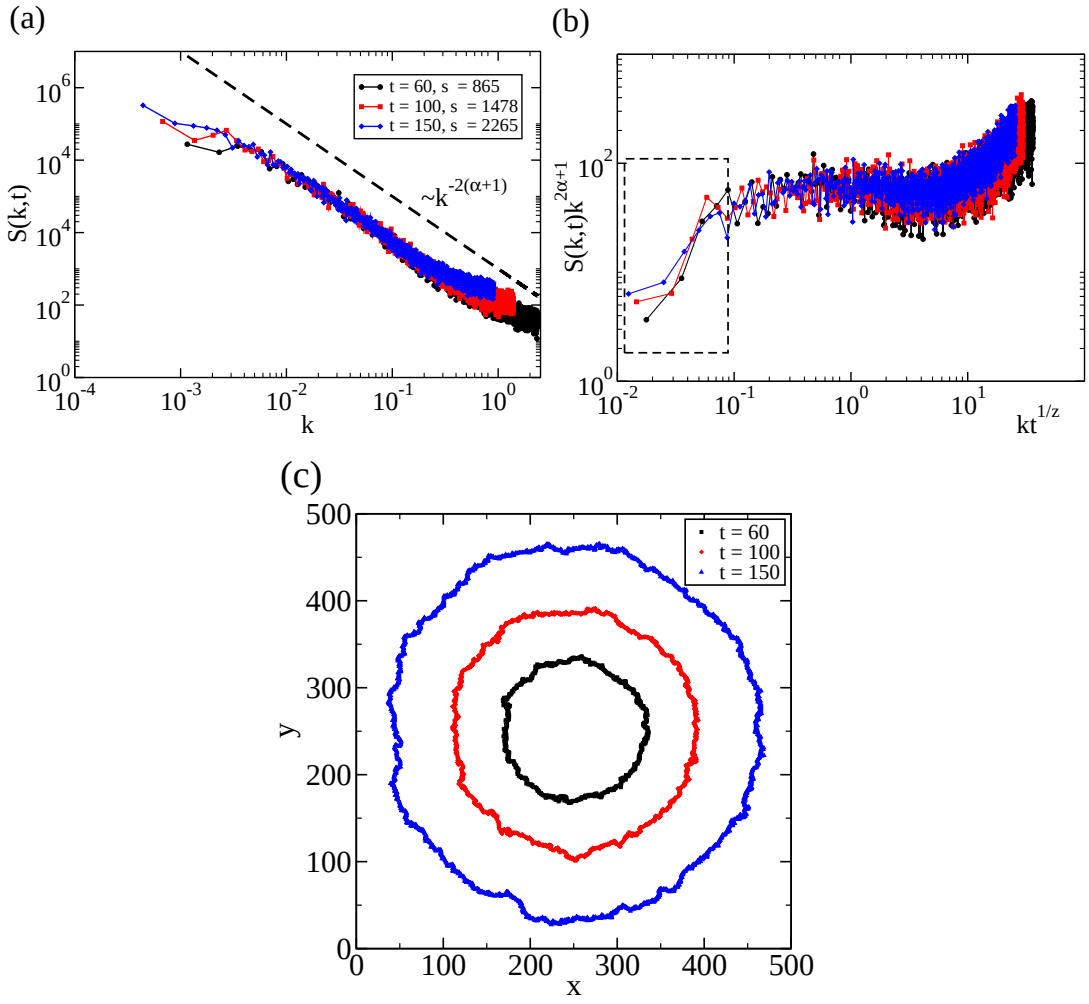

Figure 9.11: Dynamic structure function for $S(k,t)$ vs. k for different times t, $\Delta L = 0$, $\phi = 0$ and $m = 0$, (b) rescaled structure function $S(k,t)k^{2\alpha+1}$ vs. $kt^{1/z}$ by $\alpha = 0.5$ and $z = 3/2$, (c) surface border for the different times.

$t = 60, 100, 150$. The slope suggests a roughness exponent $\alpha = 0.5$. Rescaling using the Family-Vicsek relation (see Sec. 4.2.2) we get data collapse for the function (Fig. 9.11). When we use $z = 3/2$ the data collapse into a single curve, giving us clear exponents corresponding to the KPZ universality class.

Obviously this setup leads to very different scaling to that suggested by Bru *et al*.

We now proceed to vary the other parameters. In Fig. 9.12 (a) we see the behaviour for $\Delta L = 6$ under otherwise constant conditions. Here we have simulations where we calculate the structure function $S(k,t)$ for four different times and we can see that all simulations show similar scaling behaviour.

In Fig. 9.12 (b) we see Arrhenius law migration with parameters $\nu = 2$, $E_s = 1$ and $E_B = 2$ which require large migration rates and define the migration according to the explanation of Bru *et al*.

In Fig. 9.12 (e) we than take the same type of migration with realistic 'slower' rates for the parameters derived from the off-lattice model.

We also varied the sharpness of the cell cycle by $m = 5$ (Fig. 9.12 (c)). We used a setup with free migration $\phi = 100$ (Fig. 9.12 (d)) For both we did not see any MBE-like behaviour.

We have included the migration explained by Bru which should be responsible for the behaviour of MBE like growth. We also tested a lot of different setups for the binding energies but we did not find any MBE-like behaviour in the structure function, but in all simulations values for the roughness exponent close to the KPZ universality class value $\alpha = 0.5$. So we need to explain why we did not find MBE behaviour but rather exponents related to KPZ-behaviour. First we want to remind ourselves about the behaviour for 1+1 dimensions on a single line.

Here MBE-like behaviour corresponds to a system where particles are deposited at a constant rate and then relax due to diffusion on the surface [Bar95; Sar96; Mic04]. MBE describes conserved growth, so, after subtracting the mean deposition, the evolving height function has the same mean average height as when it just roughens.

Physical properties eventually require some of the terms $\nabla^2 h$ (smoothing surface tension) or $(\nabla h)^2$ (lateral growth) but the critical surface dynamics can not rely on the MBE universality class for long term behaviour [Sar96] due to the non-dominant fourth order term (see Sec. 4.4.4Sec. 5.2).

The universality class then is either EW or KPZ.

In MBE modelling the particles fall onto the surface and then relax due to diffusion. Here we have a different case. The particles form the interior of the surface. This behaviour is similar to the deposition of particles and locally the cells can grow laterally. If we take a specific radius vector from the center of mass, we find that the cells can grow in a direction perpendicular to this line.

This behaviour corresponds to lateral growth or, in terms of deposition, to a ballistic deposition model (see [Bar95; Mic04] and references therein) where before relaxation particles stick to the nearest neighbor thereby producing voids and overhangs.

Both explanations lead to KPZ-like behaviour, and we have already pointed out in Sec.7.1.4 that ballistic deposition models belong to the KPZ universality class.

These overhangs can be seen in our model and also in the observations of Bru [Brú03], so it can be seen that we have included such mechanisms in the growth.

Consequently, the behaviour in our model belongs to the KPZ class. If we include the precise mechanisms explained by Bru, then either the calculations of Bru *et al* are

wrong or different mechanisms are causing the observed behaviour.

Our results therefore agree with the critical comments by Buceta and Galeano [Buc05a].

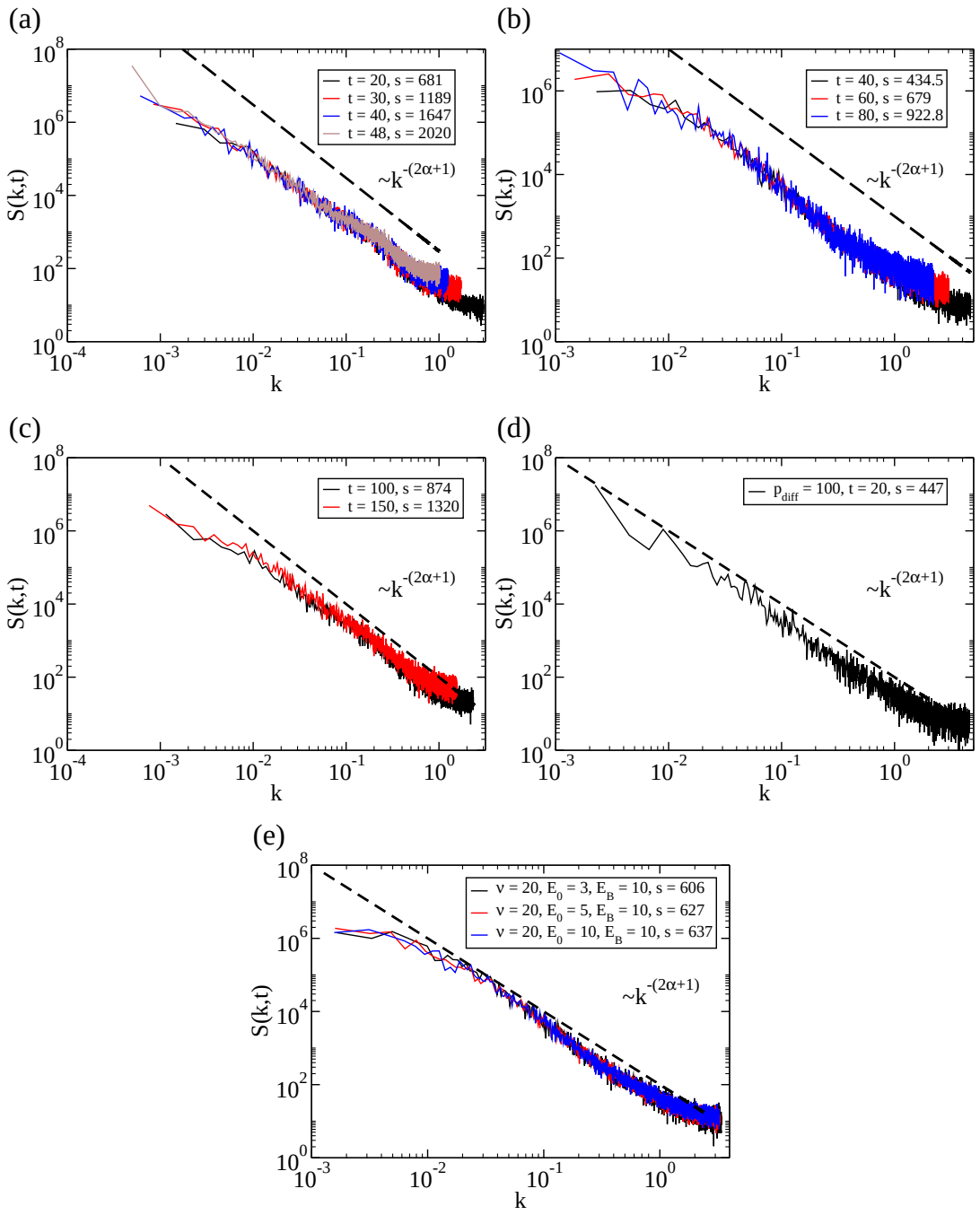

Figure 9.12: Dynamic structure function for different parameters, (a) $\Delta L = 6$, $m = 0$, $\phi = 0$ for different times, (b) $\Delta L = 0$, $m = 0$, migration depending on the coordination number (Arrhenius law) with $\nu = 2$, $E_s = 1$, $E_B = 2$ for different times, (c) $m = 5$, $\Delta L = 0$, $\phi = 0$ (d) $\phi = 100$ with border migration (e) $\Delta L = 0$, $m = 0$, migration depending on the coordination number (Arrhenius law) with $\nu = 20$, varying E_s , $E_B = 10$ corresponding to the energy derived from the off-lattice model, for the same number of cells, in all figures s denote the arclength of the border in average cell sizes, clusters contain a cell number $N \sim 3 \cdot 10^4 \ldots 3 \cdot 10^5$ cells (Bru *et al* $\sim 10^5$), s denotes the arclength in units of average cell sizes (see Fig.8.6).

9.8 Apoptosis

In normal cell populations proliferation is balanced by apoptosis. In tumor cells this balance is destroyed, so although apoptosis can still occur, the cells do not stop their uncontrolled proliferation and the population size increases. We now want to look at the two types of apoptosis we included in the simulation and their influence on the expansion of the monolayer.

9.8.1 Apoptosis with constant probability

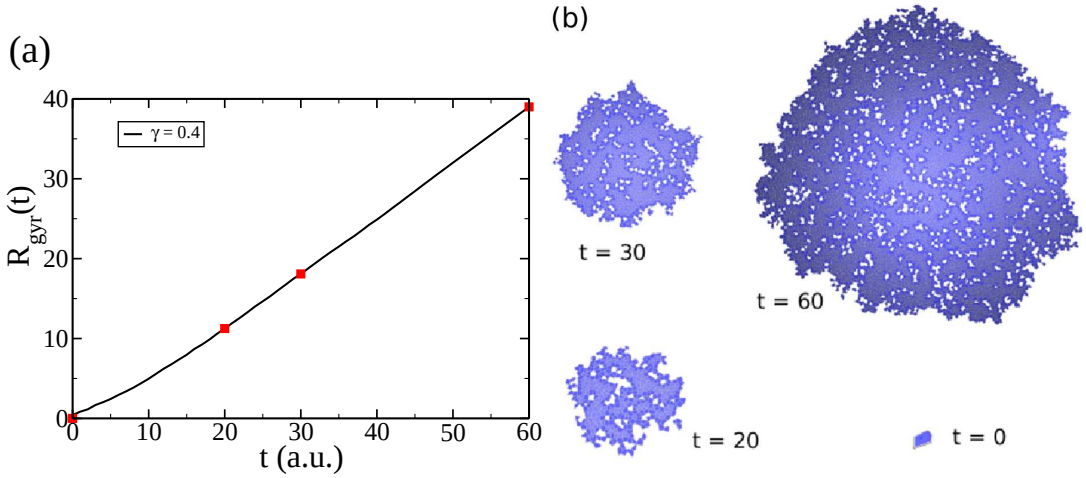

Figure 9.13: Apoptosis with constant rate. Parameters: $\phi = 0$, $m = 0$ and rate for apoptosis $\gamma = 0.4$, (a) R_{gyr} vs t/τ, (b) shows the development of the morphology of the cell cluster, dark blue: the proliferating cells at the border, light blue: quiescent cells in the interior. $\phi = 0$, $m = 0$ and $\gamma = 0.4$.

As we can see in Fig. 9.13, apoptosis, as expected, changes the velocity of population growth. It only affects the border at extremely large rates; otherwise it leads to smaller expansion velocities. The linear phase is reached later, at a stage where the rate at which cells undergo apoptosis and proliferate determines the velocity. A larger proliferating rim would compensate for this effect, but one could still not determine the expansions.

We now want to retest those setups where we expect to see the same expansion velocities. In Fig. 9.14 we have chosen setups for very different conditions both with and without migration, neglecting apoptosis and with varying proliferating rims.

In Fig. 9.14 we see that three setups show exactly the same expansion velocity for different mechanisms. So we once again see behaviour that supports the assumption that the velocity can not be the only parameter which determines the growth conditions.

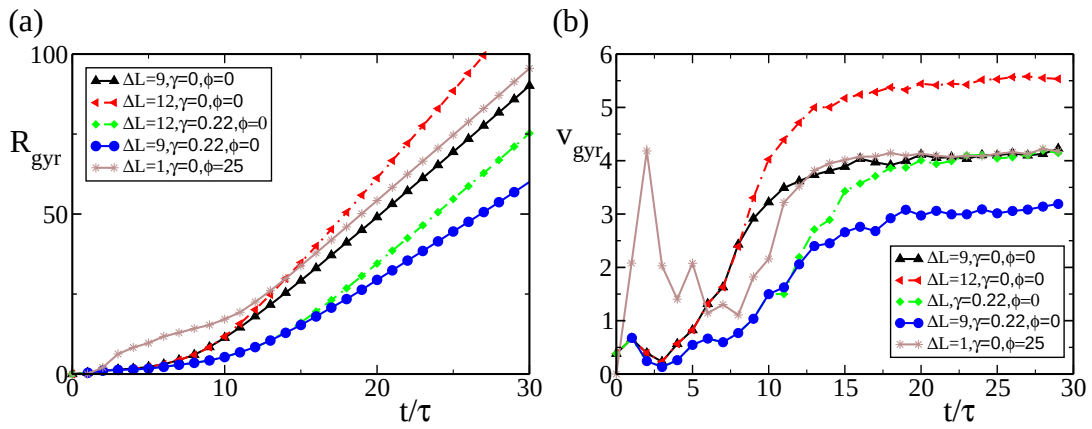

Figure 9.14: Setups with the same velocity for five setups with and without migration, different proliferating rims and different apoptosis rates: (a) $R_{gyr}(t)$, (b) the velocities of the same setups.

9.8.2 Apoptosis with mutations

For apoptosis with constant probability we now let the rate γ mutate with a variation of $\Delta\gamma$ as explained in Sec. 8.3.5. In Fig. 9.15 (a) we see the expansion of the monolayers

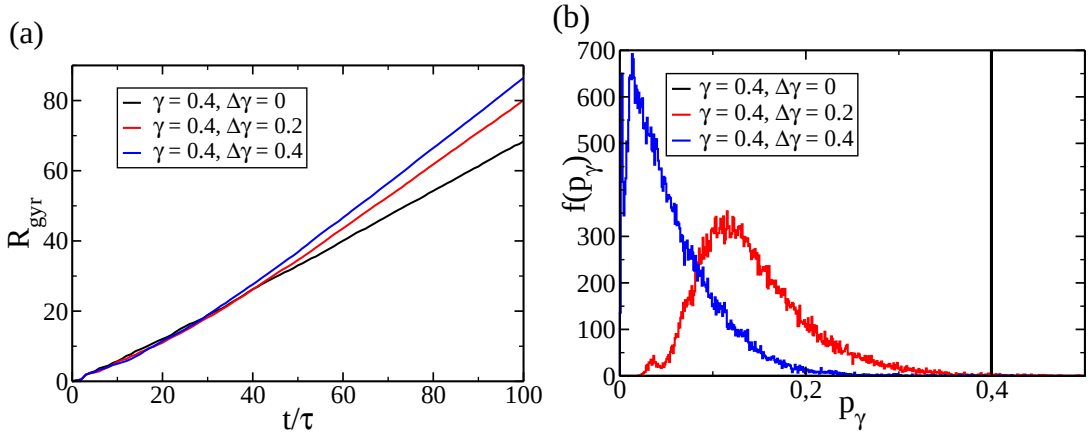

Figure 9.15: Mutation of apoptosis rate. Parameters: $\gamma = 0.4$, $t = 100$, $m = 0$ and $\Delta L = 0$, (a) Gyration radius R_{gyr} vs time scale t/τ for different mutations of the apoptosis $\Delta\gamma$ (b) distribution $f(p_\gamma)$ of probability to undergo apoptosis.

for three different rates of apoptosis mutation $\Delta\gamma \in \{0; 0.2; 0.4\}$ with a constant initial rate of apoptosis $\gamma = 0.4$. In Fig. 9.15 (b) we have depicted the histogram of successful apoptotic processes and the corresponding rates of the individual cells, and we can see in both the expansion and the histogram that the velocity increases with the mutation of the apoptosis rate, where, not surprisingly, the monolayer with more cells to divide expands faster.

Here we see a kind of competition between the cells where the mutation gives higher apoptotic rates and those with lower rates. Obviously the cells that win have a lower probability of dying, as can be seen in the distribution.

9.9 Mutations of the cell cycle

Tumor cells are characterized by uncontrolled proliferation and one basic mechanism which leads to this is cell mutation. Defects in tumor suppressor genes are one reason for the behaviour. During uncontrolled proliferation changes in the cell cycle can also appear. If the cell cycle decreases, the DNA replication phase can also be shortened, which makes it more difficult for the cell to repair defects and this again leads to mutations. We now look at simple kinds of mutations in the cell cycle.

In Fig. 9.16 we can see that both cell dynamics and expansions significantly change under mutation and that the resulting morphology reflects the mutation. Whereas in the early phase no significant differences can be seen, in the late phase the mutations lead to totally different behaviour. The expansion velocity increases rapidly and the

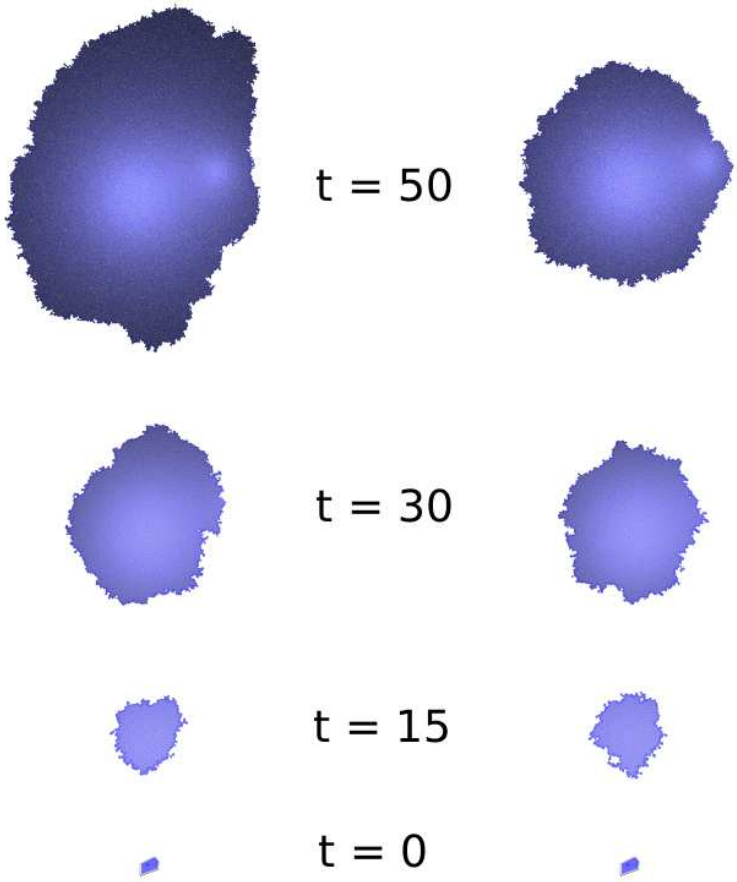

Figure 9.16: Comparison of mutated and unmutated cell morphology: $\phi = 0$, $\Delta L = 0$, and mutation of the cell cycle time $\Delta\tau = 10\%$.

nearly round shape of the cell cluster is destroyed. We start with a mutation equally distributed around the average cell cycle time and by definition no side is preferred. But as we can see, faster cells are in the lead in the expanding tumor monolayer.

That is not really surprising, since, when faster cells lead, new cells also divide fast and thereby overgrow the slow cells, which are then not equally distributed over the monolayer and so don not dominate the growth conditions.

So we have a kind of competition between the initially equally distributed fast and slow cells. The fast cells win the competition and are responsible for the behaviour of the monolayer.. In Fig. 9.17 we see that, for different strengths of the mutation,

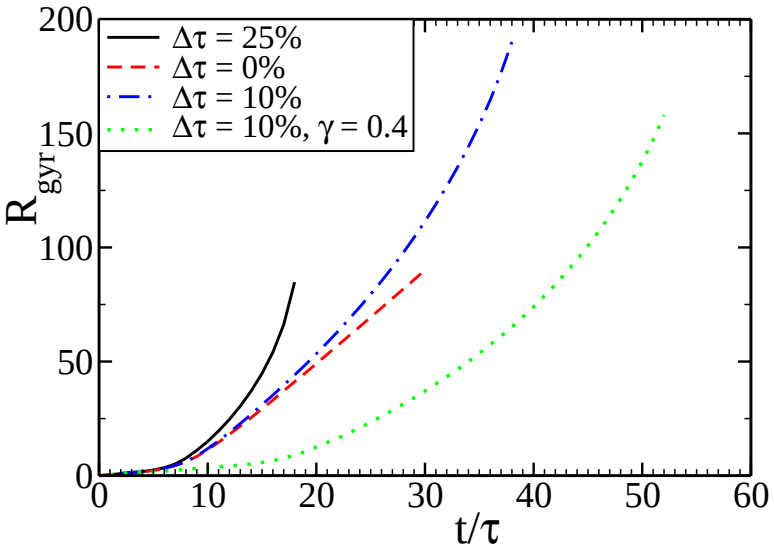

Figure 9.17: Mutation of the cell cycle and apoptosis for four different setups, all simulations with $\Delta L = 0$, no migration and $m = 0$.

velocity increases with strength and apoptosis causes a strong increase in the gyration radius in the expansion that sets in later due to the mutation.

We have now tested one specific setup, where we only varied the apoptosis rate. We took a setup with $\Delta L = 9$, $m = 60$ and $\phi = 0$, zero apoptosis and $\gamma = 0.4$. Expansion is, as expected, initially faster in the setup without apoptosis (Fig. 9.18). But, surprisingly, the expansion velocity of the setup with apoptosis increases faster and reaches the velocity of the non-apoptotic case at the intersection point. The reason is that, in the apoptotic case with a constant rate, the mutated fast and slow dividing cells undergo apoptosis. When the fast dividing cells dominate growth, the slow are destroyed by apoptosis faster than in the non-apoptotic case.

So under apoptosis the contest between fast dividing and slower dividing cells is lost earlier. Until then, velocity increases more strongly than in the non-apoptotic case and reaches it at the intersection point shown in the figure.

9.9.1 Global fluctuations

We now want to see how growth is affected by fluctuations which are not intrinsic to the individual cells but to the underlying structure. So we take a pre-described random

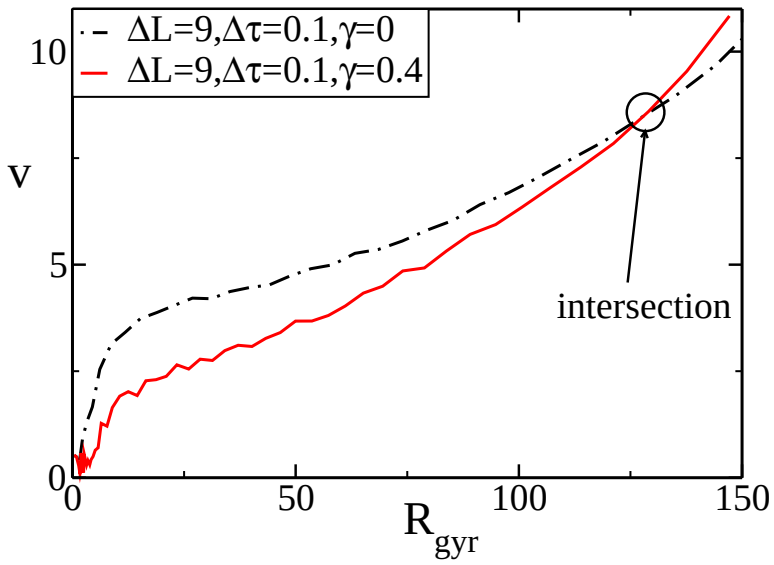

Figure 9.18: Mutation and mutation with apoptosis, parameters the same as in 9.9, additionally we include mutation $\Delta\tau = 10\%$ and for the second setup additionally apoptosis $\gamma = 0.4$.

distribution of the cell cycle time around the average $\tau \in [\overline{\tau} - \Delta\tau/2, \overline{\tau} + \Delta\tau/2]$. In our simulation we change the corresponding probabilities for a cell to divide at that point. We here test different setups with and without apoptosis and with different fluctuations. We also compare our non-intrinsic mutation with the mutation where the change of the cell cycle is coupled to the cell.

As we can see in Fig. 9.19 (a), our change does not seems to affect the dynamics for all setups. We take the setups with $\gamma = 0.0$ and $\gamma = 0.1$ as references and see that the setups with additional fluctuations ($\Delta\tau = 40\%, \Delta\tau = 5\%$) show the same behaviour. A look at the velocities in Fig. 9.19 (b) confirms this behaviour. Although we do not see differences in the general behaviour, a closer look at the setups with $\gamma = 0.1$ and zero fluctuation and $\Delta\tau = 40\%$ shows that there are larger fluctuations in the velocity. We conclude that a random fluctuating underlying cell cycle distribution has no effects on the general dynamics, as opposed to the case explained before, where an intrinsic cell cycle mutation leads to extreme changes in the dynamics with the faster cells dominating growth (shown for comparison in Fig. 9.19 (a)).

9.10 Summary and outlook

We explained in this chapter the development of tumor cell in-vitro monolayers under specific growth conditions. By means of a Kinetic Monte Carlo method we observed the expansion kinetics depending on the basic processes, namely division and migration of cells.

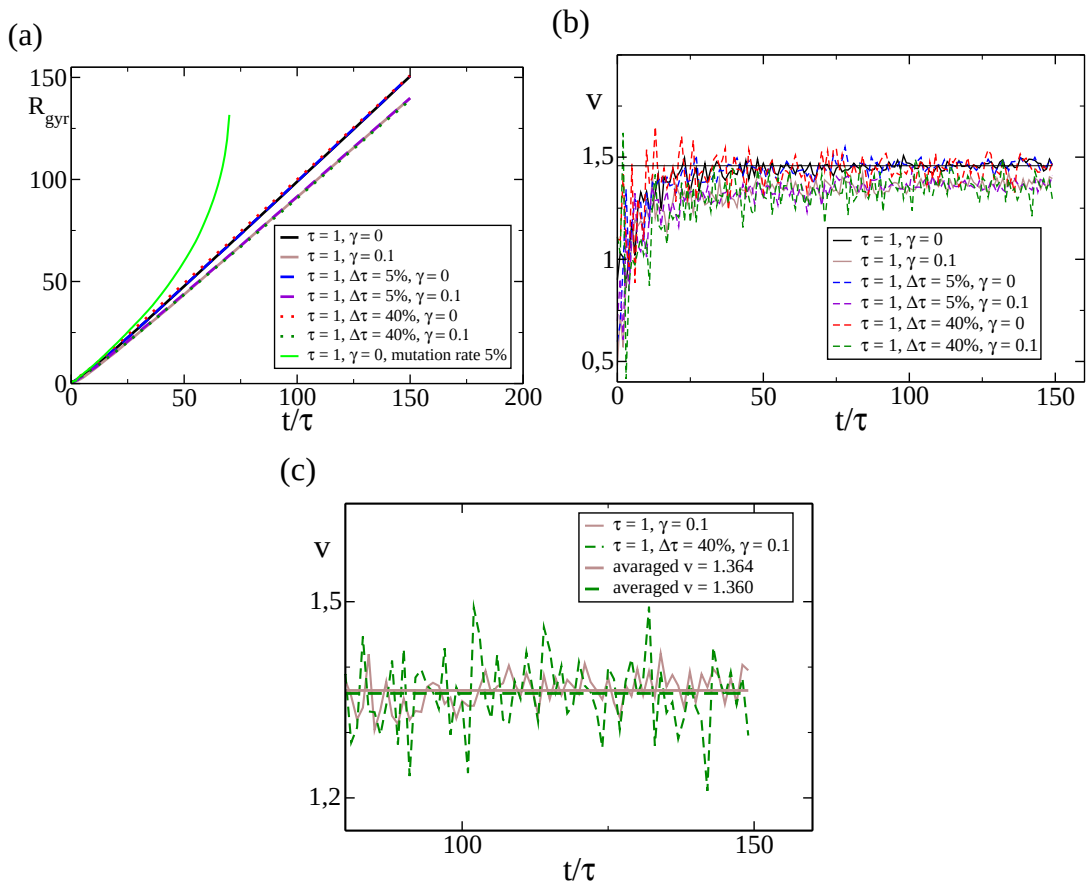

Figure 9.19: Fluctuations of cell cycle depending on the individual lattice site.

We introduced a new type of lattice, which under different kinds of noise reduction opposite to a regular structure does not show any lattice artifacts.

Guided by an off-lattice model the simulation can explain the kinetics observed in experiments.

A detailed analysis of the additionally determining parameters ΔL, ϕ and the parameter m which ensure a realistic cell cycle time distribution we observed an asymptotic expansion velocity that is reminiscent of the front velocity of the FKPP equation.

We have shown by variation of parameters that different biologically relevant mechanisms can lead to the same velocities in the development and concluded, that the velocity in the linear phase can not be the only parameter which determine this quantity.

Additionally one has to explain the proliferating rim Δ and the migration rules and the cell density at the tumor border to get indications, which mechanisms lead to the expansion.

We then included different kinds of apoptosis as a relevant parameter and again showed setups, where very different mechansims lead to the same velocity in the linear

expansion. Here, a detailed view in experiments to the early is required to decide between the different mechanisms.

Guided by the experiments of Bru *et al* and additionally motivated by the critical comments of Buceta and Galeano, we explained in detail the critical surface dynamics of the tumor border. By use of the scaling theory for self-affine types of growth we calculated the three critical exponents α, β and z. Therefore we varied the growth conditions in a wide range. In particular we also introduced the migration rules proposed by Bru *et al* to be responsible for the tumor growth of different cell lines.

While Bru *et al* claimed a MBE-like critical surface dynamics by these migration rules, we did not find by parameter variation any MBE-like behaviour but, opposite to their findings, a KPZ-like behaviour for all setups.

Thus, our observations assert the critical comments of Buceta and Galeano.

We then additionally implemented different kinds of mutations and fluctuations of the cell cycle and explained how mutated cells affect the kinetics and the morphology. We found that randomly distributed non-intrinsic fluctuations (fluctuations of the cell cycle time due to conditions depending on the underlying structure) don' t lead to significant changes, but just to a more strongly fluctuating velocity.

We have shown that a special type of the underlying structure leads to an absence of lattice artifacts, which in comparison can be clearly seen for regular lattice types.

We included a realistic cell cycle time distribution by the Erlang distribution. So our cell cycle has a predefined distribution around the mean cell cycle time.

Guided by the experiments and by use of results from an off-lattice model we could reproduce the dynamics for tumor cells observed in experiments.

Our model can explain and distinguish a variety of biologically relevant actions for the developing system and give the ability to observe the behaviour without unknown influences.

We explained the expansion kinetics and the dependence of it on the determining parameter proliferating rim ΔL, the strength of migration ϕ and the parameter m related to the sharpness of the cell cycle distribution.

We now want to briefly explain some other possible further observations, which could be made by use of the developed simulation tool.

9.10.1 Limited mutation of the cell cycle

We described the mutation of the cell cycle as a variation of the probability for division equally distributed corresponding to the variation of the cell cycle time (see Sec. 9.9). This mutation generally include the possibility of the cells to mutate to a regime, where the cells divide very fast. If we take into regard that the mitosis phase ($1 \sim 2h$) in comparison to the whole cell cycle ($\sim 24h$, in experiments for the expansion $19h$) is very small, then this approach appropiate for a model. A more detailed assumption would be the inclusion of a lower border for the cells to divide.

Mutations to lower cell cycle times lead to the reduction of the interphase, so there is less time for the cell to activate their repair mechanisms. Nevertheless there is a minimum time, which the cell need to duplicate.
In Fig. 9.20 we show a setup with such a minimum time for the cells to divide.

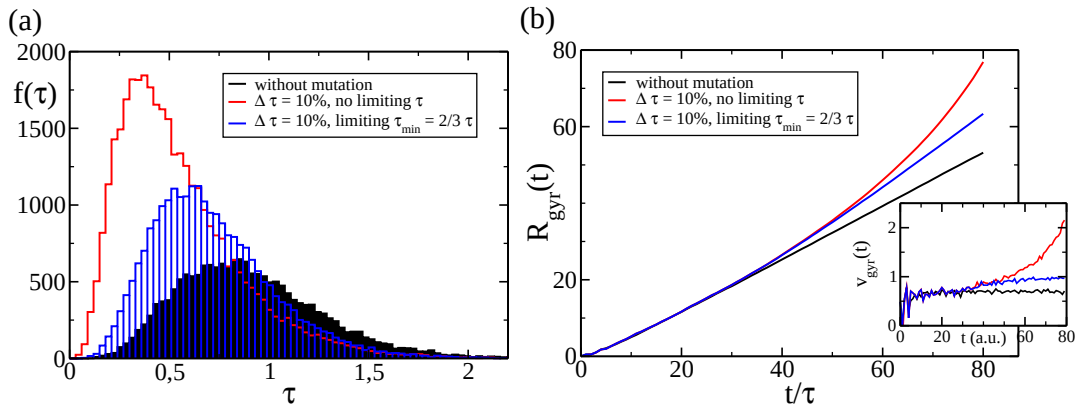

Figure 9.20: Mutation with limiting lower border τ_{min} setups used for 100000 cells, without mutations, with cell cycle mutation $\Delta\tau = 10\%$

If we consider also the upper border, such an assumption is not so evident and may be not realistic, since the cells can enlarge their gap phases in a wide range [Alb02].

The nondominating nature of the cells with larger cell cycle times in our model we have already shown for the mutations without borders, where the fast dividing cells dominate the expansion kinetics and the slower cells do not affect the growth.

The same behaviour we get by a limiting border. In Fig. 9.20 (a) we see, that the cell cycle distribution has changed to faster dividing cells also for the setup with a limiting minimum cell cycle time of $\tau_{min} = 2/3\tau$ (Fig. 9.20 (b)). Then the expansion velocity increase in comparison to the unmutated case, but has a lower velocity than the case of mutation without limiting borders (Fig. 9.20 (b)).

9.10.2 Correlated global fluctuations

We defined before the influence of the nonintrinsic fluctuations totally randomly on the lattice and see as a result no general changes in the expansion kinetics but a stronger fluctuation in the velocity as expected. A further development of thes concept would be the inclusion of nonrandom fluctuations, but defined pattern, by which the cell cycle change due to fluctuations of the environment which could be explained by differently distributed nutrient supply.

9.10.3 Different rules for division

The most important process is obviously the division of the cells. We used a division which includes a random selection of the new place in the environment for one of

the daugther cells, where the mother cell stay on the old position. For a cell in the proliferating rim, the cell select the shortest way to push the cells in this direction. This leads to a shift along this cell pushing path for the cells.

Where cells are able to sense their environment, this rule for division could differ. Possible non-random divisions could be the selection of the longest distance motivated by the aim to get as much volume for the cell as possible. Another way to reach this aim is to make the algorithm able to count the coordination number and to select the position which as less as possible neighbors.

By these different division rules we can define different model types which could lead to very different expansion kinetics. In particular we included 5 different divisions.

- 0 random selection of the new cell, shift to the shortest distance inside ΔL
- 1 random selection of the new cell, shift to direction of a random cell inside ΔL
- 2 selection of the new cell by the longest distance, shift inside ΔL to the longest distance
- 3 selection of the daughter cell by the minimum coordination number, shift to the cell inside ΔL with the lowest coordination number
- 4 selection of the daughter cell by the maximum coordination number, shift to the cell inside ΔL with the highest coordination number

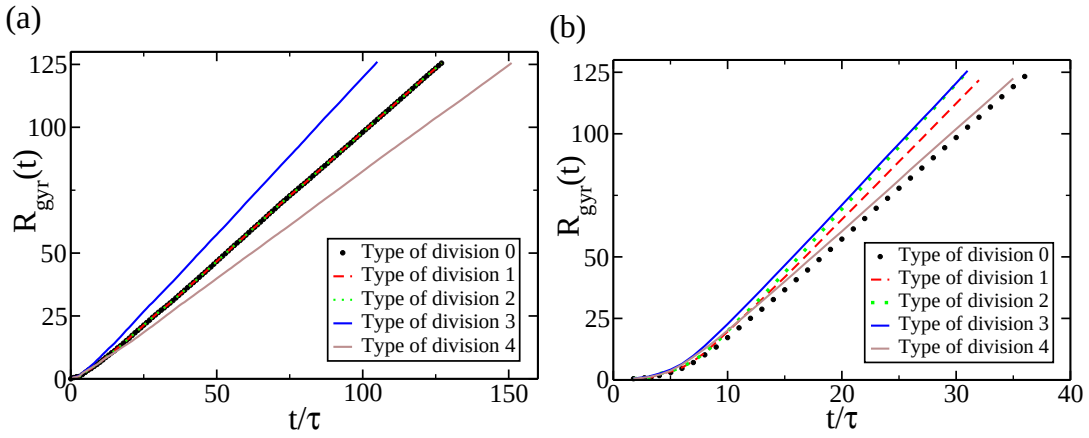

Figure 9.21: Expansion kinetics for different division rules for 100000 cells, (a) $\Delta L = 0$ in all cases, (b) $\Delta L = 6$ in all cases, simulations without migration.

In Fig. 9.21 we see that the expansion kinetics differ depending on the division rule. We do not see different velocities for the first three types and a proliferating rim $\Delta L = 1$. However the rule depending on the coordination number changes here the kinetics. That is not surprising, since the the rules here just affect the cells, which are inside the

proliferating rim and not at the border. For a larger proliferating rim all expansion kinetics differ, where not only the linear phase is changed, but also the initial expansion. So defining these rules, we can investigate by the simlation tool different model types for the division guided by the assumption, that cells could sense their environment.

9.10.4 Different rules for migration

Before, we used different migration rules, where we included free migration, free migration at the tumor border and a migration depending on the coordination number by an Arrhenius law. In Fig. 9.22 we show that by all of these different migrations defining different types of model one can reach the same expansion velocities as for the experiments of Bru [Brú98]. Here the velocity (Fig. 9.22 (b)) is in $\mu m/days$ corresponding to the shown development of the radius in Fig. 9.22 (a). The velocity is consistent with the experimentally observed velocity $v = 2.9\mu m/h$ for C6 rat astrocyte glioma [Brú98].

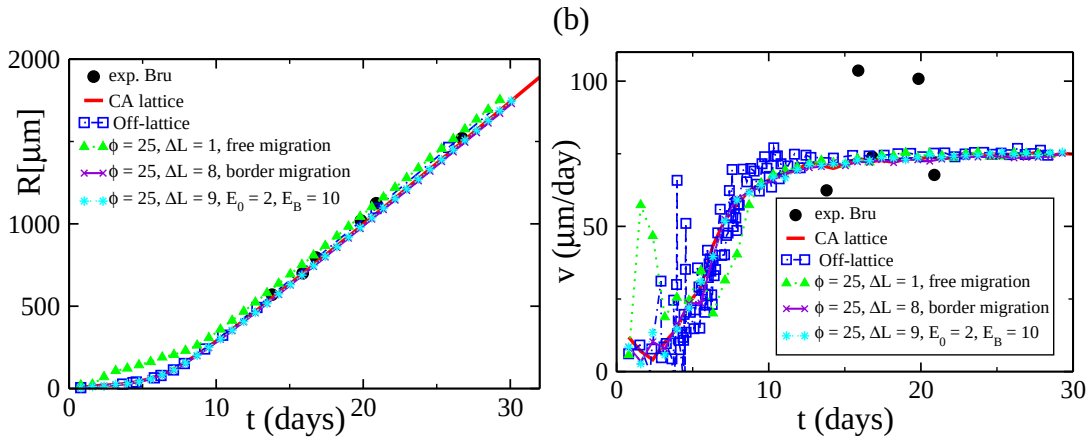

Figure 9.22: Expansion kinetics for different migration rules for (a) Mean radius $\overline{R}$ of the cell aggregate vs. time t. Full black circles experimental findings for C6 rat astrocyte glioma cells ([Brú03]), three different migration rules, free migration (green), to border restricted free migration (violet) and Arrhenius law migration (light blue) (b) expansion velocity for the same setups.

In case of the coordination number dependent rule, the choice of different setups is thereby possible by definition of the 'binding energies' which define the ΔE in the Arrhenius law. For particles in crystal growth, namely effective atoms, the effective binding is always positive. We have normally a surface binding and a neighbor binding. In case of cells, which we inlcude as points, the behaviour may vary. If we assume a cell-cell adhesion to the tissue, the cells could nevertheless by sensing tend to migrate to position with more free volume. This could be included by including the cells to migrate preferently to positions with less neighbors. In our algorithm, that is just a setting of the different sign of the neighbor binding.

In conclusion here we also have shown some possibilities which the simulation tool additionally offer for further investigations.

Chapter 10

Conclusions and Outlook

In this work the self-organized growth was extensively studied for two different types of systems.

First we modeled epitaxial crystal growth by use of the well-established stochastic differential equations. Additionally we applied the theory of time-delayed feedback methods to develop a tool to study the control of the roughening phase of surfaces by time-delayed feedback control. For different growth equations we showed, how the corresponding growth exponent β could be adjusted by such a scheme.

In the second part a powerful model for simulation of cell population growth by means of a Kinetic Monte Carlo method was developed. Aimed to model the growth of tumor cells in an in-vitro monolayer, the tool includes a large variety of properties of biological relevance. By extensive simulations we have investigated the generic kinetical behaviour and have shown that our single cell based cellular automaton model reproduces the kinetics of experimental studies and can explain the critical surface dynamics of the tumor borders.

In both parts we made use of the well-established scaling theory, which gives for self-affine types of growth phenomena the ability to determine the surface roughness evolution by means of three exponents, namely the growth exponent β, the roughness exponent α and the dynamic exponent z, where only two of those are independent.

For the crystal growth we additionally established a new type of control method to adjust the growth exponent. For the tumor growth we developed a simulation tool which combines advantages of lattice models and off-lattice models by definition of an irregular lattice free of artefacts.

In particular by numerical schemes we solved the stochastic growth equations, namely the Kardar-Parisi-Zhang and the Molecular Beam Epitaxy equation in 1+1 and 2+1 dimensions. Detailed analysis lead to observations of the three critical exponents β, α and z which determine the universality classes for the growth.

We could exactly reproduce by our scheme the exponents for the MBE equation in both dimensions, but for the KPZ equation we get stable values only for 1+1 dimensions and some indications during control for the 2+1 dimensional case.

We then defined a time-delayed feedback method to control the early roughness evolution by adjusting the growth exponent β during the roughening process.

Our method in particular includes two different schemes, the *digital control*, which acts by a control step a on the sign of the difference to the desired exponent and a *differential control* which contains an amplification factor K, which determines the control force F.

We explained in detail, how one can define, restrict and calculate parameters which could be useful for control.

The control after that gave precise results for two types of control with predictions for possible experiments. Indications for possible setups were explained by comparison with recent experiments [Oje00; Oje03]. Here, for a specific system, the relation between the nonlinear term λ from the KPZ equation to the temperature is explained in detail and it is shown that one can tune it by changing the temperature.

A lot of additional observations identify the KPZ equation as relevant for low temperature behaviour in experiments due to the nonlinear term which is related to lateral growth. In high temperature systems, diffusion processes dominate the growth process, so the MBE equation then is responsible for the universality of the growth.

For both types of behaviour, the tuning of temperature can change the behaviour and a relation to the theory could be given by experiments where the exponents dependent on temperature have to be measured.

While further explanations by experimental setups have to reproduce the theoretical investigations, the method could then give predictions how the roughness development can be tuned by time-delayed feedback.

We have explained in detail limits of control for both the digital and the differential scheme. These findings should also be reproduced by different types of methods, namely a Kinetic Monte Carlo method for a solid-on-solid approximation of crystal growth.

For the single cell based tumor growth model we explained in detail the dynamics and the surface morphology depending on different parameters.

We have defined a new lattice type consisting of Voronoi cells related to the biological cells. A construction by a Delauney triangulation gives a well defined average cell size with a well defined sharp distribution around the mean area.

The relation of the cell cycle to an Erlang distribution included in the model ensures realistic cell cycle time distributions.

By extensive simulations we observed the expansion kinetics of tumor cell in-vitro monolayers.

By the special lattice construction we ensured that our model is free from any lattice artefacts. So the model establishes a tool where one combines the advantage of

off-lattice models which are independent from any underlying lattice structure and the advantage of well-defined neighborhood which leads to a faster simulation.

We have shown that the expansion kinetics covers the findings observed in experiments and the observations made by an off-lattice model. It was in detail explained that very different biological actions included in our model can lead to the same expansion velocities in growth. Recently, mathematical models based on the Fisher-Kolmogorov-Petrovskii-Piskounov (FKPP) equation were used to predict the distribution of tumor cells for high-grade glioma in regions which are below the detection threshold of medical image techniques [Swa00]. We found that the asymptotic expansion velocity has a form that is reminiscent of the front velocity of the FKPP equation, nevertheless the same expansion velocity can be obtained for different combinations of the migration and division activities of the cell and of the cycle time distribution.

So in conclusion we believe such predictions must fail since the FKPP equation lacks some important parameters such as the proliferation depth which is why it is not sensitive to relative contributions of the proliferation depth and free migration.

We observed in our simulations that these relative contributions in fact determine the cell density profile at the tumor-medium interface: the larger the fraction of free migration is, the wider is the front profile even if the average expansion velocity is constant.

We additionally included apoptosis with different rules consistent with biological interpretations of that process and again determined the expansion kinetics, where we showed in detail that a large variety of different mechanims leads to the same velocities in the linear regime of the expansion.

We found the determining processes and thus can give suggestions for possible experiments to decide these different cell actions, for instance the measurement of the cell density at the tumor border or the migration activity or the early phase to observe large apoptosis rates.

By additional inclusion of various intrinsic mutations of the cell cycle and nonintrinisic fluctuations of the underlying structure we then showed scenarios which could determine the kinetics in cell lines under strong mutational behaviour.

For these observations by construction we don not prefer mutations to fast or slow dividing cells, nevertheless we see a strong regime, in which after a certain time range the faster cells always dominate the growth and thus determine the expansion.

Bru *et al* propose the cell lines, they investigated to show universal scaling related to the MBE universality class, we included a calculation of the corresponding critical exponents. For a wide range of different setups under inclusion of the migration proposed by Bru *et al* to be responsible for this type of universality class, we did not find any MBE-like behaviour, but strong KPZ-like critical behaviour. Our findings thereby comply with the critical comment of Buceta and Galeano.

We here stronlgy suggest further experimental investigations.

So in conclusion we investigated two systems related to complex growth phenomena, where in both parts scaling theory played an essential rule. For stochastic differential equations applied to epitaxial growth we established a new method of a time-delayed feedback control and gave predictions, how possible experimental setups have to act to tune the roughness evolution 'in situ'.

In addition, these findings could in general be applied to any system, which belong to the explained equations, where one then has to define the relation between the equation parameters and the growth phenomena.

For the second system, the tumor growth of an in-vitro monolayer, we explained in detail how the biological actions on the scale of an individual cell determine both the expansion kinetics and the critical surface dynamics.

We could reproduce the kinetics in consitstency with an off-lattice model and with experiments. However, our investigations for the universality class of tumor growth don not comply with previous interpretations of the experiments and require new experimental investigations.

Thus we investigated problems on the nanometer scale for materials grown by epitaxial methods and cell behaviour from the length scale of an individual cell to large cell populations and hopefully contributed in some way to the problem of the 'nanobot' outlined in the preface.

Appendix A

Simulations of stochastic growth equations

A.1 Additional simulations KPZ 1+1

In Fig. A.1 and Fig. A.2 we show the control for a larger system size $L = 32768$. In Fig. A.1 the results for three initial setups $\lambda_0 = 0$ and $\beta_0 = 0.33$ (black), $\lambda_0 = 0.1$ and $\beta_0 = 0.29$ (red), and $\lambda_0 = 0.25$ and $\beta_0 = 0.25$ (blue) are shown, the digital (Fig. A.1 (a)) and the differential (Fig. A.1 (b)). The roughness evolution shows, that all setups can be controlled and the evolution of the nonlinearity $\lambda(t)$ show the general properties of the control method, increase of the function for the first setup (black), nearly stable function for the second setup (red) and a decrease for the third setup (blue).

In Fig. A.2 the results for three initial setups $\lambda_0 = 0$ and $\beta_0 = 0.29$ (black), $\lambda_0 = 0.1$ and $\beta_0 = 0.29$ (red), and $\lambda_0 = 0.25$ and $\beta_0 = 0.29$ (blue) are shown, the digital (Fig. A.1 (a)) and the differential (Fig. A.2 (b)). The roughness evolution shows, that all setups can be adjusted to the same desired exponent $\beta_0 = 0.29$ (guide to the eyes: green).

In Fig. A.3 - A.6 we show the results for the KPZ equation in 1+1 dimensions for digital and differential control with initial nonlienarities $\lambda_0 = 0.05$ and $\lambda_0 = 0.15$. As for the results shown in Sec. 7.1.3 (Fig. 7.9 - 7.15), five setups with different β_0 for each control type and nonlinearity are chosen. The results show again the general behaviour of the control methods.

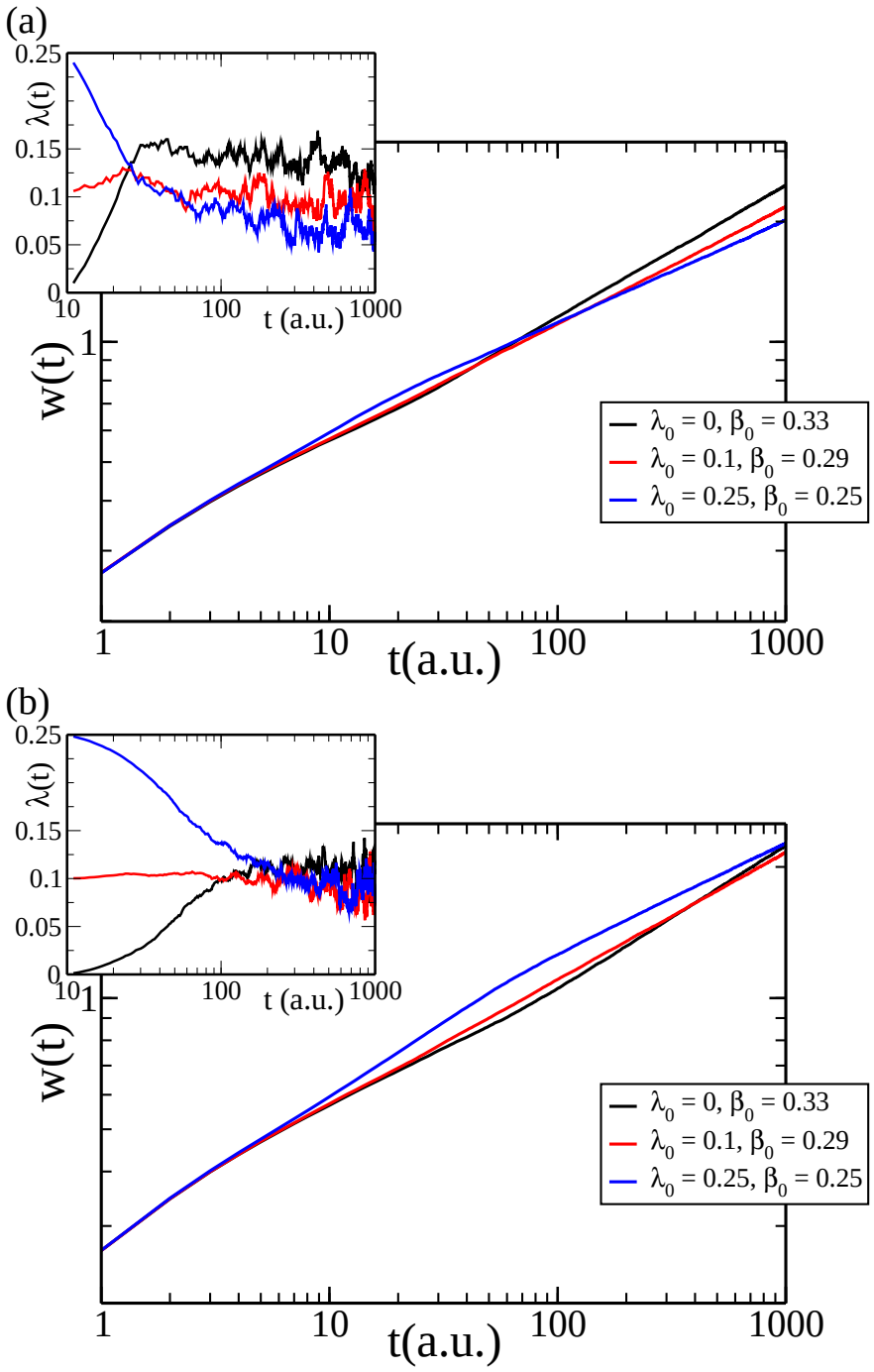

Figure A.1: Control for the KPZ equation in 1+1 dimensions with L = 32768: Three setups for the digital and the differential control $\lambda_0 = 0$ and $\beta_0 = 0.33$ (black), $\lambda_0 = 0.1$ and $\beta_0 = 0.29$ (red), and $\lambda_0 = 0.25$ and $\beta_0 = 0.25$ (blue). (a) digital control with $a = 0.01$, (b) differential control with $K = 0.02$, time discretization $dt = 0.01$ for all setups, upper left insets show the functions $\lambda(t)$..

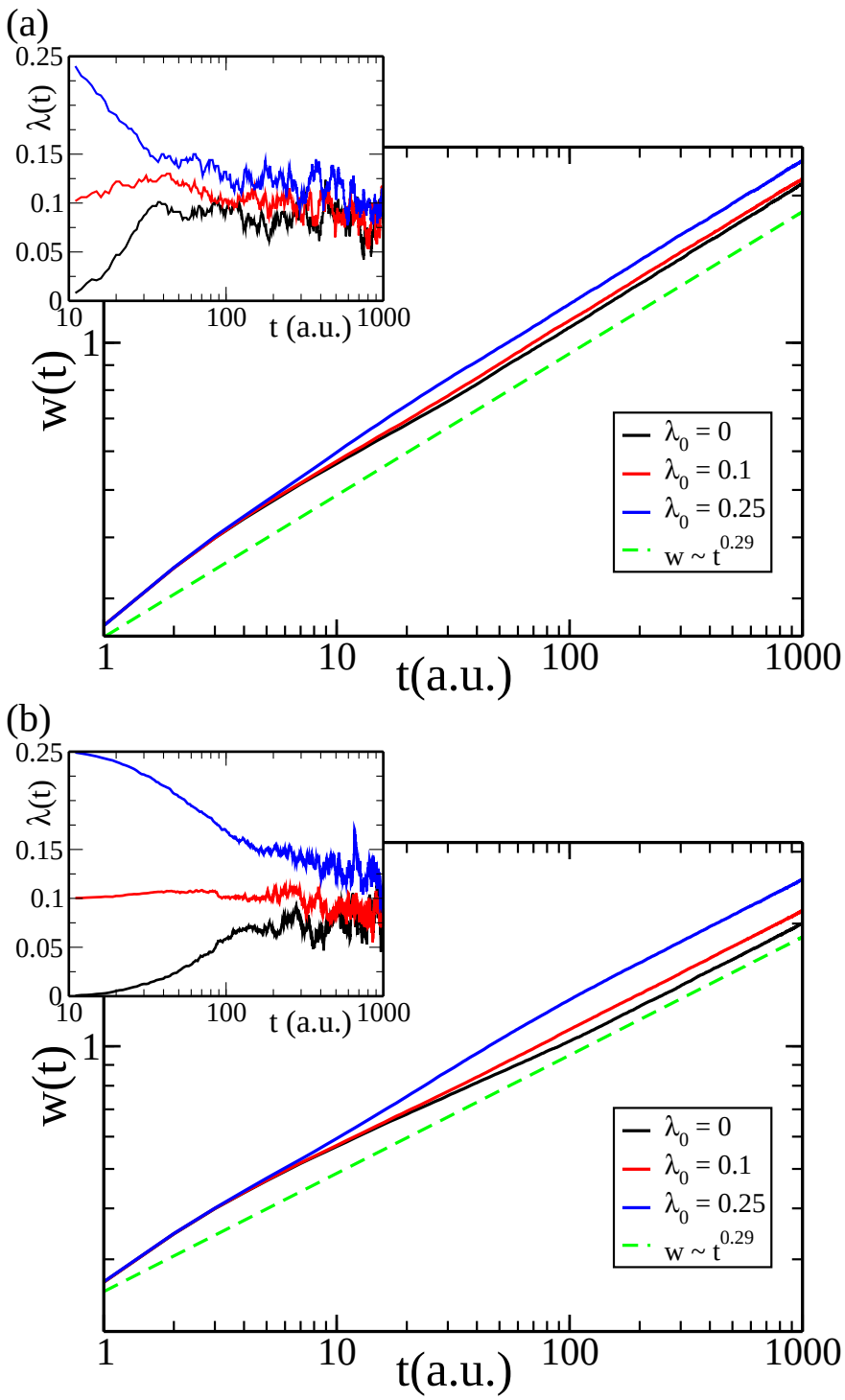

Figure A.2: Control for the KPZ equation in 1+1 dimensions with L = 32768: Three setups for the digital and the differential control with constant $\beta_0 = 0.29$, $\lambda_0 = 0$ (black), $\lambda_0 = 0.1$ (red), and $\lambda_0 = 0.25$ (blue). (a) digital control with $a = 0.01$, (b) differential control with $K = 0.02$, time discretization $dt = 0.01$ for all setups, upper left insets show the functions $\lambda(t)$.

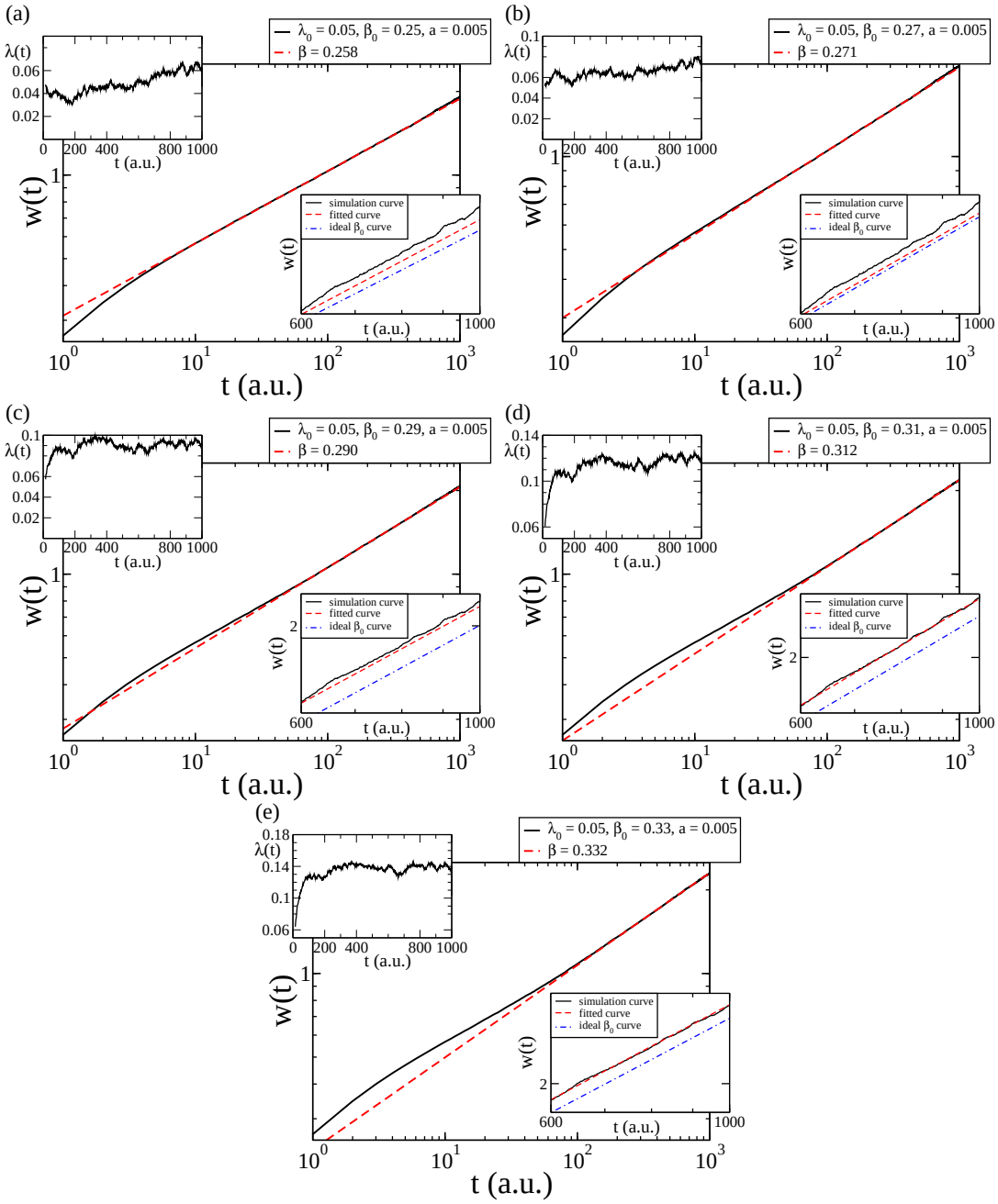

Figure A.3: Digital control for the KPZ equation in 1+1 dimensions with a control setup: $\lambda_0 = 0.05$ and $a = 0.005$ for five different desired control values of: (a) $\beta_0 = 0.25$, (b) $\beta_0 = 0.27$, (c) $\beta_0 = 0.29$, (d) $\beta_0 = 0.31$, (e) $\beta_0 = 0.33$, time discretization $dt = 0.005$, upper left insets show the functions $\lambda(t)$, lower right insets show the roughness in the late phase in double logarithmic plot.

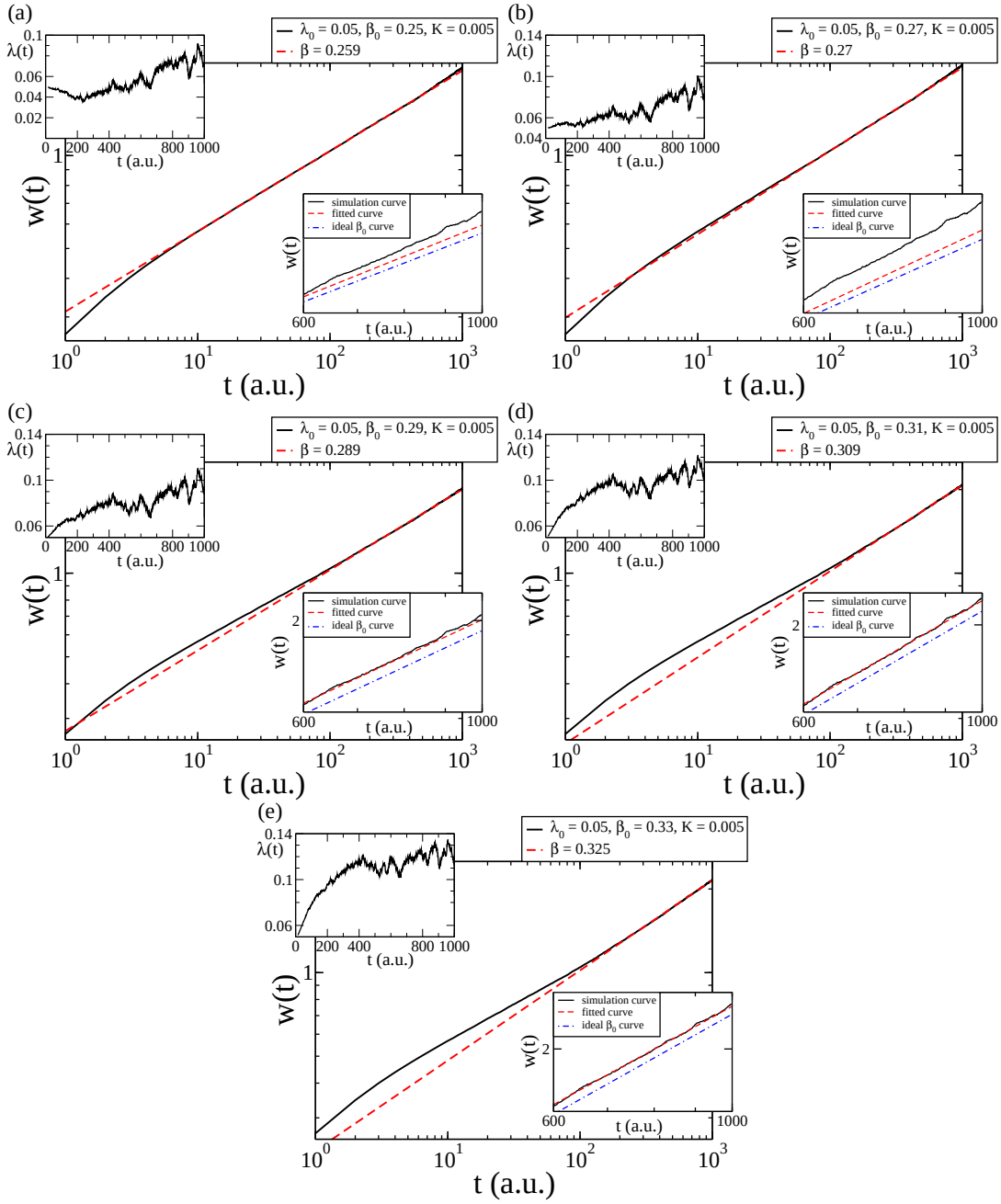

Figure A.4: Digital control for the KPZ equation in 1+1 dimensions with a control setup: $\lambda_0 = 0.05$ and $K = 0.005$ for five different desired control values of: (a) $\beta_0 = 0.25$, (b) $\beta_0 = 0.27$, (c) $\beta_0 = 0.29$, (d) $\beta_0 = 0.31$, (e) $\beta_0 = 0.33$, time discretization $dt = 0.005$, upper left insets show the functions $\lambda(t)$, lower right insets show the roughness in the late phase in double logarithmic plot.

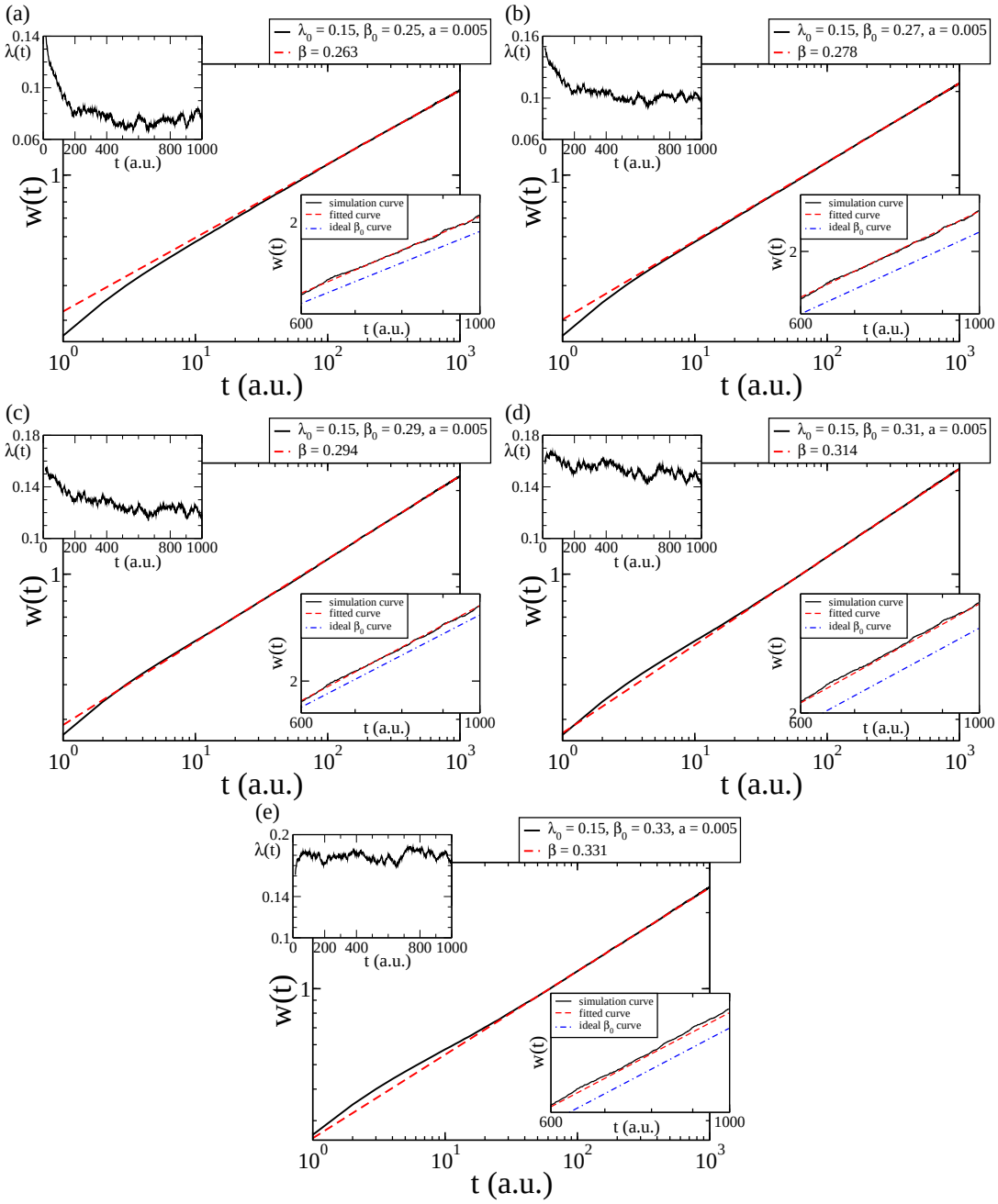

Figure A.5: Digital control for the KPZ equation in 1+1 dimensions with a control setup: $\lambda_0 = 0.15$ and $a = 0.005$ for five different desired control values of: (a) $\beta_0 = 0.25$, (b) $\beta_0 = 0.27$, (c) $\beta_0 = 0.29$, (d) $\beta_0 = 0.31$, (e) $\beta_0 = 0.33$, time discretization $dt = 0.005$, upper left insets show the functions $\lambda(t)$, lower right insets show the roughness in the late phase in double logarithmic plot.

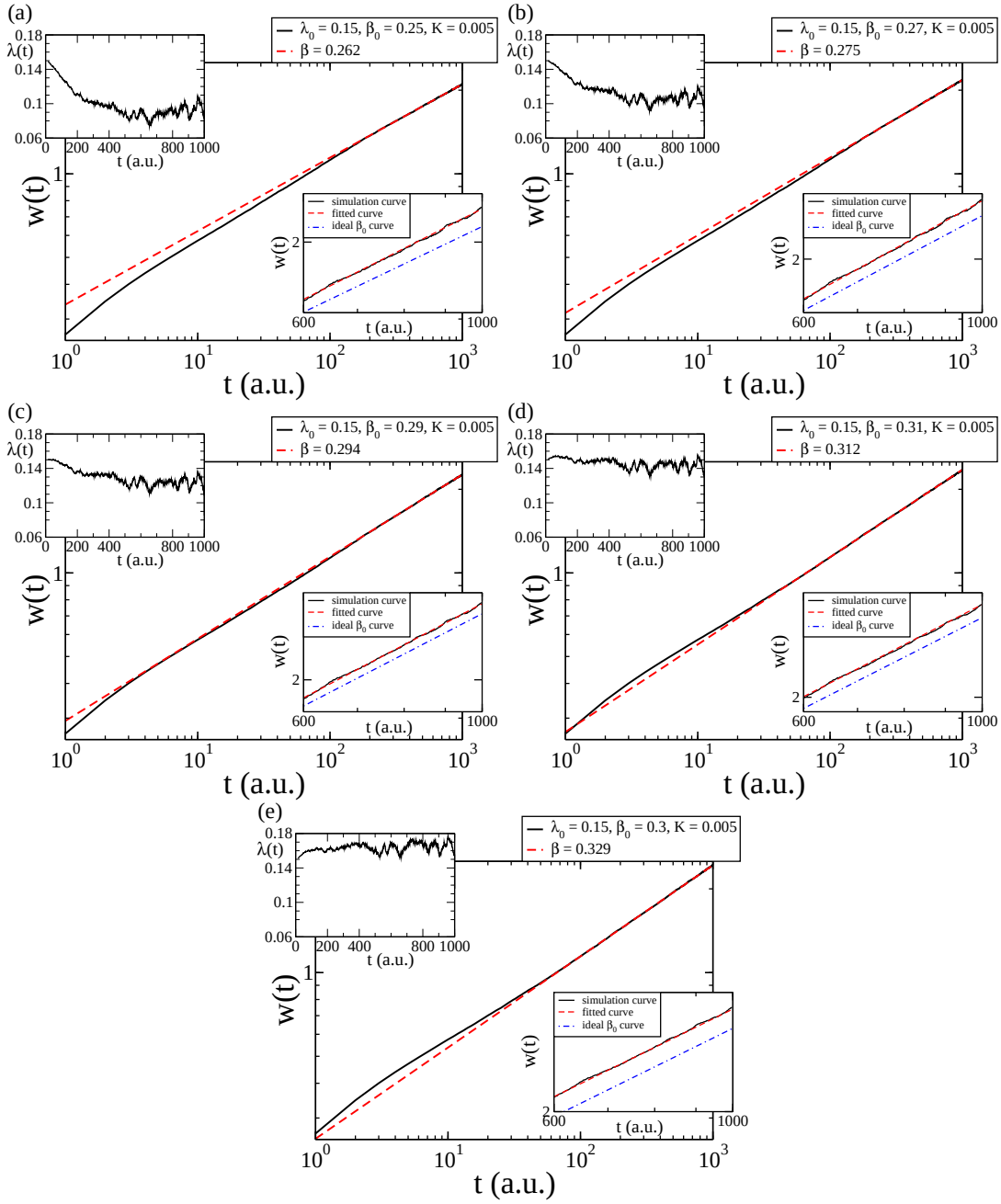

Figure A.6: Digital control for the KPZ equation in 1+1 dimensions with a control setup: $\lambda_0 = 0.15$ and $K = 0.005$ for five different desired control values of: (a) $\beta_0 = 0.25$, (b) $\beta_0 = 0.27$, (c) $\beta_0 = 0.29$, (d) $\beta_0 = 0.31$, (e) $\beta_0 = 0.33$, time discretization $dt = 0.005$, upper left insets show the functions $\lambda(t)$, lower right insets show the roughness in the late phase in double logarithmic plot.

A.2 Additional simulations KPZ 2+1

In Fig. A.7 we show the control of the KPZ equation in 2+1 dimensions with an initial nonlinearity $\lambda_0 = 0.05$. The left figures (Fig. A.7 (a,c,e)) show the digital control for three values of the desired exponent β_0 with $a = 0.005$, the right figures (Fig. A.7 (b,d,f)) show the control with the same setups for $K = 0.005$. The results show the same behaviour as for the control with other initial nonlinearities.

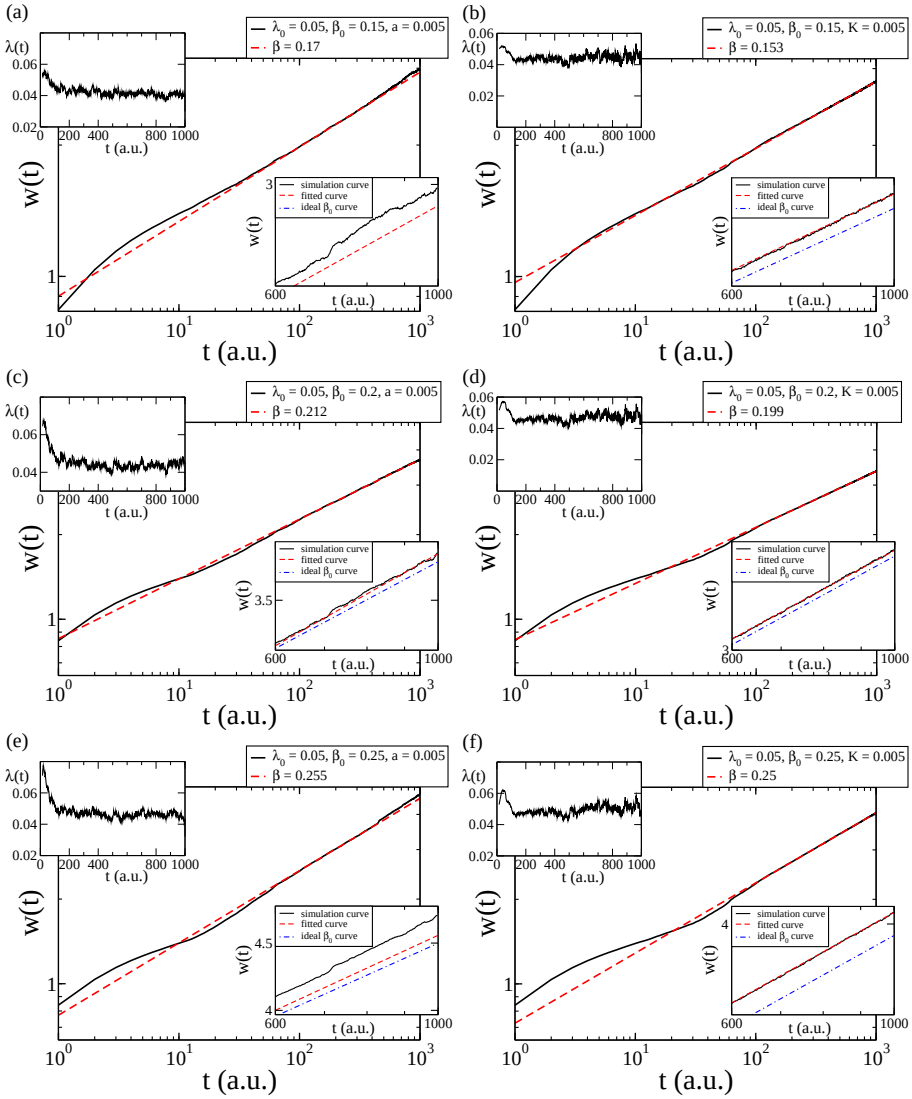

Figure A.7: Control for the KPZ equation in 2+1 dimensions with a control setup: $\lambda_0 = 0.05$, $a = 0.005$ for digital and $K = 0.005$ for differential control, three desired control values of: (a,b) $\beta_0 = 0.15$, (c,d) $\beta_0 = 0.20$, (e,f) $\beta_0 = 0.25$, time discretization $dt = 0.005$, upper left insets show the functions $\lambda(t)$, lower right insets show the roughness in the late phase in double logarithmic plot.

A.3 Additional simulations MBE 1+1

In Fig. A.8 we show the results for the control of the MBE equation in 1+1 dimensions with an initial nonlinearity $\lambda_{1,0} = 0.05$. The left figures (Fig. A.8 (a,c,e)) show the digital control for three values of the desired exponent β_0 with $a = 0.0005$, the right figures (Fig. A.8 (b,d,f)) show the control with the same setups for $K = 0.0005$.

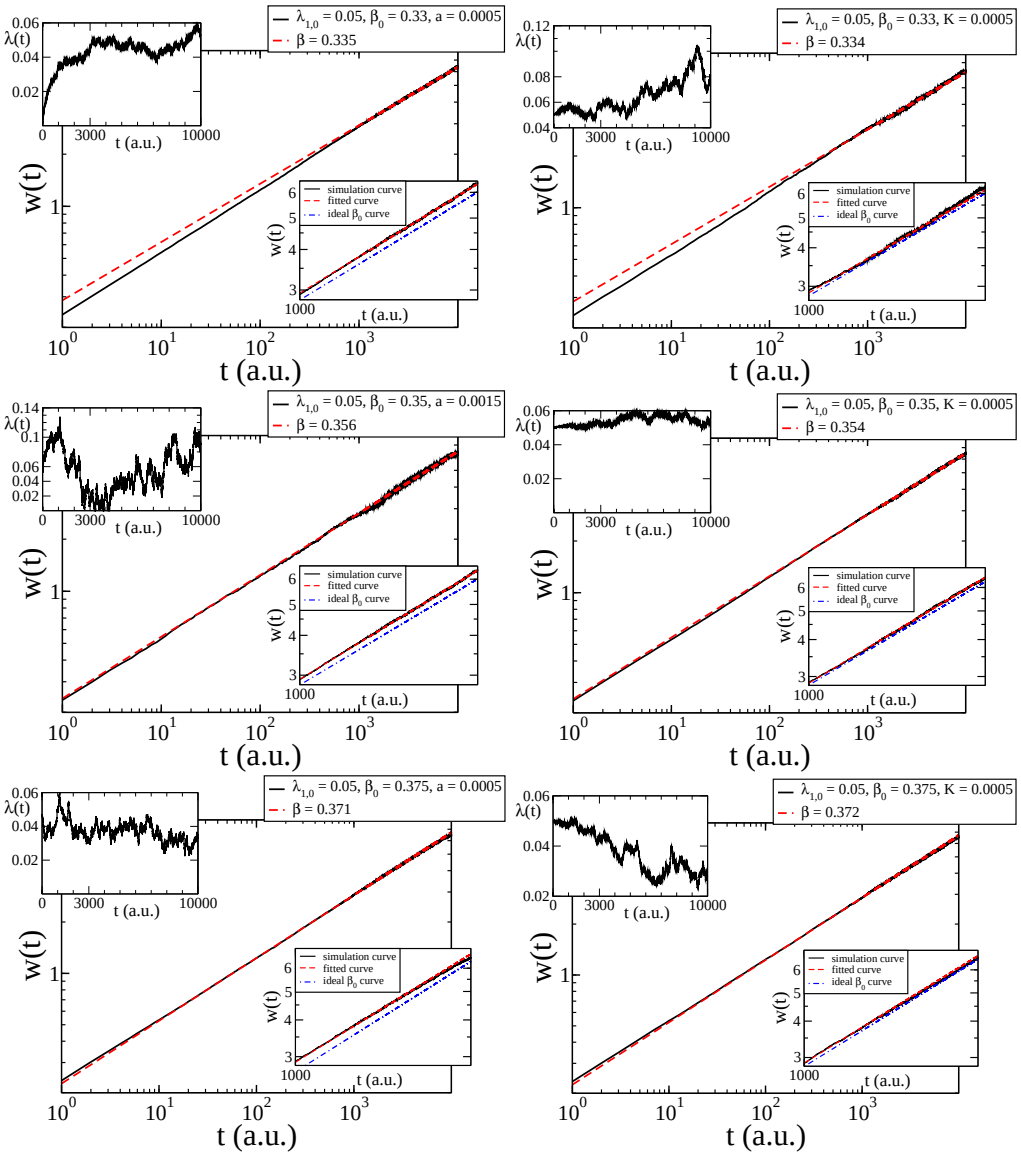

Figure A.8: Digital control for the MBE equation in 1+1 dimensions with a control setup: $\lambda_{1,0} = 0.05$, $a = 0.0005$ for digital and $K = 0.0005$ for differential control, three desired control values of: (a,b) $\beta_0 = 0.33$, (c,d) $\beta_0 = 0.35$, (e,f) $\beta_0 = 0.375$, time discretization $dt = 0.01$, upper left insets show the functions $\lambda(t)$, lower right insets show the roughness in the late phase in double logarithmic plot.

The results show the same general properties as explained for $\lambda_{1,0}$.

A.4 Noisy Kuramoto-Sivashinsky equation

With the time-delayed feedback method we investigated the KPZ and the MBE equation. An equation combining the terms of both and possibly also controllable is the noisy Kuramoto-Sivashinsky equation. Fig. A.9 show for 1+1 and 2+1 dimensions

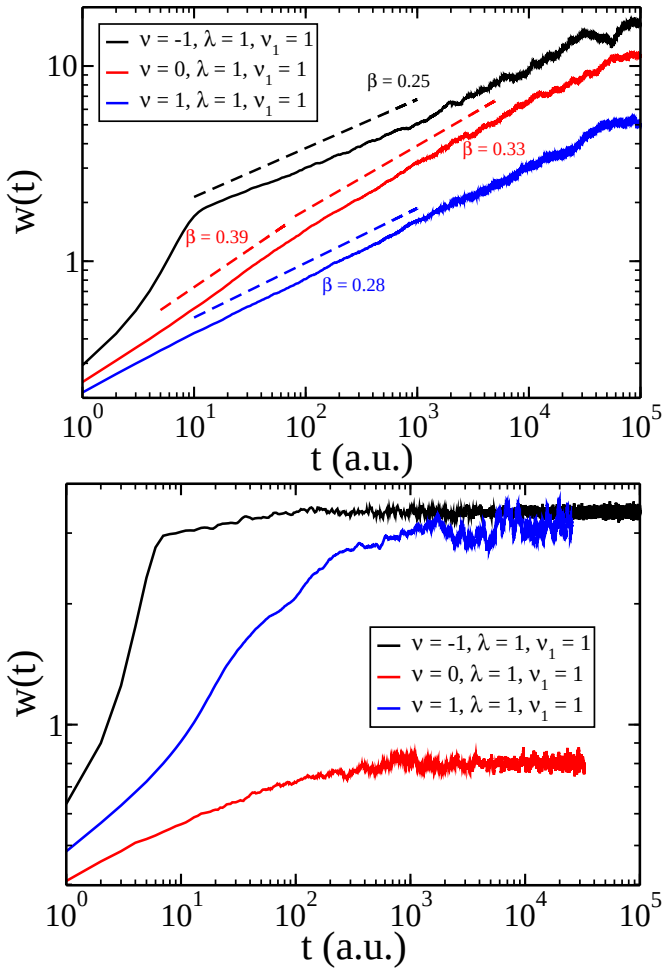

Figure A.9: Solutions of the noisy KS equation in 1+1 and 2+1 dimensions with three different parameter setups: $\nu = 1$, $\lambda = 1$ and $\nu_1 = 1$ (blue), $\nu = 0$, $\lambda = 1$ and $\nu_1 = 1$ (red), and $\nu = 1$, $\lambda = 1$ and $\nu_1 = 1$ (black), (a) in 1+1 dimensions with local exponents β as guides to the eye, (b) in 2+1 dimensions.

solutions for different initial terms ν (EW term). In 1+1 dimensions we show, that different phases of roughening appear. Further investigations could make a control as in this work explained possible also for this type of equation.

Appendix B

Deposition models

B.1 Ballistic deposition

In Fig. B.1 we show the results of the simple ballistic deposition in 1+1 dimensions. The rule for the deposited particles is to stick on the first nearest neighbor [Bar95]. The ballistic deposition is often used to get a relation form Solid-on-solid models to the KPZ equation. In Fig. B.1 we show that the effective exponent $\beta \sim 0.3$ is close to the KPZ exponent ($\beta = 1/3$) as expected.

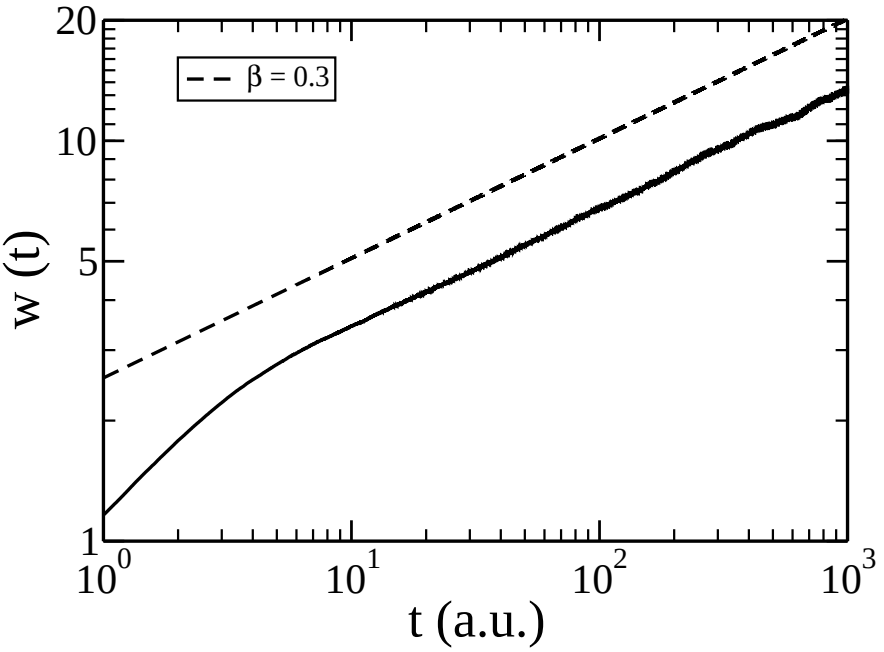

Figure B.1: Roughness evolution in the simple ballistic deposition model with nearest neighbor sticking rule [Bar95] for $L = 131072$ and $t = 1000$.

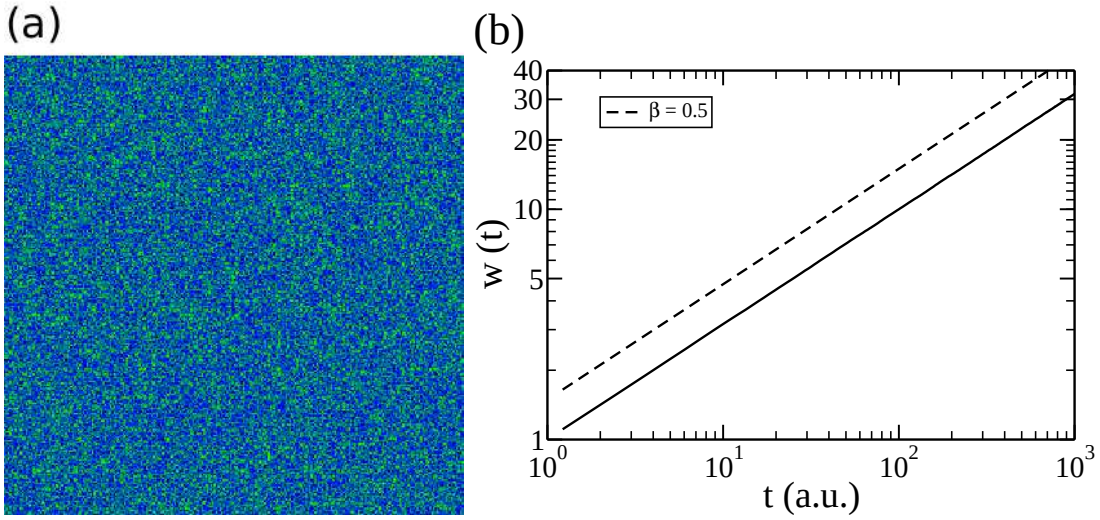

Figure B.2: Roughness evolution in the random deposition model, (a) shows a density plot of the height profile from lower values (blue) to higher values (green), (b) show the roughness vs time t for a system of $256 \times 256 l.s.$.

B.2 Random deposition

In Fig. B.2 we show the results for a random deposition on a $256 \times 256 l.s.$ system. We get the well-known exponent $\beta = 0.50$ and do not see any correlations in the density plot (B.2 (a)) as expected.

Appendix C

Simulation tool for the tumor model

C.1 Short manual

Table C.1 and table C.2 give short descriptions for the options of the simulation tool.

Option	Description
-h	show the help
-i	load lattice file (see options z, w)
-v	the probability for division (corresponding to the rate)
-f	the probability for migration (corresponding to the rate)
-k	the proliferating rim ΔL
-a	the factor $\tau/value$ by which the cell cyle time mutates
-m	the parameter for the Erlang distribution (sharpness) of the cell cycle time
-c	the probability for a cell to undergo apoptosis
-G	the probability for a mutation of the cell cyle time depending on the lattice point
-x	the number of averages
-y	time
-A	animation flag for graphic output

Table C.1: Short manual for the usage of the tool for cell population evolution

Option	Description
-D	Type of migration
	0 free migration
	1 free migration restricted to the border
	2 Arrhenius law migration
	3 Arrhenius law migration just depending on the migrating cell
	4 Arrhenius law migration restricted to the border
-M	Type of division
	0 migration to randomly selected free points, shift to shortest distance
	1 migration and shift to randomly selected free points
	2 migration and shift to the free points with the longest distance
	3 migration and shift to the free point with the lowest coordination number
	4 migration and shift to the free point with the highest coordination number
-N	prefactor for Arrhenius migration
-E	E_0 for Arrhenius migration
-B	E_B for Arrhenius migration
-z	size of lattice to create (100 for 100×100 lattice)
-w	type of lattice to create
	4 square lattice
	6 hexagonal lattice
	8 octagonal lattice
-C	Maximum of cells
-U	Maximum of Gyration radius
-Z	the factor of mutation of the apoptosis probability
-T	maximum of the probability to divide under mutation (corresponds to an average minimum of the cell cycle time
-K	probability to knock out apoptosis
-s	seed for random number generator
-o	Output rate
-n	number of divisions

Table C.2: Short manual for the usage of the tool for cell population evolution

List of Figures

Bibliography

[Alb02] B. Alberts, A. Johnson, J. Lewis, M. Raff, K. Roberts, and P. Walter: *The Cell* (Garland Science Publ., New York, 2002), third edn.

[Ama90] J. G. Amar and F. Family: *Numerical solution of a continuum equation for interface growth in 2+1 dimensions*. Phys. Rev. A **41**, 3399 (1990).

[Ama02] A. Amann, J. Schlesner, A. Wacker, and E. Schöll: *Chaotic front dynamics in semiconductor superlattices*. Phys. Rev. B **65**, 193313 (2002).

[Ama03] A. Amann, K. Peters, U. Parlitz, A. Wacker, and E. Schöll: *A hybrid model for chaotic front dynamics: From semiconductors to water tanks*. Phys. Rev. Lett. **91**, 066601 (2003).

[And05] A. R. A. Anderson: *A hybrid mathematical model of solid tumor invasion: the importance of cell adhesion*. Math. Med. Biol. **22**, 163 (2005).

[Åst95] K. T. Åstrom and T. Hägglund, eds.: *PID Controllers: Theory, Design, and Tuning* (Instrument Society of America, Research Triangle Park, N.C., 1995).

[Bab02] N. Baba, A. Amann, E. Schöll, and W. Just: *Giant improvement of time-delayed feedback control by spatio-temporal filtering*. Phys. Rev. Lett. **89**, 074101 (2002).

[Bai88] R. Baiod, D. Kessler, P. Ramanlal, L. Sander, and R. Savit: *Dynamical scaling of the surface of finite-density ballistic deposition*. Phys. Rev. A **38**, 3672 (1988).

[Bal04] A. G. Balanov, N. B. Janson, and E. Schöll: *Control of noise-induced oscillations by delayed feedback*. Physica D **199**, 1 (2004). Special issue: Trends in Pattern Formation: Stability , Control and Fluctuations - Edited by M. Bär, E. Schöll. H. Engel and A. Torcini.

[Bal05] A. G. Balanov, N. B. Janson, and E. Schöll: *Delayed feedback control of chaos: Bifurcation analysis*. Phys. Rev. E **71**, 016222 (2005).

[Bal06] A. G. Balanov, V. Beato, N. B. Janson, H. Engel, and E. Schöll: *Delayed feedback control of noise-induced patterns in excitable media*. Phys. Rev. E **74**, 016214 (2006).

[Bar95] A.-L. Barabási and H. E. Stanley: *Fractal concepts in surface growth* (Cambridge University Press, Cambridge, U.K., 1995).

[Bat91] M. Batchelor and B. Henry: *Limits to Eden growth in two and three dimensions*. Phys. Lett. A **157**, 229 (1991).

[Bec35] R. Becker and W.Döring: Ann. Phys. (Leipzig) **24**, 719 (1935).

[Bec02] O. Beck, A. Amann, E. Schöll, J. E. S. Socolar, and W. Just: *Comparison of time-delayed feedback schemes for spatio-temporal control of chaos in a reaction-diffusion system with global coupling*. Phys. Rev. E **66**, 016213 (2002).

[Ben02] H. Benner and W. Just: *Control of chaos by time delayed feedback in high power ferromagnetic resonance experiments*. J. Kor. Phys. Soc. **40**, 1046 (2002).

[Ber97] M. D. Berg, M. van Kreveld, M. Overmars, and O. Schwarzkopf: *Computational Geometry* (Springer, Berlin, 1997), first edn.

[Bey00] D. Beysens, G. Forgacs, and J. Glazier: *Cell sorting is analogous to phase ordering in fluids*. Proc. Natl. Acad. Sci. USA **97**, 9467 (2000).

[Bim96] D. Bimberg, N. N. Ledentsov, M. Grundmann, N. Kirstaedter, O. G. Schmidt, M. H. Mao, V. Ustinov, A. Egorov, A. Zhukov, P. Kop'ev, Z. Alferov, S. Ruvimov, U. Gösele, and J. Heydenreich: *InAs-GaAs quantum pyramid lasers: in situ growth, radiative lifetimes and polarization properties*. Jpn. J. Appl. Phys. **35**, 1311 (1996).

[Bim99] D. Bimberg, M. Grundmann, and N. Ledentsov: *Quantum Dot Heterostructures* (John Wiley & Sons Ltd., New York, 1999).

[Blo04] M. Block, R. Kunert, E. Schöll, T. Boeck, and T. Teubner: *Kinetic Monte Carlo simulation of formation of microstructures in liquid droplets*. New J. Phys. **6**, 166 (2004).

[Blo06a] M. Block and E. Schöll: *Adjusting surface roughness in growth processes by time delayed feedback control*. In *Proc. 28th Int. Conference on Physics of Semiconductors (ICPS-28), Vienna 2006*, edited by W. Jantsch and F. Schaffler (Springer, Berlin, 2006).

[Blo06b] M. Block and E. Schöll: *Time Delayed Feedback Control in growth phenomena*. J. Crystal Growth (2006). In print.

[Boc00] S. Boccaletti, C.Grebogi, Y. C. Lai, H. Mancini, and D. Maza: *The control of chaos: theory and applications*. Phys. Rep. **329**, 103 (2000).

[Boe99] T. Boeck, T. Teubner, K. Schmidt, and P. M. Wilde: *A method to grow silicon crystallites on glass*. J. Crystal Growth **198/199**, 420 (1999).

[Bor75] A. B. Bortz, M. H. Kalos, and J. L. Lebowitz: *A new algorithm for Monte Carlo simulations of Ising spin systems*. J. Comp. Phys. **17**, 10 (1975).

[Bos99a] S. Bose and E. Schöll: *Kinetic Monte Carlo Simulation of the Nucleation of Self-Assembled Quantum Dots*. In *Proc. 24th International Conference on The Physics of Semiconductors (ICPS-24), Jerusalem, Israel*, edited by D. Gershoni (World Scientific, Singapore, 1999).

[Bos99b] S. Bose and E. Schöll: *Optimization of the size distribution of self-organized quantum dots*. In *Proceedings of the 7^{th} International Symposium on Nanostructure: Physics and Technology*, pp. 506–509 (Ioffe Institut, St. Petersburg, 1999).

[Bos00] S. Bose: *Pattern formation at semiconductor interfaces and surfaces*. Ph.D. thesis, Technische Universität Berlin (2000).

[Boy04] P. Boyle and J. Ferlay: *Cancer incidence and mortality in Europe, 2004*. Ann. Onc. **16**, 481 (2004).

[Brú98] A. Brú, J. M. Pastor, I. Fernaud, S. Melle, and I. Brú: *Super-rough dynamics on tumor growth*. Phys. Rev. Lett. **81**, 4008 (1998).

[Brú03] A. Brú, S. Albertos, J. L. Subiza, J. L. García-Asenjo, and I. Brú: *The Universal Dynamics of Tumor Growth*. Biophys. J. **85**, 2948 (2003).

[Buc05a] J. Buceta and J. Galeano: *Comments on the Article "The Universal Dynamics of Tumor Growth*. Biophys. J. **88**, 3734 (2005).

[Buc05b] R. C. Buceta: *Generalized discretization of the Kardar-Parisi-Zhang equation*. Phys. Rev. E **72**, 017701 (2005).

[Byr03] B. Byrappa: *Crystal Growth Technology* (William Andrew Publishing/Noyes, bla, 2003).

[Cha89] A. Chakrabarki and R. Toral: *Numerical study of a model for interface growth*. Phys. Rev. B **40**, 11419 (1989).

[Chi99] C.-S. Chin and M. den Nijs: *Stationary-state skewness in two-dimensional Kardar-Parisi-Zhang type growth*. Phys. Rev. E **59**, 2633 (1999).

[Dic04] K. A. Dick, K. Deppert, M. W. Larsson, T. Mårtensson, W. Seifert, L. R. Wallenberg, and L. Samuelson: *Synthesis of branched 'nanotrees' by controlled seeding of multiple branching events*. Nature **3**, 380 (2004).

[Dra05a] D. Drasdo: *Coarse Graining simulated cell populations*. Adv. Complex Syst. **2 & 3**, 319 (2005).

[Dra05b] D. Drasdo and S. Hoehme: *A single-cell based model to tumor growth invitro:monolayers and spheroids*. Phys. Biol. **2**, 133 (2005).

[Eag90] D. J. Eaglesham and M. Cerullo: *Dislocation-Free Stranski-Krastanow Growth of Ge on Si(100)*. Phys. Rev. Lett. **64**, 1943 (1990).

[Edw82] S. F. Edwards and D. R. Wilkinson: *The Surface Statistics of a Granular Aggregate*. Proc. R. Soc. London A **381**, 17 (1982).

[Els03] F. Elsholz, M. Meixner, and E. Schöll: *Kinetic Monte Carlo simulation of self-organized pattern formation in thin film deposition*. Nucl. Instruments and Methods B **202C**, 249 (2003).

[Els04] F. Elsholz, E. Schöll, and A. Rosenfeld: *Control of surface roughness in amorphous thin film growth*. Appl. Phys. Lett. **84**, 4167 (2004).

[Els05a] F. Elsholz: *Kinetic Monte Carlo Simulations of Thin Film Growth*. Ph.D. thesis, TU Berlin (2005).

[Els05b] F. Elsholz, E. Schöll, C. Scharfenorth, G. Seewald, H. J. Eichler, and A. Rosenfeld: *Roughness evolution in thin film growth of SiO_2 and Nb_2O_5*. J. Appl. Phys. **98**, 103516 (2005).

[Fam85] F. Family and T. Vicsek: *Scaling of the active zone in the Eden process on perculation networks and the ballistic deposition model*. J. Phys. A **18**, L75 (1985).

[Fam86] F. Family: *Scaling of rough surfaces: Effects of surfac diffusion*. J. Phys. A **19**, L441 (1986).

[Far95] R. F. C. Farrow, ed.: *Molecular Beam Epitaxy* (Noyes Publications, Park Ridge, 1995).

[Fic91] K. Fichthorn and W. Weinberg: *Theoretical foundations of dynamical Monte Carlo simulations*. J. Chem. Phys. **95**, 1090 (1991).

[Fog06] H. C. Fogedby: *Kardar-Parisi-Zhang equation in the weak noise limit: Pattern formation and upper critical dimension*. Phys. Rev. E **73**, 031104 (2006).

[Fra49] F. C. Frank and J. H. van der Merwe: *One-dimensional dislocations. I. Static theory*. Proc. R. Soc. London, Ser. A **198**, 205 (1949).

[Fra99] G. Franceschini, S. Bose, and E. Schöll: *Control of chaotic spatiotemporal spiking by time-delay autosynchronisation*. Phys. Rev. E **60**, 5426 (1999).

[Fra03] S. Franchi, G. Trevisi, L. Seravalli, and P. Frigeri: *Quantum dot nanostructures and molecular beam epitaxy*. Progress in Crystal Growth and Characterization of Materials **47**, 166 (2003).

[Gea98] J. Gearhart: *CELL BIOLOGY: New Potential for Human Embryonic Stem Cells*. Science **282**, 1061 (1998).

[Gha06] S. V. Ghaisas: *Stochastic model in the Kardar-Parisi-Zhang universality class with minimal finite size effects*. Phys. Rev. E **73**, 022601 (2006).

[Gil76] D. T. Gillespie: *A General Method for Numerically Simulating the Stochastic Time Evolution of Coupled Chemical Reactions"*. J. Comput. Phys. **22**, 403 (1976).

[Gol85] L. Goldstein, F. Glas, J. Y. Marzin, M. N. Charasse, and G. L. Roux: *Growth by molecular beam epitaxy and charakterization of InAs/GaAs strained-layer superlattices*. Appl. Phys. Lett. **47**, 1099 (1985).

[Guo90] H. Guo, B. Grossmann, and M. Grant: *Kinetics of interface growth in driven systems*. Phys. Rev. Lett. **64**, 1262 (1990).

[Hau06] B. Hauschildt, N. B. Janson, A. G. Balanov, and E. Schöll: *Noise-induced cooperative dynamics and its control in coupled neuron models*. Phys. Rev. E **74**, 051906 (2006).

[Her50] C. Herring: *Effect of change of scale on sintering phenomena*. J. Appl. Phys. **21**, 301 (1950).

[Hiz06] J. Hizanidis, A. G. Balanov, A. Amann, and E. Schöll: *Noise-induced oscillations and their control in semiconductor superlattices*. Int. J. Bifur. Chaos **16**, 1701 (2006).

[Ho04] G. W. Ho, A. S. W. Wong, D.-J. Kang, and M. E. Welland: *Three-dimensional crystalline SiC nanowire flowers*. Nanotechnology **15**, 996 (2004).

[Hor06] C. M. Horowitz and E. V. Albano: *Dynamic properties in a family of competitive growing models*. Phys. Rev. E **73**, 031111 (2006).

[Höv03] P. Hövel and J. E. S. Socolar: *Stability domains for time-delay feedback control with latency*. Phys. Rev. E **68**, 036206 (2003).

[Höv04] P. Hövel: *Effects of chaos control and latency in time-delay feedback methods*. Master's thesis, Technische Universität Berlin (2004).

[Höv05] P. Hövel and E. Schöll: *Control of unstable steady states by time-delayed feedback methods*. Phys. Rev. E **72**, 046203 (2005).

[Jan04] N. B. Janson, A. G. Balanov, and E. Schöll: *Delayed feedback as a means of control of noise-induced motion*. Phys. Rev. Lett. **93**, 010601 (2004).

[Jus03a] W. Just, H. Benner, and E. Reibold: *Theoretical and experimental aspects of chaos control by time-delayed feedback*. Chaos **13**, 259 (2003).

[Jus03b] W. Just, S. Popovich, A. Amann, N. Baba, and E. Schöll: *Improvement of time–delayed feedback control by periodic modulation: analytical theory of Floquet mode control scheme*. Phys. Rev. E **67**, 026222 (2003).

[Kar86] M. Kardar, G. Parisi, and Y.-C. Zhang: *Dynamic scaling of growing interfaces*. Phys. Rev. Lett. **56**, 889 (1986).

[Ker72] J. R. Kerr, A. H. Wyllie, and A. R. Currie: *Apoptosis: a basic biological phenomenon with wide-ranging implications in tissue kinetics.* Br. J. Cancer **26**, 239 (1972).

[Kim89] J. M. Kim and J. M. Kosterlitz: *Grwoth in a restricted solid-on-solid model*. Phys. Rev. Lett. **62**, 2289 (1989).

[Kol06] A. Kolakowska, M. A. Novotny, and P. S. Verma: *Universal scaling in mixing correlated growth with randomness*. Phys. Rev. E **73**, 011603 (2006).

[Kru92] J. Krug, P. Meakin, and T. Halpin-Healy: *Amplitude universality for driven interfaces and directed polymers in random media*. Phys. Rev. A **45**, 638 (1992).

[Kun06a] R. Kunert: *Monte Carlo Simulation of stacked Quantum Dot Arrays*. Ph.D. thesis, Technische Universität Berlin (2006).

[Kun06b] R. Kunert and E. Schöll: *Strain-controlled correlation effects in self-assembled quantum dot stacks*. Appl. Phys. Lett. **89**, 153103 (2006).

[Kun06c] R. Kunert, E. Schöll, T. Hammerschmidt, and P. Kratzer: *Strain field calculations of quantum dots — a comparison study of two methods*. In *Proc. 28th International Conference on the Physics of Semiconductors (ICPS-28), Vienna 2006*, edited by W. Jantsch and F. Schaffler (Springer, Berlin, 2006).

[Lai65] K. J. Laidler: *Chemical Kinetics* (McGraw-Hill, London, 1965).

[Lai91] Z. W. Lai and S. D. Sarma: *Kinetic roughening with surface relaxation: Continuum versus atomistic models*. Phys. Rev. Lett. **66**, 3248 (1991).

[Lam98a] C.-H. Lam and F. G. Shin: *Anomaly in numerical integrations of the Kardar-Parisi-Zhang equation*. Phys. Rev. E **57**, 6506 (1998).

[Lam98b] C.-H. Lam and F. G. Shin: *Improved discretization of the Kardar-Parisi-Zhang equation*. Phys. Rev. E **58**, 5592 (1998).

[Lan05] P. T. Landsberg: *Detailed balance*. In *Encyclopedia of Nonlinear Science*, edited by A. Scott (Routledge, London, 2005).

[Läs98] M. Lässig: *Quantized Scaling of Growing Surfaces*. Phys. Rev. Lett. **80**, 2366 (1998).

[Led95] N. N. Ledentsov, M. Grundmann, N. Kirstaedter, J. Christen, R. Heitz, J. Böhrer, F. Heinrichsdorff, D. Bimberg, S. S. Ruvimov, P. Werner, U. Richter, U. Gösele, J. Heydenreich, V. M. Ustinov, A. Y. Egorov, M. V. Maximov, P. S. Kop'ev, and Z. I. Alferov: *Luminescence and Structural Properties of (In,Ga)As/GaAs Quantum Dots*. In *Proc. 22nd Int. Conf. Phys. Semicond., (ICPS-22), (Vancouver, Canada, 1994)*, edited by D. J. Lockwood (World Scientific, Singapore, 1995).

[Lev06] H. Levine, D. A. Kessler, and W.-J. Rappel: *Directional sensing in eukaryotic chemotaxis: A balanced inactivation model*. Proc. Natl. Acad. Sci. USA **103**, 9761 (2006).

[Liu01] B.-G. Liu and E. Schöll: *Strained growth in surfactant mediated heteroepitaxy*. Vacuum **61**, 145 (2001).

[Man03] L. Mandreoli, J. Neugebauer, R. Kunert, and E. Schöll: *Adatom Density kinetic Monte Carlo: A hybrid approach to perform epitaxial growth simulations*. Phys. Rev. B **68**, 155429 (2003).

[Mar87] P. M. J. Maree, K. Nakagawa, F. M. Mulders, J. F. van der Veen, and K. I. Kavanagh: *Thin epitaxial Ge-Si(111) films: Study and control of morphology*. Surf. Sci. **191**, 305 (1987).

[Mav03] C. Mavroidis and A. Dubey: *From Pulses to Motors*. Nature **9**, 573 (2003).

[McM94] T. J. McMaster, T. Hickish, T. Min, D. Cunningham, and M. J. Miles: *Application of Scanning Force Microscopy to Chromosome Analysis*. Cancer Genet. Cytogenet. **76**, 93 (1994).

[Mea86] P. Meakin, P. Ramanlal, L. M. Sander, and R. C. Ball: *Ballistic deposition on surfaces*. Phys. Rev. A **34**, 2364 (1986).

[Mea90] P. Meakin and R. Jullien: *Spatially correlated ballistic deposition on one- and two-dimensional surfaces*. Phys. Rev. A **41**, 983 (1990).

[Mea93] P. Meakin: *The growth of rough surfaces and interfaces*. Phys. Rep. **235**, 189 (1993).

[Mei87] H. Meinhardt and M. J. Klingler: *A Model for Pattern Formation on the Shells of Molluscs*. J. Theor. Biol. **126**, 63 (1987).

[Mei01a] M. Meixner, R. Kunert, S. Bose, E. Schöll, V. A. Shchukin, D. Bimberg, E. Penev, and P. Kratzer: *Monte Carlo simulation of the self-organized growth of quantum dots with anisotropic surface diffusion*. In *Proc. 25th International Conference on the Physics of Semiconductors (ICPS-25), Osaka 2000*, edited by N. Miura and T. Ando, p. 381 (Springer, Berlin, 2001).

[Mei01b] M. Meixner, E. Schöll, M. Schmidbauer, H. Raidt, and R. Köhler: *Formation of Island Chains in SiGe/Si Heteroepitaxy by Elastic Anisotropy – A Monte Carlo Study*. Phys. Rev. B **64**, 245307 (2001).

[Mei01c] M. Meixner, E. Schöll, V. A. Shchukin, and D. Bimberg: *Self-assembled quantum dots: Crossover from kinetically controlled to thermodynamically limited growth*. Phys. Rev. Lett. **87**, 236101 (2001). Ibid **88**, 059901 (2002).

[Mei02] M. Meixner: *Simulation of self-organized growth kinetics of quantum dots*. Ph.D. thesis, TU Berlin (2002).

[Mei03a] H. Meinhardt: *The Algorithmic Beauty of Sea Shells* (Springer, Heidelberg New York, 2003), third edn.

[Mei03b] M. Meixner, R. Kunert, and E. Schöll: *Control of strain-mediated growth kinetics of self-assembled semiconductor quantum dots*. Phys. Rev. B **67**, 195301 (2003).

[Mei03c] M. Meixner and E. Schöll: *Kinetically enhanced correlation and anticorrelation effects in self-organized quantum dot stacks*. Phys. Rev. B **67**, 121202 (2003).

[Met49] N. Metropolis and S. Ulam: *The Monte Carlo method*. J. Am. Stat. Assoc. **44**, 335 (1949).

[Mic04] T. Michely and J. Krug: *Islands, Mounds and Atoms* (Springer, Berlin, 2004), 1 edn.

[Mo90] Y.-W. Mo, D. E. Savage, B. S. Swartzentruber, and M. G. Lagally: *Kinetic pathway in Stranski-Krastanov growth of Ge on Si(001)*. Phys. Rev. Lett. **65**, 1020 (1990).

[Moo96] R. L. Moon: *MOVPE: is there any other technology for optoelectronics?* J. Crystal Growth **170**, 1 (1996).

[Mor01] E. Moro: *Internal fluctuations effects on Fisher waves*. Phys. Rev. Lett. **87**, 238303 (2001).

[Mor02] J. Moreira and A. Deutsch: *Cellular automata models of tumour development - a critical review*. Adv. Complex Syst. **5**, 247 (2002).

[Mos91] K. Moser, D. E. Wolf, and J. Kertész: *Numerical solution of the Kardar-Parisi-Zhang equation in one, two and three dimensions*. Physica A **178**, 215 (1991).

[Mul57] W. W. Mullins: *Theory of thermal grooving*. J. Appl. Phys. **24**, L449 (1957).

[Mur02] J. D. Murray: *Mathematical Biology I, volume 17 of Interdisciplinary Applied Mathematics* (Springer, Berlin Heidelberg, 2002), third edn.

[Nat92] T. Nattermann and L.-H. Tang: *Kinetic surface roughening. I. The Kardar-Parisi-Zhang equation in the weak-coupling regime*. Phys. Rev. A **45**, 7156 (1992).

[Oje00] F. Ojeda, R. Cuerno, R. Salvarezza, and L. Vázquez: *Dynamics of Rough Interfaces in Chemical Vapor Deposition: Experiments and a Model for Silica Films*. Phys. Rev. Lett. **84**, 3125 (2000).

[Oje03] F. Ojeda, R. Cuerno, R. Salvarezza, F. Agulló-Rueda, and L. Vázquez: *Modeling heterogeneity and memory effects on the kinetic roughening of silica films grown by chemical vapor deposition*. Phys. Rev. B **67**, 245416 (2003).

[Oka00] A. Okabe, B. Boots, K. Sugihara, and S. N. Chiu: *Spatial tessellations: Concepts and applications of Voronoi diagrams*. Probability and Statistics (Wiley, New York, 2000), second edn.

[Osk06] E. N. Oskoee and M. Sahimi: *Transport properties of composite solid films with rough self-affine surfaces*. Phys. Rev. B **74**, 045413 (2006).

[Ott90] E. Ott, C. Grebogi, and J. A. Yorke: *Controlling Chaos*. Phys. Rev. Lett. **64**, 1196 (1990).

[Pam75] B. R. Pamplin: *Crystal Growth* (Pergamon Press, Oxford, 1975).

[Par85] E. H. C. Parker, ed.: *The Technology and Physics of Molecular Beam Epitaxy* (Plenum Press, New York, 1985).

[Par99] C. A. Parent and P. N. Devreotes: *A Cell's Sense of Direction*. Science **284**, 765 (1999).

[Pas98] K. M. Passino and S. Yurkovich, eds.: *Fuzzy Control* (Addison-Wesley, 1998).

[Pim98] A. Pimpinelli and J. Villain: *Physics of Crystal Growth* (Cambridge University Press, Cambridge, 1998).

[Pom05] J. Pomplun, A. Amann, and E. Schöll: *Mean field approximation of time-delayed feedback control of noise-induced oscillations in the Van der Pol system*. Europhys. Lett. **71**, 366 (2005).

[Pyr92] K. Pyragas: *Continuous control of chaos by self-controlling feedback*. Phys. Lett. A **170**, 421 (1992).

[Rai00a] M. Raible, S. J. Linz, and P. Hänggi: *Amorphous thin film growth: Minimal deposition equation*. Phys. Rev. E **62**, 1691 (2000).

[Rai00b] M. Raible, S. Mayr, S. J. Linz, M. Moske, P. Hänggi, and K. Samwer: *Amorphous thin film growth: Theory compared with experiment*. Europhys. Lett. **50**, 61 (2000).

[Rai01] M. Raible, S. J. Linz, and P. Hänggi: *Amorphous thin film growth: Effects of density inhomogeneities*. Phys. Rev. E **64**, 031506 (2001).

[Ram00] J. Ramasco, J. Lopez, and M. Rodriguez: *Generic Dynamic Scaling in Kinetic Roughening*. Phys. Rev. Lett. **84**, 2199 (2000).

[Rei06] F. D. A. A. Reis: *Scaling in the crossover from random to correlated growth*. Phys. Rev. E **73**, 021605 (2006).

[Sar91] S. D. Sarma and P. Tamborenea: *A new universality class for kinetic growth: One-dimensional molecular-beam epitaxy*. Phys. Rev. Lett. **66**, 325 (1991).

[Sar96] S. D. Sarma, C. Lanczycki, R. Kotlyar, and S. Ghaisas: *Scale invariance and dynamical correlations in growth models of molecular beam epitaxy*. Phys. Rev. E **53**, 359 (1996).

[Sch89] H. G. Schuster: *Deterministic Chaos* (VCH Verlagsgesellschaft, 1989).

[Sch93] E. Schöll and K. Pyragas: *Tunable semiconductor oscillator based on self-control of chaos in the dynamic Hall effect*. Europhys. Lett. **24**, 159 (1993).

[Sch98] E. Schöll and S. Bose: *Kinetic Monte Carlo Simulation of the Nucleation Stage of the Self-organized Growth of Quantum Dots*. Sol. State El. **42**, 1587 (1998).

[Sch99] H. G. Schuster, ed.: *Handbook of Chaos Control* (Wiley-VCH, Weinheim, 1999).

[Sch01] E. Schöll: *Nonlinear spatio-temporal dynamics and chaos in semiconductors* (Cambridge University Press, Cambridge, 2001). Nonlinear Science Series, Vol. 10.

[Sch03a] H. J. Scheel: *Crystal Growth Technology* (Wiley, New York, 2003).

[Sch03b] J. Schlesner, A. Amann, N. B. Janson, W. Just, and E. Schöll: *Self-stabilization of high frequency oscillations in semiconductor superlattices by time–delay autosynchronization*. Phys. Rev. E **68**, 066208 (2003).

[Sch04] E. Schöll: *Pattern formation in semiconductors: control of spatio-temporal dynamics*. Ann. Phys. (Leipzig) **13**, 403 (2004). Special Topic Issue, ed. by R. Friedrich, T. Kuhn and S. Linz.

[Sch05] E. Schöll, A. Balanov, N. B. Janson, and A. Neiman: *Controlling stochastic oscillations close to a Hopf bifurcation by time-delayed feedback.* Stoch. Dyn. **5**, 281 (2005).

[Sch06a] S. Schikora, P. Hövel, H.-J. Wünsche, E. Schöll, and F. Henneberger: *All-optical noninvasive control of unstable steady states in a semiconductor laser*. Phys. Rev. Lett. **97**, 213902 (2006).

[Sch06b] J. Schlesner, V. Zykov, H. Engel, and E. Schöll: *Stabilization of unstable rigid rotation of spiral waves in excitable media*. Phys. Rev. E **74**, 046215 (2006).

[Sch07] E. Schöll and H. G. Schuster, eds.: *Handbook of Chaos Control* (Wiley-VCH, Weinheim, 2007). Second completely revised and enlarged edition.

[Shc04a] V. A. Shchukin, N. N. Ledentsov, and D. Bimberg: *Epitaxy of Nanostructures* (Springer, Berlin, 2004).

[Shc04b] V. A. Shchukin, N. N. Ledentsov, and D. Bimberg: *Epitaxy of Nanostructures* (Springer, Berlin, 2004).

[Soc94] J. E. S. Socolar, D. W. Sukow, and D. J. Gauthier: *Stabilizing unstable periodic orbits in fast dynamical systems*. Phys. Rev. E **50**, 3245 (1994).

[Spr00] G. Springholz, M. Pinczolits, P. Mayer, V. Holy, G. Bauer, H. Kang, and L. Salamanca-Riba: *Tuning of Vertical and Lateral Correlations in Self-Organized PbSe/$Pb_{1-x}Eu_xTe$ Quantum Dot Superlattices*. Phys. Rev. Lett. **84**, 4669 (2000).

[Ste96] E. Steimetz, J.-T. Zettler, F. Schienle, T. Trepk, T. Wethkamp, W. Richter, and I. Sieber: *In-situ Monitoring of InAs-on-GaAs Quantum Dot Formation in MOVPE by Reflectance-Anisotropy-Spectroscopy and Ellipsometry*. Appl. Surf. Science **107**, 203 (1996).

[Ste06] G. Stegemann, A. G. Balanov, and E. Schöll: *Delayed feedback control of stochastic spatiotemporal dynamics in a resonant tunneling diode*. Phys. Rev. E **73**, 016203 (2006).

[Str39] I. N. Stranski and L. Krastanow: *Sitzungsberichte der Akademie der Wissenschaften in Wien*. Akad. Wiss. Lit. Mainz Math.-Natur. Kl. IIb **146**, 797 (1939).

[Swa00] K. Swanson, E. Alvord, and J. Murray: *quantitativ model for differential motility of gliomas in gey and white matter*. Cell. Prolif. **33**, 317 (2000).

[Tho98] J. A. Thomson, J. Itskovitz-Eldor, S. S. Shapiro, M. A. Waknitz, J. J. Swiergiel, V. S. Marshall, and J. M. Jones: *Embryonic Stem Cell Lines Derived from Human Blastocysts*. Science **282**, 1145 (1998).

[Unk03] J. Unkelbach, A. Amann, W. Just, and E. Schöll: *Time–delay autosynchronization of the spatio-temporal dynamics in resonant tunneling diodes*. Phys. Rev. E **68**, 026204 (2003).

[Vil91] J. Villain: *Continuum models of crystal growth from atomic beams with and without desorption*. J. Phys. I **1**, 19 (1991).

[Vol26] M. Volmer and A. Weber: *Novel growth mechanism in heteroepitaxial semiconductor growth*. Z. Phys. Chem. **119**, 277 (1926).

[Vor08] G. Voronoi: *Nouvelles applications des parametres continusa la theorie des formes quadratiques. Deuxieme memoire: Recherches les paralleloedres primitifs*. J. Reine Angew. Math. **134**, 198 (1908).

[Wal06] P. Walter, E. Welcomme, P. Hallégot, N. J. Zaluzec, C. Deeb, J. Castaing, P. Veyssière, R. Bréniaux, J.-L. Lévêque, and G. Tsoucaris: *Early Use of PbS Nanotechnology for an Ancient Hair Dyeing Formula*. Nano Lett. **0**, 0 (2006).

[Wan04] X.-D. Wang, N. Liu, C. K. Shih, S. Govindaraju, and A. L. Holmes, Jr.: *Spatial correlation-anticorrelation in strain-driven self-assembled InGaAs quantum dots*. Appl. Phys. Lett. **85**, 1356 (2004).

[Wet04] R. Wetzler, R. Kunert, A. Wacker, and E. Schöll: *Inhomogeneous charging and screening effects in semiconductor quantum dot arrays*. New J. Phys. **6**, 81 (2004).

[Wil88] K. T. Wilke and J. Bohm: *Kristallzüchtung* (Verlag Deutscher Wissenschaften und Verlag H. Deutsch, Leipzig, 1988), second edn.

[Wol87] D. E. Wolf and J. Kertész: *Surface width exponents for three- and four-dimensional Eden growth*. Europhys. Lett. **4**, 651 (1987).

[Wol90] D. E. Wolf and J. Villain: *Growth with surface diffusion*. Europhys. Lett. **13**, 389 (1990).

[Wün07] M. Wünscher: *Kinetische Monte-Carlo-Simulation des epitakischen Wachstums unter Rückkopplungskontrolle*. Master's thesis, TU Berlin (2007).

[Yan06] S. Yanchuk, M. Wolfrum, P. Hövel, and E. Schöll: *Control of unstable steady states by long delay feedback*. Phys. Rev. E **74**, 026201 (2006).

[Zan88] A. Zangwill: *Physics at surfaces* (Cambridge University Press, Cambridge, 1988).